IMPERIAL COLLEGE LONDON

Towards The Development of Caspase-3/7 Inhibitor(s) for In Vivo PET Imaging of Cancer Apoptosis.

A thesis submitted by

Angela Udemba

In partial fulfilment of the requirements for the degree of

Doctor of Philosophy

Department of Surgery and Cancer
Imperial College
South Kensington
London
SW7 2AZ

30th September 2013

The copyright of this thesis rests with the author and is made available under a Creative Commons Attribution Non-Commercial No Derivatives licence. Researchers are free to copy, distribute or transmit the thesis on the condition that they attribute it, that they do not use it for commercial purposes and that they do not alter, transform or build upon it. For any reuse or redistribution, researchers must make clear to others the licence terms of this work.

Declaration of Originality

I, Angela N. Udemba certify that the research described within this thesis was accomplished under the co-supervision of Dr. Matthew J. Fuchter, Imperial College London and Professor Eric O. Aboagye, Imperial College London; along with some supervision from Dr. Graham Smith and Dr. Laurence C. Carroll; and is my own work unless stated otherwise.

Angela N. Udemba
London, September 2013

Abstract

The ability to image caspase activation provides a powerful tool for the evaluation of the oncologic therapeutic response via the apoptotic cascade. Research efforts have focused on the development of radiolabelled non-peptidyl caspase inhibitors to be utilised for imaging purposes. Isatin sulfonamides are of particular interest because of their specificity and potency for inhibiting the "apoptotic executioner" caspase-3. However, imaging attempts using the radiolabelled lead isatin **i** have shown low target-to-background radiotracer uptake.

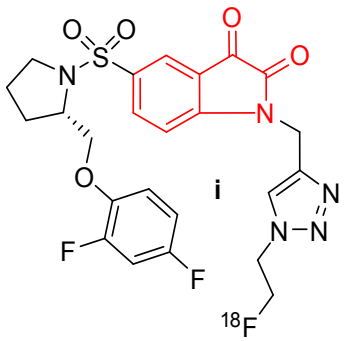
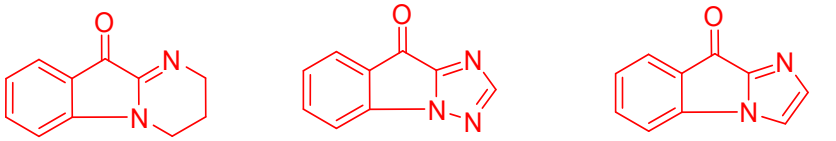


Figure A1: The lead isatin sulfonamide radiotracer

The research aim was to explore alternative series of caspase-3 inhibitors as radioligands with optimal properties for the PET imaging of apoptosis. The series based on the pyrimidoindolone **ii**, triazoleindolone **iii** and imidazoleindolone **iv** heterocycles are structurally similar to the isatin core heterocycle **i**, with all containing the crucial ketone responsible for caspase inhibition via the formation of a thiohemiketal with an active site cysteine residue.



ii Pyrimidoindolone heterocycle

iii Triazoleindolone heterocycle

iv Imidazoleindolone heterocycle

Figure A2: Proposed alternative heterocycles to the isatin scaffold

Using computational modelling studies combined with UV-vis titrations, these heterocycles were shown to have the propensity to favourably form thiohemiketals and therefore potentially inhibit caspase-3. Initial target structures **v** - **vii**, modelled on the structure of the lead isatin **i**, were subsequently designed for synthesis and biological characterisation. Pyrimidoindolone target **v** was

synthesised and radiolabelled using modified literature conditions. Biological results showed the pyrimidoindolone to have a similar biological profile to isatin **i**.

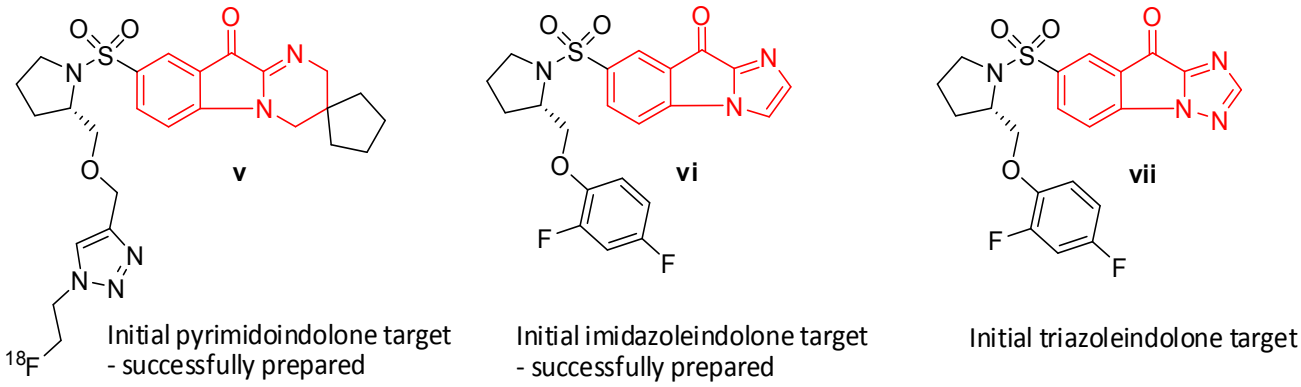


Figure A3: Initial target pyrimidoindolone, imidazoleindolone and triazoleindolone heterocycles

Four different synthetic strategies were investigated for the synthesis of the imidazoleindolone and triazoleindolone heterocycles including, the use isatin sulfonamide intermediates, an intramolecular S_NAr cyclisation process, Friedel-Crafts cyclisation method and nucleophilic addition to a benzonitrile. Preparation of imidazoleindolone **vi** was achieved with the S_NAr cyclisation route. Preparation of triazoleindolone **vii** proved challenging with synthesis of only the core heterocyclic precursors, hydrazone **ix** and ketal **vii** achieved using the S_NAr cyclisation route. Acid-sensitivity of the ring system hindered deprotection reactions and led to ring destruction.

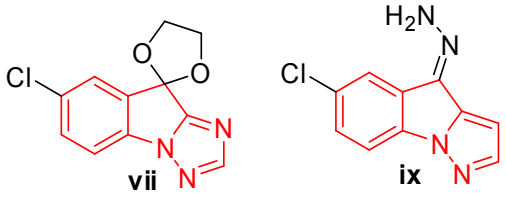


Figure A4: Prepared precursors to the core triazoledindolone heterocycle

Acknowledgements

Firstly I would like to thank Professor Eric Aboagye for providing me with the opportunity to research an exciting and certainly challenging project. Dr Matthew Fuchter, thank you for patiently sitting through all my frustrating research updates and reports. I am grateful for the group socials that provided much need distraction and entertainment.

I must acknowledge Dr Graham Smith for his continuous support from the very first day on this project. You taught me everything I know about radiochemistry for which I am grateful.

Dr Laurence Carroll, thank you so very much for your invaluable contribution to radiosynthesis. I am grateful for your patience and support with completing biological studies.

I would like to extend my immense gratitude to Dr Quang-De Nguyen and Dr Maciej Kaliszczak for conducting the biological experiments.

To the members of the Barrett/Fuchter group, many thanks for creating a stimulating and enjoyable working environment.

Abbreviations

Å	Angstrom
A	Absorption
Ac	Acetyl
ACN	Acetonitrile
Ala	Alanine
AMC	Aminomethylcoumarin
Arg	Arginine
Asn	Asparagine
Asp	Aspartic acid
β^+	Positron
Boc	Di-*tert*-butyl dicarbonate
BPDS	Bathophenanthroline disulfonic acid
Bq	Becquerel
br	Broad
Bu	Butyl
CBR	Caspase binding radioligand
cf	Compare
Ci	Curie
CI	Chemical Ionisation
δ	Chemical Shift
CPA	Cyclophosphamide

CT	Computerised Tomography
Cys	Cysteine
Δ	Delta / 'change in'
d	Doublet
DBU	1,8-Diazabicyclo[5.4.0]undec-7-ene
DCM	Dichloromethane
dd	Doublet of doublets
ddd	Doublet of doublet of doublets
DEVD	Aspartic acid-glutamic acid-valine-aspartic acid
DFT	Density Functional Theory
DMA	Dimethylacetamide
DMAP	4-Dimethylaminopyridine
DME	Dimethoxyethane
DMF	*N,N*-Dimethylformamide
DMSO	Dimethyl sulfoxide
DNA	Deoxyribose nucleic acid
dt	Doublet of triplets
E	Energy
ED_{50}	Effective dose for 50% inhibition
EI	Electron ionisation
EOB	End of Bombardment
EOS	End of Synthesis

eq.	Equivalent
ES	Electrospray
Et	Ethyl
et. al	And others
Et_3N	Triethylamine
Et_2O	Diethyl ether
EtOAc	Ethyl acetate
EtOH	Ethanol
g	Gram(s)
GBq	Gigabecquerel
Gln	Glutamine
Glu	Glutamic acid
Gly	Glycine
GSH	Glutathione
4-HC	4-Hydroperoxycyclophosphamide
His	Histidine
HMDS	Hexamethylsiloxane
HPLC	High Performance Liquid Chromatography
HRMS	High Resolution Mass Spectrometry
hrs/hr	Hour(s)
Hz	Hertz
i	*Iso*

IC_{50}	Inhibitor concentration for 50 % inhibition of an enzyme *in vitro*
ID	Injected dose
IMA	Isatin Michael Acceptors
J	Coupling constant
K	Equilibrium constant
K_{222}	Kryptofix$_{222}$ (4,7,13,16,21,24-Hexaoxa-1,10-diazabicyclo[8.8.8]hexacosane)
kDa	Kilodalton
keV	Kiloelectron volt
KJ	Kilojoules
L	Litre
LCMS	Liquid Chromatography Mass Spectrometry
LDA	Lithium diisopropylamide
LG	Leaving group
LOR	Line of response
LR	Lawesson's Reagent
M	Molar
m	Multiplet
µ	Micro (10^{-6})
mCi	Millicurie
Me	Methyl
MeI	Methyl iodide
Met	Methionine

MeV	Megaelectron volt
MHz	Mega Hertz
min(s)	Minute(s)
MK	Merz Kollman
mL	Millilitre
mmol	Millimole(s)
mol	Mole(s)
MRI	Magnetic Resonance Imaging
MS	Mass Spectrometry
m/z	Mass to charge ratio
n	Nano
n / N	Normal
NBS	*N*-Bromosuccinimide
NIR	Near Infrared
nM	Nanomolar
NMM	*N*-methylmorpholine
NMR	Nuclear Magnetic Resonance
Nu	Nucleophile
OMs	Mesylate
OTf	triflate
p	*Para*
PAC-1	First procaspase activating compound

PBS	Phosphate buffered saline
(p,n)	*(proton, neutron)*
PET	Positron Emission Tomogragraphy
PG	Protecting group
Pgp	P-glycoprotein
pH	Potential hydrogen
Ph	Phenyl
Phe	Phenylalanine
PhMe	Toluene
pKa	Acid dissociation constant
pM	Picomolar
PMB	Paramethoxy benzyl
PMBSH	Paramethoxybenzyl thiol
ppm	Parts per million
PPTS	Pyridinium *p*-toluenesulfonate
pr	Propyl
prep	Preparative
Pro	Proline
Prod.	Product
PS	Phosphatidylserine
psi	Per square inch
PTSA	Paramethoxytoluene sulfonic acid

q	Quartet
QSAR	Quantitative Structure Activity Relationship
R	Boltzmann Constant
RC	Radiochemical
React.	Reactant
R_f	Retention factor
RIF-1	Radiation-induced murine fibrosarcoma tumour cells
rpm	Rotations per minute
rt	Room temperature
s	Singlet
SAR	Structure Activity Relationship
SCRF	Self-Consistent Reaction Field
sec (s)	Second(s)
SEM	2-(Trimethylsilyl)ethoxymethyl
± SEM	± Structural equation modelling
Ser	Serine
S_N2	Bimolecular nucleophilic substitution
S_NAr	Nucleophilic aromatic substitution
SPAAC	Strain-promoted alkyne-azide coupling
SPE	Solid Phase Extraction
SPECT	Single Photon emission Computed Tomography
t	Triplet

T	Temperature
TAC	Tumour time versus radioactivity curve
TBAI	Tetrabutylammonium iodide
Temp.	Temperature
tert or t	Tertiary
THF	Tetrahydrofuran
Thr	Threonine
TLC	Thin Layer Chromatography
Tr	Trityl
Trp	Tryptophan
TS	Transition state
Ts/Tos	Tosylate
tt	Triplet of triplets
Tyr	Tyrosine
UV-vis	Ultraviolet-visible
Val	Valine
Veh	Vehicle or control
Ver	Verapamil
Vs	Versus

Table of Contents

DECLARATION OF ORIGINALITY **2**

ABSTRACT **3**

ACKNOWLEDGEMENTS **5**

ABBREVIATIONS **6**

I. INTRODUCTION **18**

I.1. An Overview **18**

I.2. Molecular Imaging Modalities **20**
I.2.1. The Basic Principles of PET 23
I.2.1.1. Radiotracer/ Probe Design for PET Imaging 25
I.2.1.2. [18F] - Ideal PET Radionuclide 27
I.2.1.3. Radiosynthesis of PET Tracers 28

I.3. Apoptotic Imaging Markers and Biological Targets **29**
I.3.1. Imaging Phosphatidylserine (PS) Reorganisation using Annexin-V 31
I.3.2. Imaging Apoptotic Cell Membranes using the Aposense Family 31
I.3.3. Imaging Early Apoptotic Events by Targeting Caspase-3(7) 33

I.4. Design and Development of Radiotracers Targeting Caspase-3/7 ..... **35**
I.4.1. Isatin Sulfonamides as Potent and Selective Inhibitors of Caspase-3/7: SAR 35
I.4.2. Development of Radiolabelled Isatin Sulfonamides 41
I.4.2.1. Radiochemistry of Caspase-3 PET Imaging Agents 44
I.4.3. Pyrimidoindolones: A New Class of Caspase-3/7 Inhibitors 47

I.5. Proposed Research **51**

II. INITIAL COMPUTATIONAL MODELLING & UV-VIS TITRATIONS **54**

II.1 Introduction **54**

II.2. Computational Analysis of the Heterocycles **55**
II.2.1. Computational Methods 56
II.2.2. Calculation of Ketone Partial Charges 57
II.2.3. Transition States and Gibbs Free Energies 59

II.3. Experimental UV-Vis Analysis of the Heterocycles **63**
II.3.1. UV-Vis Spectroscopic Titrations of Thiohemiketal Formation 64

II.3.2. Calculating Equilibrium Constants using Benesi-Hildebrand Plots 66
II.3.3. Experimental Results 69
II.3.3.1. The Substituent Effect 72

II.4. Conclusion 76

III. [18F]-FLUORINATED PYRIMIDOINDOLONE TO IMAGE CASPASE-3 79

III.1. Introduction: Target Structure Design 79

III.2. Target Pyrimidoindolone Synthesis 81
III.2.1. Halomethylation of Cyclopentylcarbonitrile 83
III.2.2. Pyrimidoindolone Target Probe Synthesis; Part 2 86
III.2.2.1. Exploring a Different Route to the Pyrimidoindolone Target 91
III.2.2.2. Synthesis of the Pyrimidoindolone Core Heterocycle / Pharmacophore 93

III.3. Radiochemistry of the Pyrimidoindolone Target 94

III.4. Biological Characterisation of the Pyrimidoindolone Target 102
III.4.1. *In vitro* Caspase Enzyme Inhibition Assay 102
III.4.2. *In Vitro* Cell Uptake Studies 102
III.4.3. *In vivo* Tissue Biodistribution & Metabolic Profiles 105
III.4.4. Transwell / Efflux Ratio Assay 110

III.5. Conclusion 114

IV. IMIDAZOLEINDOLONE AND TRIAZOLEINDOLONE SYNTHESIS 116

IV.1. Introduction 116

IV.2. Imidazoleindolone and Triazoleindolone Synthesis via Isatin Sulfonamide Intermediates 119

IV.3. Imidazoleindolone and Triazoleindolone Synthesis via S_NAr Fluoride displacement 133
IV.3.1. Imidazoleindolone Synthesis 134
IV.3.2. Triazoleindolone Synthesis 148

IV.4. Alternative Routes to the Imidazoleindolone and Triazoleindolone Targets 159
IV.4.1. Investigating the Friedel-Crafts Route 161
IV.4.1.1. Imidazoleindolone Synthesis 161
IV.4.1.2. Triazoleindolone Synthesis 164
IV.4.2. Investigating the 'Addition to Benzonitrile' Route 166

IV.5. Conclusion 167

GENERAL SUMMARY & PERSPECTIVE 170

EXPERIMENTAL 175

REFERENCES **229**

APPENDIX **239**

Appendix 1: Gaussian Data Output from Computational Modelling of the Heterocycles **240**

Appendix 2: UV-Vis Absorption Data **241**

Appendix 3: Crystal Data and Structure Refinement for the Ketal Protected Triazoleindolone 212 ..... **244**

CHAPTER I:

GENERAL INTRODUCTION

I. INTRODUCTION

I.1. An Overview

Molecular imaging is a rapidly growing research area that allows the non-invasive characterisation of biological processes within a living organism[1] by exploiting the interaction of different forms of energy with tissue.[2] Conventional imaging technologies are primarily based on imaging gross anatomy and changes in physiological features.[1, 3] Today, imaging employs molecularly targeted contrast agents in visualising the expression and activity of biomarkers such as, growth factor receptors, proteases, protein kinases, as well as, detecting key biological processes including apoptosis.[3, 4] The available imaging modalities include magnetic resonance imaging (MRI), optical imaging, contrast-enhanced ultrasound and radionuclide imaging encompassing, Positron Emission Tomography (PET) and Single Photon Emission Computed Tomography (SPECT). The phenomenon of molecular imaging is poised to aid the earlier detection of cancer, personalised anticancer therapy and staging, and monitoring of response to therapy.[4, 5]

Apoptosis or programmed cell death serves to maintain homeostasis in multicellular organisms. Abnormal apoptosis has been observed in a large number of pathologies but, more specifically, mechanisms hindering apoptosis are implicated in most malignancies.[6] The induction of apoptosis is thus an essential part of non-surgical anticancer therapies such as, radiotherapy, chemotherapy and hormonal treatments. It follows that the rapid and accurate visualisation of the apoptotic response to therapy has a great potential in aiding diagnostic and treatment monitoring. Apoptosis is characterised by specific changes in the cell. These changes are exploited in the imaging and detection of cell death and include; membrane alterations, DNA fragmentation, enzyme expression/ activation and plasma membrane leakage.[7] Traditional assessment of cell death involved the invasive removal of microscopic samples from tissues using biopsy or post-mortem.[8] The fact that these microscopic methods are invasive limits applicability and utilisation. Molecular imaging offers the advantage of non-destructively imaging apoptosis *in vivo*.[5] The cysteine-aspartyl protease, caspase-3 has been found to be activated in most models of apoptosis and is thus a biochemical target for apoptotic imaging. Current research strategies are aimed at identifying non-peptidyl, small molecule inhibitors of caspase-3 that can be utilised in the targeted molecular imaging of cell death.

The imaging of apoptosis began with the nuclear magnetic resonance (NMR) characterisation of apoptotic cells *in vitro*.[8] This was closely followed by MRI,[9] then nuclear imaging[10] together with,

optical imaging[11] and contrast-enhanced ultrasound.[12] Of all the available imaging modalities, nuclear medicine is considered the superior technology as it is currently the most sensitive and specific method for studying molecular processes.[13, 14] Realistic goals of nuclear medical imaging in oncology include: i) the early detection of molecular or physiological changes that signal the presence of cancer when a tumour is still at a curable stage; ii) the ability to evaluate response to therapy and modify treatment procedures in real time; and iii) the acceleration of the anticancer drug development process by allowing earlier clinical testing of new therapeutics.[3, 5] In this introductory chapter, an overview of the available imaging modalities is provided, placing particular emphasis on nuclear medicine techniques and the selection of PET for the molecular imaging of apoptosis. The present status of research into targeted radiopharmaceutical probes for the imaging of cell death will be highlighted, leading to the objectives behind our proposed research, aimed at designing optimal caspase-3 binding probes for the PET imaging of apoptosis. In subsequent chapters, research results are presented and discussed, including synthesis of designed probes, computational modelling of properties, radiolabelling and biological characterisation. The report then concludes with an overall perspective from the research report and future work towards realising the research goals.

I.2. Molecular Imaging Modalities

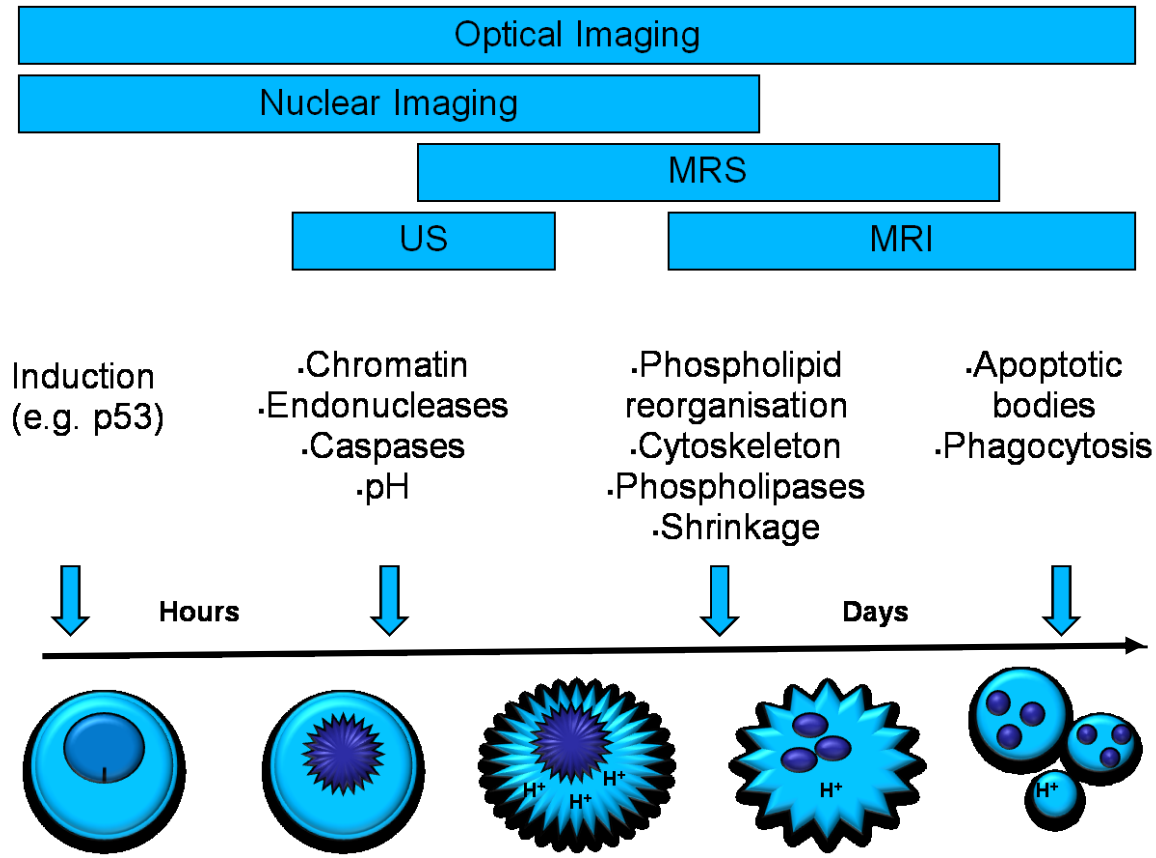


Figure 1.1: Timeline showing the application of the different imaging modalities at different stages of the apoptotic cascade, characterised by a number of biomolecular and biophysical events. Since molecular events precede the biophysical changes, nuclear imaging techniques are more sensitive at the early phases of apoptosis. Figure adapted from Hakumaki *et al*.[8]

Figure **1.1** shows the biomolecular and biophysical events that characterise the onset of apoptosis which can be exploited by the different imaging modalities in the detection of apoptosis. The concept of targeted imaging is illustrated in Figure **1.2**: specific biomarkers such as, enzymes and receptors involved in biological activities such as, apoptosis are identified and targeted using chemicals or biomolecules that selectively bind to the chosen biomarker. These targeting moieties are labelled with signalling agents used to 'visualise' the biomarkers and therefore the biological activity being imaged.[15] The signalling agents are designed for use in specific imaging modalities including, ultrasound, optical imaging, MRI and nuclear medicine techniques comprising, PET and SPECT.

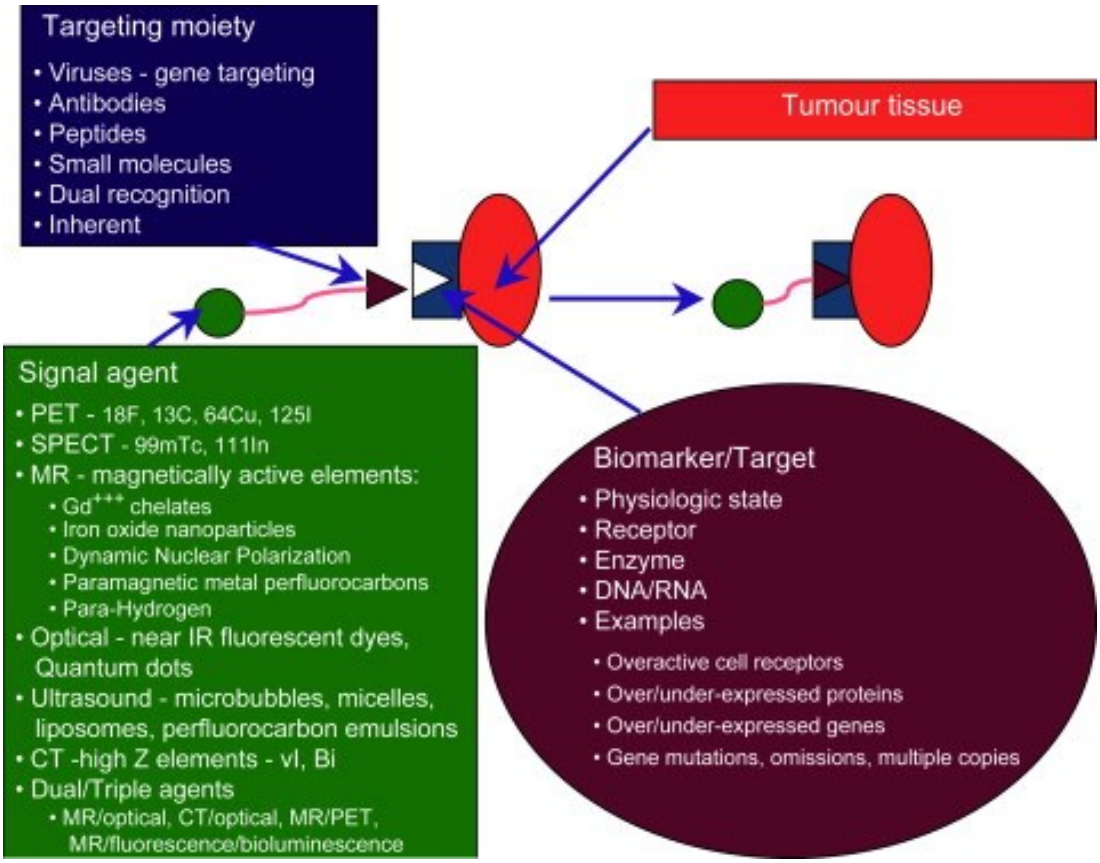


Figure 1.2: Targeted Biomarker imaging. Figure taken from Fass *et al*.[15]

Ultrasound employs high frequency sound waves (> 20 kHz) to produce images of structures within the body.[8] The technique is regularly used to guide biopsies and is one of the most common methods used in the diagnosis of tumours in the thyroid, breast, prostate, liver and kidneys.[15] It has been shown that ultrasound may be able to detect the biophysical effects of apoptosis such as the subcellular nuclear chromatin condensation and DNA fragmentation which signal the onset of apoptosis.[8, 16] However, deep-seated tumours can prove difficult to image.[8] Notable advantages of ultrasound imaging in comparison to other modalities include, its low cost, easy availability and portability. A key disadvantage of the technique in the field of apoptosis is its inability differentiate apoptosis from necrosis (uncontrolled cell death).[8]

Optical imaging is an imaging modality that relies on radiation penetrating the body for image construction using high-speed and often sensitive detection of fluorescent tracers. However, photons of the UV-vis range are absorbed by tissue chromophores and hence cannot penetrate more than 1-2 mm into tissues. This has limited the use of optical imaging to millimetre-scale resolution, largely restricting the method to the planar imaging of small animals.[1, 13]

MRI is the modality of choice for the evaluation of tumour size, shape and anatomical appearance in many areas of the body.[17] The technique is based on the magnetic relaxation of water protons contained in different tissue types, and therefore benefits from the high concentration of water in living organisms. Excellent spatial resolution and tissue contrast are achieved by the enhancement of local water proton relaxation in the presence of an exogenous contrast agent, usually a paramagnetic gadolinium(III) complex.[18] MRI is however limited by low sensitivity, requiring the use of relatively large concentrations of tracers for imaging purposes, which can potentially have toxic side effects. Thus, difficulties lie in the design and development of MR contrast agents that can increase sensitivity without compromising the safety. Despite the sensitivity issues, MRI has been successfully applied in research to the molecular imaging of apoptotic cell membranes using the endogenous protein, Annexin-V as the probe.[19, 20]

Nuclear medicine imaging can be regarded as the non-invasive monitoring of biological processes using trace amounts of positron-emitting and gamma-emitting radiopharmaceuticals for PET and SPECT respectively. Nuclear imaging techniques cannot match the spatial resolution of MRI or ultrasound due to the nature of the physics involved. However, this technique maintains a position of prominence in molecular imaging because of the extreme sensitivity the technique is capable of. Very high sensitivities mean that *in vivo* imaging by both SPECT and PET can be performed at sub-pharmacological tracer doses.[13, 21] This makes it possible to label and administer even highly potent or toxic compounds without the manifestation of pharmacological or toxicological effects.[21] We were particularly interested in molecular imaging using PET which is further described in the subsequent sections.

Figure **1.3** below summarises the advantages and disadvantages of the available molecular imaging modalities. Despite the obvious trade-offs between all the imaging modalities, the advent of molecular imaging has contributed to the great progress observed in the understanding of apoptosis in cancer.[8]

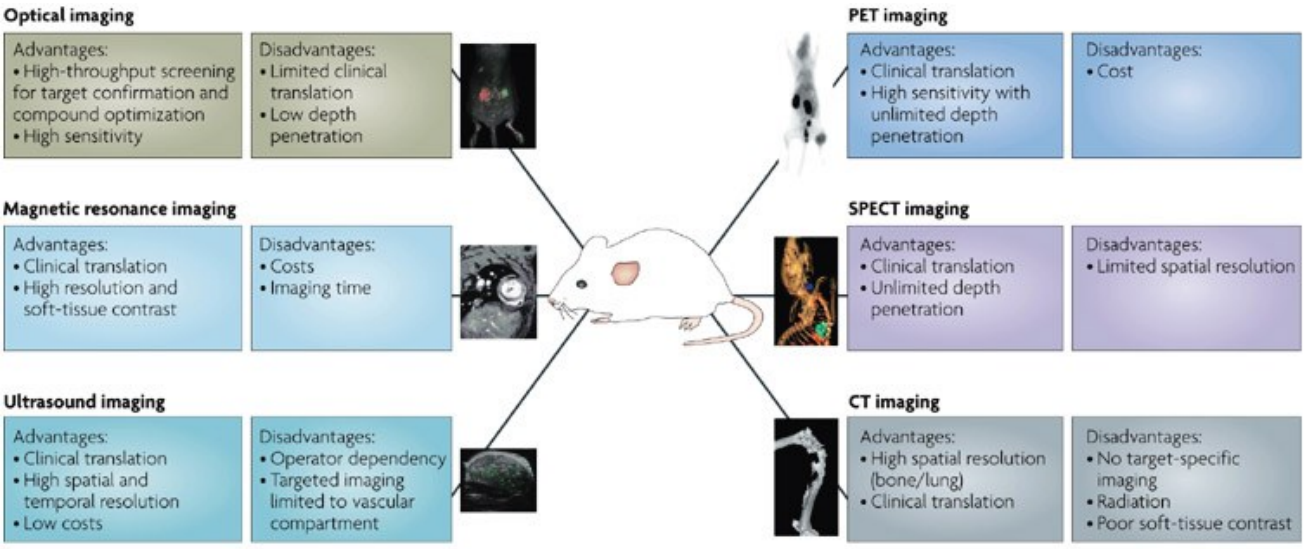


Figure 1.3: A summary of the advantages and disadvantages of different molecular imaging modalities. Image taken from Willmann *et al*.[22]

I.2.1. The Basic Principles of PET

Since positron-emitting atoms are not naturally occurring, the radionuclides used in PET are produced by a cyclotron. In a cyclotron, high power electric and magnetic fields are used to accelerate charged particles (e.g. protons, deuterons or alpha particles) to high energies which then bombard stable atoms in a target to give rise to radioactive isotopes. Table **1.1** gives a brief summary of the nuclear reactions used to produce the principal radionuclides used in PET (^{11}C, ^{15}O, ^{18}F, and ^{13}N).[14, 23] As shown in Table **1.1**, there are generally more protons than neutrons in each radionuclide. The excess positive charge is released during nuclear disintegration by the emission of a positron.[17] The emitted positron travels a short distance and is annihilated by colliding with an electron, producing two 511 keV photons.[17] Simultaneous detection of the annihilation photons along a line of response (LOR) between two detectors provides a distribution summation of the radiotracer which is computed into PET images of the process under investigation.[14, 17, 23, 24]

Table 1.1: Production and characteristics of the principal PET radionuclides[14]

Positron emitting radionuclide	Stable element	Nuclear Reaction	No. of protons (p) and neutrons (n) in the product nucleus	Half-life (mins)	Stable nucleus after positron emission
^{11}C	Nitrogen (^{14}N)	$^{14}N(p,\alpha)^{11}C$	6p, 5n	20.4	^{11}B
^{13}N	Carbon (^{12}C)	$^{12}C(d,n)^{13}N$	7p, 6n	10.0	^{13}C
^{15}O	Nitrogen (^{14}N)	$^{14}N(d,n)^{15}O$	8p, 7n	2.03	^{15}N
^{18}F	Oxygen (^{18}O)	$^{18}O(p,n)^{18}F$	9p, 9n	109.8	^{18}O

In oncology, functional information from PET provides advantages over anatomic information from ultrasound and MRI. Whole body PET imaging allows the early identification of disease, differentiation between benign and malignant lesions, examinations of all organs for metastases, and the determination of therapeutic effectiveness.[23] PET has also been shown to have 8 - 43 % higher diagnostic accuracy than conventional procedures in trials for lung and colorectal cancers.[23, 25] Of the two nuclear imaging techniques available (PET and SPECT), PET is considered superior for a number of reasons.[13] Firstly, the principal PET radionuclides (^{11}C, ^{15}O, ^{13}N and ^{18}F) are physiologically important elements and their biogenicity makes it possible to directly label organic molecules of interest without altering their biological activities.[18] Common SPECT nuclei include ^{99m}Tc and ^{123}I which are not biologically important elments.[13] Secondly, the spatial resolution of PET clinical cameras is in the range of 1 - 2 mm compared to the 6 - 7 mm of SPECT clinical cameras[13] i.e. PET acquires data with higher spatial resolution than SPECT.

However, PET is not without limitations. The requirement for an in-house cyclotron to produce the short-lived isotopes used in PET limits the application of the technique. This is more problematic with ^{11}C which has a short half-life of 20.4 mins. The second limitation of PET is also imposed by the short half-lives of the principal positron emitters, forcing the synthesis, purification, analysis and formulation of radiolabelled probes to occur within the order of minutes. The larger positron emitting isotopes such as, ^{64}Cu, ^{89}Zr and ^{124}I with longer half-lives of 12.7 hours, 78.4 hours, and 4.17 days respectively, could be used.[26] However, the longer half-lives of these radionuclides would prolong exposure of the subject (patient or laboratory animal) to ionising radiation, resulting in significantly higher radiation doses. Nonetheless, the limitations imposed by the short half-lives of the principal PET radionuclides are compensated for by the advantages they offer to their use as tracers. In addition to being physiologically important elements, the principal PET radionuclides allow the possibility of repeating studies in the same subject within a short time interval,[21] which is beneficial in reducing the number of animals required for an experiment without compromising statistical significance.

In addition, PET has the ability to measure chemical changes that occur before the macroscopic anatomical signs of a disease can be observed.[27] Despite the challenges imposed by the short-lived positron emitters, a wide variety of selective PET radiotracers have been developed including, enzyme substrates and inhibitors, receptor ligands, amino acids and markers of blood flow and blood volume.[23] PET is the preferred method for imaging receptor/enzyme function and

biochemical mechanisms, since its high sensitivity makes it possible to visualise biomolecules typically present in the nanomolar range.[8, 28] In oncology, conventional methods may be insensitive to assessing therapeutic response where tumour shrinkage is not anticipated, but where functional changes may be marked. It is here that PET imaging can particularly play an important role using targeted radiopharmaceutical probes.

I.2.1.1. Radiotracer/ Probe Design for PET Imaging

PET imaging requires specific molecules labelled with a positron-emitting radionuclide which can be quantified *in vivo* by the detection of photons emitted as a result of positron annihilation. In a typical PET imaging assay, a radiotracer is injected intravenously and scanned to measure the tracer concentration in tissues and plasma over time. The development of new PET imaging probes is a multidisciplinary area consisting of biological target selection, organic synthesis, radiosynthesis and the *in vitro* and *in vivo* evaluation of the radiopharmaceutical. The main challenge in oncological PET imaging is the design and development of targeted radiopharmaceuticals with high affinity and high specificity that can allow the quantitation of molecular processes in a reproducible and repeatable manner. In targeted imaging, the radionuclide or the signalling moiety is attached to a molecule that binds to a specific biological target, such as an enzyme of interest (Figure **1.2**). The ideal radiotracer agent binds only to the biological target of interest so that little or no non-specific interactions are observed. In order to obtain images with high target-to-background ratio, a number of prerequisites for the development of imaging probes must be met. These are extensively reviewed in the published literature.[29, 30] Some common criteria, applicable to PET as well as to other imaging modalities include:

I. **High Sensitivity** – biomarkers or targets such as receptors and proteins are commonly expressed at very low concentrations. Hence, the ability of imaging techniques to detect concentrations in the sub-micromolar or often, sub-nanomolar scale is crucial.

II. **High Specificity and Affinity** – a high affinity of a probe for its biological target ensures the probe accumulation in the target tissue, resulting in high-contrast images. The affinity of the radiotracer should also be compatible with the concentration of the molecular target of interest i.e. molecular targets present in high concentrations can be imaged using radiotracers with a relatively low affinity (10 - 30 nM), compared to the sub-nanomolar radiotracer affinity required for a target which is expressed in lower concentrations.[31] In other words, the lower

the concentration of a molecular target, the higher the affinity requirement of a radiotracer to provide sufficient specific binding signals.

III. **Favourable pharmacokinetics** – low peripheral metabolism and plasma clearance times of minutes to hours are desirable. Labelled metabolites can undergo non-specific binding or take part in other biological processes, reducing target-to-background ratio. Hence, where the radiotracer is extensively metabolised *in vivo*, the preference is for the compound to be labelled in a position which produces labelled metabolites that are least likely to interfere with the process under investigation.

IV. **Lipophilicity** – the lipophilicity of a probe is an important factor since it determines the aqueous solubility of the probe for intravenous administration or the ability of the probe to permeate barriers such as membrane bilayers and the blood brain barrier. Highly lipophilic tracers often exhibit non-specific binding interactions. In general, successful radiotracers have sufficient lipophilicity that they are able to diffuse across cell membranes but not so lipophilic that their concentration in lipid-rich tissues hinders their binding at the molecular target of interest.

V. **Ease of Radiolabelling** – the molecular structure of a radiotracer precursor should allow rapid labelling with the appropriate radionuclide, given the restriction imposed by the short half-lives of PET nuclides and the limited scope of available radiolabelling methods.

I.2.1.2. [18F] - Ideal PET Radionuclide

Table 1.2: Positron ranges in soft tissues for selected positron emitters.[32]

Positron emitting radionuclide	Half-life (mins)	Theoretical specific activity (Ci/ μmol)	Decay % β^+	Positron Energy (MeV)		Positron range in soft tissue (mm)	
				Maximum (E_{max})	Mean	Maximum	Mean
^{11}C	20.4	9220	99.77	0.970	0.386	4.2	1.23
^{18}F	109.8	1710	96.7	0.635	0.250	2.6	0.61
^{124}I	6048	31	11.0	1.532	0.686	6.3	2.3
			12.0	2.135	0.974	8.7	3.5
^{68}Ga	68.3	2766	87.7	1.899	0.836	8.2	2.9
^{64}Cu	768	245	17.87	0.653	0.278	2.9	0.64

Table **1.2** shows a number of PET radionuclides that can be used in the development of radiopharmaceuticals.[32] The biogenicity and high specific activity (the concentration of cold, unradiolabelled material present in a formulated dose) of ^{11}C make it ideal for labelling biological or organic molecules of interest. However, the physical half-life of 20.4 mins is too short for extensive application in terms of commercialisation and distribution. The radiometals are appropriate for labelling peptides and proteins via chelation chemistry, and the availability of ^{68}Ga via generator production is advantageous. ^{124}I can also be used for radiolabelling peptides and proteins, but its low specific activity is far from ideal and the much longer half-life is unfavourable with respect to radiation dose to a subject. With ^{124}I, the very high energy positron emissions also results in blurry images and imaging is further complicated by a second gamma emission. ^{18}F is generally the preferred PET radionuclide for the development of radiopharmaceuticals for a number of reasons:[32]

I. It has the lowest positron energy (0.635 MeV) which limits the distance travelled by the emitted positron before annihilation, restricting the tissue range to a maximum of 2.6 mm. The result is high resolution images compared to PET images obtained with other PET radionuclides
II. ^{18}F can be produced in high specific activity and is readily available from small medical cyclotrons
III. ^{18}F decays with almost 100 % positron efficiency
IV. ^{18}F-PET tracers typically have well established radiochemistry for synthesis in relatively high yields
V. The physical half-life of 109.8 mins allows the possibility of distribution to clinics without access to a cyclotron

VI. The combination of intermediate half-life and medium energy photo emission provides an acceptable radiation dosimetry profile to allow repeated studies in patients.

I.2.1.3. Radiosynthesis of PET Tracers

PET radiosynthesis involves the radiolabelling of a drug molecule by the incorporation of a cyclotron-produced radionuclide. The radionuclides obtained from a cyclotron are sometimes used directly but are often converted into more reactive chemical species to allow their facile incorporation into the molecules of interest.

Fluorine can react with a range of organic and inorganic molecules both as a nucleophile and as an electrophile. For the production of ^{18}F, two types of targets are used in a cyclotron; a liquid target for the production of nucleophilic $^{18}F^-$ and a gas target for the production of electrophilic fluorine gas, $[^{18}F]F_2$. Typically the nuclear reactions involve the proton bombardment of ^{18}O-enriched water and deuteron bombardment of ^{20}Ne atoms for the production of $^{18}F^-$ and $[^{18}F]F_2$ respectively.[14, 32] Cyclotron produced electrophilic $[^{18}F]F_2$ is diluted with carrier (cold) fluorine gas, leading to low specific activity not optimal for the synthesis of high specific activity radiopharmaceuticals. In addition, in electrophilic radio-fluorination reactions, the labelling reaction yield is limited to a maximum of 50 % because the $[^{18}F]F_2$ precursor has only one atom as ^{18}F and the other atom as the stable ^{19}F.

In contrast to the carrier added $[^{18}F]F_2$, non-carrier added $^{18}F^-$ can be produced in high specific activity (2 - 10 Ci/μmol) and is therefore usually preferred for radiolabelling reactions.[32, 33] The synthesis of radiopharmaceuticals using $[^{18}F]$fluoride are typically achieved via the nucleophilic substitution of the corresponding mesylate, tosylate or a triflate precursor (S_N2), or by nucleophilic aromatic substitution (S_NAr).[32, 34] These labelling reactions differ from normal organic synthesis, owing to the short half-lives of the radionuclides requiring fast reaction times and simple procedures. Trace amounts of the radioactive isotope are usually reacted with relatively large amounts of a substrate. Typically, aqueous $[^{18}F]$fluoride delivered from a cyclotron is dried in the presence of Kryptofix-222 (K_{222}) and potassium carbonate via azeotropic distillation with successive additions of acetonitrile to give the 'naked' $[^{18}F]$fluoride, a very reactive nucleophile. Nucleophilic fluorination is then carried out in an aprotic solvent (e.g. DMSO, DMF or ACN) under basic conditions, with conventional heating or microwave irradiation.[35, 36]

With a growing interest to widen the reaction scope and therefore the radiochemistry precursor compounds that can be used, new radiosynthetic strategies have been developed. Traditionally, radiolabelling with [^{18}F]fluoride focused on nucleophilic substitution reactions.[37] Recently, the copper(I) catalysed 1,3-dipolar cycloaddition of terminal alkynes with substituted azides, the so-called 'click' reaction has been widely employed.[37] An example of the application of the click reaction in the radiosynthesis of a PET radiotracer is discussed in Section **I.4**. The 'click' radiolabelling technique has been recently expanded to a copper-free reaction, where the alkyne-azide coupling is promoted by strain without the need to use the cytotoxic copper catalyst.[38, 39] The reaction of a strained cyclooctyne and an azide in strain-promoted alkyne-azide coupling (SPAAC) reaction has shown greatly improved kinetics. The ring strain of a substituted cyclooctyne and electron-withdrawing fluorine substituents promote the [3 + 2] dipolar cycloaddition with azides. Recently, a number of groups have reported the use of copper-free click reaction for [^{18}F] radiolabelling reactions.[38, 40-43]

I.3. Apoptotic Imaging Markers and Biological Targets

Apoptosis is a cell suicide mechanism which contributes to normal physiology and pathology. Beyond cancer, apoptosis plays a key role in several other pathologies, including stroke, ischemia, osteoarthritis and neurodegenerative disorders.[44, 45] Several features of apoptotic cells differentiate them from their healthy counterparts, marking them for rapid engulfment by phagocytes and subsequent recycling of their cellular constituents.[46] One of the most distinctive features of apoptosis is condensation of the nucleus and its fragmentation into smaller pieces. Indeed, in the absence of a specific molecular target, early studies identified apoptotic cells using this characteristic.[47-49]

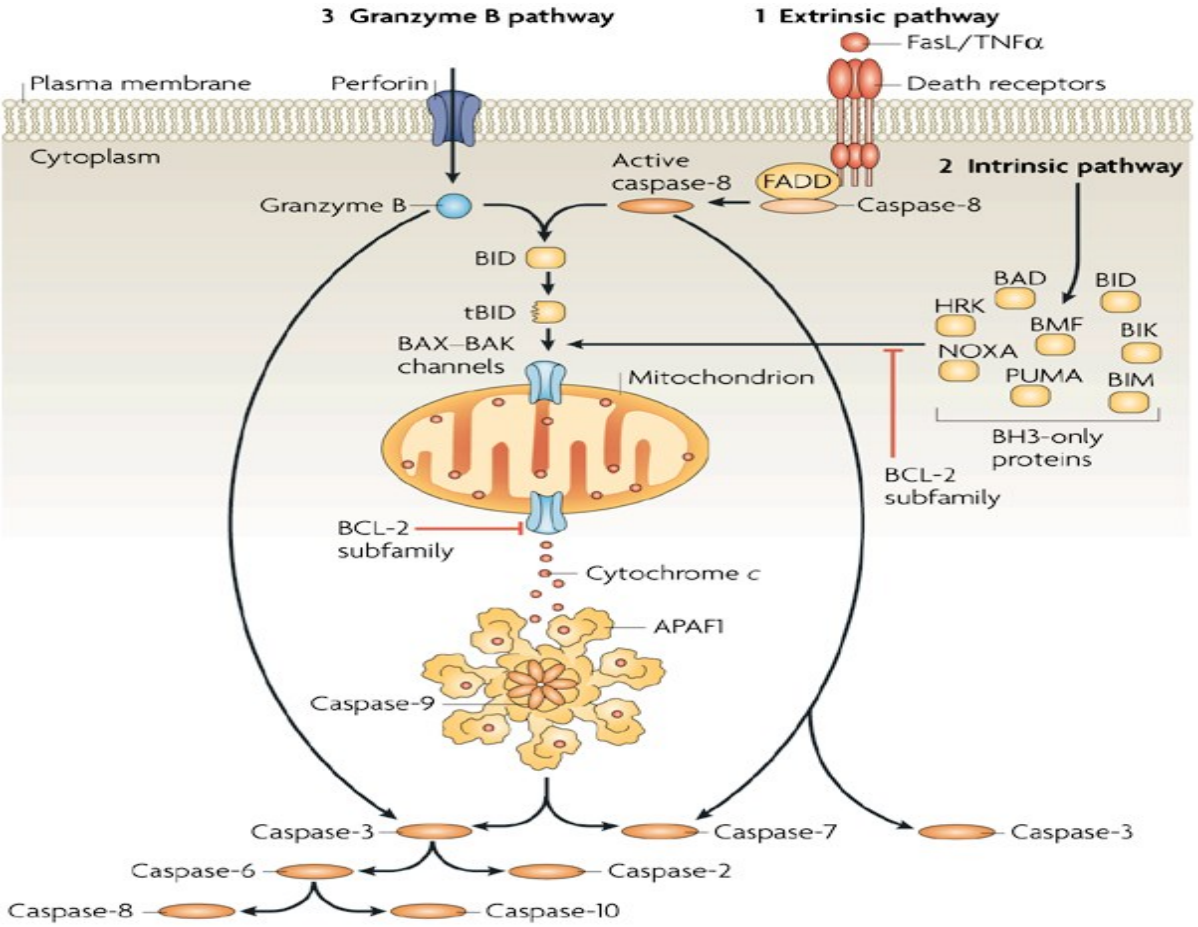


Figure 1.4: Caspase activation pathways, initiating of apoptosis. Image taken from Taylor *et al*.[46]

The evasion of apoptosis is one of the six hallmarks of cancer and the induction of cell death is thought to be an essential part of the successful treatment of tumours.[50] It is generally believed that molecular imaging will enable the implementation of personalised treatment, rapid assessment to therapy and optimisation of treatment strategies in real time. Early imaging of apoptosis used the radiolabelled protein, Annexin-V[51] and more recently, the Aposense family of molecules have been developed for apoptotic PET imaging.[52-55] Both Annexin-V and the Aposense tracers target the apoptotic cell membranes. Of late, inhibitors targeting the caspase enzymes in the early stages of apoptosis have received much attention.[56-58] These 3 classes of apoptotic imaging agents are described in the following sections.

I.3.1. Imaging Phosphatidylserine (PS) Reorganisation using Annexin-V

The terminal stage in the apoptotic cascade is phagocytosis, the consumption of the dead cells by phagocytes.[46] Phagocytes recognise and coordinate to specific sites on the cell membrane of the dead cells. Phosphatidylserine (PS) which is the most characterised phagocytic ligand is confined to the inner cell membrane in healthy cells, but is externalised to the outer membrane in response to pro-apoptotic stimuli where it serves as a signal for cell ingestion by phagocytes without inflammation.[59, 60] This translocation of PS has been exploited in the molecular imaging of apoptosis.[46]

Annexin-V, a 36 kDa human protein which undergoes Ca^{2+} dependent binding to negatively charged phospholipid surfaces, was initially discovered as an anticoagulant protein, where the anticoagulant mechanism is based on the protein's high affinity for PS.[61] Blankenberg *et al.* first demonstrated the feasibility of SPECT imaging of apoptosis in tumours using ^{99m}Tc-labelled Annexin-V.[51] Though ^{99m}Tc-Annexin-V was able to predict tumour response in cancer patients, the target-to-background ratio was low as a result of high uptake in the liver and kidneys and comparatively low uptake in tumours. The strong affinity of Annexin-V for the intact renal cortex has been attributed to the high concentration of PS in the kidneys.[51] Annexin-V binding also occurs non-specifically during necrosis, a process also characterised by PS exposure.[51] In contrast to apoptosis, necrosis is accompanied by the release of cellular contents into the extracellular space, triggering an inflammatory response.[46] But similarly to apoptosis, necrosis is characterised by rapid loss of membrane integrity and the externalisation of PS. This has implications in the molecular imaging of apoptosis using PS as a biomarker. The use of Annexin-V is also limited by relatively slow clearance from non-targeted tissues, attributed to its large protein structure.[62] As a result, Annexin-V probes are not considered optimal for apoptotic imaging.

I.3.2. Imaging Apoptotic Cell Membranes using the Aposense Family

Aposense is a family of low molecular weight amphipathic molecular probes that detect and accumulate within cells undergoing apoptosis.[52-55] This class of probes recognise the apoptotic cell membrane and undergo a process that enables them to cross the membrane and accumulate within the cytoplasm in the early stages of the cell death process. Studies have shown that the uptake of these probes correlates with Annexin-V binding, loss of mitochondrial membrane potential and caspase activation, which are all associated with apoptosis.[55] The Aposense probes are particularly

notable for their excellent clearance profiles and favourable biodistribution. Intracellular accumulation, as opposed to Annexin-V binding to the cell surface, means that Aposense probes can potentially exhibit increased signal-to-noise ratio.

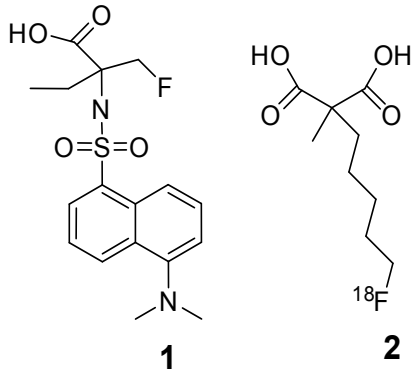


Figure 1.5: Members of the Aposense family of apoptotic probes

A member of the Aposense family, the dansyl derivative **1** (Figure **1.5**), comprising of a fluorophore and a fluorine atom was developed for both fluorescence and potential PET imaging using ^{18}F.[55] *In vitro* fluorescence imaging has shown the irreversible, selective and rapid accumulation of dansyl **1** in various cell types undergoing apoptosis. Similar results were also observed in *in vivo* studies of tumour models. In subsequent studies, ^{18}F-labelled 5-fluoropentyl-2-methyl-malonic acid **2** (Figure **1.5**), was designed as a radiotracer for the clinical evaluation of apoptosis by PET imaging. This probe was also found to selectively accumulate in apoptotic but not in necrotic cells, demonstrating utility for selective imaging of tumour-induced apoptosis.[52, 53, 63] However, the biomarker targeting mechanism of the Aposense family of radiotracers is yet to be fully defined; though it is believed that the amphipathic tracers function through the electrostatic attraction of their anionic carboxylate 'head' groups to the positively charged PS residues on the surface of the apoptotic cells, followed by the attachment of their lipophilic 'tail' inside the phospholipid cell membrane.[52]

The radiolabelled malonic acid species **2** has proceeded to clinical trials with phase 1 completed in healthy volunteers and phase 2 reportedly underway. Results of the phase 1 clinical trials showed favourable attributes for a PET apoptotic tracer including, favourable dosimetry, biodistribution, stability and safety profile, encouraging further development of the Aposense probe for the clinical PET imaging of apoptosis.[64] However, further studies are required to elucidate the cell

membrane target of the amphipathic probes and the exact mechanism of translocation from the cell membrane to the cytoplasm.

I.3.3. Imaging Early Apoptotic Events by Targeting Caspase-3(7)

With regards to the initiation of apoptosis, numerous proteins are released from the mitochondrial intermembrane space. One of these proteins, cytochrome *c*, triggers the assembly of a caspase-activating complex called the apoptosome (Figure **1.4**). Many of the apoptotic events are then initiated as a result of caspase-mediated cleavage of substrate proteins. The caspases represent an exclusive intracellular target for the development of new apoptotic imaging agents. This class of cysteine-aspartyl proteases are receiving increasing attention as targets for therapeutic assessment and drug development, owing to their central role in mediating the initiation and propagation of the apoptotic cascade.[44, 45] Of the fourteen known human caspases, the functions of caspase-2 and caspases 11 to 14 are unclear. The remainder have been characterised and can be divided into 3 functional groups: i) caspases-1, 4, and 5 which are associated with inflammation, ii) the initiator caspases-8, 9 and 10 and, iii) the effector caspases-3, 6 and 7. The initiator caspases are activated at the top of the apoptotic signalling cascade and then proceed to activate the effector caspases. Three main routes have been proposed for the induction of apoptosis; an extrinsic or receptor mediated pathway, an intrinsic or mitochondrial pathway and the granzyme B pathway (Figure **1.4**).[46, 65] All three routes lead to the activation of the effector caspases-3, 6 and 7 which then carry out the proteolysis associated with the propagation of apoptosis.[46, 66-68] Studies have shown that the effector caspase-3 is particularly activated in virtually every model of apoptosis.[66] Thus, the ability to image caspase-3 activation non-invasively provides a unique tool for diagnosis and evaluation of therapeutic response via the apoptotic cascade. To realise this aim, radioligands based on small molecule inhibitors of caspase-3 (and the structurally similar caspase-7 enzyme) must be identified and demonstrated to be efficacious. The section that follows reviews the recent history in the development of radiotracers based on caspase-3(7) inhibitors.

Table 1.3: The effect of stereochemistry, pyrrolidine substituents and isatin *N*-alkylation on caspase-3 inhibition potency.[56, 69]

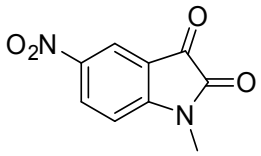
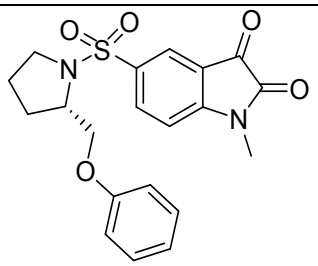
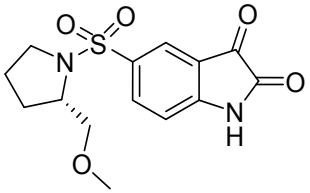
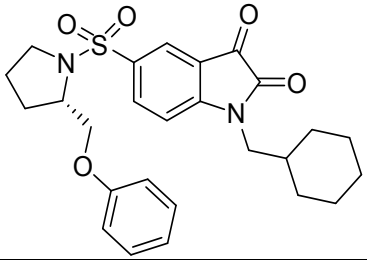
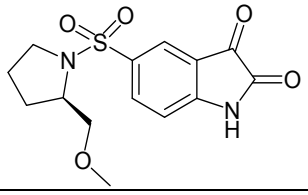
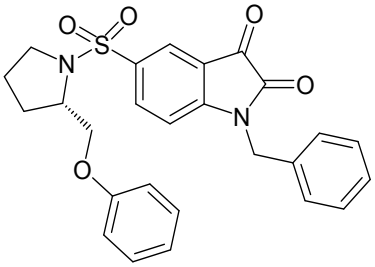
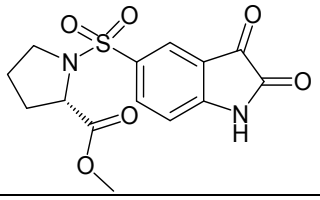
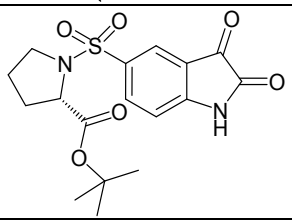
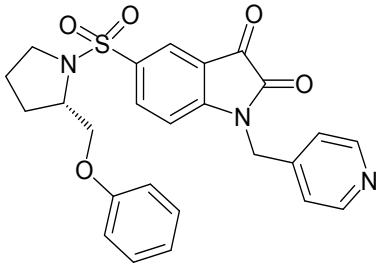
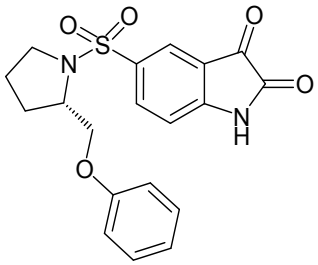
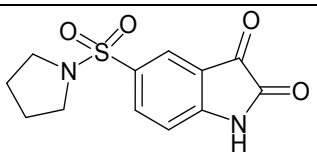
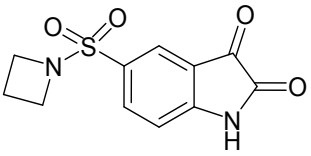
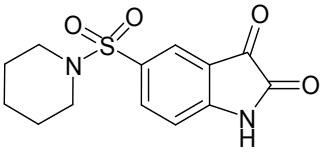
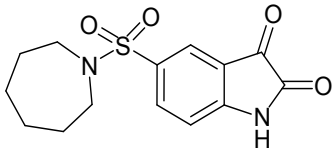
Pyrrolidine ring substitution			**Isatin N-alkylation**		
No.	Structure	Casp-3 IC_{50} (nM)	No.	Structure	Casp-3 IC_{50} (nM)
3	 (Initial hit)	1000	**9**		30
4		120	**10**		5.2
5		18000	**11**		2.5
6		170			
7		70	**12**		4.2
8		44			

Table 1.4: The importance of ring size on casp-3 potency[56]

No.	Structure	Casp-3 IC_{50} (nM)
13		170
14		2800
15		2200
16		1900

I.4. Design and Development of Radiotracers Targeting Caspase-3/7

Peptide-based compounds were amongst the first compounds reported to be potent inhibitors of caspase-3.[70, 71] However, these compounds were found to possess poor cell permeability due to their high polarity, preventing *in vivo* applications. The peptidyl inhibitors were also shown to be moderately selective with poor metabolic stability. To overcome this problem, much effort has been devoted to developing non-peptidyl, small molecule inhibitors. Several classes of caspase-3/7 inhibitors have been reported including, the pyrroloquinoline-1,3-diones series,[72] isatin Michael acceptors (IMA) and isatin sulfonamides.[73] The isatin sulfonamide series have been extensively studied due to their high potency and selectivity for caspase-3/7.

I.4.1. Isatin Sulfonamides as Potent and Selective Inhibitors of Caspase-3/7: SAR

Following high throughput screening aimed at discovering caspase-3 inhibitors, Lee *et al*. identified the hit, 5-nitroisatin **3** (Table **1.3**) as a caspase-3/7 inhibitor.[56, 69] With the goal of optimising the initial hit, in order to avoid the metabolic liabilities of nitro aromatics, and integrate a chemical functionality with appropriate electronic properties that would also allow the incorporation of

molecular diversity, a variety of derivatives were evaluated. This resulted in the identification of 5-*N,N*-dialkylisatin sulfonamides as caspase-3 inhibitors (Table **1.3**).[56] The isatin sulfonamides also possessed much improved selectivity for caspase-3/7 inhibition compared to nitroisatin **3**. Initial studies demonstrated the importance of stereochemistry on the *5-N,N*-dialkylisatin sulfonamides, where the *S*-configuration at the chiral pyrrolidine or azetidine carbon atom was crucial for potency (Table **1.3**, isatin **4** and **5**).[56, 72]

During the initial hit optimisation, Lee *et al*. found that increasing the ring size from 5 to 7 or replacing the pyrrolidine ring with an azetidine led to decreased potency for caspase-3 (Table **1.4**, isatins **13 - 16**). The increase in potency from isatin **6** to **8** (Table **1.3**), as the pyrrolidine ring is substituted with larger alkyl/aryl groups, suggested hydrophobic binding interactions in the enzyme active site. Similarly, alkylating the isatin nitrogen with larger hydrophobic groups led to further increase in inhibitory activity, though polar moieties could also be accommodated as shown by the retained potency of the 4-pyridlymethyl derivative (Table **1.3** isatins **9 - 12)**. Introduction of a phenyl group on both the left side ether and the isatin nitrogen resulted in a dramatic increase in potency, giving the isatin sulfonamide **11** as the lead compound.

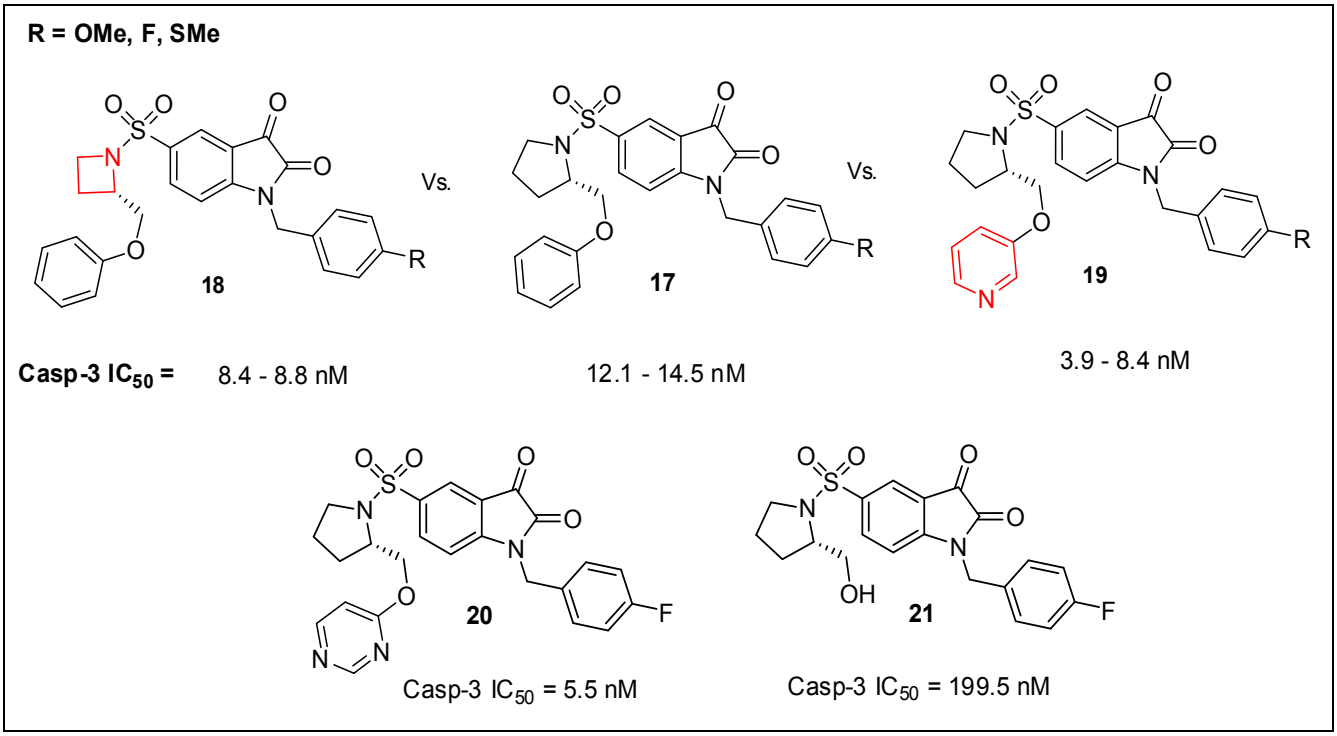


Figure 1.6: Similar potencies were reported for the pyrrolidine analogues **17** and their azetidine equivalents **18**, but replacing the phenyl ring with a pyridine **19** or a pyrimidinyl ring **20** resulted in higher potencies. The unalkylated prolinol derivative **21** showed the importance of the left side ether for caspase-3 inhibition potency.[57, 73]

In subsequent studies by Chu *et al.*, aimed at optimising the lead compound **11**, the group showed that para substituents on the *N*-benzyl had no appreciable effect on caspase-3 inhibition potency (Figure **1.6**, isatin series **17**).[73] This correlated with the earlier observations by Lee *et al.*, regarding the alkylation of the isatin nitrogen with hydrophobic groups (Table **1.3**). That is, both sets of SAR studies suggested that hydrophobic groups are preferred to the N1-Me or the unalkylated isatin-N1. However, there was no strong preference between different hydrophobic groups. This was accounted for using molecular field maps (Figure **1.8**)[74] of isatin sulfonamide binding interactions with caspase-3. The molecular field maps denoted the binding pocket around the isatin nitrogen as hydrophobic, where both aliphatic and aromatic rings at the isatin N-1 would create desirable close contacts with amino acid residues in the active site (Figures **1.7**).

Chu *et al.* reported similar potencies between the pyrrolidine analogues **17** and their azetidine equivalents **18** (Figure **1.6**), despite the difference in potency reported by Lee *et al.* for compounds **13** and **14** (Table **1.4**).[73] Interestingly, replacing the benzene ring of the 2-(phenoxymethyl) pyrrolidine with a pyridine ring resulted in higher potencies (Figure **1.6**, isatin **19**). In further SAR studies by Smith *et al*., it was found that, similarly to the results reported by Chu *et al.*, increases in potency was observed when the benzene ring of the 2-(phenoxymethyl)pyrrolidine was replaced with polar moieties bearing H-bond acceptors such as, a pyrimidinyl ring (Figure **1.6**, isatin **20**).[57] In addition, the isatin sulfonamide **21** demonstrated the importance of the left side ether in bonding interactions with the enzyme (Figure **1.6**).

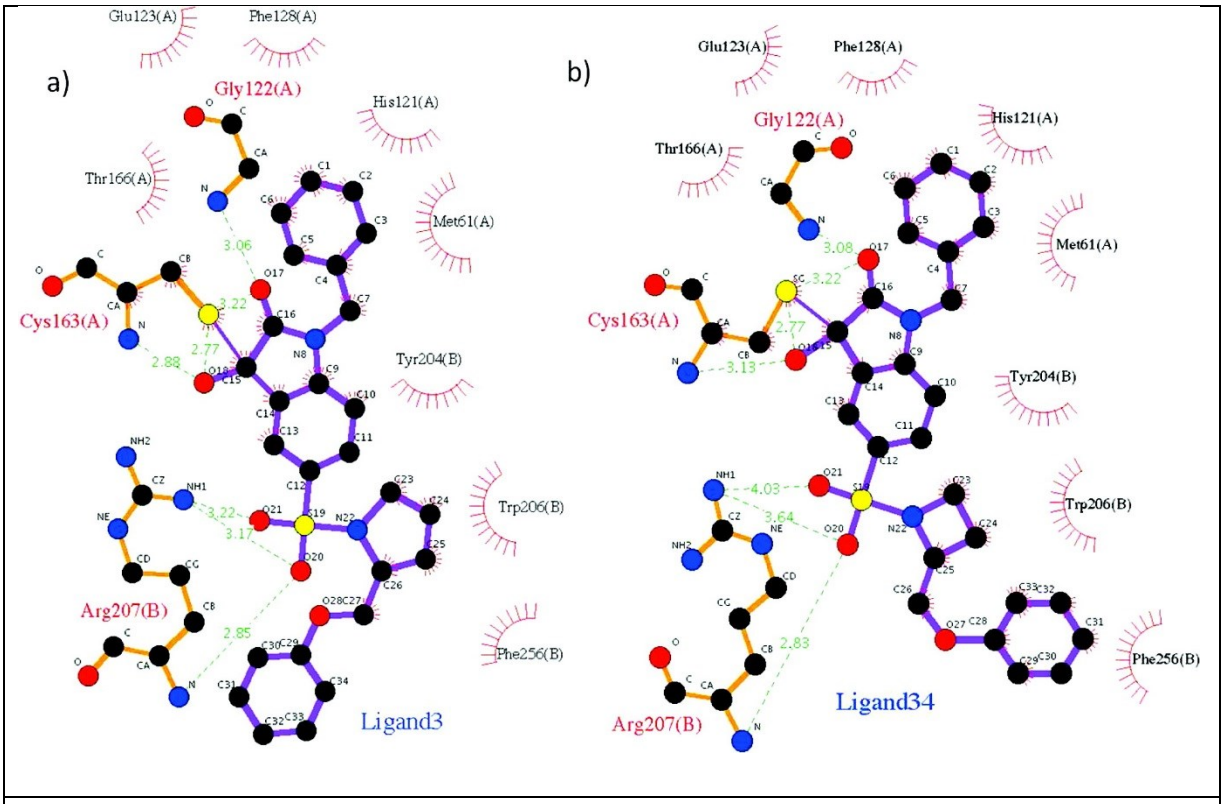


Figure 1.7: Binding interactions of **a)** isatin sulfonamide analogue **11** (ligand 3 in the image), and **b)** its azetidine equivalent (ligand 34 in image). Figure taken from Wang *et al*.[74]

The basis of the SAR observations was revealed from sequence alignements[69] and docking studies.[74] It was found that the three hydrophobic residues (Tyr204, Trp206 and Phe256) in the S_2 pocket of caspase enzymes are unique to caspases-3 and 7.[69] A superimposition of 59 derivatives from the pyrrolidine (**17**) and azetidine (**18**) series showed that the isatin core and the flexible pyrrolidine or azetidine ring make extensive hydrophobic contacts with these residues in the S_2 pocket, thus conferring binding specificity to the isatin sulfonamides (Figure **1.7**).[74] In addition to the key π-π interactions in the S_2 pocket, the molecular field maps (Figure **1.8**) showed that groups containing hydrogen bond acceptors were accommodated due to the presence of Ser381 residue within hydrogen bonding distance of this region, as well as the partial exposure of this region to solvent.[73, 74] This accounted for the retained or increased potencies of inhibitors where the benzene ring of the phenoxymethyl moiety was replaced with a heteroaromatic ring such as a pyridine or pyrimidyl ring (Figure **1.6**, isatins **19** and **20**).[56, 57, 73]

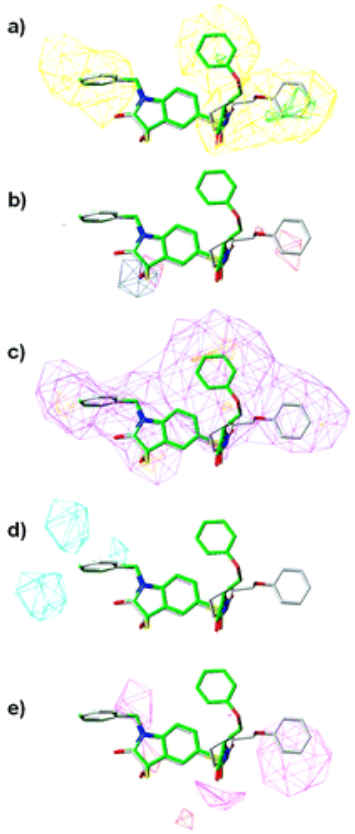


Figure 1.8: Molecular field maps derived from a model with isatin **11** and its azetidine equivalent; **a)** steric map, **b)** electrostatic map, **c)** hydrophobic map, **d)** hydrogen bond donor map, **e)** hydrogen bond acceptor map. Figure taken from Wang *et al*.[74]

Aside from the hydrophobic interactions at the S_2 subsite, the essential binding modes also include, electrostatic interactions formed between the sulfonamide group and Arg207 backbone amide or its guanidino group (Figures **1.7**, **1.8**). Importantly, an X-ray co-crystal structure of a complex between caspase-3 and isatin sulfonamide **9** revealed a binding model involving the reversible addition of an active site cysteine residue to the isatin C-3 carbonyl carbon, forming a tetrahedral thiohemiketal intermediate.[69] Thus, it was expected that isatin sulfonamides would distribute reversibly into cells but would only be trapped specifically within cells with active caspase-3/7. The inhibitor-enzyme covalent bond formation consequently inhibits caspases-3/7.

X-ray crystallography has also shown that the substrate preferences for caspase-3 and 7 are identical, since they are structurally and functionally very similar.[75, 76] These two caspases differ only in the composition of their S_4 subsite where the chemical content of caspase-3 is predominantly hydrophobic while caspase-7 is more hydrophilic.[76] Hence, selectivity between caspases-3 and 7 may be obtainable by designing inhibitors with extended binding in the S_4 subsite. However, given that

both caspase-3 and 7 are effector caspases with similar roles in the propagation of the apoptotic cascade,[44, 45] the simultaneous inhibition of the two caspases has not been shown to be problematic.

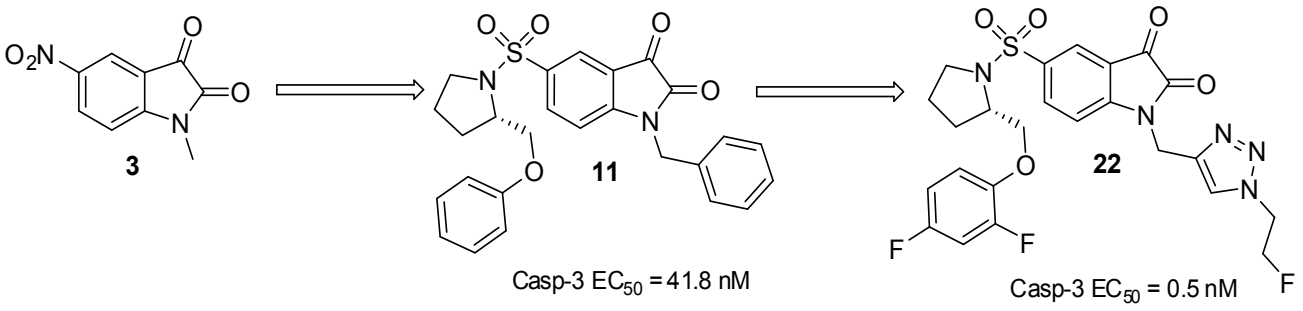


Figure 1.9: From the initial hit **3**[56, 69] to lead structure **11**[73] and the current lead **22**[57]

SAR studies by different groups in the past decade led to the current lead caspase-3 inhibitor, isatin sulfonamide **22** (Figure **1.9**).[57] The studies established isatin sulfonamides as potent and selective inhibitors of caspase-3/7. Although a good correlation was found between the cell-based and the *in vitro* caspase-3 activities of the compounds, a significant shift in activity was observed when comparing *in vitro* activities to the corresponding potencies in intact cells.[57, 69, 77] The observed activity shift has been attributed to non-specific inhibitor interactions with nucleophilic moieties in the cytosol.[56, 69] Studies are ongoing to optimise the specific binding properties of the isatin sulfonamides with progression of lead compounds to radiolabelling and *in vivo* PET imaging in animal models.

I.4.2. Development of Radiolabelled Isatin Sulfonamides

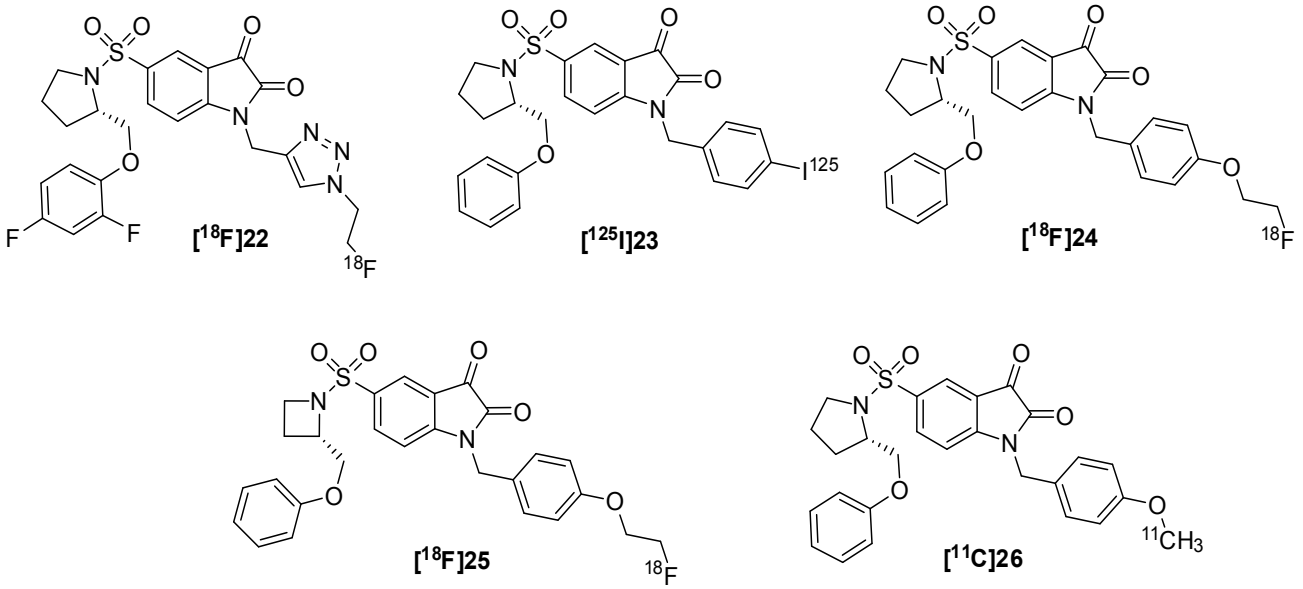


Figure 1.10: Developed Caspase Binding Isatin Radioligands.[57, 78, 79]

Following the establishment of isatin sulfonamides as putative inhibitors of caspase-3/7, Kopka *et al*. proposed these inhibitors as caspase binding radioligands (CBRs) for the *in vivo* imaging of apoptosis.[77] The group synthesised a number of isatin sulfonamide precursors for radiolabelling, incorporating structural modifications at the N-1 position which was proven to tolerate a wide range of chemical groups without the loss of caspase-3/7 inhibition potency.[56, 73] The suitability of the isatin sulfonamides for development as CBRs commenced with the radiosynthesis of the first isatin radiotracer [^{125}I]**23** (Figure **1.10**) for SPECT imaging.[77] However, in later studies by Smith *et al*., this radioligand was reported to have poor biological stability, attributed to a rapid *in vivo* aromatic hydroxylation of the phenyl ether, with the possibility of the majority of the detected radioactivity originating from the metabolic product.[57]

Taking advantage of the metabolic-blocking effect of electron-withdrawing fluorine substituents and the metabolic stability of 1,2,3-triazole groups, Smith *et al*. designed a library of isatin sulfonamides incorporating the triazole heterocycle and fluorine substituted aromatic groups.[57] The lead compound, [^{18}F]**22** was subsequently selected on the basis of subnanomolar affinity for activated caspase-3, high selectivity for the target enzyme, moderate lipophilicity and high metabolic stability with no evidence of *in vivo* defluorination. Isatin sulfonamide **22** was demonstrated to bind to a range of drug-induced apoptotic cancer cells *in vitro* and *in vivo*, by up to 2-fold and as early as 24 hrs post-treatment, compared to control treatment.[57] Whole body *in vivo*

microPET in mice detected an increased signal intensity in tumours after drug treatment which was associated with drug-induced apoptosis and caspase-3 activation (Figure **1.11**).[57]

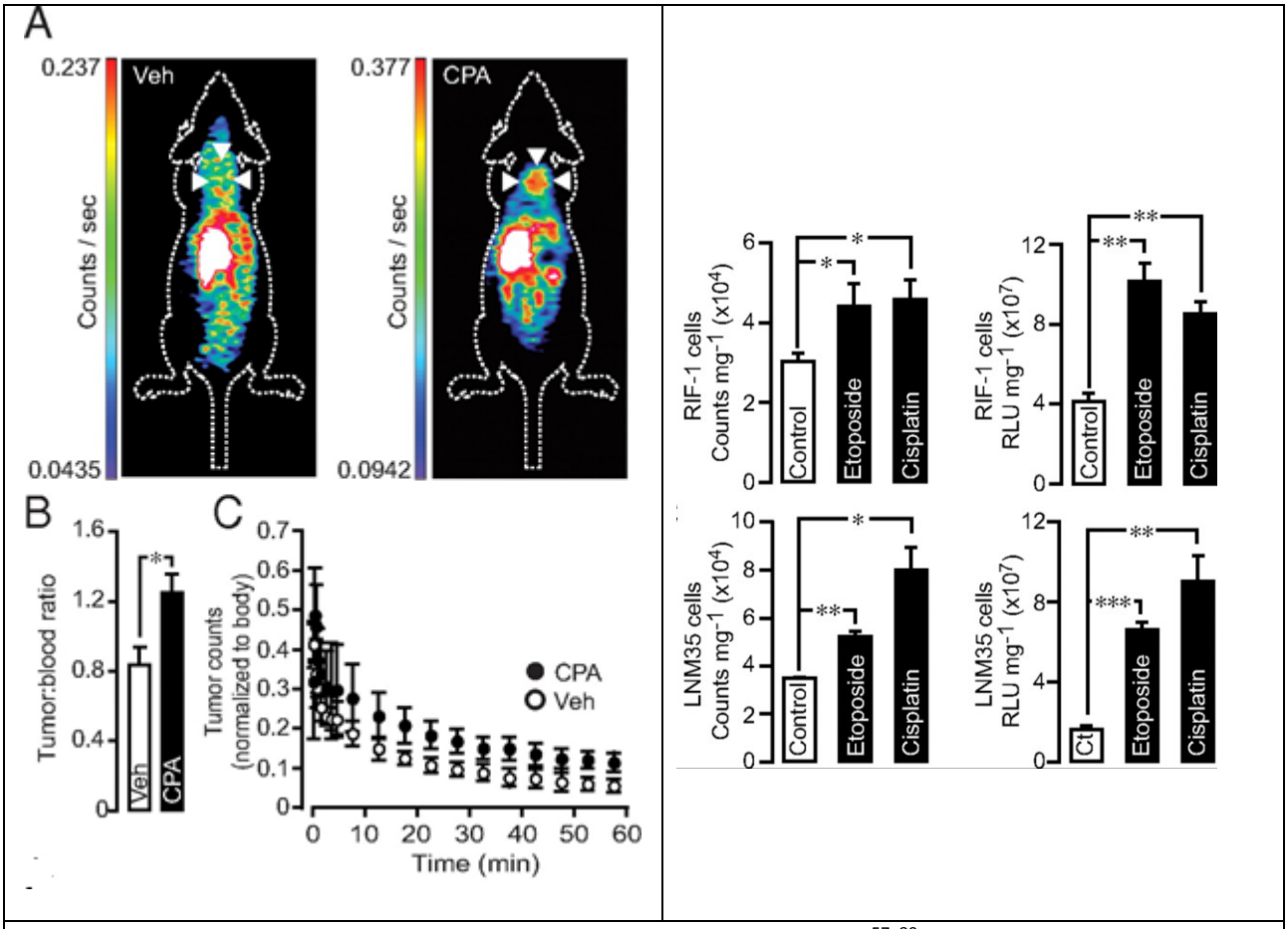


Figure 1.11: Figure taken from Smith *et al*.[57, 80]

[^{18}F]**22** PET imaging analysis. 38C13 xenografts bearing mice were treated with 100 mg/kg cyclophosphamide CPA (*n* = 3) or vehicle (*n* = 3) for 24 hrs and subsequently subjected to 60 min dynamic PET imaging. **(*a*)** [^{18}F]**22** PET images of CPA-treated, 38C13 xenograft bearing mice and the vehicle/control mice. White arrowheads indicate the tumour position. **(*b*)** [^{18}F]**22** tissue uptake in tumour and blood samples removed after PET scan. **(*c*)** The tumour time versus radioactivity curve (TAC).	[^{18}F]**22** binding and active caspase-3/7 content analysis in cancer cells undergoing drug-induced apoptosis. Left panel: the effect of cisplatin (100 µM; 24 hrs) or etoposide (100 µM; 24 hrs) treatment on [^{18}F]**22** uptake. Right panel: caspase-3/7 activity in RIF-1 fibrosarcoma and LNM35 lung carcinoma cells, correlating with [^{18}F]**22** uptake and showing that radiotracer uptake was due to caspase-3 activation. For each set of treated and control samples, radioactivity data was expressed as decay-corrected counts per milligram of total cellular protein.

The results obtained demonstrated [^{18}F]**22** as a caspase-3 targeted PET radiotracer with potential utility in the evaluation of oncologic therapeutic response.[57] Notably however, low baseline uptake of [^{18}F]**22** in tumours was observed. PET images also showed a high retention of the radiotracer in the liver and intestines. Thus, the use of an anatomical imaging modality such as MRI

for the localisation of the tumour may be necessary in the translation of this tracer into clinical practice, with limited application in the abdominal region.

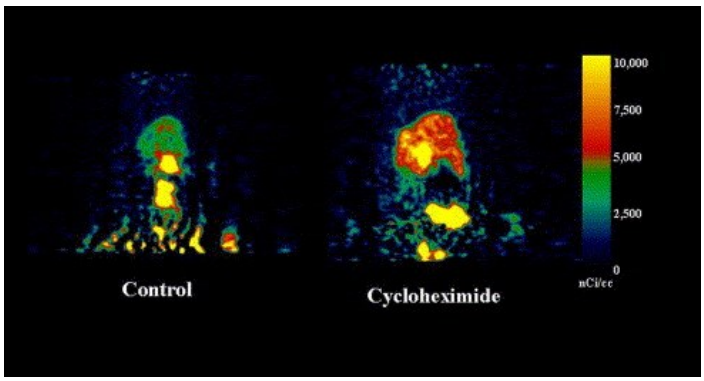


Figure 1.12: Whole-body microPET image of [^{18}F]**24** distribution in a control rat (left) and cycloheximide-treated rat (right). Images summed from 10 to 60 mins after intravenous injection of ~150 μCi [^{18}F]**24**. Figure taken from Zhou *et al*.[78]

Table 1.5: Inhibitor profile of the leading caspase-binding isatin radioligands

Compound	Casp-1 (nM)	Casp-3 (nM)	Casp-6 (nM)	Casp-7 (nM)	Casp-8 (nM)	Log P	Specific activity (mCi/μM)
[^{18}F]24[78]	>50000	9.7	3700	23.5	>50000	4.19	1500
[^{18}F]25[79]	>20000	8.6	4930	26.1	>25000	3.65	2280
[^{11}C]26[79]	>20000	14.5	10000	21.8	>2500	3.97	1400
[^{18}F]22[57]	>5000	0.5	>5000	2.2	>5000	1.61	32.34*
[^{18}F]22[81]	>5000	0.5	>5000	2.2	>5000	1.61	18513**

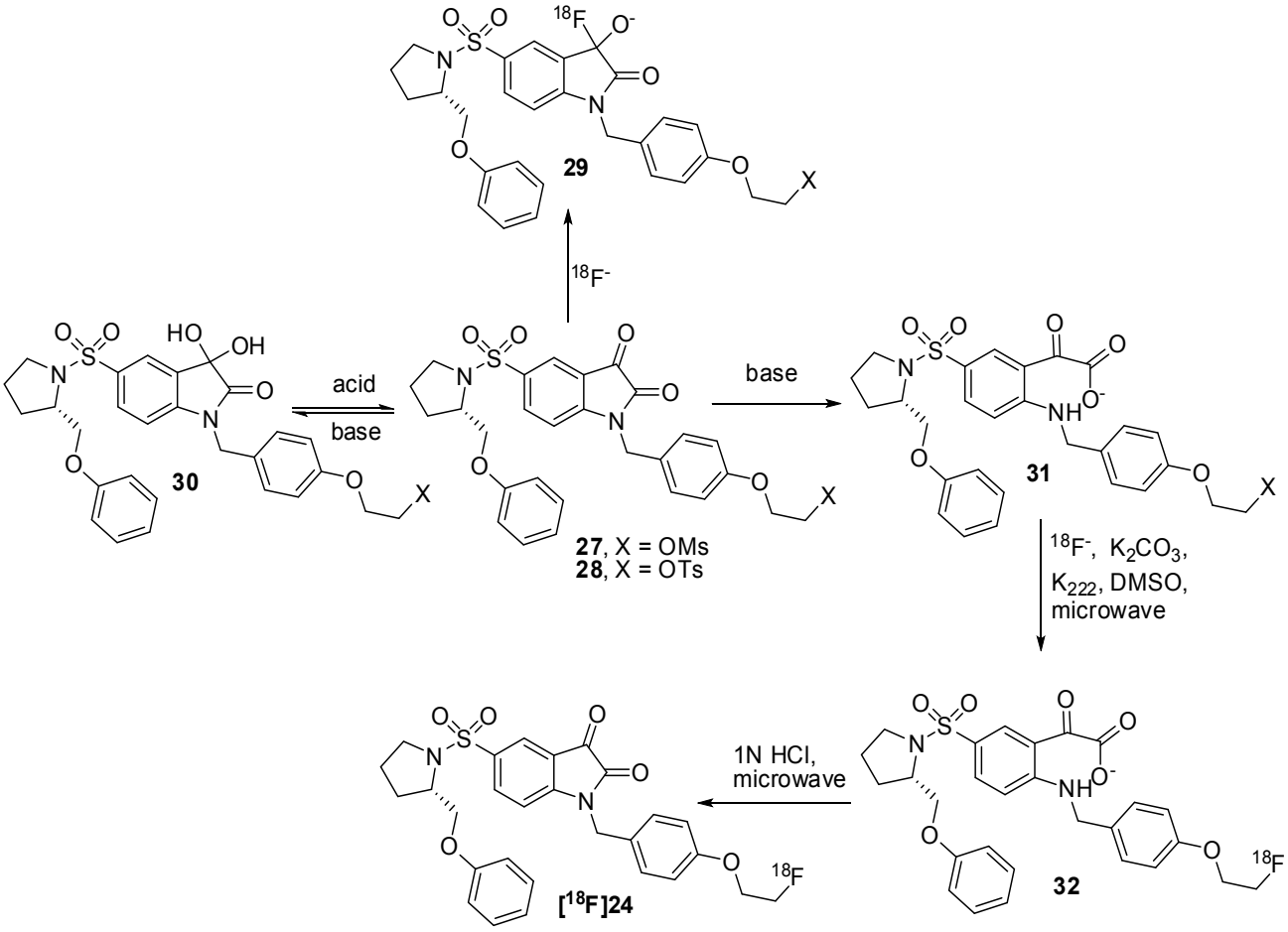
*Specific activity from click radiolabelled [^{18}F]**22**, calculated from the reported value of 1.2 GBq/μM
** Specific activity from the direct radiolabelling of [^{18}F]**22** by automated S_N2 [^{18}F]fluoride displacement of a tosylate precursor, calculated from the reported value of 685 GBq/μM

Zhou and Chu *et al.* also demonstrated the feasibility of apoptotic PET imaging using the radiolabelled isatin sulfonamides [^{18}F]**24**, [^{18}F]**25** and [^{11}C]**26** (Figure **1.10**, page 41).[78, 82] The inhibition potencies of these inhibitors are shown in Table **1.5** above. In all cases, results of microPET studies using a cycloheximide-induced liver model of apoptosis revealed an increased uptake of the inhibitor in treated versus control animals (Figure **1.12**), with slower washout of radioactivity from the liver and spleen in the treated animals. The levels of uptake were shown to be consistent with chemically induced apoptosis and caspase-3 activation. However, the liver model used in the microPET studies was limited by the induction of a high level of apoptosis which is not representative of the levels that are typically observed clinically. Similarly to [^{18}F]**22**, biodistribution studies of these tracers showed

the retention of inhibitor-derived radioactivity in the liver, attributed to a rapid hepatic clearance, therefore precluding the use of these tracers in the abdominal region.

Of the four caspase binding radioligands reported to date (Table **1.5**), [^{18}F]**22** incorporating 1,2,3-triazole and 2,4-difluorophenyl moieties is the most potent. However, the initial modest specific activity of 1.2 GBq/μM (32.4 mCi/μM),[57] though sufficient for initial evaluation, was not optimal for more complex *in vivo* models or clinical development. Thus, ongoing optimisation of the probe continues, with improved radiosynthesis to increase the specific activity as briefly described below.[81]

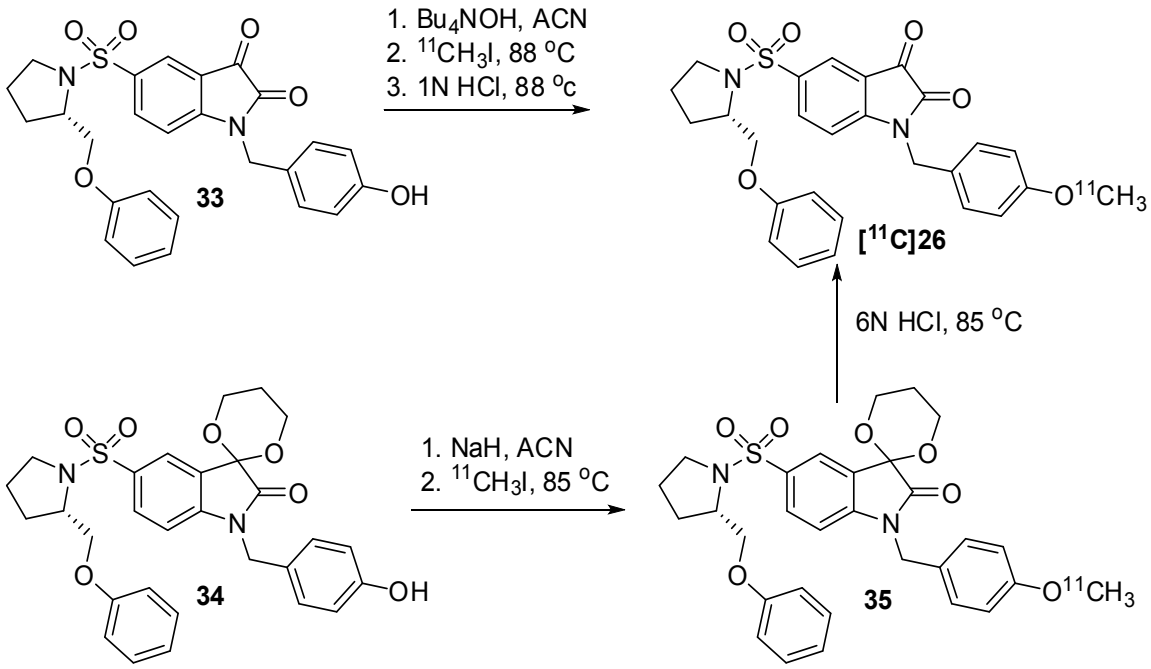
I.4.2.1. Radiochemistry of Caspase-3 PET Imaging Agents



Scheme 1.1: The process of ^{18}F-labelling by the displacement of a leaving group.[83]

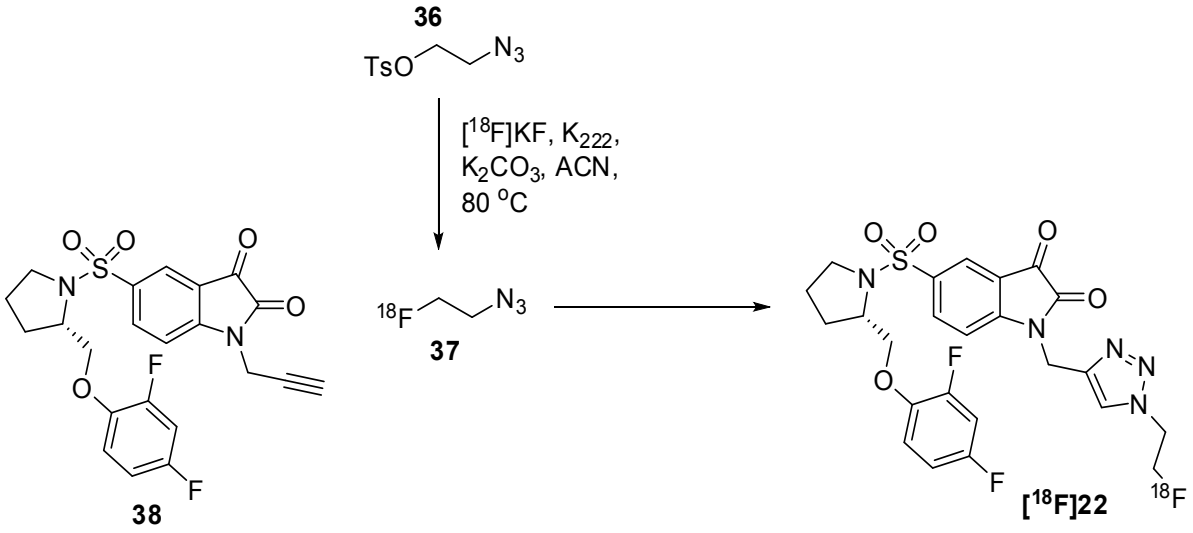
Research efforts have focused on utilising radiopharmaceuticals labelled with ^{18}F because, as discussed in section **I.2**, its properties make it ideal for clinical imaging purposes. It is worth

considering the essential radiolabelling methods employed in the radiosynthesis of caspase binding isatin radioligands. The reactive isatin ring has proven problematic for radiolabelling with [^{18}F]fluoride, owing to nucleophilic attack on the C-3 carbonyl carbon (Scheme **1.1**).[83, 84] It was found that attempts to radiolabel isatin sulfonamide derivatives by the displacement of a leaving group led the trapping of the [^{18}F]fluoride nucleophile by the C-3 carbonyl of the isatin scaffold, giving the species **29**, instead of the desired radiolabelled derivative [^{18}F]**24** (Scheme **1.1**).[83]



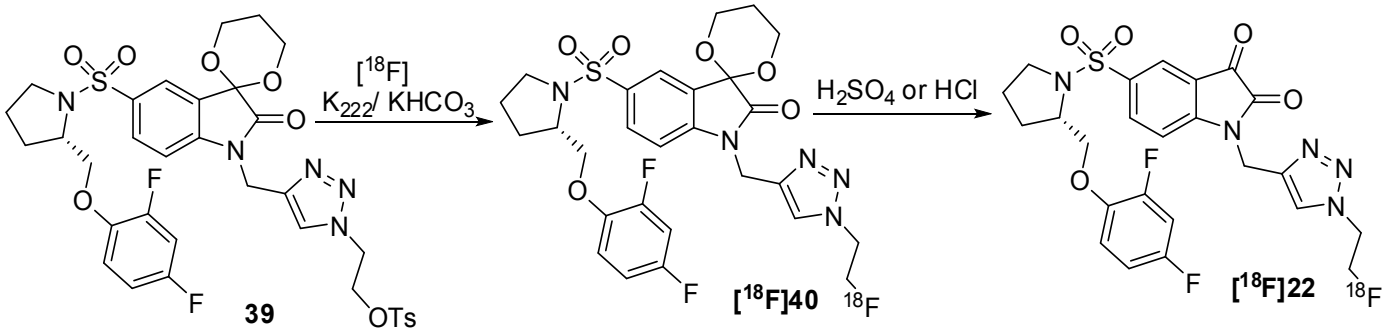
Scheme 1.2: ^{11}C-labelling of isatin sulfonamides.[83]

Zhou *et al*. subsequently demonstrated that the radiolabelling reaction proceeded efficiently via the acid-base ring opening/recyclisation procedure shown in Scheme **1.1**.[83] The precursor (**27/28**) was initially treated with a strong base (e.g. Bu$_4$NOH) which resulted in ring opening to give the intermediate **31**. [^{18}F]Fluoride could then undergo the intended nucleophilic substitution to displace the tosylate or mesylate leaving group of intermediate **31**, before converting the resulting radiolabeled product **32** to the desired radioligand, [^{18}F]**24** under acidic conditions (Scheme **1.1**). This ring-opening-reclosure method was also utilised in ^{11}C-labeling of isatin sulfonamides (Scheme **1.2**). An alternative route avoiding the trapping effect of the C-3 carbonyl involved protection of the ketone as a 1,3-dioxane, followed by radiolabelling under standard conditions and subsequent hydrolysis of the protecting group (Scheme **1.2**). Both reaction routes reportedly afforded the isatin probes [^{18}F]**24** and [^{11}C]**26** in high yields and high specific activities (Figure **1.10**, Table **1.5**).



Scheme 1.3: ^{18}F-labelling of isatin sulfonamide **22** by copper catalysed click chemistry.[57]

Isatin sulfonamides can also be radiolabelled via the copper catalysed cycloaddition of 2-[^{18}F]fluoroethylazide **37** to an alkyne precursor, commonly called 'click' radiolabelling (Scheme **1.3**).[57] This reaction can be carried out without the need for protecting groups with the procedure shown to be highly regioselective for the 1,4-disubstituted 1,2,3-triazoles.[85] However, the click reaction gave the radiolabelled lead isatin [^{18}F]**22**, in poor specific activity; Table **1.5** shows that the specific activity at the end of synthesis is lowest for the click-labelled [^{18}F]**22**. In successive studies, direct radiolabelling by the S_N2 displacement of a tosylate precursor with [^{18}F]fluoride, gave isatin [^{18}F]**22** in significantly increased specific activity (Scheme **1.4**).[81] An automated procedure for the S_N2 method has been developed and validated to clinically acceptable standards.[81] This improved specific activity combined with increased purity, synthesis time and automation have projected the radiotracer [^{18}F]**22** to the early stages of clinical development.[86]



Scheme 1.4: ^{18}F-labelling of isatin sulfonamide **22** by direct displacement of a tosylate leaving group.[81]

I.4.3. Pyrimidoindolones: A New Class of Caspase-3/7 Inhibitors

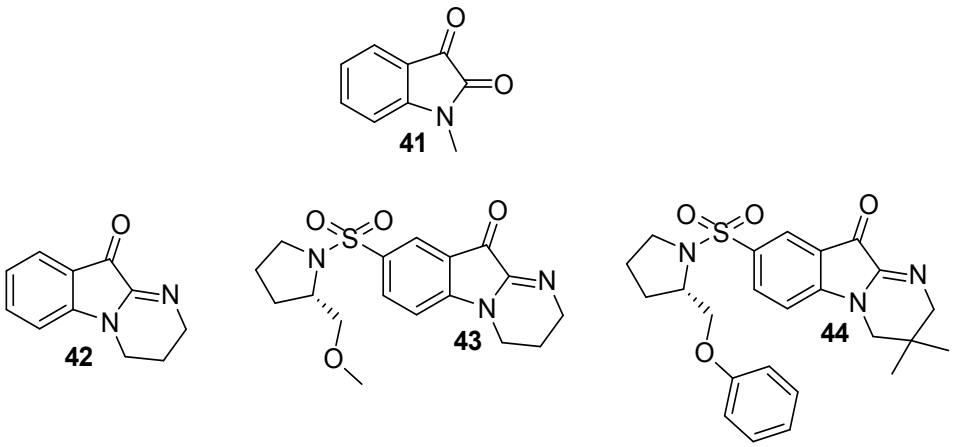
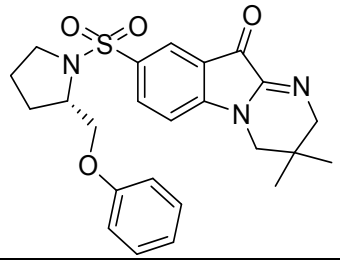
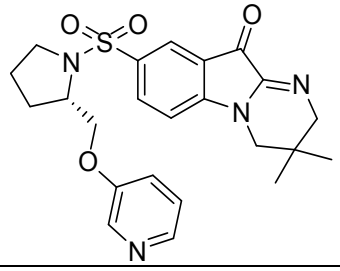
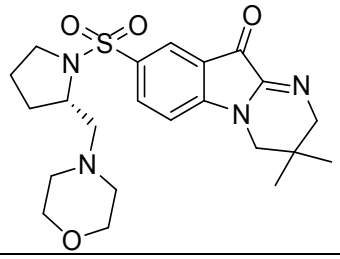
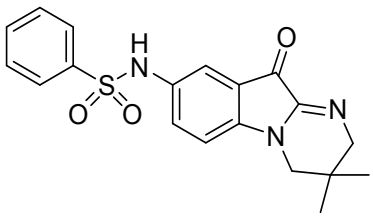
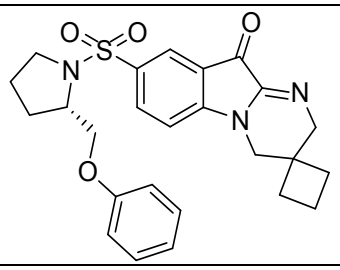
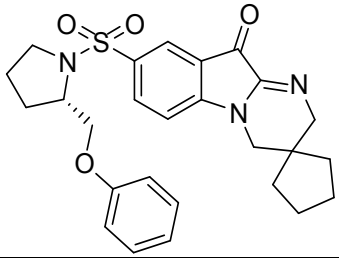


Figure 1.13: Core isatin heterocycle **41**, the pyrimidoindolone heterocycle **42** and the sulfonamide-substituted pyrimidoindolones **43** and **44**.[58]

While radioligands based on isatin sulfonamides were demonstrated to be sensitive and selective radiotracers of *in vivo* apoptosis, imaging results of the developed tracers, including the lead compound [^{18}F]**22**, have shown low target-to-background activities. For clinical imaging purposes, improvements in the signal-to-noise ratio is crucial. Hence, studies are ongoing to further optimise this class of inhibitors in clinically relevant models. Nevertheless, the structurally similar pyrimidoindolones have emerged as a new class of caspase-3/7 inhibitors.[58] Probes based on the pyrimidoindolone heterocycle have the potential to decrease non-specific *in vivo* binding activities, by modulating the reactivity of the ketone carbonyl responsible for caspase inhibition through the formation of a thiohemiketal in the enzyme active site (Figure **1.13**).

Active caspases have been shown to be homodimers with two identical active sites.[87] A recent study showed that isatin sulfonamides bind to a single domain of the enzyme, distorting the second active site and dramatically reducing the binding affinity to this site.[87] Enzyme activity is abolished upon binding of an isatin sulfonamide to only one active site of the caspase homodimer, resulting in half-site reactivity.[87] In contrast, the pyrimidoindolones (Figure **1.13**) have been shown to inhibit caspase-3 by binding to both active sites with equal affinity. Thus, the stoichiometry of inhibitor to dimeric caspase-3 is 1/1 and 0.5/1 for the pyrimidoindolones and the isatins respectively. However, consideration of the enthalpies, free energies and entropies of pyrimidoindolone and isatin binding to caspase-3 showed similar affinities for the two heterocycles, despite the different stoichiometries.[87]

Table 1.6: A selection of the pyrimidoindolone derivatives prepared by Havran *et al*.[58]

Compound No.	R	Caspase-3 IC_{50} (nM)	Solubility @ pH 7.4 (μg/mL)
44		7	11
45		2.40	>100
46		4.99	34
47		364	-
48		1.29	69*
49		2.32	89*

* % parent compound @ 24 hrs

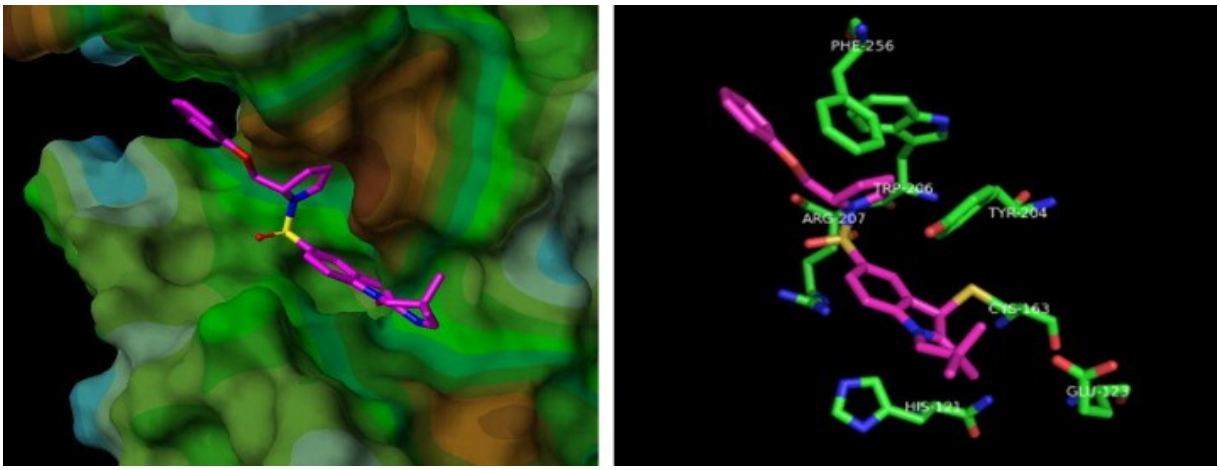
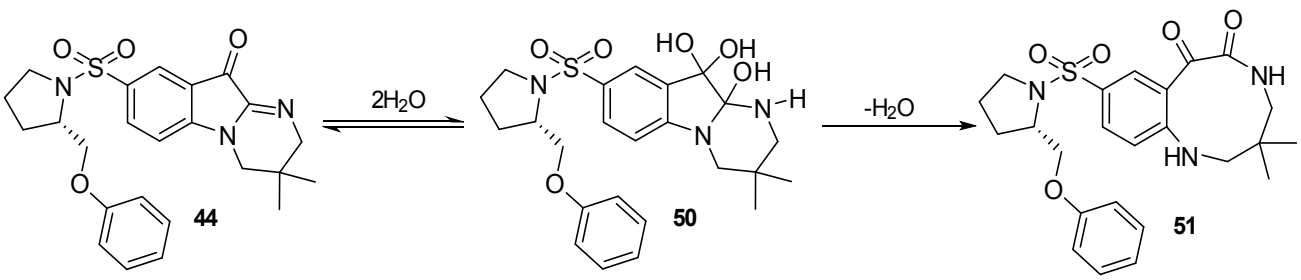


Figure 1.14: X-ray co-crystal structure of pyrimidoindolone **44** with human caspase-3 (left) and with the residues illustrated on the right, showing similar binding interactions observed with isatin sulfonamides. Figure taken from Havran *et al*.[58]

An X-ray co-crystal structure of caspase-3/inhibitor **44** (Figure **1.14**) revealed that the inhibition of caspase-3 involved the formation of a covalent bond between the electrophilic C-10 carbonyl and an active site cysteine residue. That is, similarly to the isatins, an electrophilic carbonyl carbon in the correct position is crucial for the inhibitory activity of the pyrimidoindolones. The initial SAR studies by Havran *et al*. revealed similarities with the isatin sulfonamides, showing analogous hydrophobic and hydrophilic binding interactions with caspase-3/7.[58] As with the isatin SAR studies, a 2-(phenoxymethyl)pyrrolidine substituent on the pyrimidoindolone heterocycle gave a potent inhibitor, but the replacement of the benzene ring with a pyridine ring further increased potency, with the added advantage of increased solubility (Table **1.6**, **44** vs. **45**).



Scheme 1.5: Reported hydration of the pyrimidoindolone scaffold leading to the formation of the 9-membered ring, **51** under standard aqueous conditions.[58]

Interestingly, studies showed a decrease in the potency of the pyrimidoindolones in aqueous solution over time.[58] Using NMR studies, this decrease was attributed to hydration of the parent inhibitor under neutral conditions (Scheme **1.5**). Addition of two molecules of water to the

pyrimidoindolone ring gave a dihydrate intermediate **50**, with subsequent expulsion of water and ring opening to give the nine-membered keto-amide **51** (Scheme **1.5**).[58] As trace amounts of a radiotracer are typically administered intravenously during imaging, the poor aqueous stability may prove problematic in potential clinical applications of this class of caspase-3/7 inhibitors. Nonetheless, hydration of the pyrimidoindolone scaffold was only significant after 24 hours, and since ^{18}F-PET imaging is typically performed on very short time scales, within the order of minutes, the limited aqueous stability may not preclude the use of pyrimidoindolones as apoptotic imaging agents.

Further biological evaluation using experimental models of apoptosis is required to assess the extent of this low aqueous stability. However, attempts have been made to improve such aqueous stability.[58] With the goal of improving solubility, Havran *et al*. investigated the effect of replacing the phenoxy ether moiety with simple amines. Morpholine proved to be the optimal amino substituent, retaining inhibitory activity but with no improvement on aqueous solubility (Table **1.6**, **46**). The reverse sulfonamides were subsequently proposed, aiming to improve stability by reducing the electrophilicity of the C-10 carbonyl group, minimising nucleophilic attack by water whilst retaining an ability to form a covalent bond with the active-site cysteine. Unfortunately, the reverse sulfonamides resulted in significantly decreased potency and poorer aqueous stability (Table **1.6**, **47**). Based on the group's earlier observation that compounds with an unsubstituted dihydropyrimido ring such as the 2-(methoxymethyl)pyrrolidine derivative **43** (Figure **1.13**) were extremely unstable in aqueous solution compared to ones incorporating a gem-dimethyl group in the 3-position, spiroannulated structures were proposed. The aim was to improve stability whilst avoiding the metabolic liabilities of the 'free' methyl groups. The spirocyclobutyl derivative proved to be very potent but without improved aqueous stability (Table **1.6**, **48**). In contrast, the spirocyclopentyl analogue (Table **1.6**, **49**) showed an improved stability profile whilst maintaining nanomolar affinity for caspase-3. The reason for this improved stability is not yet known. Nevertheless, the results of the SAR studies, in addition to the ability to improve aqueous stability demonstrated that the pyrimidoindolones could potentially find utility as radiotracers for the imaging of apoptosis.[58]

I.5. Proposed Research

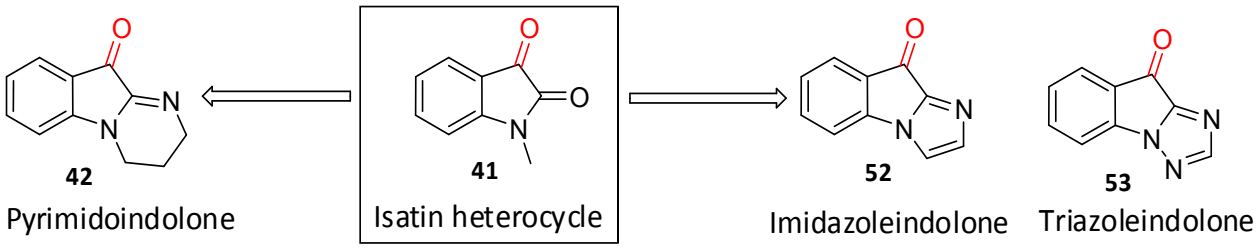


Figure 1.15: From the isatin radiotracer to pyrimidoindolone based caspase inhibitors and the newly proposed imidazoleindolone and triazoleindolone heterocycles.

Based on the observations that PET imaging using isatin sulfonamides is hampered by low target-to-background activities, we aimed to design and develop alternative heterocycles with the potential to increase the signal-to-noise ratio of apoptotic PET images through specific caspase-3 binding interactions. We were particularly interested in further investigating the pyrimidoindolone heterocycle as a caspase-binding radioligand. Although *in vitro* models had shown the pyrimidoindolones as relatively potent caspase-3 inhibitors,[58] there were no reported radiolabelled pyrimidoindolone-based radiotracers for the PET imaging of apoptosis. The selection of a potential pyrimidoindolone radiotracer for further studies was based on the hypothesis that:

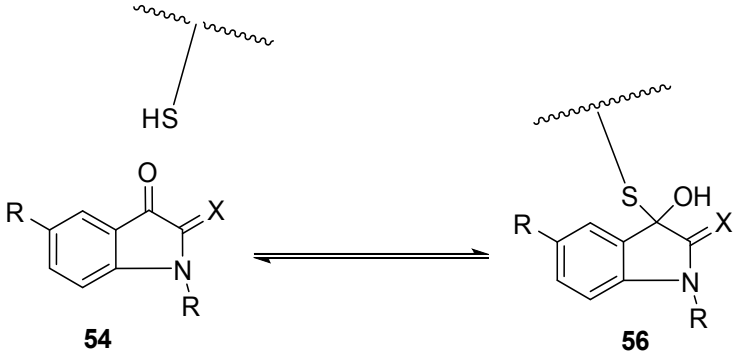
i) Their dual binding mode to the caspase-3 dimer compared to the half-site activity of the isatin sulfonamides[87] would provide greater scope for specific binding interactions and reduce *in vivo* background uptake of the radioligand and;

ii) The conversion of the isatin C-2 carbonyl to an amidine in the equivalent position of the pyrimidoindolone ring would modulate the electrophilicity of the ketone carbonyl, thereby minimising non-specific interactions with nucleophilic moieties (e.g. thiols) of cytosolic proteins (Figure **1.15**).

Our initial strategy therefore involved the preparation of a model pyrimidoindolone radiotracer for preliminary biological characterisation as a potential caspase-3 binding apoptotic PET probe. Chapter **III** covers the design, synthesis, radiolabelling and biological characterisation of the initial pyrimidoindolone radiotracer, with comparisons to the lead isatin sulfonamide **22**.

Given the problems reported with aqueous stability of the pyrimidoindolone scaffold,[58] a 'back-up' strategy was implemented, involving the exploration of novel heterocycles as potential caspase-3 inhibitors. The proposed heterocycles were based on the imidazoleindolone **52** and

triazoleindolone **53** heterocycles (Figure **1.15**). Both these heterocycles possess the crucial ketone carbonyl responsible for caspase inhibition. Similarly to the pyrimidoindolone, it was hoped that the replacement of the isatin C-2 carbonyl with an electron rich imidazole and triazole ring in the imidazoleindolone and triazoleindolone heterocycles respectively would favourably modify the ketone reactivity and thiohemiketal stability. To our knowledge, there were no reported information on the synthesis and biological properties of the imidazoleindolone and triazoleindolone heterocycles, unlike the previously described pyrimidoindolone heterocycle. Thus, initial research on these heterocycles focused on computational modelling in order to validate their potential as caspase inhibitors compared to the known isatin and pyrimidoindolone systems.



Scheme 1.6: Computational calculations of the favourability of thiohemiketal formation for all four heterocycles shown in Figure **1.15** are descried in Chapter **II**

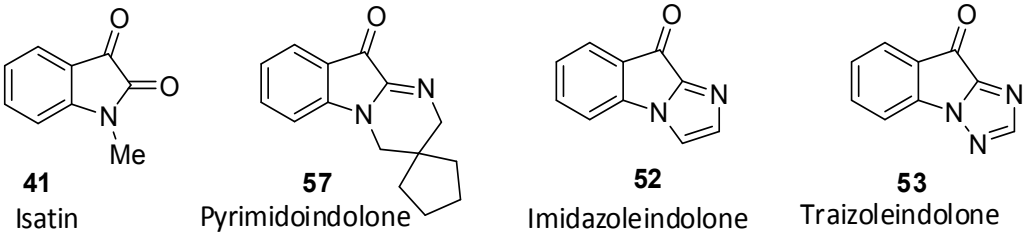
Chapter **II** describes the initial computational studies combined with UV-vis experimental titrations employed for modelling the relative thiohemiketal formation properties of the imidazoleindolone and triazoleindolone heterocycles, alongside the pyrimidoindolone and the isatin ring systems. The aim was to study the kinetics and thermodynamics of thiol addition to the ketone groups of the different heterocycles as an indication of their propensity to inhibit caspase-3. (Scheme **1.6**). Chapter **IV** details the design and synthesis of the initial imidazoleindolone and triazoleindolone target heterocycles.

CHAPTER II:

INITIAL COMPUTATIONAL MODELLING & UV-VIS TITRATIONS

II. INITIAL COMPUTATIONAL MODELLING & UV-VIS TITRATIONS

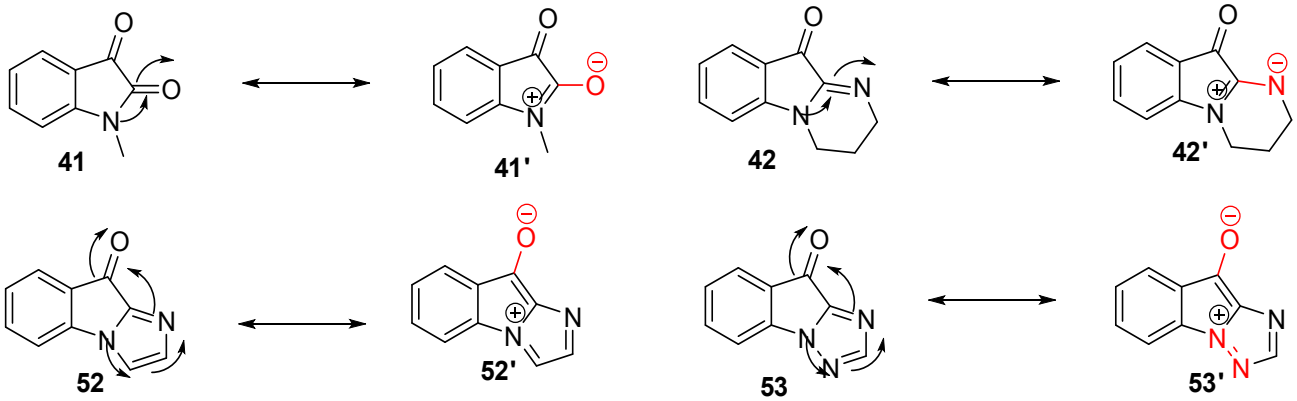
II.1 Introduction



Core heterocycles used for computational studies

Figure 2.1: The core isatin heterocycle **41** and the heterocycles under study as caspase-3 inhibitors

As discussed in Chapter **I**, the inhibition of caspase-3 stems from the formation of a covalent bond between the enzyme and the ketone carbonyl of a substrate, resulting in a tetrahedral thiohemiketal intermediate.[69] As a result of this inhibition mechanism, an electrophilic carbonyl carbon in the correct position is crucial for inhibitory activity. However, a highly electrophilic or reactive carbonyl may result in non-specific interactions with nucleophilic moieties in biological systems. Indeed, the isatin sulfonamides are suboptimal as caspase-3 binding apoptotic imaging probes due to poor signal-to-noise ratio of PET images, attributed to background interactions of the highly electrophilic isatin ketone (Chapter **I**).[57, 80]



Scheme 2.1: Electron density delocalisation of the isatin **41**, pyrimidoindolone **42**, imidazoleindolone **52** and triazoleindolone **53** heterocycles

Like the pyrimidoindolone **42**, the triazoleindolone **53** and imidazoleindolone **52** are structurally similar to the isatin heterocycle **41**, with all being aromatic heterocycles bearing the crucial ketone carbonyl in analogous positions. Scheme **2.1** shows that direct delocalisation onto the ketone carbonyl can occur with the imidazoleindolone and triazoleindolone heterocycles, but not

with the pyrimidoindolone and isatin structures. This is expected to impact on the overall reactivity of the ketone carbonyls. It was hoped that the presence of an imidazole and triazole rings in the imidazoleindolone and triazoleindolone heterocycles would give extended aromatic systems that would favourably modulate the ketone reactivity, limiting unwanted interactions with nucleophiles in the cytosol of biological systems.

II.2. Computational Analysis of the Heterocycles

Molecular properties and mechanisms involved in the biological actions of molecules are generally too complex to be described by a detailed computational model for the design of new biologically active compounds.[88] Nevertheless, by means of statistical treatment of a set of molecules, qualitative properties of molecular structures may be determined for various descriptors such as, octanol-water partition coefficient,[89] Van der Waals interactions,[90, 91] electronegativity/electropositivity, molecular dipole moment[92] and bond distances or connectivity.[93]

Unlike experimental measurements, there is no statistical error in quantum-chemical calculations but there are inherent accuracy issues associated with the derived assumptions required to facilitate the calculations.[94] In calculations of properties in a series of related compounds, the computational error is considered to be approximately constant throughout the series.[88, 94] Thus, relative values are calculated, which can be meaningful in revealing characteristic trends even though the absolute values may not be quantitatively correct.[88, 94]

Computational studies are considered of vast importance in modern drug design and have been successfully used to predict or account for correlations between structure and activity.[94] As such, computational calculations have been effectively used to predict hemiacetalisation equilibrium constants with clear correlations with experimental data.[95] To assess, and attempt to predict the potential potencies of the imidazoleindolone and triazoleindolone structures, as well as the pyrimidoindolone heterocycle in comparison to the isatin ring, computational studies were initially employed. That is, by using computational studies to analyse the relative favourability of thiol addition to the heterocycles' ketone groups, we aimed to deduce the likelihood of the heterocycles acting as effective caspase-3 inhibitors.

As shown in Figure **2.1**, the core heterocycles were used for the computational calculations as we aimed to examine the relative properties of the pharmacophores, excluding the added effects of substituents. The N-methyl substituted isatin **41** was chosen instead of the unsubstituted

equivalent in order to avoid any complexities of the amide tautomer. For the pyrimidoindolone heterocycle, the spirocyclopently substituted structure **57** was used as this was shown to be the ideal substituent in SAR studies conducted by Havran *et al*., with regards to aqueous stability (Chapter **I**).[58] As we intended to incorporate the spirocyclopently substituent in the initial radiolabelled pyrimidoindolone target to be synthesised for biological characterisation, we chose to also employ this substituent for computational studies, though it was not expected to have a major impact on the results obtained.

II.2.1. Computational Methods

Density Functional Theory (DFT) is employed as a quantum mechanical modelling method with which to investigate the electronic structure in realistic models of atoms, molecules and their surfaces.[96] DFT predicts a variety of molecular properties ranging from molecular structures, vibrational frequencies, atomisation energies to ionization energies, electric & magnetic properties and reaction pathways.[96] Specific DFT functionals are used when calculating the properties of many-electron systems, with the reliability of computational calculations depending on the functional chosen for the studies. There are various types of DFT functionals designed for use in various areas of computational chemistry calculations.[97] An extensive list of density functionals developed for calculations can be found in the cited review.[97] For the purpose of our calculation, two different functionals were employed:

a) **wB97xD** - a functional that includes dispersive non-covalent interactions, optimised for van der waals long-range corrected interactions for empirical atom–atom dispersion. This functional has been reported to be significantly superior for non-bonded interactions, with satisfactory performance for covalently bonded interactions.[98] This functional was therefore ideal for predicting transition state energies involved in thiohemiketal formation, where long range interactions, such as weak S…C and H…O bonds are important. Since this functional is used for predicting non-covalent as well as covalent interactions, it was expected to produce adequate results relating to the ground state energies of the reactants and products involved in the thiohemiketal formation.

b) **M062X** - a functional that considers charge transfer between bonds as well as thermochemistry properties.[97] As thermochemistry combines thermodynamics with bond energies in the calculation of quantities such as enthalpy, entropy and free energy, this

functional was expected to give an efficient model for the equilibrium constant of thiohemiketal formation derived from free energy calculations.

In computational chemistry calculations, functionals are combined with a relevant basis set. In the present study, calculations were performed using the wB97xD and M062X functionals with the commonly used **'6-31G (2d,2p)'** basis set, which adds the polarisability function of molecular orbitals including s, p and d orbitals, denoted by "(2d,2p)".[99-102] For 'heavy atoms' (defined as atoms heavier than hydrogen), up to 2 d orbitals are added, while up to 2 p orbitals are added for the hydrogen atom. In cases where transition metals are involved, 2 f orbitals are added to the basis set.[99-102]

In addition, all calculations were simulated in DMSO, employing the self-consistent reaction field method (SCRF)[103] to account for solute-solvent interactions, described in terms of a dipole moment.[104] Water was not used as the 'solvent' to avoid hydration and strong hydrogen-bonding effects interfering with results.

All calculations were performed with the Gaussian 09 software for the ground states of the molecules with values directly extracted from the Gaussian output file.[105]

II.2.2. Calculation of Ketone Partial Charges[a]

Using the 6-31G (2d,2p) basis set combined with the chosen functionals wB9xD and M062X, two types of partial charges were calculated for the heterocycles; the MK (Merz Kollman)[106, 107] and Mulliken[108] charges, which use electrostatic potential and normal electron population respectively. These are the two most commonly used methods for determining atomic charges.[109] While Mulliken analysis divides electronic population equally between the two atoms of a bond (the so called Mulliken population analysis) using linear combinations of atomic and molecular charges to determine partial charges,[108] the MK or electrostatic approach assigns point charges to atomic centres in order to best reproduce the electrostatic potential. [106, 107]

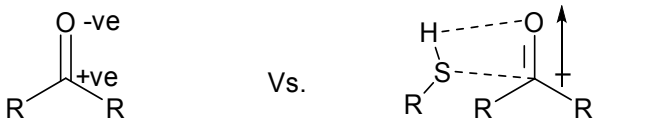
[a] Computational calculations of partial charges were carried out by the computational chemist, Alexandra Simperler, Imperial College London

Table 2.1: Calculated partial charges on the ketone carbon atom of the heterocycles

Heterocycle	wB97xD		M062X	
	MK Charges	Mulliken Charges	MK Charges	Mulliken Charges
Isatin **(a)**	+0.48	+0.26	+0.46	+0.29
Pyrimidoindolone **(b)**	+0.47	+0.27	+0.41	+0.30
Imidazoleindolone **(c)**	+0.51	+0.28	+0.49	+0.31
Triazoleindolone **(d)**	+0.52	+0.29	+0.51	+0.33

Results obtained from the computational calculation of the two types of partial charges are listed in Table **2.1**. In general, there were very little differences in partial charges across the four different heterocycles, with both sets of data for each functional in agreement. That is, MK charges obtained with wB97xD functional correlates in trend with those obtained with the M062X functional and the same goes for the Mulliken charges. However, the figures obtained for MK charges were generally larger than those obtained for Mulliken charges. The computational definition of atomic charge is arbitrary and typically do not correspond to direct experimentally measurable quantities.[94] In addition, the methods are mostly defined to reproduce heats of formation, ionization potentials, and/or geometric characteristics of molecules.[94] In spite of this, obtained numerical quantities can give at least a qualitative picture of the charge distribution in a molecule.[94, 110]

The ketone carbon partial charges for the different heterocycles suggested that, the electrophilicity of their ketone groups are similar and may therefore have a similar reactivity with thiol nucleophiles. From the small differences in the data obtained, it would appear that the partial charges of the triazoleindolone and the imidazoleindolone heterocycles are similar and slightly more electrophilic than the pyrimidoindolone and isatin heterocycles which are in turn also similar. Nonetheless, the Mulliken and MK partial charges only considered the charge distribution within the carbonyl bond of the heterocycles, in the absence of the thiol nucleophile and therefore did consider the effect of a dipole induced when the ketone is in close proximity with a thiol, as shown by the schematic below (Figure **2.2**). The error margins in computational studies make it unfeasible for small differences to be analysed. It was therefore concluded that the electrophilicities of the heterocycles are likely to be similar.



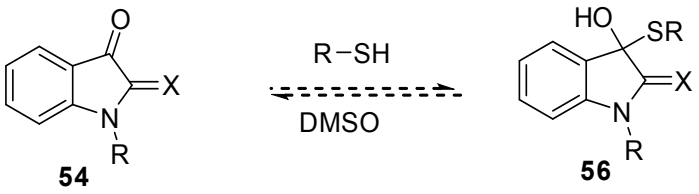
MK and Mulliken partial charges with no intermolecular influence

Dipole induced upon thiol approach

Figure 2.2: Ketone carbon partial charges Vs the dipole induced when a ketone is in close proximity to a thiol nucleophile

II.2.3. Transition States and Gibbs Free Energies[b]

Following the partial charge measurements, the activation energy and Gibbs free energy influencing the likelihood of the forward and back reactions were calculated. These were expected to better represent the reaction profile of thiohemiketal formation. Unlike the MK and Mulliken charges, the use of functionals such as M062X and wB97xD, and basis sets such as 6-31G (2d,2p) have been shown to successfully predict chemical properties that were directly supported by experimental results.[94, 110]



54 **56**

R = Me−SH Vs More complex thiols

Scheme 2.2: The equilibria between the ketone heterocycles and their thiohemiketal products

The simple methylthiol was used as the model thiol for the computational calculations in order to avoid potential non-nucleophilic effects of more complex thiols (Scheme **2.2**). The flexibility of larger or more complex thiols would result in a number of conformations with different energies, while the presence of aryl groups in thiols was shown to lead to intramolecular π-π stacking which may enhance the stability of the transition states, influencing observed results. This is exemplified with paramethoxybenzylthiol in Figure **2.3** whose flexible Ar-**CH_2**-SH moiety gave a thiohemiketal product with two different conformations and one conformer showing π-π stacking.

[b] Gibbs free energies and hydrogen bonding distances were calculated by the computational chemist, Alexandra Simperler, Imperial College London

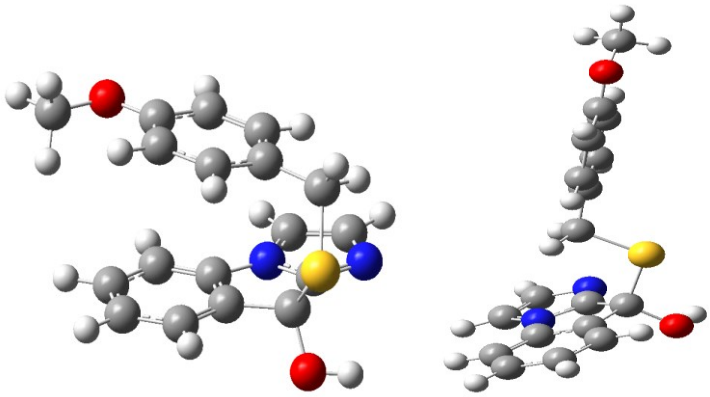


Figure 2.3: Parallel (left) and perpendicular (right) approach of PMBSH resulting in π-π stacking or vertical alignment of the thiol with the imidazoleindolone heterocycle **52**

Table 2.2: Computational results of thiol addition to the heterocycles calculated using wB97xD and M062X functionals with the 631G (2d,2p) basis set, including intramolecular hydrogen bonding distances and equilibrium constants calculated from free energy values

wB97xD	Energies$_{298K}$ [kJ/mol]			H-bonding distance (Å)	*K*
Ketone	G_{TS}-G_{React}	G_{Prod}-G_{React}	G_{TS}-G_{Prod}		
Isatin **(a)**	151	**-3.69**	155	2.67	4.43
Pyrimidoindolone **(b)**	163	**+7.25**	155	2.33	0.05
Imidazoleindolone **(c)**	162	**+7.83**	154	2.86	0.04
Triazoleindolone **(d)**	171	**+1.02**	171	3.10	0.66

For the free energy ΔG, wB97xD: **a < d < b ≤ c**; for the equilibrium constant, *K*: **a > d > b ≥ c**

For the activation energy, wB97xD: **a < c ≤ b < d**

Intramolecular hydrogen bonding distance, wB97xD: **b < a < c < d**

M062X	Energies [kJ/mol]			H-bonding distance (Å)	*K*
Ketone	G_{TS}-G_{React}	G_{Prod}-G_{React}	G_{TS}-G_{Prod}		
Isatin **(a)**	141	**-18.73**	160	2.51	1920
Pyrimidoindolone **(b)**	139	**-9.74**	149	2.32	51
Imidazoleindolone **(c)**	154	**-4.71**	159	3.03	7
Triazoleindolone **(d)**	163	**-12.41**	175	3.13	150

For the free energy ΔG, M062X: **a < d < b < c**; for the equilibrium constant, *K*: **a > d > b > c**

For the activation energy, M062X: **b ≤ a < c < d**

Intramolecular hydrogen bonding distance, M062X: **b ≤ a < c ≤ d**

The relative activation energies, Gibbs free energies and equilibrium constants obtained using the functionals wB97xD and M062X, combined with the 6-31G (2d,2p) basis set are shown in Table **2.2**.

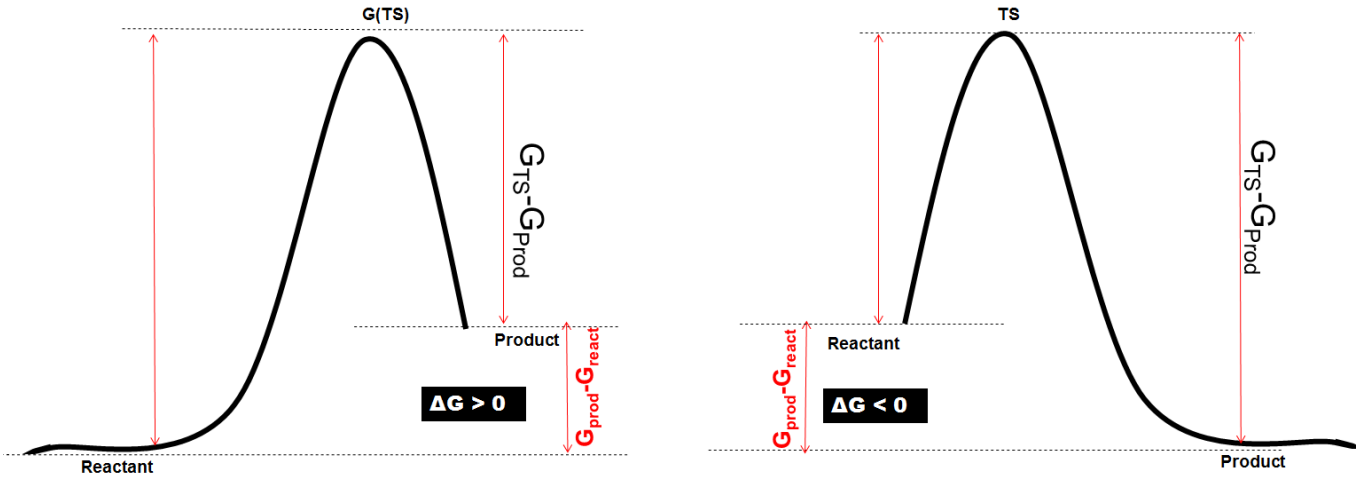


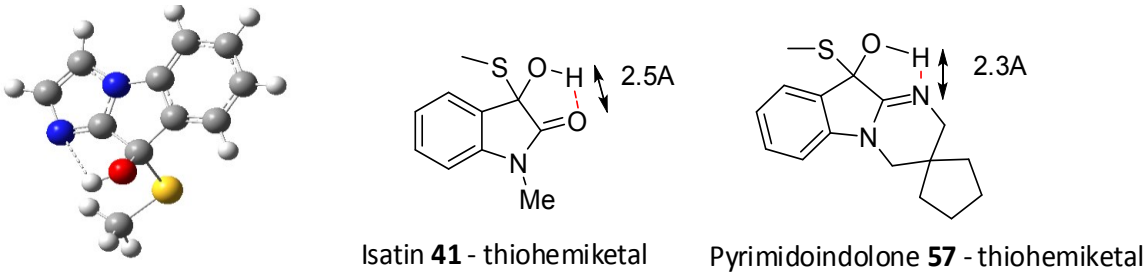
Figure 2.4: Plots of the calculated reaction pathway energies

Analysis of the wB97xD data suggested that the free energy, ΔG of thiol addition increases in the order; **isatin < triazoleindolone < pyrimidoindolone ≤ imidazoleindolone**. That is, the favourability of thiohemiketal formation decreases in the same order with thiol addition to the isatin shown to be the most favourable, followed by the triazoleindolone and then the pyrimidoindolone and the imidazoleindolone heterocycles. Reactions with negative ΔG values are favourable because a high energy compound reacts to give a lower energy product, while reactions with positive ΔG values are not favoured. In the data calculated using the wB97xD functional, only the isatin heterocycle has a negative free energy and is apparently the only heterocycle that would favourably react with a thiol to form a thiohemiketal. Computational data are however qualitative results, showing predicted relative free energies of thiol addition to the heterocycles and hence the positive free energies were not taken as indications that thiohemiketal formation from the other heterocycles are unfavourable.

Unlike the results obtained with the wB97xD functional, negative ΔG values were obtained for all four heterocycles using the M062X functional. Despite the quantitative differences, both the wB97xD and the M062X functionals showed the same order of thiol addition favourability according to the obtained ΔG values: **isatin > triazoleindolone > pyrimidoindolone > imidazoleindolone**.

For both functionals, the lowest activation energy was obtained for the isatin ring, indicating that thiol addition may also be fastest with the isatin heterocycle. The pyrimidoindolone and the

imidazoleindolone structures were shown to have comparatively lower activation energies compared to the triazoleindolone heterocycle, suggesting that, though thiohemiketal formation may be more favourable for the triazoleindolone heterocycle, the rate of thiol addition to the pyrimidoindolone and imidazoleindolone heterocycles would be faster. Nevertheless, the lower free energy for the triazoleindolone heterocycle would result in a high proportion of the triazoleindolone-thiohemiketal product at equilibrium.



Isatin **41** - thiohemiketal Pyrimidoindolone **57** - thiohemiketal

Figure 2.5: Intramolecular hydrogen bonding, forming a 5-membered ring in the isatin **41** and pyrimidoindolone **57** thiohemiketal products

Intramolecular hydrogen bonding distances, shown for the isatin and pyrimidoindolone thiohemiketal products in Figure **2.5**, were measured in attempt to account for the trends observed. From the M062X data, the pyrimidoindolone and isatin ring systems have the shortest hydrogen bonding distances of 2.32 Å and 2.51 Å respectively, a distance range that is reported to result in 'strong, mostly covalent' hydrogen bonding.[111, 112] Hydrogen bonding distances of 3.03 Å and 3.13 Å were obtained for the triazoleindolone and imidazoleindolone heterocycles respectively, a range reported to form hydrogen bonds that are 'mostly electrostatic'.[111, 112] Intramolecular hydrogen bonding was expected to favourably impact the stability of the thiohemiketal products. However, the obtained hydrogen bonding distances for the thiohemiketal products did not directly correlate with ΔG values.

$$\frac{[\text{Thiohemiketal}]}{[\text{Ketone}]\ [\text{Thiol}]} = K \qquad \textbf{Equation 2.1}$$

$$\Delta G = -RT\ln K \qquad \textbf{Equation 2.2}$$

$$K = e^{-\Delta G/RT} \qquad \textbf{Equation 2.3}$$

Using the obtained ΔG values, the equilibrium constants for thiol addition were calculated, using Equation **2.3**, derived from Equations **2.1**. The equilibrium constant is directly related to, and inversely proportional to free energy; the lower the free energy the higher the equilibrium constant and the more favourable the forward reaction. A *K* value of above 1 was obtained for all heterocycles using the M062X functional, indicating that that the reaction with a thiol lies on the thiohemiketal product side at equilibrium, albeit to different extents for the different heterocycles. The two functionals showed the isatin to have the highest *K* value by a significant margin.

Both the wB97xD and M062X functionals are regularly used in computational calculations with the two functionals considering such a wide spectrum of properties that it cannot be conclusively determined which functional gave the most accurate representation of the favourability of thiohemiketal formation. Both functionals however, are in agreement with the obtained trend in the free energy of thiol addition to the heterocycles; **isatin > triazoleindolone > pyrimidoindolone > imidazoleindolone**.

II.3. Experimental UV-Vis Analysis of the Heterocycles

Initial computational analysis of the three heterocycles in comparison to the isatin ring suggested that all three heterocycles under study have the propensity to inhibit caspase-3 through the favourable addition of a cysteine thiol group to the ketone carbonyls. The next step was to experimentally study the heterocycles in order to validate these predictions. For initial experimental studies, UV-vis absorption spectroscopy was employed for the determination of thiohemiketal equilibria. The experimental values were then compared to the relative trend in the values calculated from the computational model.

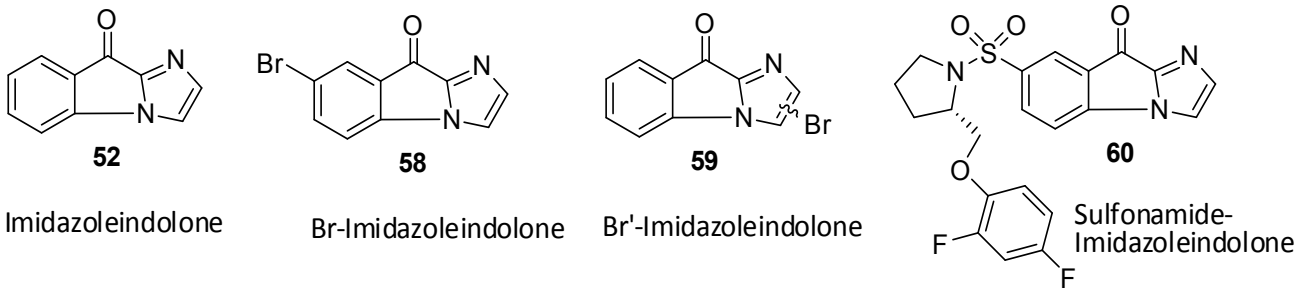


Figure 2.6: Unsubstituted and substituted imidazoleindolone heterocycles

In order to carry out the UV-vis titrations, the first step was to synthesise the core heterocycles. For the purpose of not diverting beyond the scope of this chapter, the synthesis of the pyrimidoindolone, imidazoleindolone and triazoleindolone heterocycles are described in subsequent Chapters **III** and **IV**. The pyrimidoindolone heterocycle **57** and imidazoleindolone heterocycle **52** were successfully synthesised. Isatin **41** is commercially available and was purchased from Sigma-Aldrich. Unfortunately, the synthesis of the novel triazoleindolone heterocycle proved very problematic and was ultimately not achieved.

Additionally, the bromide and sulfonamide-substituted imidazoleindolone heterocycle **58**, **59** and **60** were prepared and used to analyse substituent effects on thiohemiketal formation (Figure **2.6**). The bromide substituent was chosen due to facile synthesis of this derivative while the sulfonamide substituent was included to closely resemble the isatin sulfonamides.

II.3.1. UV-Vis Spectroscopic Titrations of Thiohemiketal Formation

The interaction of the relevant ketone with a thiol was monitored from the decrease in the ketone absorption at the maximum absorption wavelength. A similar experiment was successfully conducted by Aulabaugh *et al*. who employed UV-vis spectroscopy to monitor the interaction of isatin with caspase-3 resulting from thiohemiketal formation in the enzyme active site.[87] The formation of a thiohemiketal results in the reduction of the ketone absorption. As a result, the concentration of the thiohemiketal formed is proportional to the difference in the UV-vis absorption before and after thiol addition to the ketone solution.

To experimentally determine the equilibria between the ketone derivatives and their thiohemiketal products, anhydrous DMSO was used as the solvent, in order to limit the possible ketone hydration by residual water. Aiming to closely emulate the cysteine thiol residue found in the caspase-3 active site, the tripeptide, glutathione was initially employed as the thiol for the study but this was insoluble in DMSO. As a result, the simple thiol, PMBSH was used instead. Methanethiol, which was employed in the computational studies was not used in order to avoid problems with handling this toxic gaseous compound. The use of different thiols should not restrict comparisons of the computational data with the experimental results, since relative trends, rather than absolute figures were to be compared for the two sets of data, each with the thiol nucleophile kept constant. Given the sensitivity of thiols to oxidation in air, solutions were degassed and stoppered UV cuvettes under argon were used for all experiments.

The UV-vis absorption of all the heterocycles under study were measured in DMSO over the course of 24 hours to ascertain the stability of the ketone substrates in DMSO. All heterocycles were proven to remain stable in DMSO with no signs of decomposition after 24 hours. The UV-vis absorption of mixtures of PMBSH were shown to be constant for 15 minutes after which the solutions were assumed to have reached equilibrium. Prolonged measurements for up to 12 hours showed that the absorption spectra of the ketone/PMBSH mixtures remained unchanged. The UV-vis absorption spectra and the resulting plots of absorption at varying thiol concentration are shown below in Figures **2.7** to **2.9**. The table of absorption data for all heterocycles can be found in the appendix. The more favourable thiol addition to the isatin ring is evident from the UV-vis absorption spectra of thiol addition to the isatin ring (Figure **2.7**), showing significant decreases in the ketone absorption with increasing thiol concentration. By contrast, the UV-vis absorption spectra of the imidazoleindolone and pyrimidoindolone heterocycles only show small decreases in ketone absorption for the same ketone/thiol concentrations (Figures **2.8** – **2.9**).

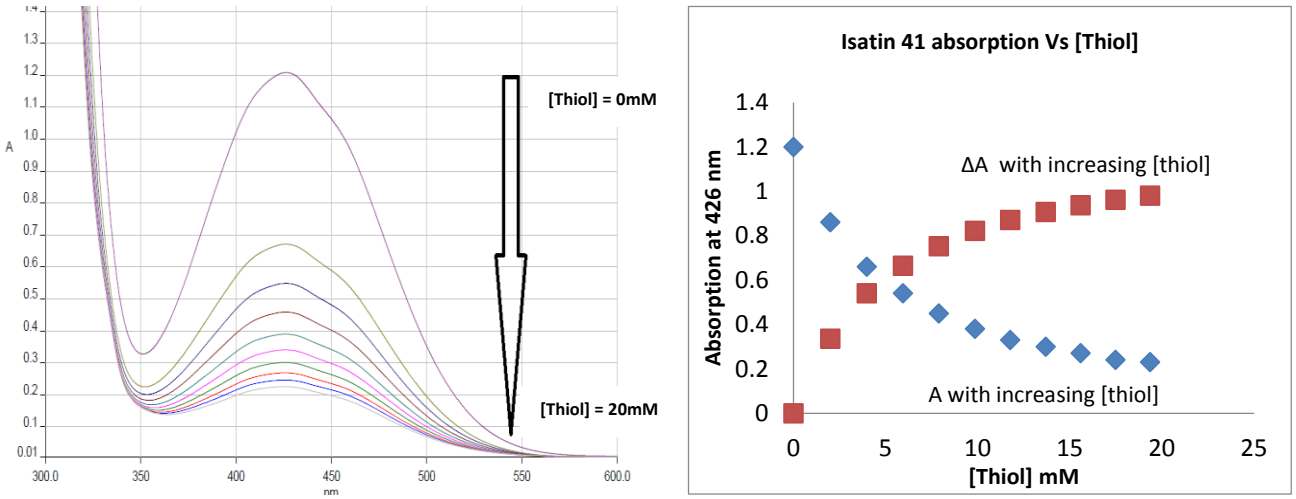


Figure 2.7: The UV-vis absorption spectra (left); and a plot of absorption (A) and ΔA Vs [thiol] for 2mM isatin **41** solution titrated with 0 – 10 equivalents of PMBSH. For details of the absorption values at the different concentrations, see the Appendix (page 240).

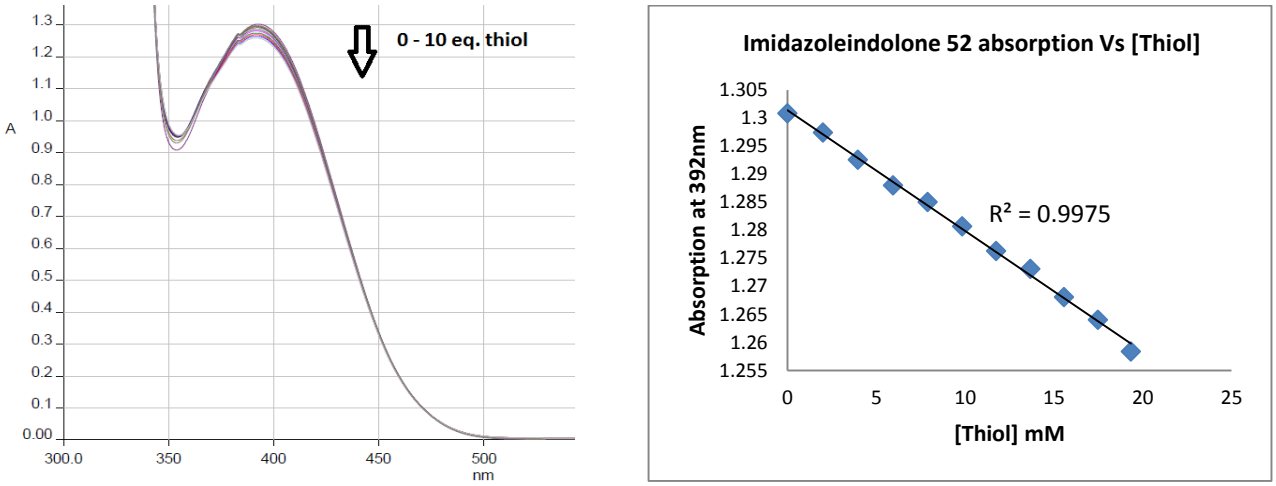


Figure 2.8: The UV-vis spectra and a plot of absorption Vs [thiol] for 2mM imidazoleindolone **52** titrated with 0 – 10 equivalents of PMBSH

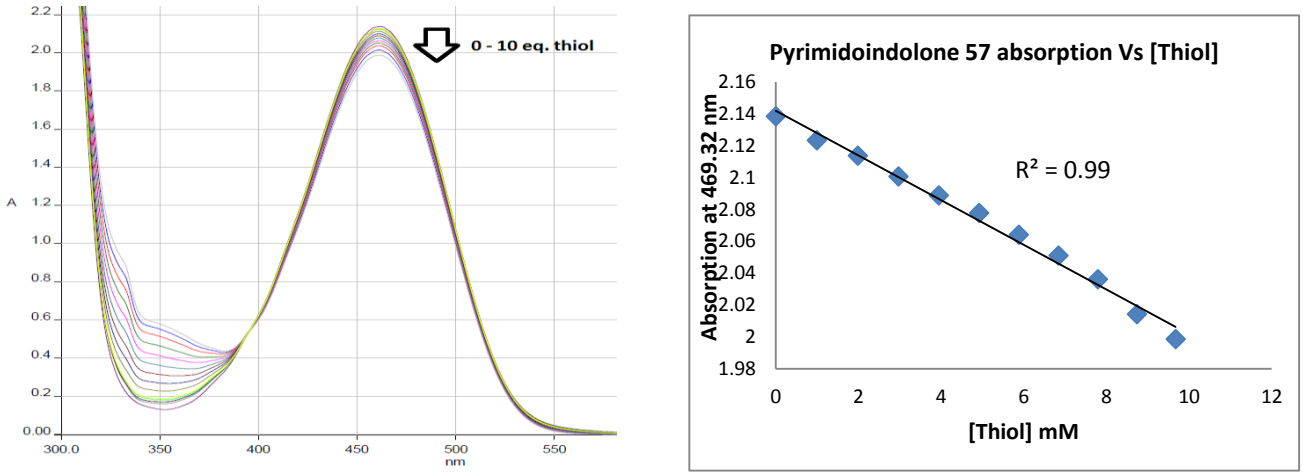


Figure 2.9: The UV-vis spectra and a plot of absorption Vs [thiol] for 2mM pyrimidoindolone **57** titrated with 0 – 10 equivalents of PMBSH

II.3.2. Calculating Equilibrium Constants using Benesi-Hildebrand Plots

The Benesi-Hildebrand plot[113, 114] is a convenient and widely used method for calculating binding constants and reaction equilibria when one-to-one conjugates are formed. The method relies on the measurement of characteristic electronic absorptions before and after the formation of an adduct.[114] The mathematical derivation of the Benesi-Hildebrand equation is summarised below. Modification of the equation allows equilibrium constants to be calculated from plots showing the relationship between the UV-vis absorption and the concentration of one reaction component that was varied and used in excess amounts, without the need to determine the absorption coefficient of the reaction species.

$$\Delta A = \frac{K\,\Delta\varepsilon\,[th]\,[kt]_o}{1 + K\,[th]}$$ **Equation 2.4**

where ΔA is the change in absorption at a particular wavelength, ε is the absorption coefficient, $[kt]_o$ is the initial ketone concentration and [th] is the thiol concentration.

Modification of the equation to a double reciprocal plot gives:

$$\frac{1}{\Delta A} = \frac{1}{[th]\,\Delta\varepsilon\,[kt]_o\,K} + \frac{1}{\Delta\varepsilon\,[kt]_o}$$ **Equation 2.5**

Hence, from a plot of the reciprocal of the change in absorption (1/ ΔA) versus the reciprocal of the thiol concentration (1/[th]), where the ketone concentration is kept constant and the thiol concentration is varied, ***K* = intercept/slope** . The Benesi-Hildebrand plots of 1/ ΔA against 1/[th] for the heterocycles are shown below in Figures **2.10** - **2.12**.

$$\frac{1}{\Delta A} = \frac{1}{[th]} \cdot \underbrace{\frac{1}{\Delta\varepsilon\,[kt]_o\,K}}_{\text{Slope}} + \underbrace{\frac{1}{\Delta\varepsilon\,[kt]_o}}_{\text{Intercept}}$$ **Equation 2.5'**

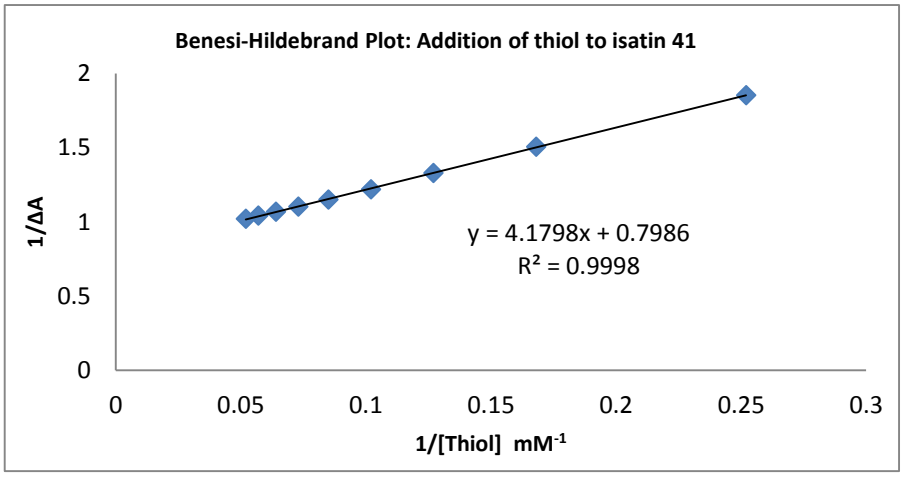


Figure 2.10: The Benesi-Hildebrand plot for thiol addition to isatin **41**, giving a *K* value of 0.19 mM^{-1}

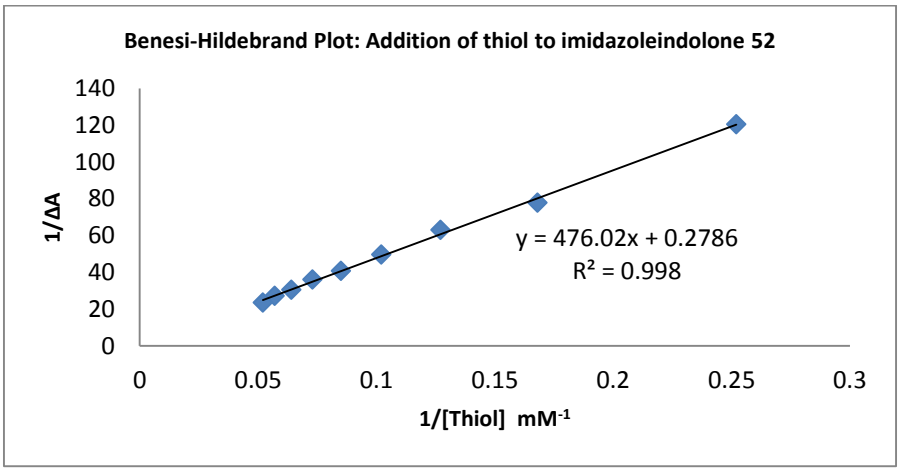


Figure 2.11: The Benesi-Hildebrand plot for thiol addition to imidazoleindolone **52**, giving a *K* value of 5.85 x 10^{-4} mM^{-1}

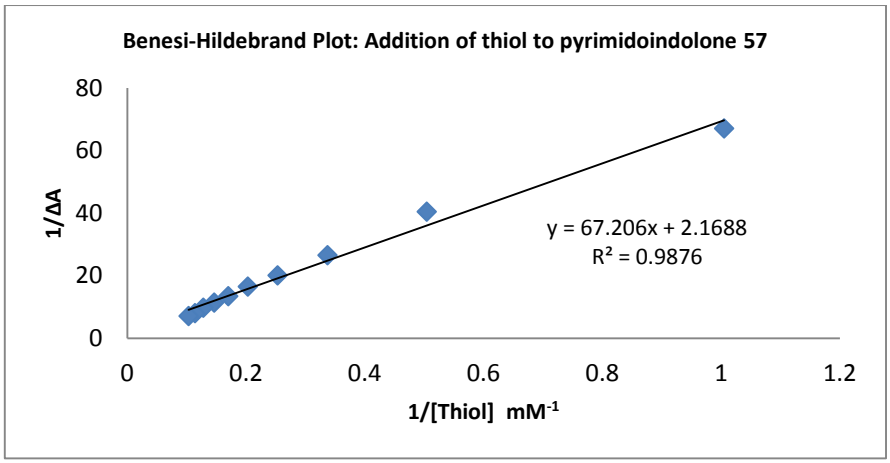


Figure 2.12: The Benesi-Hildebrand plot for thiol addition to the pyrimidoindolone **57**, giving a *K* value of 0.03 mM^{-1}

II.3.3. Experimental Results

Table 2.3: Calculated *K* values for thiol addition

Ketone	Thiohemiketal *K* / mM^{-1}
Isatin **41**	0.19
Pyrimidoindolone **57**	0.03
Imidazoleindolone **52**	0.0005

The equilibrium constants calculated from the Benesi-Hildebrand plots in Figures **2.10** – **2.12** are summarised in Table **2.3**. In contrast to the computational results (using the M062X functional), all the experimental *K* values are less than 1, suggesting that the ketone dominates over the thiohemiketal product at equilibrium for all the heterocycles. This was apparent from the UV-vis absorption spectra of the pyrimidoindolone and imidazoleindolone heterocycles where small changes in the ketone absorption were observed upon thiol addition (Figures **2.8** and **2.9**). However, the trend in experimental *K* values and therefore the favourability of thiol addition reflects the trend obtained from computational studies:

Isatin 41 > Pyrimidoindolone 57 > Imidazoleindolone 52

Experimentally, isatin thiohemiketal formation is approximately 6-fold and 380-fold more favourable than thiol addition to the pyrimidoindolone and imidazoleindolone heterocycles respectively.

It is worth noting that thiohemiketal formation was confirmed from the ^{1}H NMR of isatin **41** and PMBSH mixture in deuterated DMSO (Figures **2.13** – **2.16**). The signal intensity of the thiohemiketal increases upon increasing the ratio of thiol to isatin from 1:1 to 3:1 in order to push equilibrium further towards thiohemiketal formation. A clear NMR could not be obtained for the other heterocycles due to their low *K* values for thiohemiketal formation.

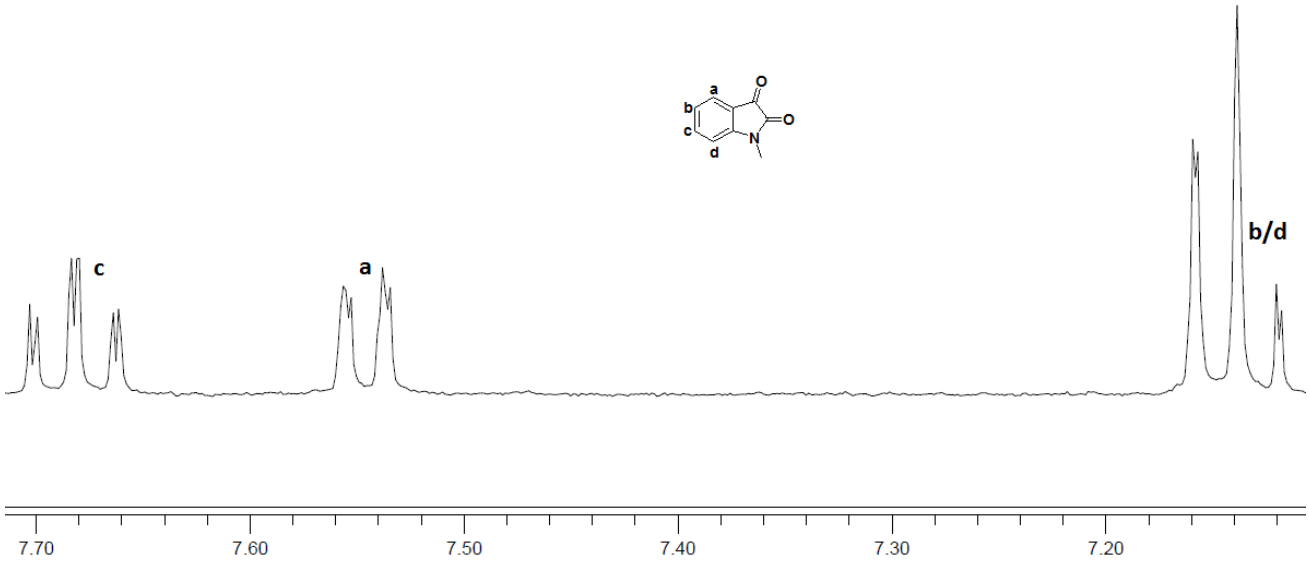


Figure 2.13: ^{1}H NMR of the isatin **41** in DMSO (aromatic region only), measured with a 400 MHz spectrometer

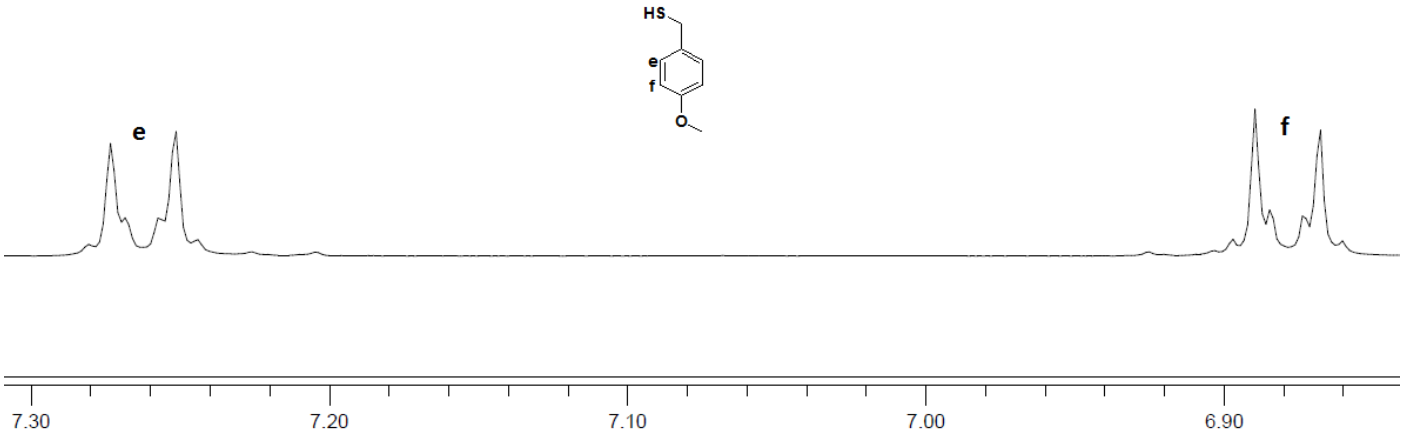


Figure 2.14: ^{1}H NMR of PMBSH in DMSO (aromatic region only), measured with a 400 MHz spectrometer

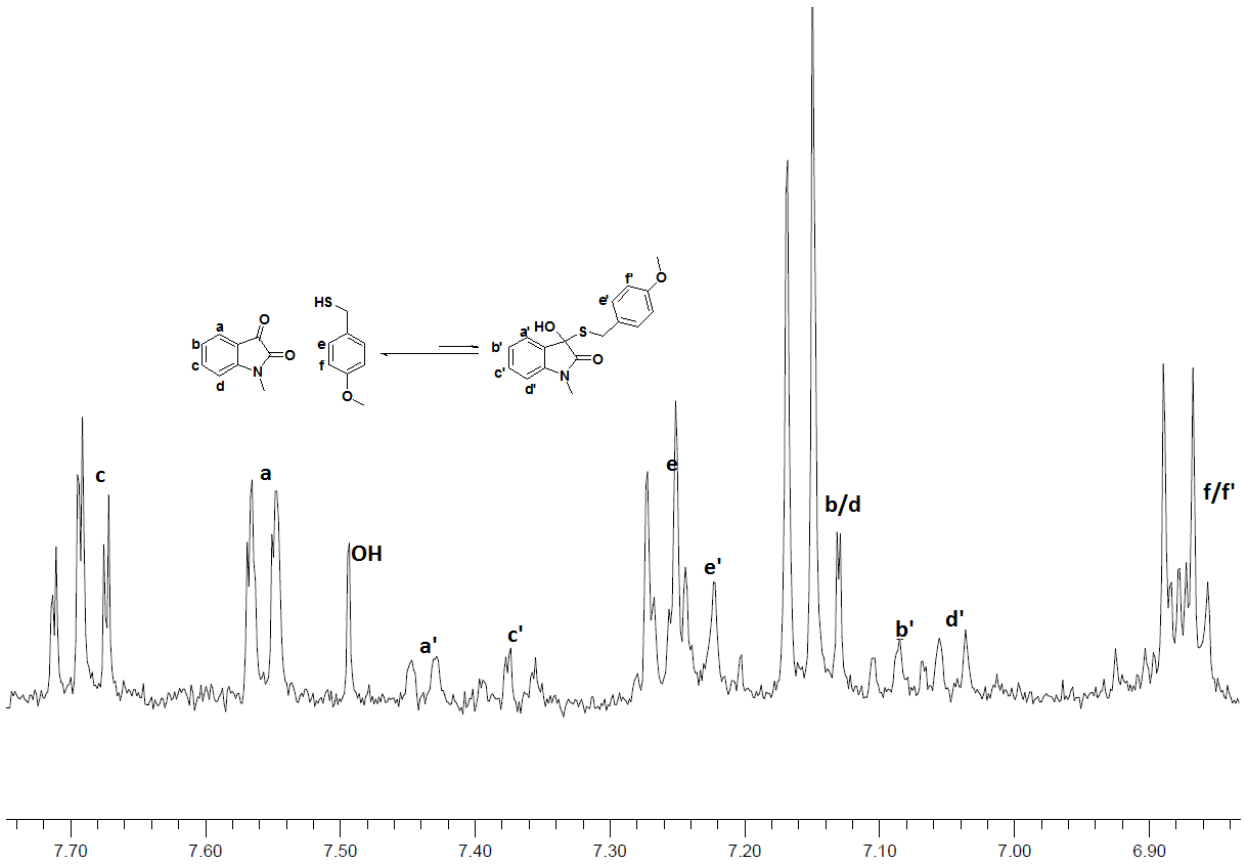


Figure 2.15: ^{1}H NMR of a 1:1 mixture of isatin **41** and PMBSH in DMSO (aromatic region only), measured with a 400 MHz spectrometer

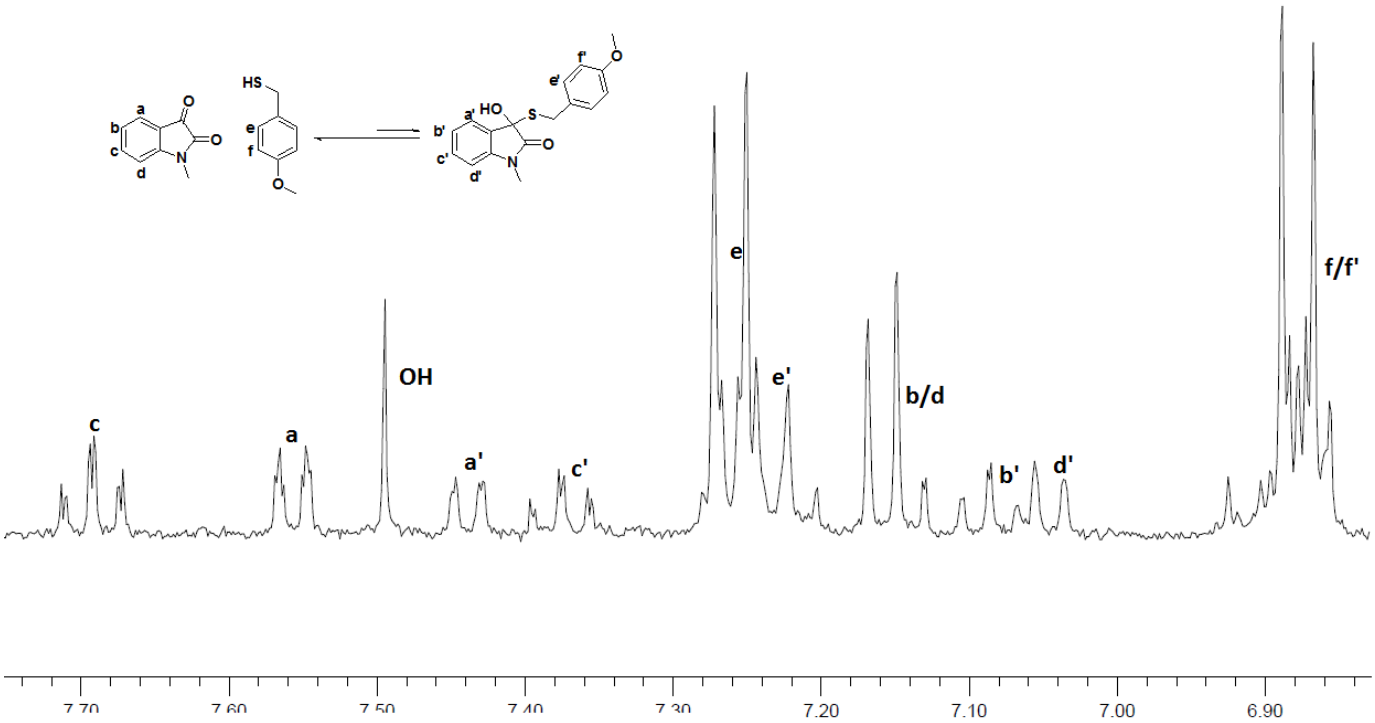


Figure 2.16: ^{1}H NMR of a 1:3 mixture of isatin **41** and PMBSH in DMSO (aromatic region only), measured with a 400 MHz spectrometer

II.3.3.1. The Substituent Effect

The UV-vis absorption spectra and the resulting plots of absorption versus thiol concentration for the bromide- and sulfonamide-substituted imidazoleindolone heterocycles **58**, **59** and **60** are shown below in Figures **2.17** – **2.19**. The corresponding Benesi-Hildebrand plots are shown in Figures **2.20** – **2.22**.

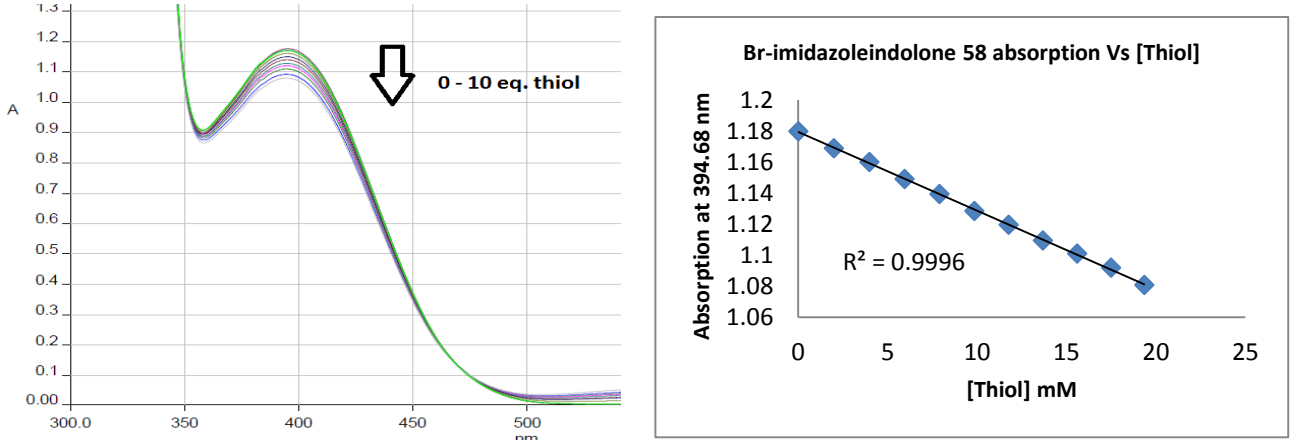


Figure 2.17: The UV-vis spectra and a plot of absorption Vs [thiol] for 2mM imidazoleindolone **58** titrated with 0 – 10 equivalents of PMBSH

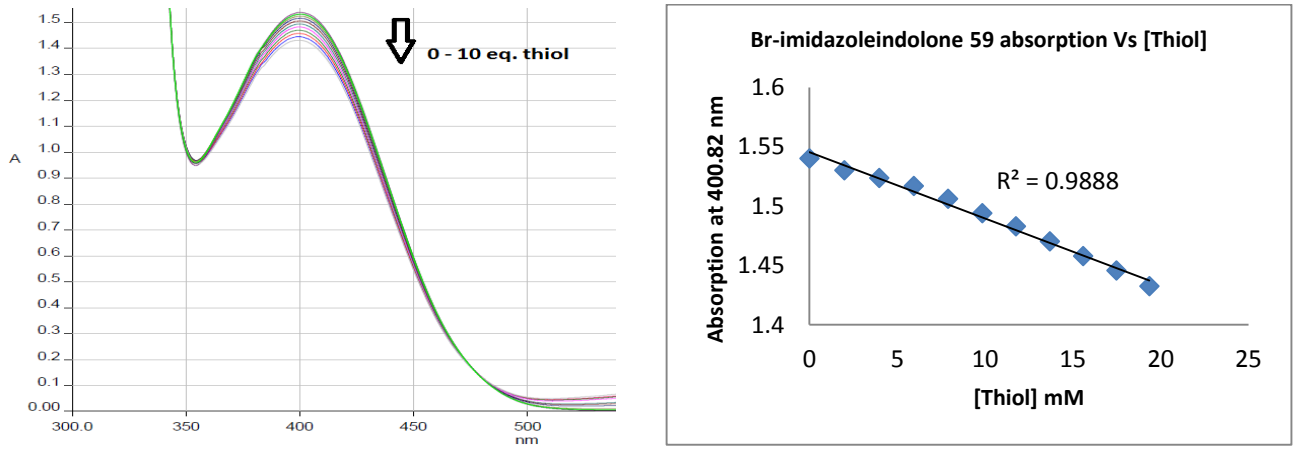


Figure 2.18: The UV-vis spectra and a plot of absorption Vs [thiol] for 2mM imidazoleindolone **59** titrated with 0 – 10 equivalents of PMBSH

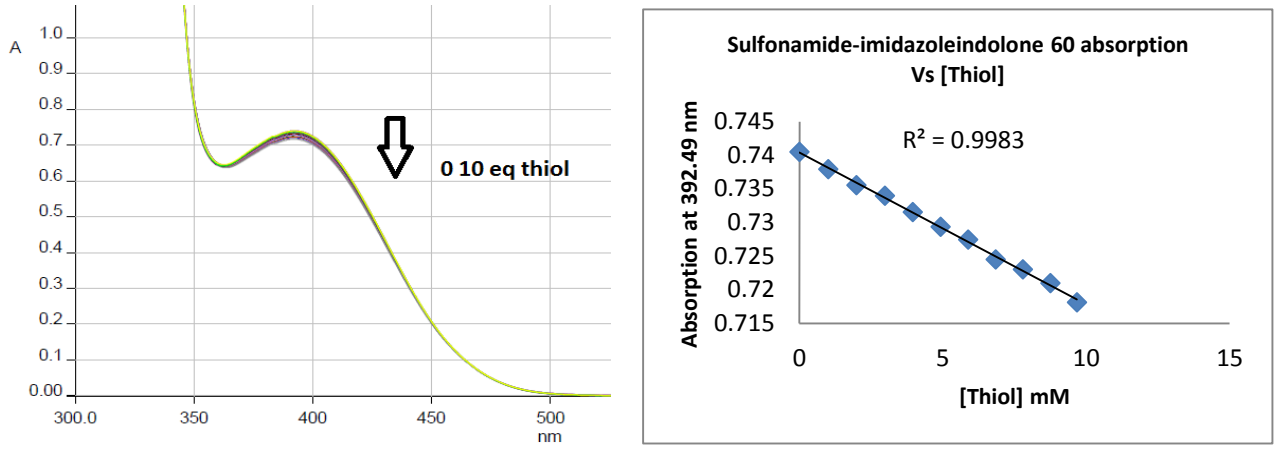


Figure 2.19: The UV-vis spectra and a plot of absorption Vs [thiol] for 1mM imidazoleindolone **60** titrated with 0 – 10 equivalents of PMBSH

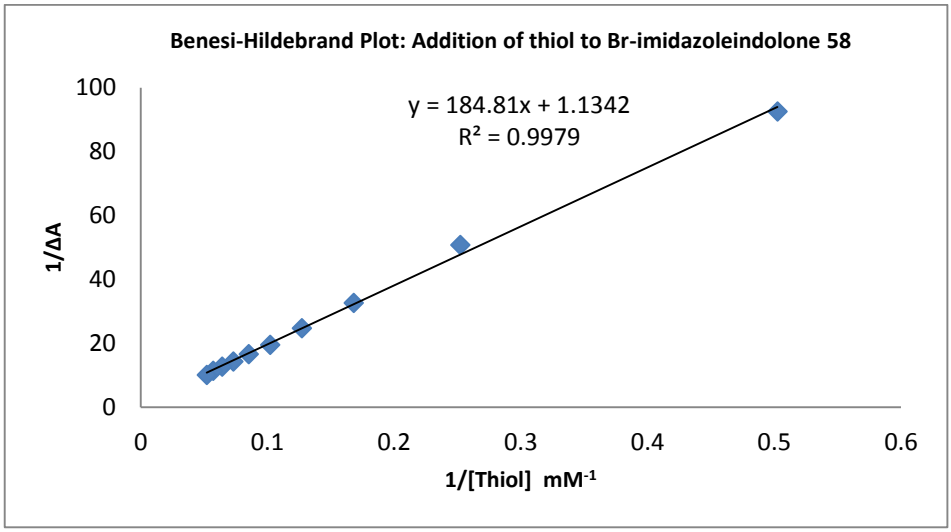


Figure 2.20: The Benesi-Hildebrand plot for thiol addition to the bromo-substituted imidazoleindolone **58**, giving a *K* value of 0.006 mM^{-1}

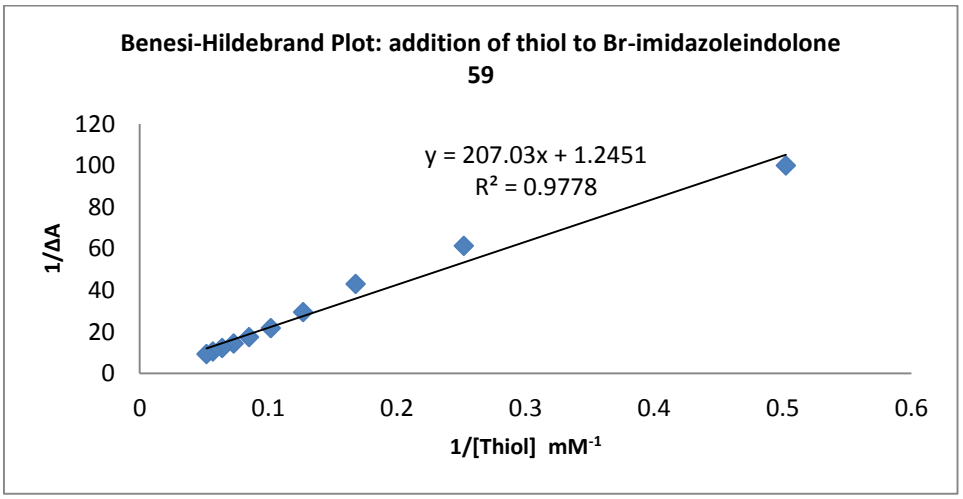


Figure 2.21: The Benesi-Hildebrand Plot for thiol addition to the bromo-substituted imidazoleindolone **59**, giving a *K* value of 0.006 mM^{-1}

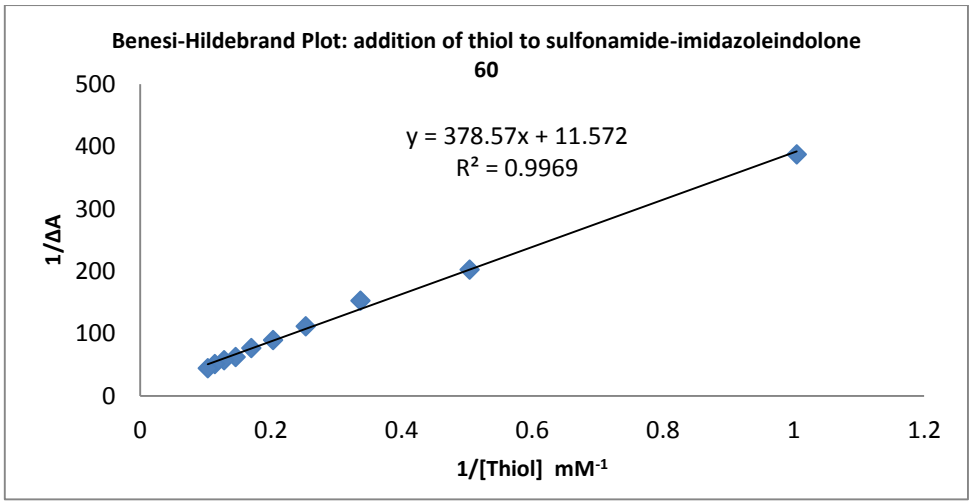


Figure 2.22: The Benesi-Hildebrand plot for thiol addition to the sulfonamide-substituted imidazoleindolone **60**, giving a *K* value of 0.03 mM^{-1}

Table 2.4: Calculated thiohemiketal *K* values of substituted imidazoleindolone heterocycles

Ketone	Thiohemiketal *K* /mM^{-1}
Imidazoleindolone **52**	0.0005
Br-Imidazoleindolone **58**	0.006
Br′-Imidazoleindolone **59**	0.006
Sulfonamide-imidazoleindolone **60**	0.03

As shown in Table **2.4**, the imidazoleindolone heterocycle becomes more susceptible to thiohemiketal formation when substituted with an electron withdrawing group. The favourability of thiohemiketal formation increases by approximately 12-fold with a bromide substituent on the phenyl ring (**58**) or on the imidazole ring (**59**), and by 60-fold when substituted with the more electron withdrawing sulfonamide group. The favourability of thiol addition to the sulfonamide substituted imidazoleindolone **60** was shown to be similar to that of thiol addition to the pyrimidoindolone **57**, but still less than the formation of a thiohemiketal from the unsubstituted isatin **41**.

Further computational analysis using the bromide substituted imidazoleindolone **58** was obtained and compared with the results obtained for the unsubstituted imidazoleindolone **52** using the M062X functional. We found that the equilibrium constant for thiohemiketal formation increased by 12-fold with the bromide substituted heterocycle **58**; the exact increase observed experimentally (Table **2.5**).

Table 2.5: The computational results of unsubstituted imidazoleindolone **52** compared to the bromo-substituted imidazoleindolone **58**

M062X	Energies$_{298K}$ [kJ/mol]			H-bonding distance (Å)	*K*
Ketone	G_{TS}-G_{React}	G_{Prod}-G_{React}	G_{TS}-G_{Prod}		
Imidazoleindolone **52**	154	**-4.71**	159	3.03	*7*
Br-Imidazoleindolone **58**	153	**-11.02**	164	3.04	*85*

For the free energy ΔG: **58 < 52** and the resulting *K*: **58 > 52**

For the barrier between the transition state and reactant (activation energy): **52 ≤ 58**

For the intramolecular hydrogen bonding distance: **52 ≤ 58**

II.4. Conclusion

In the present study, the favourability of thiol addition to the ketone group of the four heterocycles under study was established through the computational calculation of Gibbs free energy, in addition to other potentially contributing factors such as intramolecular hydrogen bonding and ketone partial charges. The predicted trend in the computationally derived favourability of thiohemiketal formation was supported by the results obtained from UV-vis titration of the ketone substrates with PMBSH.

The trend in the calculated and experimentally determined thiohemiketal equilibria may not be reflected in biological binding affinities, where the overall structure of a ketone substrate has a substantial effect on caspase-3 binding and subsequent inhibitory activity. Nevertheless, by comparing the determined properties of the three heterocycles under investigation to the extensively studied isatin sulfonamide, their relative caspase-3 inhibition potency may be predicted.

Though the computational and experimental data gave different absolute values, both sets of results showed the same trend in equilibrium constant (*K*) values and therefore the favourability of thiohemiketal addition: **Isatin 41 > Pyrimidoindolone 57 > Imidazoleindolone 52**. Both sets of results are in agreement in suggesting that the isatin heterocycle is much more favourable towards thiohemiketal formation, followed by the pyrimidoindolone **57**, with the imidazoleindolone **52** being the least favourable. While the triazoleindolone heterocycle **53** was not used the in UV-vis equilibria calculations due to synthetic difficulties, the agreement of the computational results with the experimental data for the other three heterocycles gives us the confidence to conclude the favourability of thiohemiketal formation from the triazoleindolone heterocycle **53** is second only to the isatin ring, and more favourable than the pyrimidoindolone **57** and imidazoleindolone **52** heterocycles.

Additionally, the influence of substituents on thiohemiketal formation was shown by the experimental *K* values of the bromide and sulfonamide substituted imidazoleindolone heterocycles, **58**, **59** and **60**. As expected, the presence of electron withdrawing substituents increased the favourability of thiohemiketal formation, likely due to increased electron deficiency of the ketone carbonyl.

The model of a ketone reacting with a simple thiol represents the formation of a thiohemiketal in an intermolecular reaction, whereas the intracellular formation of a thiohemiketal

resulting from a ketone-substrate binding to an enzyme active site cavity is comparable to an intramolecular reaction as the reacting groups are brought together in very close proximity.[115, 116] It has been reported that such intracellular reactions can be favoured over intermolecular reactions by a factor of 10^3-10^8 M, depending on the extent to which optimal substrate orientation in the enzyme active site is achieved, and the reduction of conformational degrees of freedom.[115, 116] With this in mind, the favourable results obtained from computational and UV-vis studies are sufficiently encouraging to warrant further study, progressing to the synthesis and biological characterisation of caspase-3 binding apoptotic PET probes based on the imidazoleindolone **52**, pyrimidoindolone **57** and triazoleindolone **53** pharmacophores.

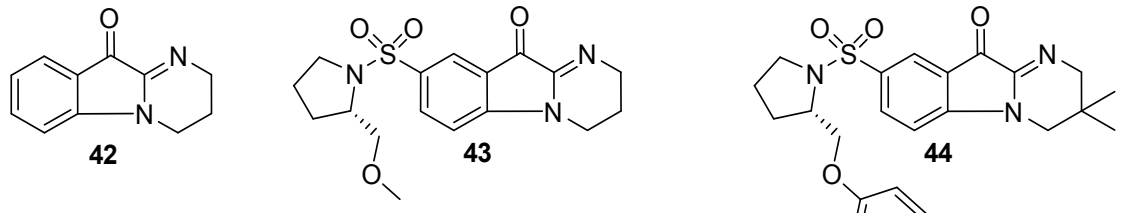
CHAPTER III:

[18F]-Fluorinated Pyrimidoindolone to Image Caspase-3 Activity

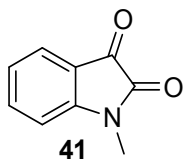
III. [18F]-Fluorinated Pyrimidoindolone to Image Caspase-3

III.1. Introduction: Target Structure Design

While the isatin sulfonamides are the current state-of-art of caspase-binding radioligands, PET imaging of apoptosis using these inhibitors is hampered by low target-to-background ratio (Chapter **I.4.2**). The pyrimidoindolones (Figure **3.1**) subsequently emerged as potential alternatives to the isatin sulfonamides with initial SAR studies reported by Havran *et al*. (Chapter **I.4.3**).[58] As previously discussed (Chapter **I.4.3**), a recent study showed that isatin sulfonamides bind to a single domain of the dimeric caspase-3 enzyme while the pyrimidoindolones bind to both domains with equal affinity.[87] It was hoped that the dual binding of pyrimidoindolones to the caspase active site compared to the half-site activity of the isatin sulfonamide would lead to increased specific binding activities, reducing non-specific background signals when used for PET imaging.



Unsubstituted and substituted pyrimidoindolone structures studied by Havran *et al*.



The core isatin heterocycle and the lead isatin sulfonamide

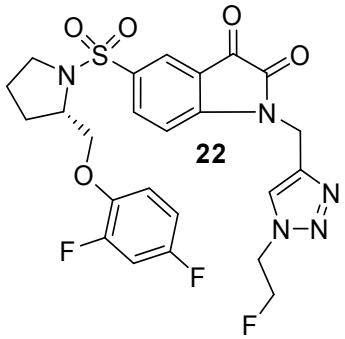


Figure 3.1: The pyrimidoindolone heterocycle and the structurally similar to isatins

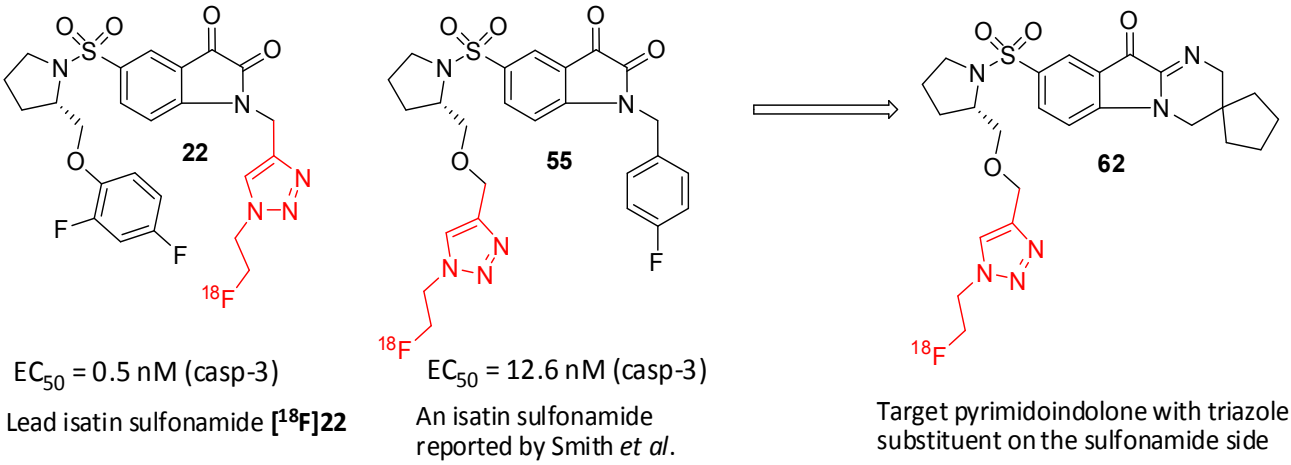


Figure 3.2: The current isatin lead compound [^{18}F]**22**, a previously tested isatin sulfonamide **55**, and the proposed initial pyrimidoindolone structure [^{18}F]**62**

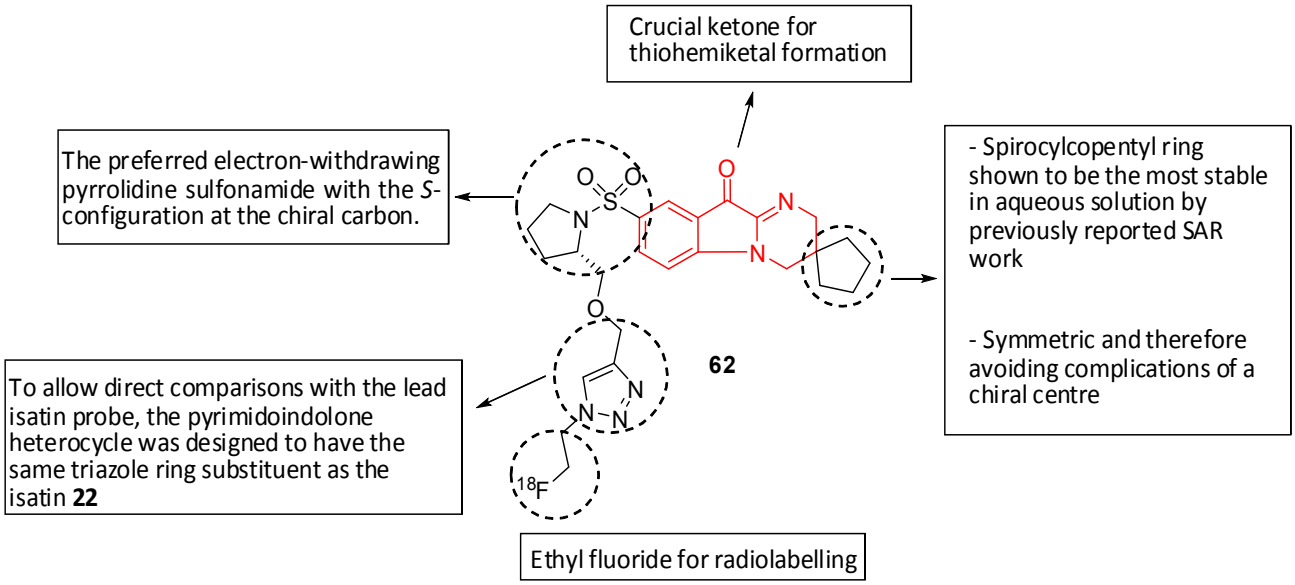
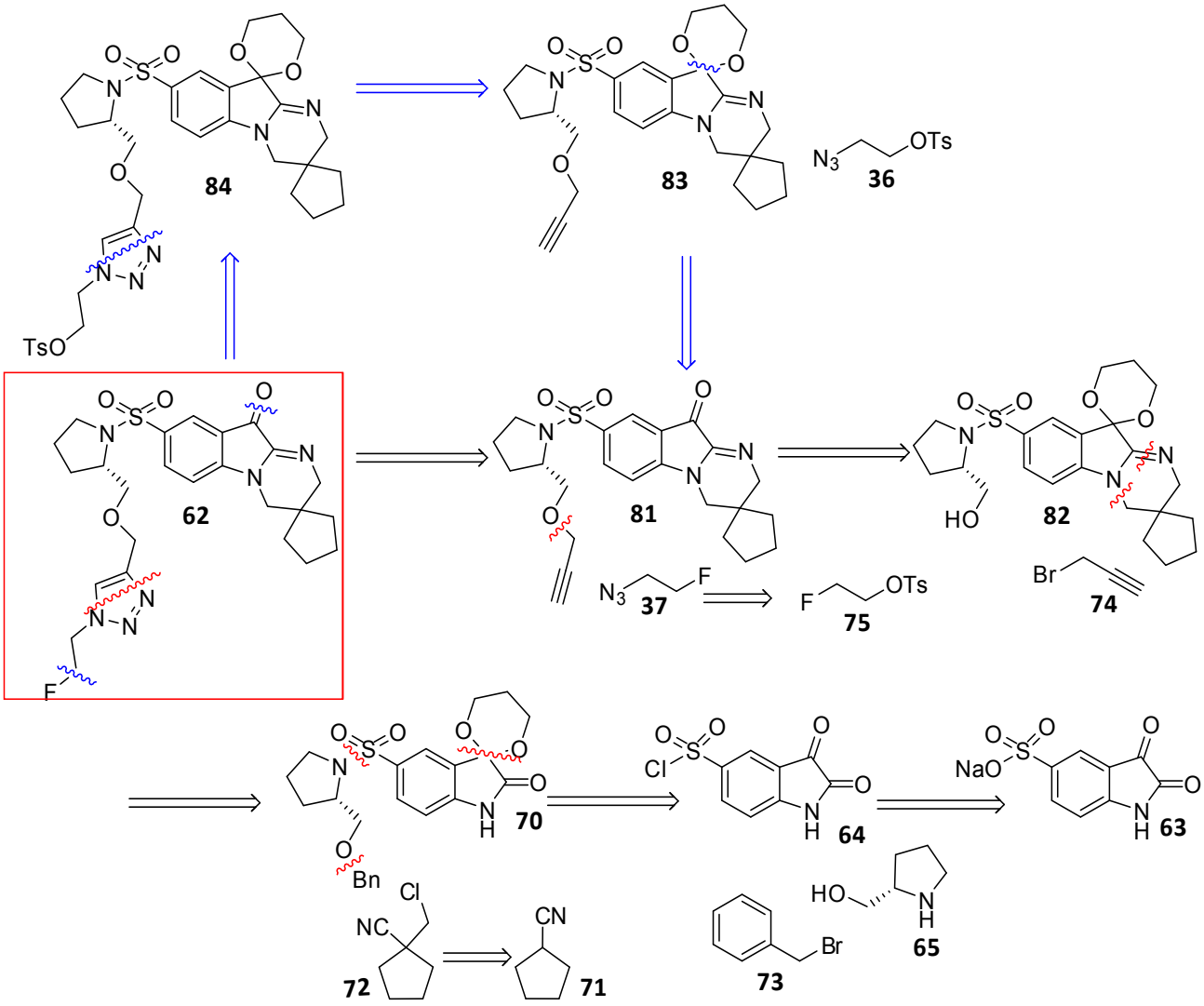


Figure 3.3: The designed pyrimidoindolone target structure **62** to be synthesised, radiolabelled and characterised for capsase-3 imaging was modelled on the structure of the lead isatin **22**.

Results of the SAR studies reported by Havran *et al*. revealed similarities to the isatin sulfonamides in terms of hydrophobic and hydrogen binding interactions with the caspase-3/7 binding cleft.[58] To allow direct comparisons with isatin sulfonamide **22**, the target pyrimidoindolone was designed with the same triazole ring substituent found in the lead isatin probe. SAR studies of the isatin sulfonamides have shown that triazole substituents are well tolerated on both the sulfonamide and amide sides of the isatin ring while maintaining high potency and selectivity as shown in Figure **3.2**. For ease of synthesis, the triazole ring was positioned on the sulfonamide side of the pyrimidoindolone ring (Figure **3.2**). On the amidine side of the pyrimidoindolone, substitution can only occur on the unfunctionalised aliphatic carbon atoms. Hence, to allow facile synthesis,

reagents for the construction of the pyrimidoindolone ring which already contain the planned substituent were preferred. For optimal aqueous stability with high potency, based on results reported by Havran *et al*. (Chapter **I.4.3**),[58] the spirocyclopentyl substituent was selected (Figure **3.3**).

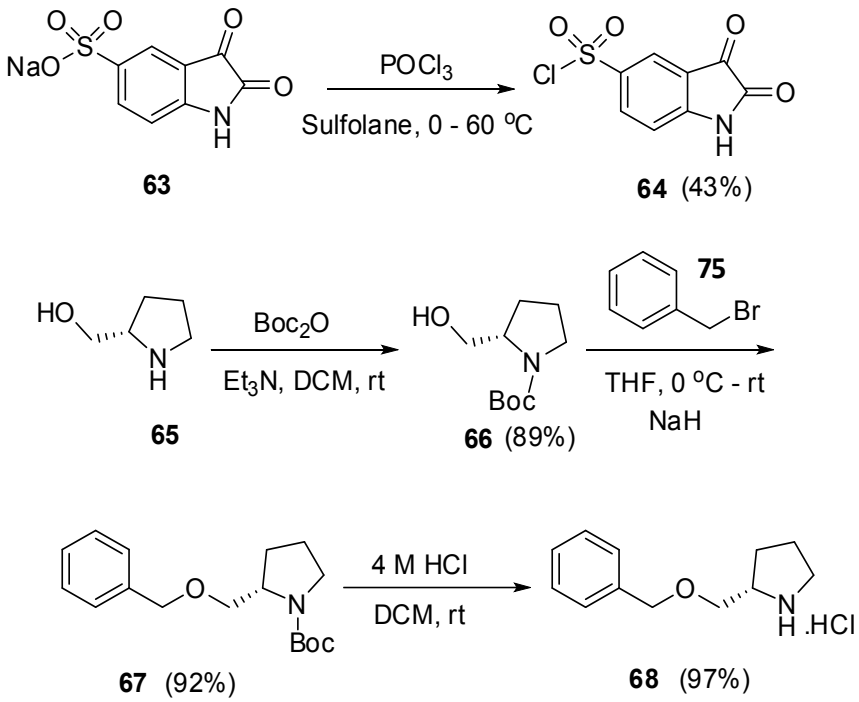
III.2. Target Pyrimidoindolone Synthesis



Scheme 3.1: Retrosynthetic analysis showing the route employed for the target pyrimidoindolone synthesis

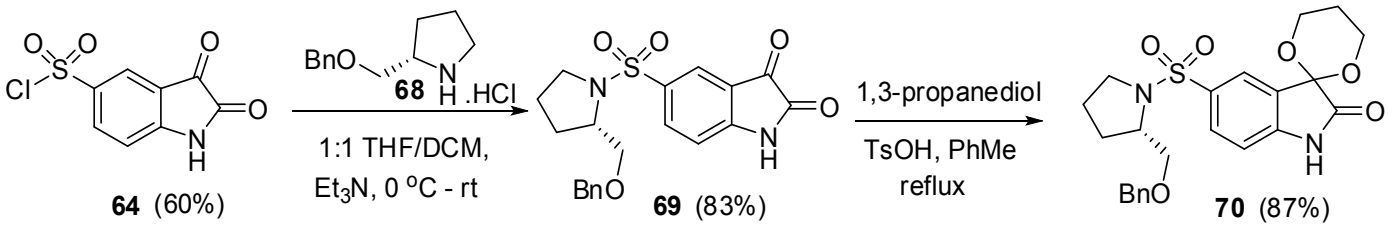
The retrosynthetic analysis, summarising the route employed for the target pyrimidoindolone is shown in scheme **3.1** and detailed in this section. The core pyrimidoindolone ring differs from that of the core isatin ring by the substitution of an amide group for an amidine group. Hence, similar reactions used to prepare the isatin sulfonamide were used for the initial steps. The synthesis of the pyrimidoindolone target **62** started with the treatment of sodium 5-isatin sulfonate **63** with

phosphorus oxychloride in sulfolane at 60 ^{o}C, converting the sulfonate group into the sulfonyl chloride **64** in 43 % yield (Scheme **3.2**).[58]



Scheme 3.2: Preparation of the (*S*)-2-(benzyloxymethyl)pyrrolidine hydrochloride **68** in 79 % yield over 3 steps and the isatin sulfonyl chloride **64**.[57, 58]

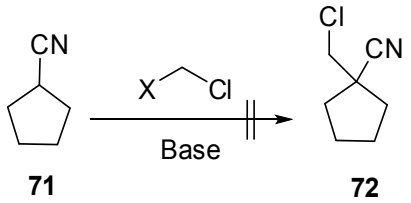
Reaction of sulfonyl chloride **64** with the required amine, (*S*)-2-(benzyloxymethyl)pyrrolidine **68** would then give the isatin sulfonamide intermediate **69**. The amine **68** was prepared from commercially available (*S*)-prolinol with an overall yield of 79 % (Scheme **3.2**). First, the amine moiety of (*S*)-prolinol **65** was protected with a Boc group to give the N-protected prolinol **66**, which was treated with NaH and benzyl bromide to give the intermediate **67** in 92 % yield. Subsequent deprotection of the Boc group then gave (*S*)-2-(benzyloxymethyl) pyrrolidine **68** as an HCl salt in quantitative yield (Scheme **3.2**).



Scheme 3.3: Preparation of isatin sulfonamide **69** and ketal protected derivative **70**

Following the preparation of the amine **68**, isatin sulfonamide **69** was prepared in 83 % yield by treatment of sulfonyl chloride **64** with amine **68** in the presence of triethylamine. To avoid possible side reactions involving the reactive ketone centre in subsequent steps, it was necessary to protect ketone **69** as ketal **70**, obtained in 87 % yield from the condensation of ketone **69** with 1,3-propanediol in the presence of catalytic TsOH (Scheme **3.3**).

III.2.1. Halomethylation of Cyclopentylcarbonitrile



71 **72**

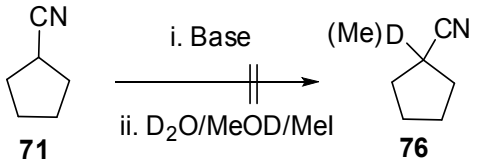
Scheme 3.4: Attempted halomethylation of cyclopentylcarbonitrile **71**.[117]

Table 3.1: Unsuccessful reaction conditions for the preparation of nitrile **72**

Entry	X	Base	Solvent	Temp (°C)	Yield (%)
1	I	LDA	THF	-78	0
2	I	LDA	THF	-60	0
3	I	NaH	THF	0	0
4	I	LDA	THF	0 to -78	0
5	Br	LDA	THF	-78	0
6	Br	LDA	THF	0	0
7	Br	LDA	PhMe	0	0

2,2-Dialkyl-3-halopropanenitriles are frequent intermediates in the synthesis of pyrimidoindolones to construct the amidine functional group. However, the preparation of these intermediates is hampered by the formation of polymeric by-products.[117] Cliffe *et al*. reported a route towards these compounds via nitrile-stabilised carbanions.[117] This involved the deprotonation of the nitrile α-proton at -65 °C using LDA as the base, followed by the addition of the anion to a mixture containing excess dihalomethane in THF.

Despite the reported high-yielding preparation of 2-cyclopentyl-3-chloropropanenitrile,[117] we encountered problems when preparing the compound **72**, the intermediate in the synthesis of our pyrimidoindolone target (Scheme **3.4**). As shown in Table **3.1**, no reaction was observed using either THF or toluene as the solvent, bromochloromethane or chloroiodomethane as the alkylating agent, LDA as the base with temperatures ranging from -78 ^{o}C to 0 ^{o}C and reaction times of 1 – 18 hours. Sodium hydride (pKa = 35 in water), which has a pKa comparable to LDA (pKa = 35 in THF) was also used as the base in a large excess at 0 ^{o}C overnight (Table **3.1**, Entry **3**). Unfortunately, only unreacted nitrile **71** was isolated from the reaction mixture. Dihalomethanes are known to form carbenoid species by the displacement of a halide following deprotonation by a strong base, which may compete with nucleophilic attack by nitrile carbanion.[118] The lack of reaction was initially attributed to dihalomethane alkylating agents undergoing deprotonation by the 1-lithiocyclopentanecarbonitrile anion or LDA under the reaction conditions, a process reported to occur readily with hindered amide bases in THF at -90 ^{o}C.[119, 120]



Scheme 3.5: Attempted deuteration/methylation of nitrile **71**

Table 3.2: Unsuccessful reaction conditions for the deuteration/methylation of nitrile **71**

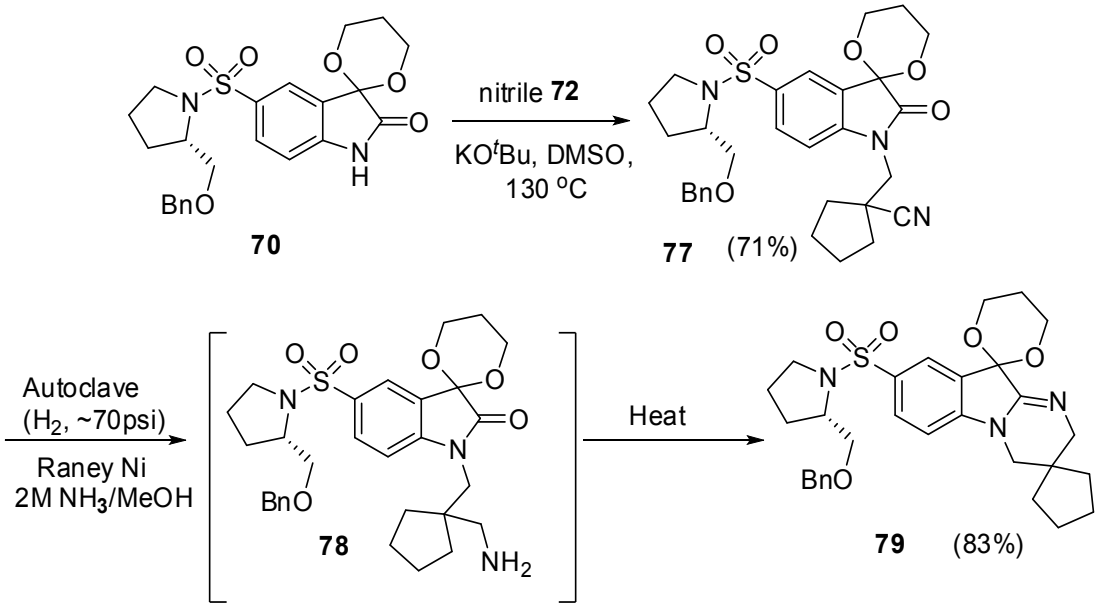
Entry	Base	Base eq.	Solvent	Temp (°C)	Time*	% D/Me incorporation
1	LDA	1	THF	-78	1-2 hrs	0
2	LDA	1	PhMe	-78	1-2 hrs	0
3	LDA	1	THF	-60	1-2 hrs	0
4	LDA	1	THF	0	1-6 hrs	0
5	LDA	1	THF	rt	1 to 18hrs	0
6	LDA	3.5	THF	rt	1 to 18hrs	0
7	NaH	1	THF	0	2 hrs	0
8	NaHMDS	1	THF	0	1 to 3hrs	0
9	NaHMDS	1	THF	rt	2 days	0
10	NaHMDS	3.5	THF	rt	3 days	0
11	$NaNH_2$	3	THF	rt	18 hrs	0

***Stirring time of a solution of the appropriate base and nitrile **71** at the stated temperature, prior to quenching with D_2O, methanol-D_4 or Me-I.

Subsequent reactions (Table **3.2**, Scheme **3.5**), designed to investigate the efficiency of nitrile deprotonation at various temperatures by treatment with a base prior to quenching with deuterium oxide, deuterated methanol or methyl iodide were undertaken. Both ^{1}H NMR and mass spectrometry of reaction samples after quenching showed no incorporation of deuterium or the methyl group to give the species **76** (Scheme **3.5**). No reaction was observed using LDA, followed by quenching at either -78 °C, -60 °C, 0 °C or room temperature, where the base-nitrile mixture was stirred for 1 - 18 hours in THF before quenching (Table **3.2**, Entries **1**, **3**, **4**, **5**). Using excess LDA made no difference to the reaction outcome (Table **3.2**, Entry **6**). Cliffe *et al*. reported toluene as a superior solvent to THF for the reaction.[117] This was attributed to toluene reducing the basicity of the carbanion so that the possible carbenoid formation from the dihaloalkane and consequent side-reactions are less likely. The reaction was consequently repeated in toluene; however no incorporation of either deuterium or a methyl group (from MeI) was observed (Table **3.2**, Entry **2**).

It became apparent that problems with the deprotonation of nitrile **71** accounted for the unsuccessful halomethylation reactions. As nitrile α-protons are known to be sufficiently acidic to be deprotonated by LDA, it was thought that the synthetic problem could stem from the stability of the carbanion formed following deprotonation of the nitrile **71**. In order to trap the apparently unstable carbanion immediately after deprotonation, a reaction was carried out in which a precooled solution of LDA was added to a solution containing both the cyclopentylcarbonitrile and excess electrophile (bromochloromethane) at -78 ^{o}C. This procedure successfully gave the desired halomethylated product **72**, though with a low yield of 24 %. ^{1}H NMR and mass spectrometry of the mixture of by-products indicated polymeric species containing several chlorine atoms, a problem reported to occur in the photochemical preparation of 2,2-dialkylethanenitrile and in the reaction of dihalomethanes with 2-arylethanenitriles.[117] A sufficient amount of the desired intermediate **72** was obtained to proceed with the synthesis of the target pyrimidoindolone probe. However, in order to prepare a library for future SAR studies of the pyrimidoindolone heterocycles, it would be necessary to improve the efficiency and yield of the 2,2-dialkyl-3-halopropanenitrile preparation.

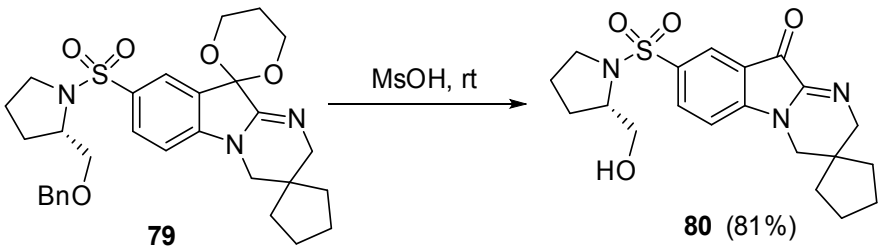
III.2.2. Pyrimidoindolone Target Probe Synthesis; Part 2



Scheme 3.6: Synthesis of Pyrimidoindolone target continued.[58]

Following the successful synthesis of the alkylating agent, 2-cyclopentyl-3-chloropropanenitrile **72**, the previously prepared ketal-protected isatin sulfonamide **70** was successfully alkylated by S_N2 nucleophilic substitution to give the corresponding nitrile **77** in 71 %

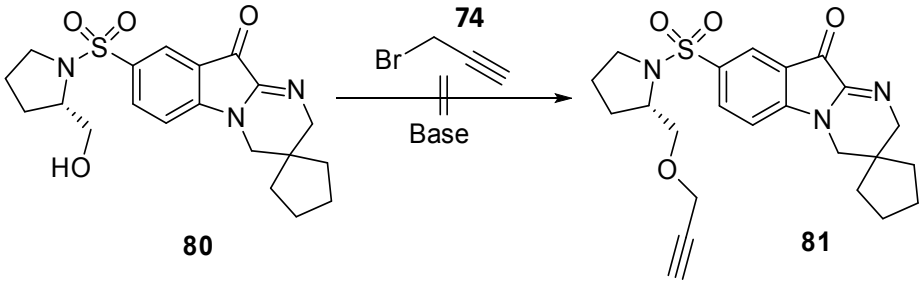
yield (Scheme **3.6**). The next step involved the reduction of the nitrile group to a primary amine which would then undergo intramolecular dehydration/cyclisation to give the amidine ring **79**. An initial reduction attempt using catalytic Raney Ni at atmospheric pressure for up to 2 days was unsuccessful. Nitrile reduction was ultimately achieved using an autoclave at a pressure of ~70 psi and a very dilute solution. An autoclave was required to increase pressure and therefore concentration of hydrogen gas in the reaction mixture, while a dilute solution prevented intermolecular reactions which may compete with the subsequent desired intramolecular cyclisation. Amidine **79**, was isolated from the hydrogenation reaction mixture as the major product and the intermediate primary amine **78** as the minor product. Filtration to remove the Raney Ni catalyst and heating the reduction reaction mixture fully converted primary amine **78** to amidine **79**, with a total yield of 83 % (Scheme **3.6**).



79 **80** (81%)

Scheme 3.7: Full deprotection reaction of amidine **79**.[58]

In the next step, the fully deprotected structure **80** was obtained in 81 % yield by the treatment of amidine **79** with methanesulfonic acid, resulting in the acid-catalysed removal of the benzyl ether and ketal hydrolysis (Scheme **3.7**). Introduction of a propargyl group by the O-alkylation of alcohol **80** would have then completed the synthesis of the radiochemistry alkyne precursor **81** (Scheme **3.8**). However, attempts to O-alkylate alcohol **80** using propargyl bromide **74** under several reaction conditions failed to give the desired alkyne precursor **81** (Scheme **3.8**, Table **3.3**).

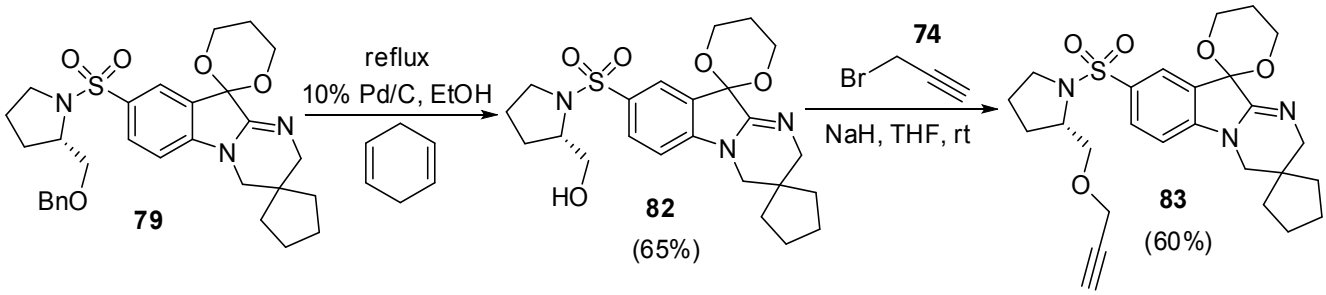


Scheme 3.8: Attempted alkylation of alcohol **80** with propargyl bromide

Table 3.3: Attempts at the preparation of alkyne **81**

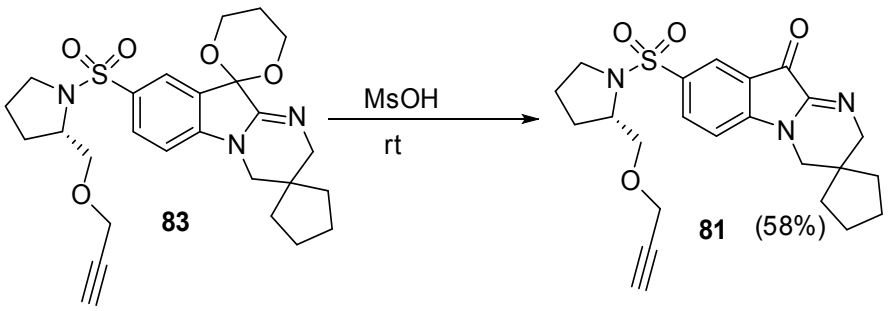
Entry	Base/ Catalyst	Solvent	Temp (^oC)	Time	Observation
1	KOH	THF	rt	5-18 hrs	No reaction
2	KOH	DMF	rt	10 mins	Decomposition
3	NaH	THF	rt	4-12 hrs	No reaction
4	NaH	DMF	rt	5-10 mins	Decomposition
5	K_2CO_3	Acetone	reflux	12 hrs	Unknown product
6	NaH / Bu_4NI	THF	rt	18 hrs	No reaction
7	NaH / Bu_4NI	THF	reflux	2 hrs	Decomposition
8	K_2CO_3/ Bu_4NI	THF	rt	3 days	No reaction
9	Cs_2CO_3	Propargyl bromide/ Acetone	reflux	18 hrs	Decomposition

As shown on **Table 3.3**, in general, no reaction was observed when the alcohol **80** was treated with base (KOH, NaH, or NaH/Bu_4NI, K_2CO_3/ Bu_4NI) in THF at room temperature which was attributed to the limited solubility of the various bases in THF (Table **3.3**, Entries **1**, **3**, **6**, **8**). However, heating the THF reaction mixture to reflux led to the decomposition of the starting material (Table **3.3**, Entry **7**). The use of catalytic amounts of Bu_4NI in an attempt to improve the reactivity of the electrophile was unsuccessful (Table **3.3**, Entry **3** Vs **6**). Reactions in DMF at room temperature quickly led to the decomposition of the starting material with either KOH or NaH as the base (Table **3.3**, Entries **2**, **4**). Repeating the reaction in acetone using K_2CO_3 and heating to reflux for 12 hours gave an unknown product (Table **3.3**, Entry **5**), while the use of Cs_2CO_3, a more soluble base than K_2CO_3 in acetone, and a large excess of propargyl bromide led to complete decomposition (Table **3.3**, Entry **9**).



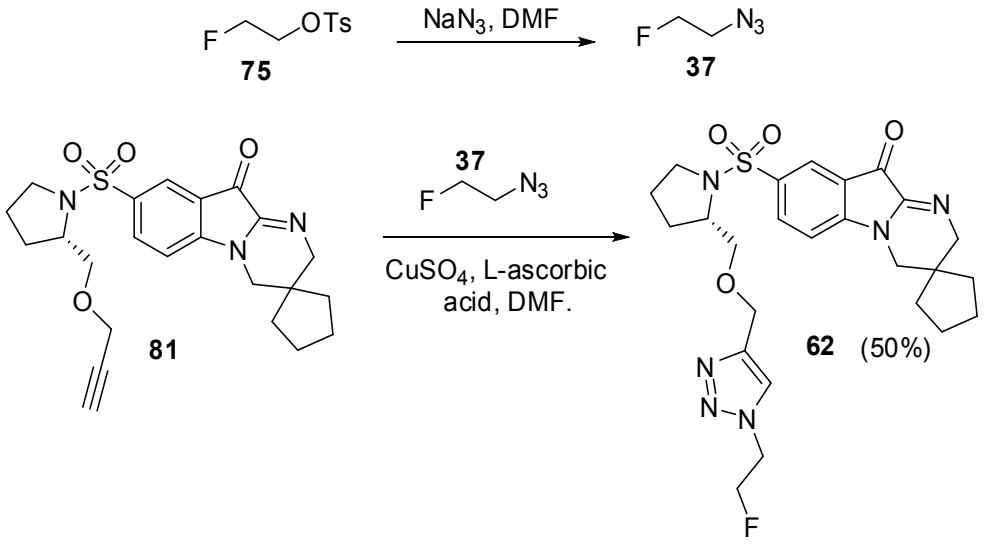
Scheme 3.9: Successful alkylation of ketal **82** to yield alkyne **83**

The unsuccessful reactions were attributed to the presence of a reactive electrophilic ketone in the pyrimidoindolone ring system of intermediate **80**. It was possible that the anion produced upon deprotonation of the alcohol group of **80** reacted faster with the highly electrophilic ketone than with propargyl bromide, ultimately resulting in decomposition. On the basis of this, we felt that that alkylation with propargyl bromide would be successful if the ketone was protected. Hence the alcohol **82** was prepared from the fully protected intermediate **79** using transfer hydrogenation with palladium in the presence of 1,4-cyclohexadiene to achieve the selective deprotection of the benzyl group (Scheme **3.9**). Ketal-protected alcohol **82** was successfully alkylated in THF at room temperature using NaH to give the desired alkyne **83** in 60 % yield (Scheme **3.9**).



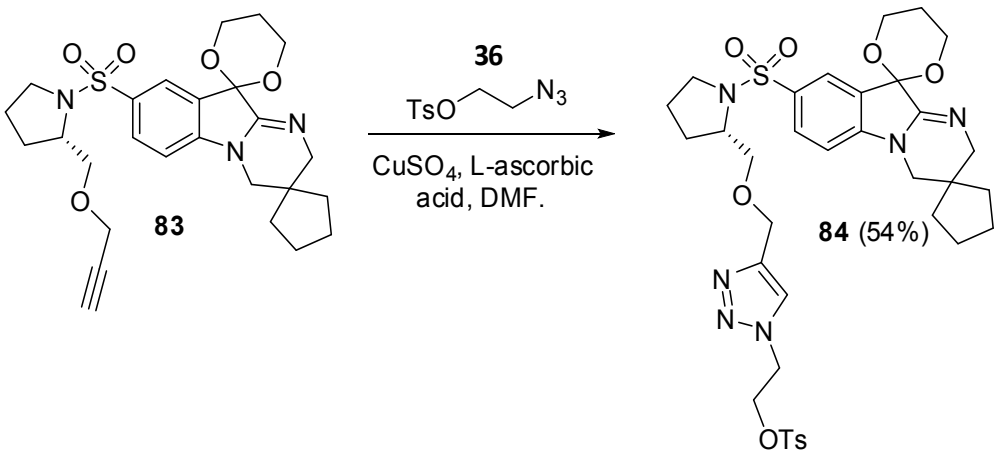
Scheme 3.10: Preparation of the precursor alkyne **81** for radiolabelling by click reaction

Subsequent ketal deprotection of alkyne **83** by treatment with methanesulfonic acid gave the radiochemistry precursor, as well as the unradiolabelled pyrimidoindolone reference precursor **81** in 58 % yield (Scheme **3.10**).



Scheme 3.11: Preparation of the pyrimidoindolone **62** cold reference by click chemistry

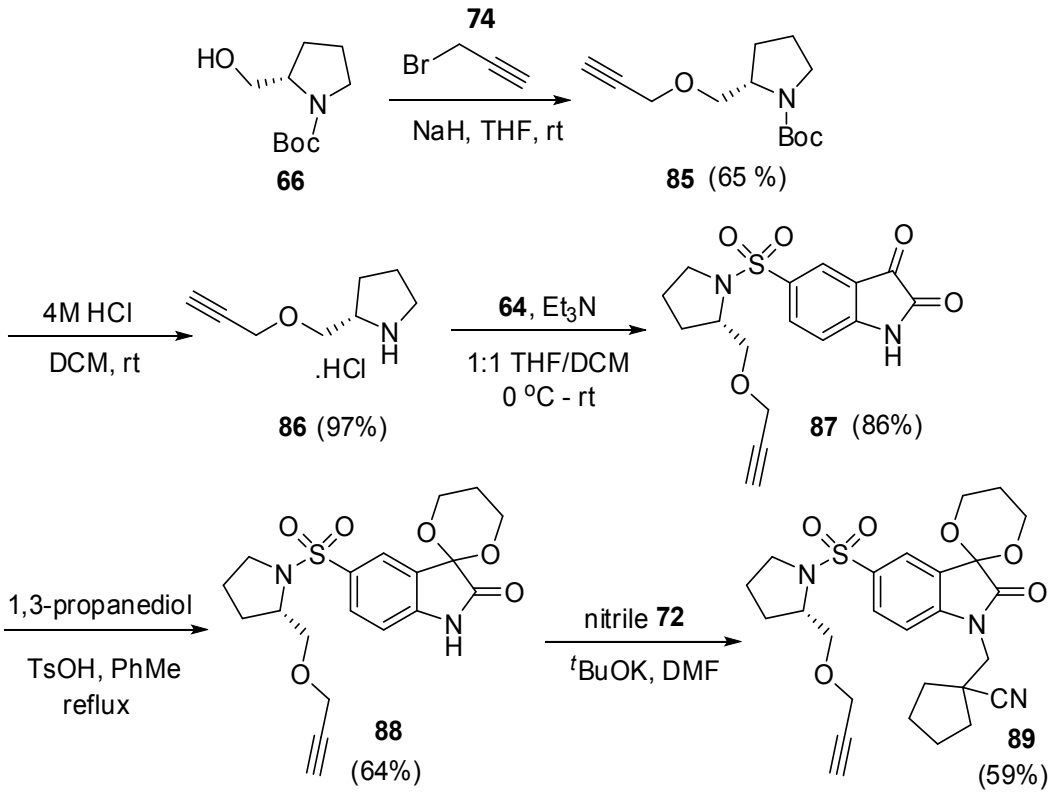
To synthesise the target pyrimidoindolone cold reference, alkyne **81** was used in a 'click' reaction, a copper catalysed azide-alkyne cycloaddition between an azide and a terminal alkyne to give a 1,2,3-triazole (Scheme **3.11**).[121] The unradiolabelled target compound **62** was obtained in the moderate yield of 50 %. For radiolabelling, alkyne **81** would be used along with [^{18}F]-fluoroethylazide **37** to give the radiolabelled target pyrimidoindolone probe [^{18}F]**62**, as described in the next section.



Scheme 3.12: Preparation of tosyl radiochemistry precursor **84**

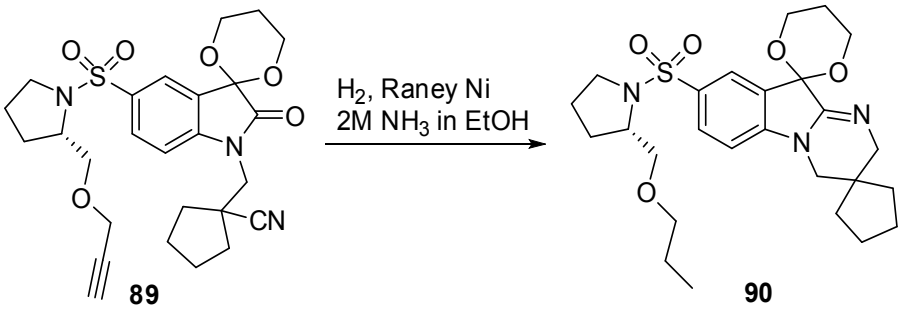
We also intended to explore radiolabelling by direct nucleophilic displacement with [^{18}F]fluoride. The tosyl triazole precursor **84** to be radiolabelled by nucleophilic displacement using [^{18}F]fluoride was therefore prepared from the copper catalysed click reaction with tosylethylazide **36** and ketal-protected alkyne **83** (Scheme **3.12**). This precursor **84** was used to obtain the radiolabelled target compound **62**, as described below in section **III.3**.

III.2.2.1. Exploring a Different Route to the Pyrimidoindolone Target



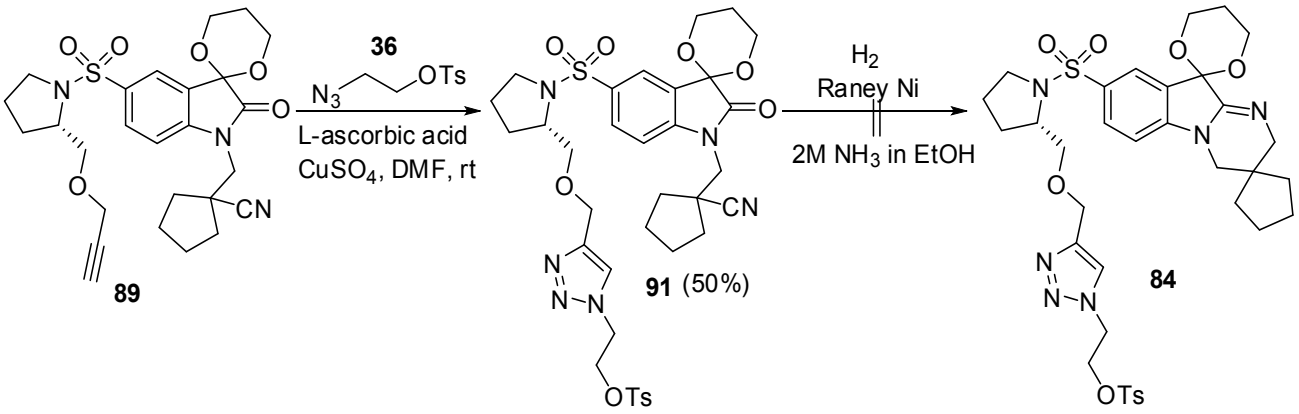
Scheme 3.13: Target pyrimidoindolone synthesis via an alternative route

In an attempt to improve the efficiency and yield of the target pyrimidoindolone synthesis, the developed route was approached in a different order but using identical reagents and reactions. This alternative route involved incorporation of the alkyne group earlier in the sequence (Scheme **3.13**). Starting from *N*-Boc-prolinol **66**, the alcohol moiety was alkylated with propargyl bromide **74** in 65 % yield, followed by Boc deprotection to give the desired amine **86** in quantitative yield. Coupling of amine **86** with sulfonyl chloride **64** led to isatin sulfonamide **87** in 86 % yield. Subsequent ketone protection as ketal **88** in 64 % yield, and amide alkylation with carbonitrile **72** using the same reactions described above for the preparation of intermediate **77** gave the amide alkylated isatin sulfonamide **89** in 59 % yield.



Scheme 3.14: Raney Ni reduction of intermediate **89**

Unfortunately, attempts to selectively reduce nitrile **89** in the presence of the alkyne group, using Raney Ni resulted in the full reduction of both the alkyne and nitrile group, giving the ether **90** (Scheme **3.14**).

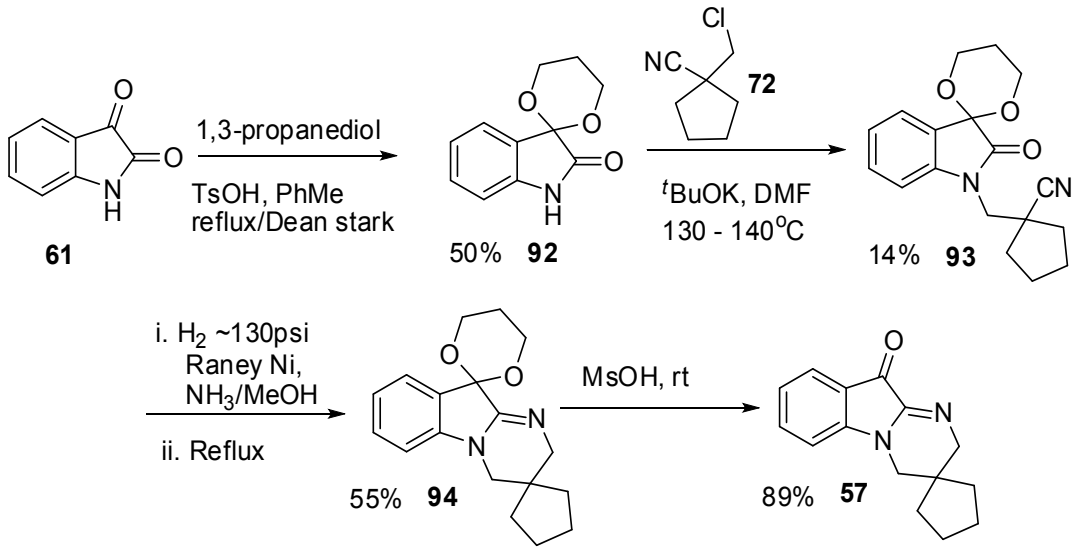


Scheme 3.15: Click reaction of intermediate **89** prior to Raney Ni reduction

To avoid the problem of non-selective reduction, a click reaction was carried out with alkyne **89** prior to nitrile reduction (Scheme **3.15**). The copper-catalysed click reaction of alkyne **89** with tosylazide **36** successfully gave 1,2,3-triazole **91** in 50 % yield. Unfortunately, Raney Ni reduction gave a mixture containing unreacted tosylate **91**, as the minor component and an unknown by-product with the tosylate group displaced according to a ^{1}H NMR spectrum (Scheme **3.15**).

In addition to problems encountered with nitrile reduction in the presence of other functional groups, the successful steps did not show any improvements on yields and reaction efficiency. As a result, pyrimidoindolone target synthesis via this alternative route was terminated, progressing with the original route described above.

III.2.2.2. Synthesis of the Pyrimidoindolone Core Heterocycle / Pharmacophore



Scheme 3.16: Preparation of the pyrimidoindolone **57**

Pyrimidoindolone heterocycle **57**, used in the UV-vis experiment described in Chapter **II** was prepared simultaneously with the target pyrimidoindolone probe **62**, in five steps starting with the commercially available isatin ring **61**. Isatin **61** was protected as a 1,3-dioxolane using 1,3-propanediol and toluenesulfonic acid in toluene to give the ketal **92** in 50 % yield. The ketal **92** was then alkylated with chloromethyl cyclopentanecarbonitrile **72** using ^{t}BuOK as a base to give nitrile **93** in 14 % yield and with less than 80 % purity. This reaction step failed to reach completion, with both the starting amide **92** and alkylating agent **72** isolated from the reaction mixture despite prolonged heating for up to three days, and using excess amounts of the base and alkylating agent. Unlike the facile amide-alkylation of the sulfonamide substituted isatin ring **70**, alkylation of the unsubstituted ring **92** proved challenging. It was likely that the presence of an electron withdrawing substituent on the phenyl ring, such as a sulfonamide was required to activate the ring towards electrophilic substitution. Reduction of the crude nitrile **93** using Raney Ni as a catalyst and methalonic ammonia as the solvent gave the primary amine which was subsequently heated to drive cyclisation/dehydration to give the amidine **94** in 55 % yield. Ketal deprotection using methanesulfonic acid then gave the pyrimidoindolone heterocycle **57** in 89 % yield (Scheme **3.16**).

III.3. Radiochemistry of the Pyrimidoindolone Target

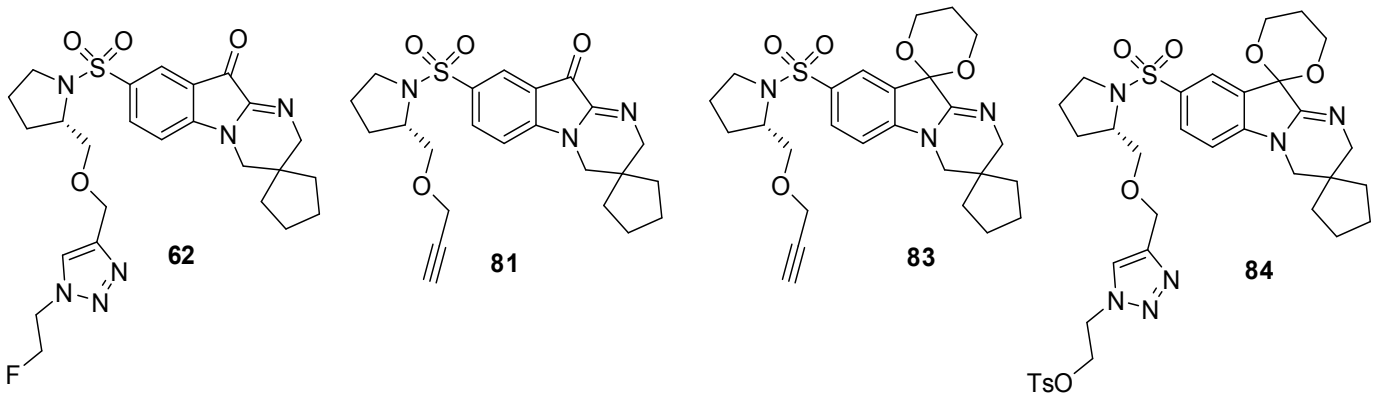
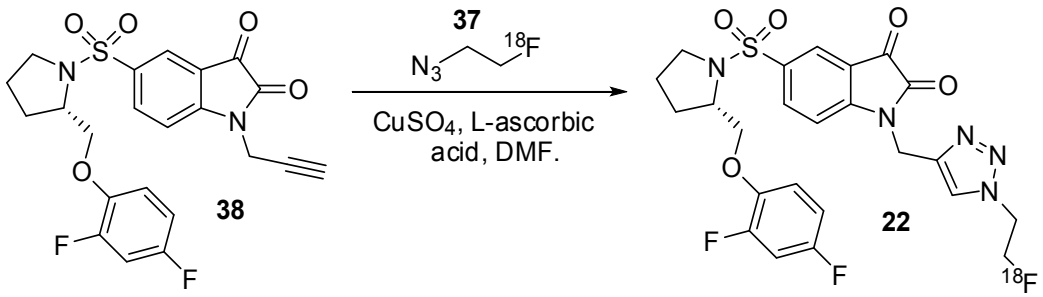


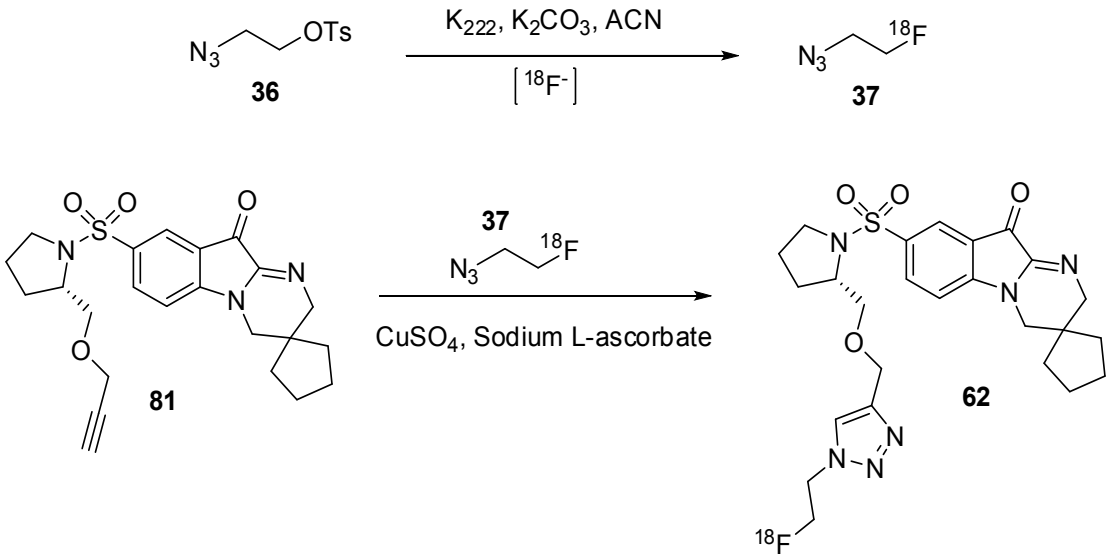
Figure 3.4: Pyrimidoindolone radiochemistry precursors (**81**, **83 and 84**) and the cold reference (**62**)

In a direct attempt to mimic the original isatin radiochemistry reported by Smith *et al*. (Scheme **2.17**),[57] radiolabelling using the copper catalysed click reaction of an alkyne precursor with [^{18}F]fluoroethylazide **37**, was initially employed for the pyrimidoindolone radiosynthesis.



Scheme 2.17: Reported click radiolabelling of the lead isatin sulfonamide **22**[57]

The first stage in the click radiosynthesis of pyrimidoindolone **62** (Scheme **3.18**) was aimed at exploring a range of reaction conditions in attempts to find the optimum condition for the radiolabelling procedure. The radiolabelling agent, [^{18}F]fluoroethylazide **37** was prepared from tosylethylazide **36** using Kryptofix-222 as a phase transfer agent and K_2CO3 as the base (Scheme **3.18**). The reaction mixture was purified by distillation using a thermospray with varying and inconsistent radiochemical yields obtained, likely due to inconsistencies in cleaning the thermospray. The possible effects of the solvent used, reaction temperature, reaction time and the presence of a ligand were investigated, monitoring the reactions by reverse-phase HPLC. The observed results are summarised in Table **3.4**.



Scheme 3.18: Click radiolabelling with precursor alkyne **81**

Table 3.4: Click radiolabelling reaction results observed by analytical HPLC

Entry	Time (mins)	Temp ^{O}C	% [^{18}F] (RC) incorporation*	
			DMF	DMSO
1	5	rt	-	10
2	10	rt	34	17
3	15	rt	32	29
4	5	rt + BPDS**	49	4
5	10	rt + BPDS	51	24
6	15	rt + BPDS	48	33
7	30	rt + BPDS	60	28
8	5	50	65	78
9	10	50	58	64
10	15	50	56	46
11	30	50	46	51
12	5	84	74	39
13	10	84	52	54
14	15	84	36	49
15	36	84	19	34

*% of total radioactivity incorporated to give the radioactive product [^{18}F]**62**, determined by analytical reverse-phase HPLC. **BPDS ligand (Figure **3.5**) added to the reaction mixture.

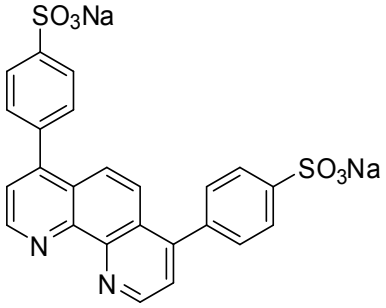


Figure 3.5: The Structure of bathophenanthroline disulfonate (BPDS), a Cu(I) stabilising ligand

Slow reactions were observed at room temperature with modest amounts of [^{18}F]fluoride incorporation (Table **3.4**, Entries **1 – 3**). Although the starting copper reagent was Cu(II) sulfate, the active metal catalyst in a click reaction is known to be Cu(I) formed from *in situ* reduction of Cu(II) by ascorbic acid. Any oxygen in the reaction mixture would act to oxidise Cu(I) back to Cu(II), hindering the reaction. In attempts to enhance the click reaction, the Cu(I) stabilising ligand, BPDS (Figure **3.5**) was employed.[122] However, the addition of BPDS had no effect on the reactions carried out at room temperature in DMSO (Table **3.4**, Entries **4 – 7**). BPDS addition initially enhanced the DMF reaction but negligible increases in the percentage of [^{18}F]fluoride incorporation were observed with time (Table **3.4**, Entries **4 – 7**). When heated to 50 ^{o}C, both solvents showed initial fast reaction followed by the gradual decomposition of both the radiolabelled product [^{18}F]**62** and the alkyne precursor **81** (Table **3.4**, Entries **8 – 11**). At 84 ^{o}C, faster reaction was observed in DMF within the first five minutes (Table **3.4**, Entry **12**). However, faster decomposition in DMF gave lower overall yield over time (Table **3.4**, Entries **12 – 15**). It was clear from the radiochemical chromatograms that the radioactive product decomposes to give an unknown radioactive compound. This decomposition became more significant at higher temperatures where the product peak area decreases as the peak for the unknown compound increases. Of the results summarised in Table **3.4**, the highest yield was observed in DMSO at 50 ^{o}C for five minutes (Entry **8**). These conditions were adopted for the preparation and isolation of the radiolabelled product by preparative reverse-phase HPLC (Table **3.5**).

Table 3.5: Click reaction results observed by prep HPLC

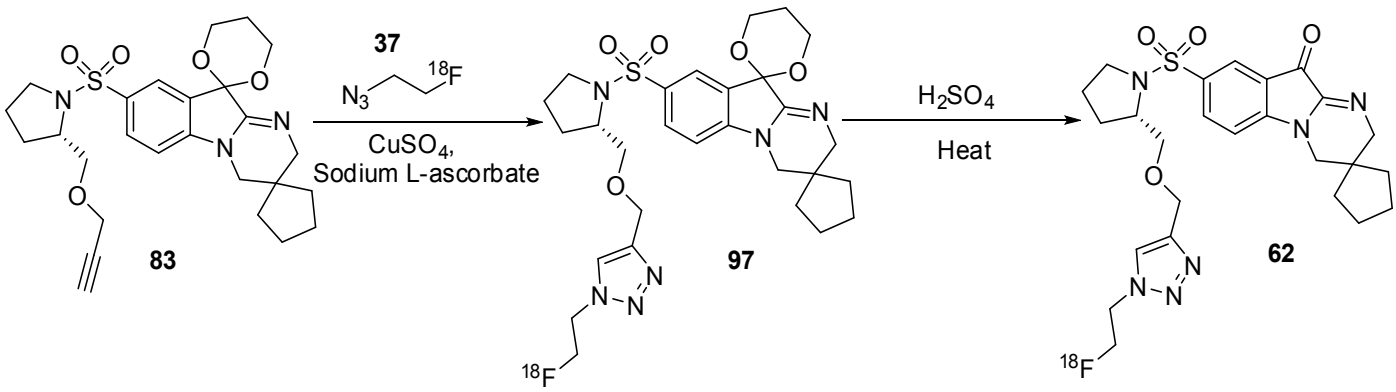
Entry	Time (mins)	Solvent (50 µL)	Temp ^{o}C	% [^{18}F] (RC) incorporation*
1	5	DMSO	50	8
2	7	DMSO	50	6
3	17	DMSO	50	6
4	10	DMF	50	21
5	5.5	DMF	80	29
6**	5	DMF	80	42

***** % of total radioactivity incorporated to give the radioactive product [^{18}F]**62**, determined by preparative reverse-phase HPLC

****** With the ketal-protected alkyne **83** used as the precursor i.e. the reaction shown in Scheme **3.19**

However, the high incorporation of radioactivity observed could not be replicated on a larger scale for the isolation of the radiolabelled product (Table **3.5**, Entries **1 – 3**). The same disappointing result was observed in DMF at 50 ^{o}C and 80 ^{o}C (Table **3.5**, Entries **4** - **5**). In addition to the poor radiochemical incorporation, product [^{18}F]**62** co-eluted with a stable but unknown by-product, giving

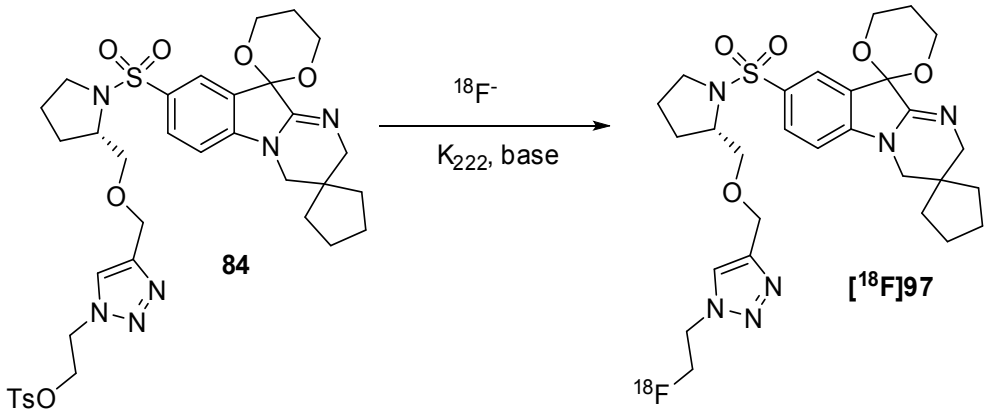
the probe in a crude mixture that could not be purified by prep HPLC. A similar problem with isatin sulfonamide 'click' radiolabelling was reported by Glaser & Co, where the desired product also co-eluted with a by-product that had an almost identical retention time.[123] The amount of impurity observed in the isolated radio-product mixture was especially significant with low levels of radiochemical incorporation. We observed from the synthesis of the pyrimidoindolone cold reference that the ketone moiety, when not protected had the propensity to react to give unwanted products. Hence, we proceeded to use the ketal-protected alkyne precursor **83** in click radiolabelling with the hope of improving the purity profile of the pyrimidoindolone radio-probe (Scheme **3.19**).



Scheme 3.19: Click radiolabelling with ketal-protected precursor alkyne **83**

Consequently, click radiolabelling reaction was attempted with ketal-protected alkyne **83** as the precursor (Scheme **3.19**). While a comparatively better result was observed (Table **3.5**, Entry **6**), a modest radiochemical incorporation of 42 % was obtained. This modest yield, combined with incomplete ketal deprotection upon treatment of the reaction mixture with sulfuric acid, resulted in a poor overall yield. Increasing the reaction time in order to achieve complete ketal deprotection resulted in radiochemical decomposition, further decreasing the overall yield. Although improved, co-eluting impurities remained problematic. In addition, the click reaction proved irreproducible with yields ranging from 0 % to 42 % radiochemical incorporation under analogous conditions.

Following the irreproducible results and impurities observed for the click process, radiolabelling by direct $^{18}F^-$ S_N2 displacement of a tosylate was examined, adopting the reaction shown in Scheme **3.20**. The results observed under different reaction conditions by analytical HPLC are summarised in Table **3.6** below.



Scheme 3.20: Radiolabelling by $^{18}F^-$ displacement of a tosyl leaving group

Table 3.6: $^{18}F^-$ tosyl displacement radiolabelling results observed by analytical HPLC

Entry	Time	Solvent (μL)	Temp (^oC)	Base	% [^{18}F] (RC) incorporation*
1	5	DMF (100)	80	K_2CO_3	14
2	10	DMF (100)	80	K_2CO_3	29
3	15	DMF (100)	80	K_2CO_3	30
4	20	DMF (100)	80	K_2CO_3	40
5	5	DMF (100)	110	$KHCO_3$	22
6	10	DMF (100)	110	$KHCO_3$	26
7	15	DMF (100)	110	$KHCO_3$	36
8	20	DMF (100)	110	$KHCO_3$	37
9	5	DMF (100)	110	K_2CO_3	63
10	10	DMF (100)	110	K_2CO_3	76
11	10	DMF (150)	110	K_2CO_3	36

*% of total radioactivity incorporated to give intermediate ketal [^{18}F]**97** as determined by analytical HPLC

Table **3.6** shows the percentage radiochemical incorporation giving the intermediate ketal-protected intermediate, [^{18}F]**97**. Again the effects of reaction time and temperature, as well as concentration were examined. As shown in Table **3.6**, increasing the reaction temperature from 80 ^oC to 110 ^oC significantly increased the radiochemical yield when K_2CO_3 was used as the base (Table **3.6**, Entries **2** and **10**). The precursor tosylate was consumed via the desired reaction as well as by decomposition within ten minutes at all temperatures examined. The observed decomposition was likely due to side reactions with residual water or chloride from the [^{18}F]fluoride mixture generated from a cyclotron, or tosyl elimination to give the corresponding alkene which was reportedly observed during the radiosynthesis of [^{18}F]isatin **22**.[123]

At 80 ^{o}C, precursor decomposition was faster than the desired reaction, while using $KHCO_3$ as the base resulted in both faster radiochemical and precursor decomposition. $KHCO_3$ (pKa = 6.37) being much less basic than K_2CO_3 (pKa = 10.25) may have been less efficient at neutralising the reaction, leading to increased side reactions. Aiming to examine the effect of concentration on the reaction, where the solvent volume was increased from 100 µL to 150 µL, the obtained radiochemical incorporation suggested that decomposition of the precursor tosylate **84** was faster with a more dilute reaction mixture (Table **3.6**, Entries **10** and **11**). The possible consumption of the precursor tosylate **84** by side reactions with other nucleophiles such as water and chloride was counteracted by the use of a large excess of the precursor. The procedure of radiolabelling by S_N2 [^{18}F]fluoride displacement of the tosylate group generally gave significantly improved purity profile (95 – 100 %), compared to the click labelling process as there was no co-eluting by-product.

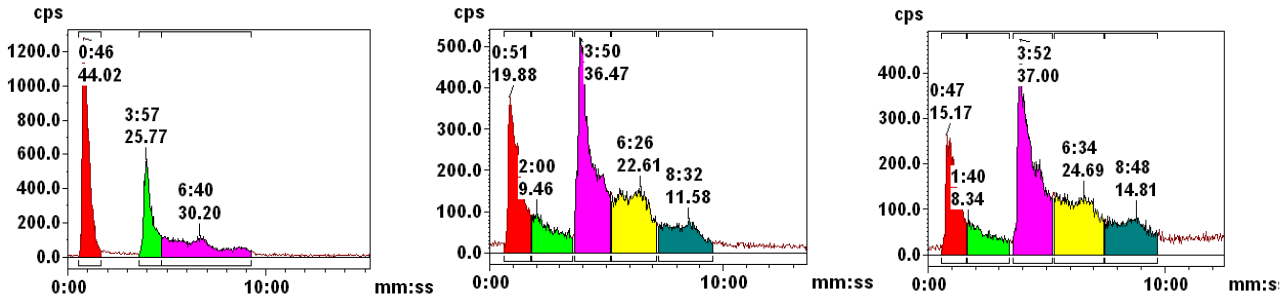


Figure 3.6: Radiolabelling reactions with $KHCO_3$ as the base in DMF at reaction times of 10 mins (left), 15 mins (middle) and 20 mins (right), showing increased decomposition with time (Table **3.6**, Entries **6**, **7** and **8**). The radiolabelled ketal-protected intermediate [^{18}F]**97** is shown on the chromatograms at 3:52 to 3:57 mm:ss. Chromatograms were obtained by reverse-phase HPLC elution.

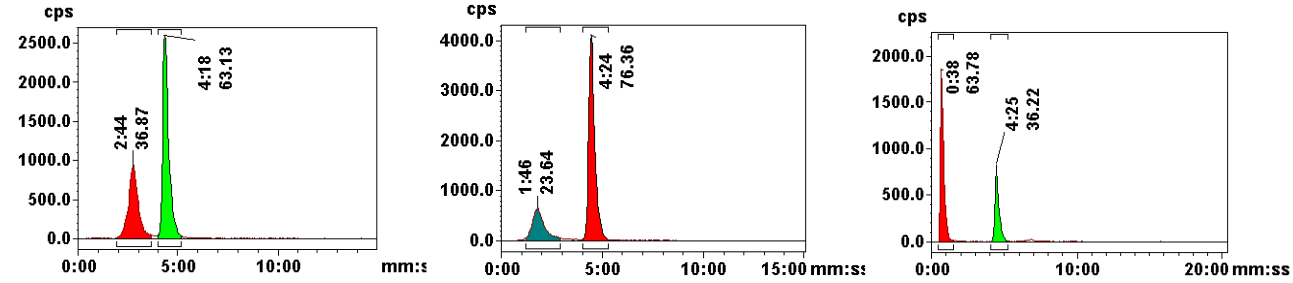
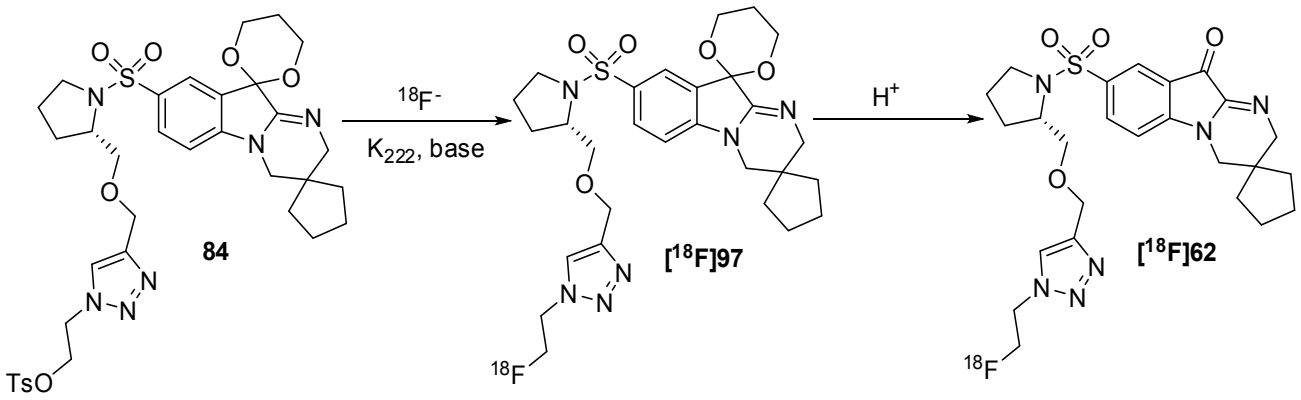


Figure 3.7: Radiolabelling reactions with K_2CO_3 as the base in DMF at reaction times of 5 mins (left) and 10 mins (middle), showing increased radiochemical yield of [^{18}F]**97** shown on the chromatograms at around 4 minutes (Table **3.6**, Entries **9** and **10**). The chromatogram on the right shows the result of a diluted mixture with a reaction time of 10 mins, showing poor radiochemical yield of [^{18}F]**97** (Table **3.6**, Entry **11**). Chromatograms were obtained by reverse-phase HPLC elution.



Scheme 3.21: Acid catalysed ketal deprotection following radiolabelling by tosyl displacement

Hydrochloric acid was initially employed for ketal deprotection of the radioactive intermediate [^{18}F]**97** to give the target probe [^{18}F]**62**, monitoring the disappearance of the ketal intermediate by analytical HPLC. The deprotection reaction involved diluting the [^{18}F]fluoride displacement reaction mixture with a 3M HCl solution and heating to 110 ^{o}C. In this case, slow and incomplete deprotection was observed despite increasing the HCl concentration to 5M and the reaction time to 30 mins. A moderate 50 % deprotection was obtained using 5M HCl and heating at 110 ^{o}C for 30 mins. Diluting with sulfuric acid drove ketal deprotection to completion within 10 mins at the same temperature. Unfortunately, problems with product isolation were encountered during neutralisation of the sulfuric acid mixture with 3N to 6N NaOH solution. The semi-prep HPLC ^{18}F chromatogram of the mixture showed broad, unseparated peaks. Solid-phase extraction, where the product was immobilised on a C-18 cartridge and eluted with ACN, then with 5 mM HCl in EtOH, gave a much improved semi-prep HPLC profile with product isolation. However, this method resulted in poor radiochemical yield due to incomplete elution of the lipophilic product, and/or loss of the protonated product in acidic aqueous mixture, given that the pH of the reaction mixture was 4 or less. Attempts to quench the reaction mixture to a more basic pH resulted in decomposition of the product probe. Isatin sulfonamides demonstrated similar instability under basic conditions owing to the reaction of a base with the electrophilic ketone group (Chapter **I.4.2**).[83] Gradual addition of the base to the acidic mixture to obtain the ideal pH of 5-6 was unsuccessful because of the large and rapid pH change encountered at the equivalence point when adding a strong base to a strong acid.

As a result of the problems encountered with product isolation from the sulfuric acid mixture, deprotection using HCl was re-visited, because neutralisation of the weaker HCl acid could be more easily controlled to reach an ideal pH of 5/6. The slow rate of deprotection with HCl was addressed by investigating the effect of changing the reaction solvent from DMF or DMSO to ACN. Using ACN,

low to moderate radiochemical incorporation of 10 – 45 % was observed. Again, similarly to reactions in DMF/DMSO, the degree of ketal deprotection in a one-pot reaction using 4M – 5M HCl and heating for 15 mins at 100 – 120 ^{o}C was disappointing, consistently giving less than 50 % conversion of the ketal intermediate [^{18}F]**97** to target probe [^{18}F]**62** after 30 minutes. In successive reactions, it was found that the deprotection rate was significantly increased by removing ACN solvent by distillation prior to the addition of HCl. This resulted in a deprotection yield of 70 – 85 % within 15 minutes at 110 ^{o}C (Figure **3.9**). Similarly to deprotection reactions using sulfuric acid, lack of HPLC peak separation was observed, though this problem was solved by phase separation. Immobilisation of the NaOAc neutralised HCl reaction mixture on a C-18 cartridge, washing with water and then eluting the product probe with ethanol gave a sample that was successfully separated by prep HPLC to give the target probe in high purity (Figure **3.9**). A radiochemical yield of 22 % (decay-corrected, 130 mins reaction time) was obtained for biological characterisation. The chromatograms of the reaction conditions used for radiosynthesis prior to biological characterisation are shown in Figures **3.8** and **3.9** with the reaction conditions summarised in the Experimental chapter.

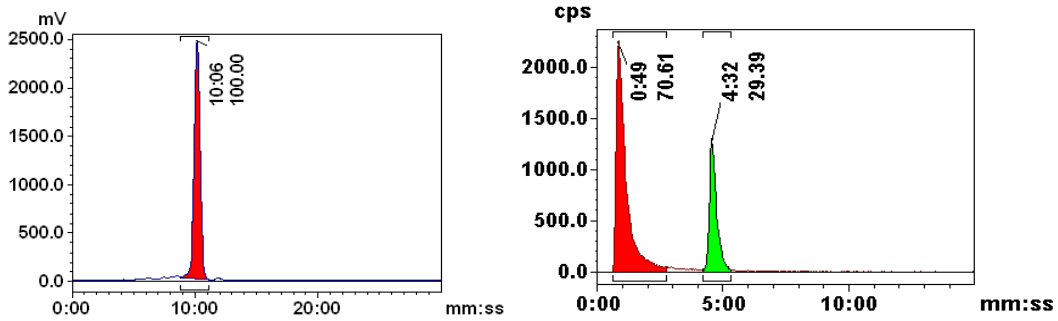


Figure 3.8: Left - semi-prep HPLC chromatogram of the cold reference of the target probe **62**. Right – analytical HPLC chromatogram showing the reaction mixture in ACN, 110 ^{o}C, 15 mins reaction time with 29% radiochemical incorporation to give the intermediate [^{18}F]**97** (at 4:32 mm:ss)

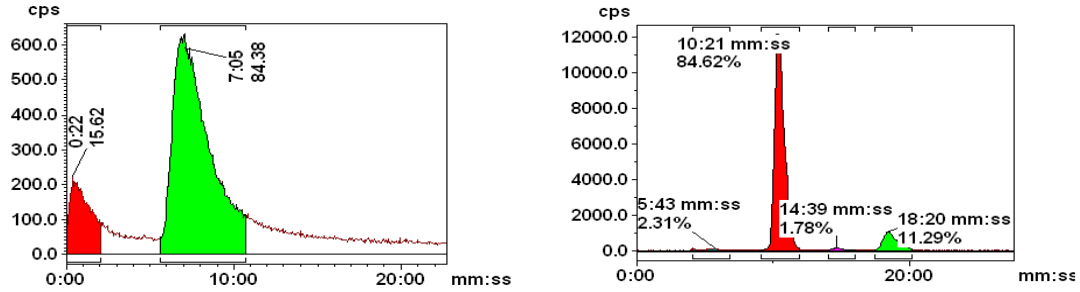


Figure 3.9: Semi-prep HPLC chromatograms of ACN reaction mixtures following acid deprotection and neutralisation. Left – chromatogram of the ketal deprotection reaction mixture without phase separation using a C-18 cartridge, showing broad peaks. Right – a prep HPLC chromatogram of the ketal deprotection reaction mixture with clear peak separation following phase separation with a C18 cartridge - with 85 % conversion of the ketal intermediate [^{18}F]**97** (at 18:20 mm:ss) to the target probe [^{18}F]**62** at 10:21 mm:ss.

III.4. Biological Characterisation of the Pyrimidoindolone Target

III.4.1. *In vitro* Caspase Enzyme Inhibition Assay

Table 3.7: Pyrimidoindolone Caspase IC_{50} Data[c]

Incubation Time (mins)	Caspase-3 IC_{50} (nM)		Caspase-8 IC_{50} (nM)	
	Pyrimido **62**	Isatin **22**	Pyrimido **62**	Isatin **22**
15	108.90	13.43	>5000	>5000
30	78.19	1.86	>5000	>5000
60	118.80	5.72	>5000	>5000
90	95.83	3.98	>5000	>5000
Mean ± SEM	**100.43 ± 8.78**	**6.25 ± 2.52**	**-**	**-**

The potency of pyrimidoindolone **62** for caspase-3 and control caspase-8 was determined by measuring the substrate concentration required to inhibit each enzyme activity by 50 % (IC_{50}). For IC_{50} determination of pyrimidoindolone **62** Vs lead isatin **22**, nine substrate concentrations ranging from 5 pM to 500 µM were used, measuring the accumulation of the fluorogenic product 7-amino-4-methylcoumarin (7-AMC) resulting from cleavage of caspase enzyme substrate Ac-DEVD-AMC by uninhibited activated caspase. 7-AMC production was measured by a fluorimetric method following incubation at 15, 30, 60 and 90 mins. The results are summarised above in Table **3.7**. Isatin **22** shows an average of 16-fold more affinity for caspase-3 than the pyrimidoindolone **62**. Both probes were shown to be poor substrates for caspase 8, showing selectivity for caspase-3.

III.4.2. *In Vitro* Cell Uptake Studies[d]

Cell uptake studies of the pyrimidoindolone tracer **62** was also carried out in control, PAC-1 (first procaspase activating compound) and 4-HC (4-hydroperoxycyclophosphamide) treated cells. The studies involved inducing apoptosis in cancer cells by treatment with anticancer agents prior to measuring cell uptake of the pyrimidoindolone probe resulting from the tracer binding to activated caspase-3. Like isatin sulfonamides, the probe was designed to be taken up by intact cells, but only retained in cells with activated caspase-3. Without the induction of caspase-3 (and therefore apoptosis), pyrimidoindolone tracer retention in cells would not be observed. It also follows that the observation of pyrimidoindolone uptake following the induction of apoptosis would successfully indicate that the probe is a caspase-binding ligand. The aim of the cell uptake studies was to first

[c]Data reported by Dr. Quang-De Nguyen who carried out the *in vitro* caspase inhibition experiment

[d] The cell uptake experiment was conducted by Dr Quang-De Nguyen, Imperial College London.

assess the caspase-binding properties of the synthesised pyrimidoindolone probe **62** before proceeding to *in vivo* studies.

The uptake of pyrimidoindolone **62** was measured approximately 24 hours after the treatment of cells with PAC-1 and 4-HC. PAC-1 is a compound (Figure **3.10**) that induces apoptosis via the selective and direct activation of the executioner caspase-3.[124] Caspase-3 is stored in cells as the inactive procaspase-3 which is inhibited by low levels of zinc. PAC-1 has been shown to activate procaspase-3 by chelating zinc and therefore releasing the zinc-mediated inhibition, converting inactive procaspase-3 to the active caspase-3, which then induces a cascade of events that lead to cell death.[124]

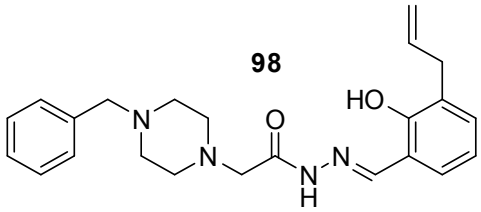
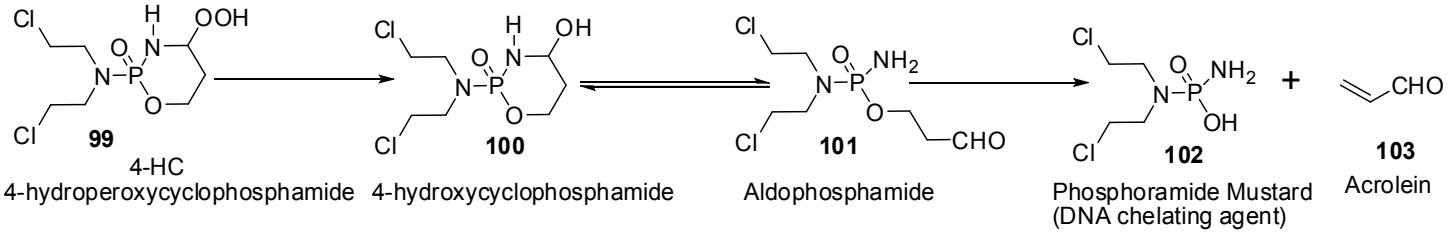


Figure 3.10: The chemical structure of PAC-1, anticancer caspase-activating agent

Whereas PAC-1 is a direct activator of caspase-3, 4-HC indirectly activates caspase-3 through the formation of metabolites that cause DNA damage, thus inducing cell death.[125] 4-HC **99**, a pre-activated form of cyclophosphamide is an anticancer agent which converts to 4-hydroxycyclophosphamide **100**, which is at equilibrium with the open-ring aldophosphamide **101** when in solution.[126, 127] Aldophosphamide **101** then generates the active alkylating metabolite, phosphoramide mustard **102** which alkylates DNA strands (Scheme **3.22**).[126, 127] The resulting DNA interstrand crosslinks and DNA damage then triggers apoptotic cell death involving prolonged cell-cycle arrest.[125]



Scheme 3.22: The formation of DNA chelating mustard from 4-HC[126]

In contrast to PAC-1 which has a more immediate effect on apoptotic induction through the direct activation of caspase-3, 4-HC indirectly induces apoptosis via a prolonged cell-cycle dependent pathway which means it activates caspase-3 at a much slower rate. It has been reported that maximum DNA crosslinking was observed at about 4 hrs following a brief exposure to DNA alkylating agents such as phosphoramide mustard.[128] The different rates of caspase-3 activation impacts on the rate of cell death and hence the rate of tracer uptake when PAC-1 is used for cell treatment compared to 4-HC treatment.

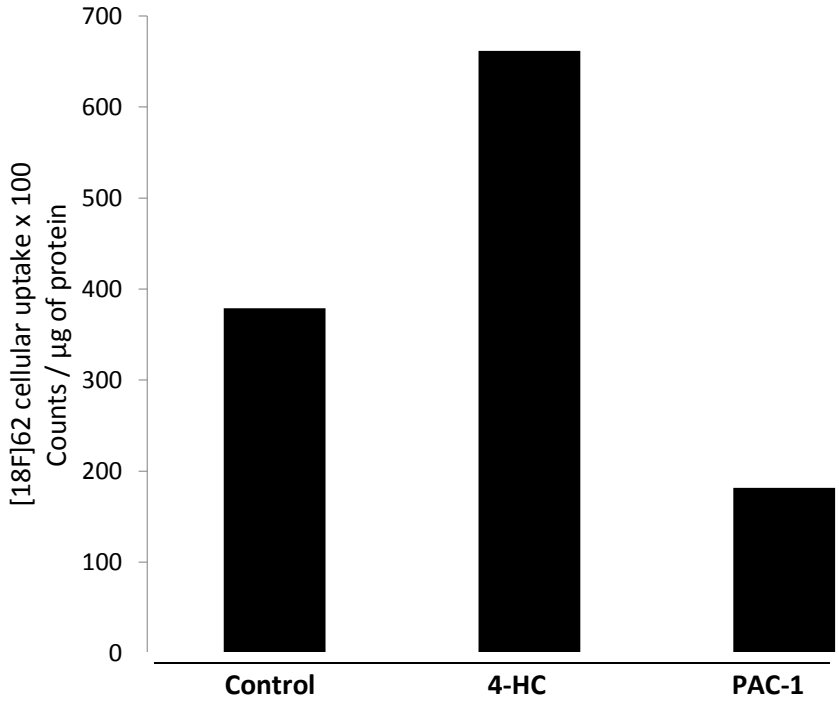


Figure 3.11: 38C13 lymphoma cell uptake of [^{18}F]-pyrimidoindolone **62** in; untreated control cells (0.1 % DMSO, 24 hrs); 4-HC treated cells (3 µg/mL, 24 hrs) and; PAC-1 treated cells (10 µM, 24 hrs) - showing a 1.5-fold uptake in 4-HC treated cells and decreased uptake in PAC-1 treated cells compared to control cells, 24 hours after treatment. For all treated and control samples, radioactivity data are expressed as decay-corrected counts per milligram of total cellular protein.

Figure **3.11** shows increased pyrimidoindolone radiotracer uptake in 4-HC treated cells compared with the control cells, measured 24 hours after treatment. The apparent low uptake observed with PAC-1 treated cells was attributed to the faster induction of apoptosis leading to faster cell death, prior to the measurement of tracer uptake. It was believed that at 24 hours after treatment with PAC-1, the majority of cells would have undergone the complete apoptotic cycle (cell death) when caspase-3 is no longer active and therefore cannot bind the radiotracer. In contrast, given the prolonged process of apoptotic induction by 4-HC, uptake measurement at 24 hours

appears to be an ideal time point with 4-HC treatment for detecting 'dying' cells still undergoing the apoptotic cycle with activated caspase-3 still present (rather than 'dead' cells). In order to detect apoptosis and the resulting pyrimidoindolone uptake with PAC-1 treatment, it would be necessary to measure radiotracer uptake at an earlier time point or at time intervals to show the process from apoptotic/caspase-3 activity to cell death.

Nevertheless, the increased radiotracer uptake of 4-HC treated cells compared with the control cells (Figure **3.11**) suggested the pyrimidoindolone **62** to be a caspase-binding ligand. Similar results were observed with the [^{18}F]-isatin radiotracer **22** which also showed increased uptake in 4-HC treated cells compared to control cells (Figure **3.12**), 24 hours after treatment.[80] A 2-fold uptake and 1.5-fold uptake of 4-HC treated cells compared with control cells were observed with the isatin and pyrimidoindolone tracers respectively, indicating that the isatin is a slightly more potent caspase substrate.

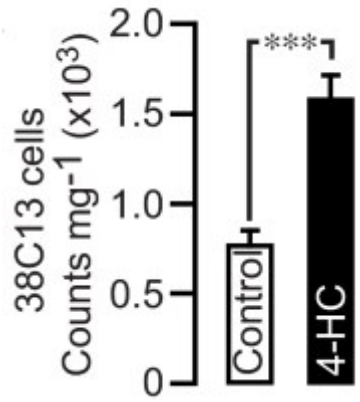


Figure 3.12. Uptake of [^{18}F]-isatin **22** in 38C13 lymphoma cells treated with 4-HC to induce apoptosis (4-HC; 1 µg/mL; 24 hrs) and in control/ untreated cells (control: 50 % DMSO, 24 hrs), showing a 2-fold uptake in treated cells compared to control cells, 24 hrs after treatment. For treated and control samples, radioactivity data were expressed as decay-corrected counts per milligram of total cellular protein. Figure taken from Nguyen *et al*.[80]

III.4.3. *In vivo* Tissue Biodistribution & Metabolic Profiles

Following the *in vitro* cell uptake measurements which showed the pyrimidoindolone **62** to be a caspase-3 substrate, *in vivo* biodistribution studies were carried out, aiming to assess the distribution of the probe in major organs. The tissue distribution studies involved intravenous injection of the pyrimidoindolone radiotracer into tumour-bearing untreated mice followed by biodistribution measurement in major organs, 60 mins after injection. At 60 mins after injection, high localization of [^{18}F]**62**-derived radioactivity was seen in the kidneys, urine and liver, suggesting the

importance of both renal and hepatic routes of elimination (Figure **3.13**). The radiotracer was completely eliminated from the plasma within 60 mins. Future work would involve assessing *in vivo* biodistribution in tumour-bearing treated mice in order to compare the distribution of the radiotracer in the tumour of treated mice compared to that of untreated or control mice. Data shown in Figure **3.13** shows the absence of pyrimidoindolone probe binding or distribution in untreated tumour, which should facilitate the measurement of tumour tracer-binding associated with caspase activation in treated mice.

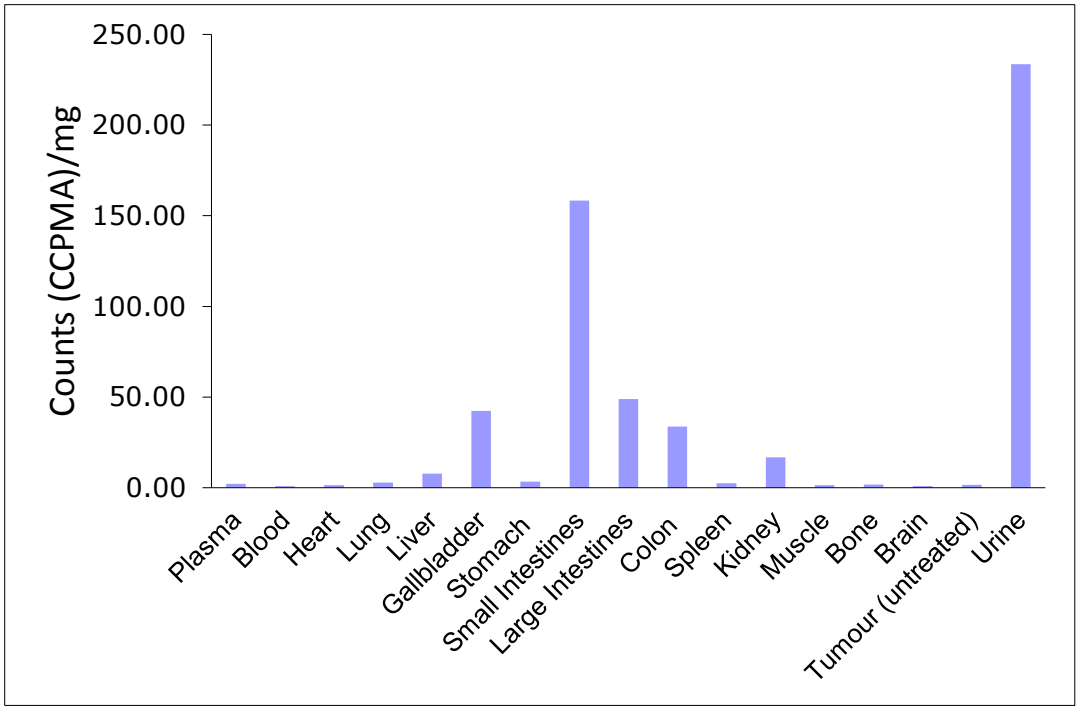


Figure 3.13: [^{18}F]**62** biodistribution in untreated RIF-1 tumour bearing mice at 60 mins after injection. Data are ± SEM; n = 3 mice

A comparison of the obtained pyrimidoindolone data with the biodistribution data reported for the isatin sulfonamide [^{18}F]**22** showed that the pyrimidoindolone probe has a similar biodistribution profile as the isatin (Figure **3.14**).[57] Both radiotracers showed elimination in the liver/gallbladder, intestines, kidneys and urine.

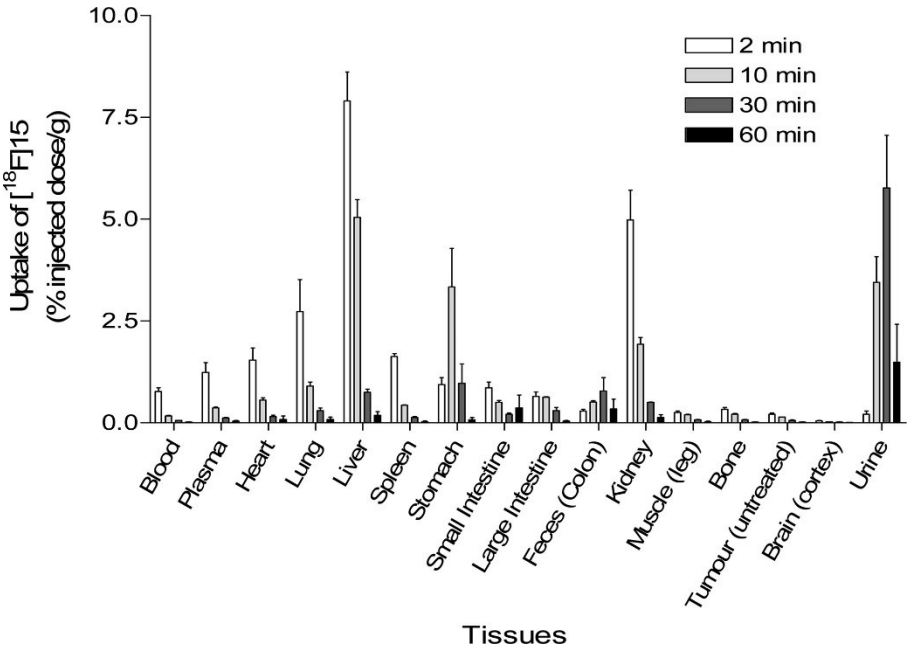


Figure 3.14: Biodistribution of [^{18}F]-Isatin **22** in untreated RIF-1 tumour bearing mice between 2 and 60 mins reported by Smith *et al*.[57]

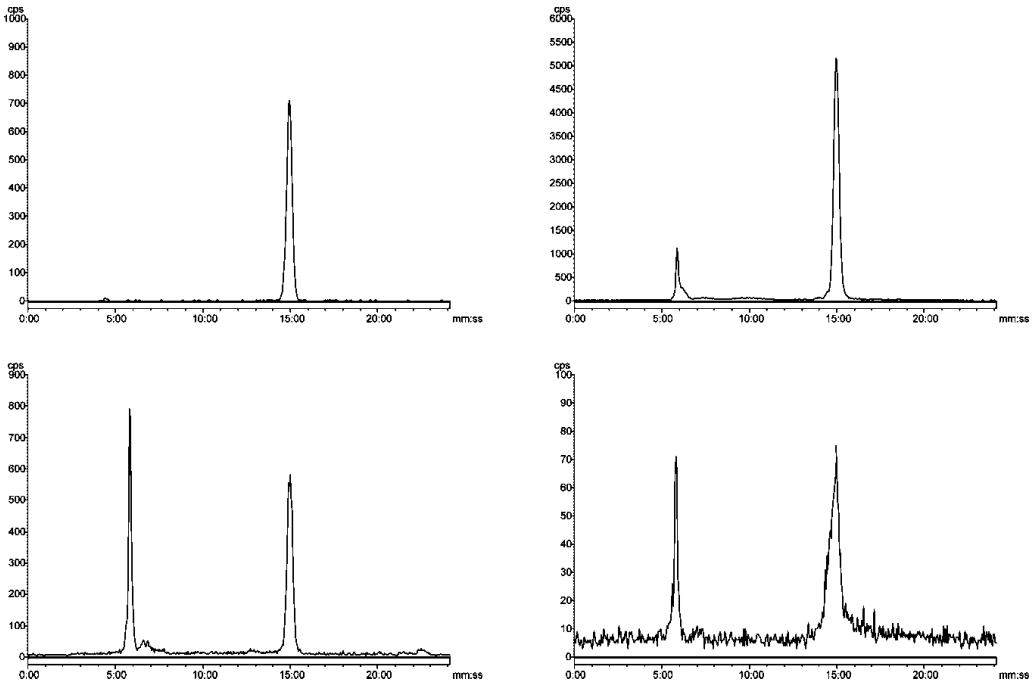


Figure 3.15: *In vivo* metabolism of [^{18}F]**22** assessed in plasma by radio-HPLC. Top left, [^{18}F]**22** standard; top right, 2 min plasma; bottom left, 15 min plasma; bottom right, 60 min plasma. Data reported by Smith *et al*.[57]

In vivo metabolic stability of the pyrimidoindolone radiotracer was also determined in liver, plasma and urine samples. Similarly to the metabolic data reported for isatin **22** (Figure **3.15**),[57] radio-HPLC analysis showed that the pyrimidoindolone radiotracer **62** produces a single polar metabolite in the plasma, urine and liver. At 60 mins after injection, traces of the unmetabolised parent pyrimidoindolone tracer was present in plasma (14 %) and in the liver (10 %), while the urine sample contained only the metabolite for elimination (Figure **3.16**).

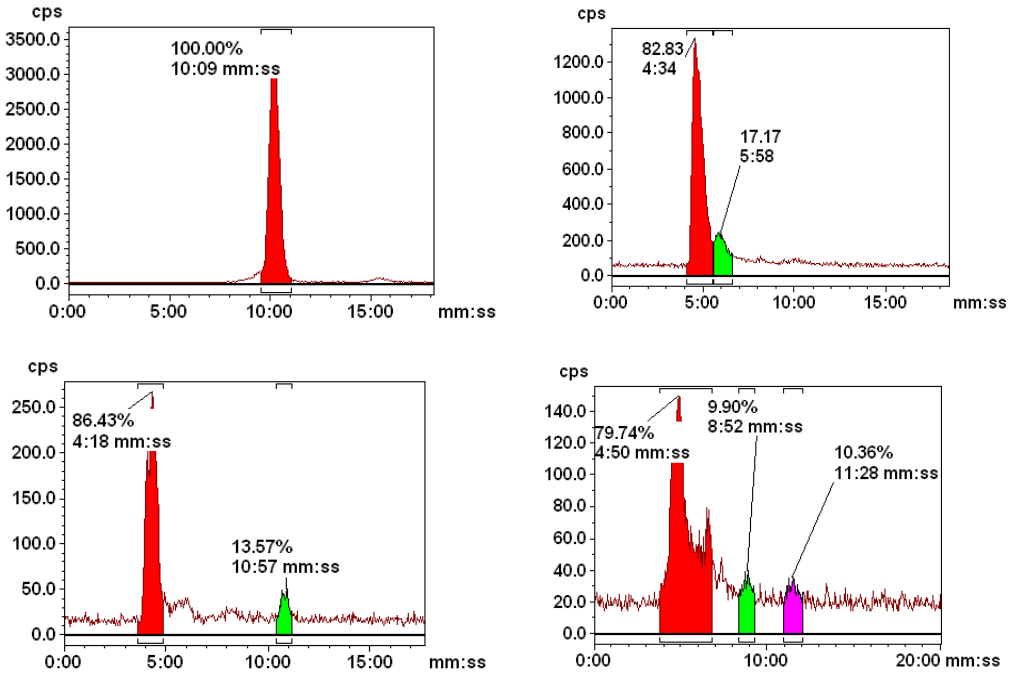


Figure 3.16: *In vivo* metabolism of [^{18}F]-pyrimidoindolone **62** in untreated RIF-1 tumour bearing mice measured in plasma, liver and urine, 60 minutes after injection. **Top left** - [^{18}F]**62** standard; **Top right** – urine; **bottom left** - plasma; **bottom right** – liver.

The results suggested that the isatin scaffold is relatively more stable than the pyrimidoindolone; although for both [^{18}F]-isatin-**22** and [^{18}F]-pyrimidoindolone-**62**, the presence of the parent tracer after 60 min is apparent in certain tissues, [^{18}F]-isatin-**22** showed a higher presence of the unmetabolised parent tracer. In the plasma for example, 14 % and 50 % of the radioactivity was due to unmetabolised parent tracer for the pyrimidoindolone and isatin probes respectively (Figures **3.15** and **3.16**).

While no attempts were made to identify the nature of the metabolites, possible metabolic pathways of the pyrimidoindolone radiotracer include glutathione conjugation[129] and glucuronidation,[130] two classic metabolic pathways for drugs to form more readily excreted hydrophilic products. Given that both the pyrimidoindolone **62** and the isatin **22** were

designed as substrates for caspase-3, binding by the addition of a thiol residue in the caspase-3 active site, possible *in vivo* metabolism of the heterocycles could be through the incorporation of glutathione (GSH) to give polar metabolites for elimination. Alternatively, metabolism of the heterocycles could occur by the reduction of the ketone to alcohol, followed by glucuronidation where glucuronic acid is added to the probe via the alcohol or possibly the amidine group in the case of the pyrimidoindolone, giving polar metabolites for excretion.[130] Metabolism of isatin sulfonamide **22** may also occur through aromatic hydroxylation.[131-133] However, it is well documented that the fluoro-substituted phenyl rings hinder *in vivo* P450-catalysed ring hydroxylation due to the electron withdrawing effect of the fluoride.[132, 133]

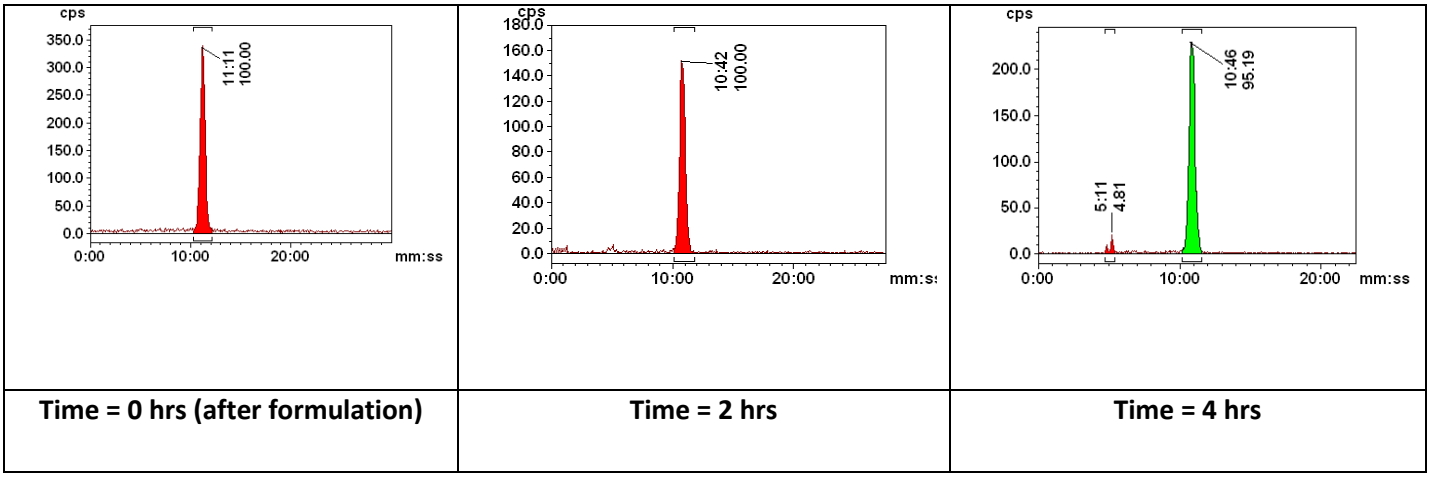


Figure 3.17: [^{18}F]-pyrimidoindolone **62** stability study with samples taken from a solution of the radiotracer in aqueous PBS buffer

Metabolism may also compete with *in vivo* aqueous decomposition for the breakdown of the pyrimidoindolone probe. As reported by Havran *et al.*,[58] the pyrimidoindolone ring may undergo hydrolysis by the addition of two molecules of water to give the multiple hydroxyl compound **50** (Chapter **I.4.4**, Scheme **1.5**, page 49) which could then undergo further metabolism such as by glucuronidation.[130] Aqueous stability may account for the apparent lower metabolic stability of the pyrimidoindolone compared with the isatin sulfonamide.

Given the reported limited aqueous stability of the pyrimidoindolone scaffold,[58] radio-HPLC was used to monitor the stability of pyrimidoindolone radiotracer **62** in aqueous solution, in order to assess stability in the timeline of a radiotracer biological use (Figure **3.17**). The resulting chromatograms showed that the radio-product in aqueous solution remained stable for at least 3 hours, with over 95 % of the parent radiotracer still present after 4 hours (Figure **3.17**). The apparent minimal aqueous decomposition 3 hours after formulation in aqueous solution is not expected to

present a problem for possible clinical use of the pyrimidoindolone. The short half-life of ^{18}F PET radionuclide means that the use of freshly synthesised radio tracers are typically conducted at short time spans, typically less than 4 hours. To reduce costs and allow off-site use with transportation of a radiotracer in clinics, a probe is typically expected to remain stable for up to 4 hours from formulation to injection.

III.4.4. Transwell / Efflux Ratio Assay[e]

When developing optimal caspase-3 binding apoptotic imaging probes, as well as considering the potency for caspase-3, it is important to assess tracer cell permeability which would impact on the ability of the probe to access the tumour being imaged. Cellular efflux is considered to be a major cause of resistance to chemotherapy in cancer patients.[134, 135] A principal cause of drug resistance in tumour cells is the active efflux of exogenous compounds affecting their concentration in tumours.[134-136] The transwell efflux assay calculates tracer properties in terms of cell permeability and extrusion from cells which is expressed as a ratio.

The ATP binding ABC transporters, P-glycoprotein (P-gp) and breast cancer resistant protein ABCG2 have been identified to play major roles in the active efflux of various exogenous and endogenous substrates across the extra- and intracellular membranes.[137] A substrate of the ABC transporters passing the membrane by passive diffusion is recognised by the transporter and through hydrolysis of ATP, is extruded out of the cell, thus limiting its intracellular concentration.[138]

The ability of Pgp-2 and ABCG2 to actively efflux molecules from cells is implicated in the tumour resistance to treatment.[134, 135] ABC transporters have been shown to be over-expressed in many tumour types, leading to increased resistance to exogenous compounds. Minimising the interaction of drugs with ABC transporters in order to increase intracellular concentrations and therefore biological effects is a key part of the tracer design and the development process. Given the significance of active drug efflux in oncology, an experiment to study the cell efflux ratio of the pyrimidoindolone probe **62** compared with the isatin lead **22** was conducted.

The transwell efflux assay involved studying the interaction of the caspase-binding probes with ABC transporters. Tracer binding to the Pgp and/or ABCG2 transporters would result in active efflux of the probes across tumour cells.

[e] Transwell/ Efflux Assay was conducted by Dr. Maciej Kaliszczak, Imperial College London

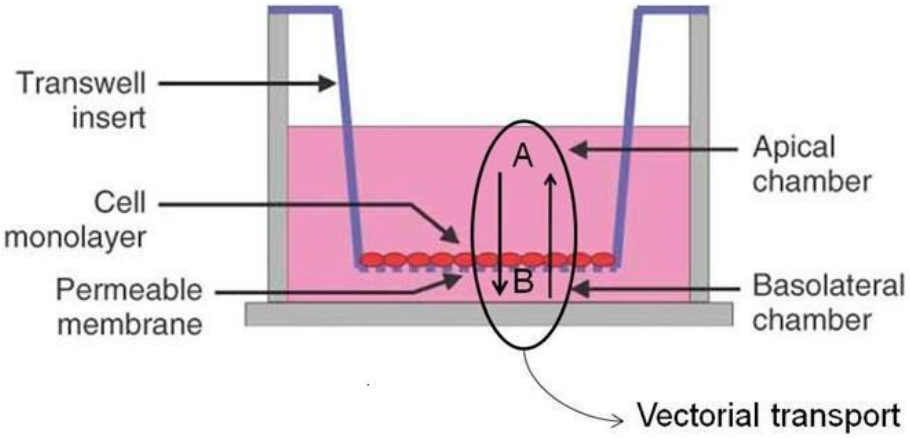


Figure 3.18: The set-up of a transwell assay experiment to assess the transport of compounds across the apical (A) and basal (B) side of a caco-2 monolayer, a cell based model for studying drug permeability. The apical side represents the extracellular surroundings while the basal side models the intracellular system.

The direct impact of the transporters on the intracellular concentration of the probes was assessed by measuring the permeability of the isatin lead and pyrimidoindolone probe across a monolayer of differentiated caco-2 cells, the most extensively characterised cell-based model for studying the cell permeability of compounds. Permeability was measured from the apical (A) to the basal (B) side (Papp A→B), and extrusion or efflux was measured from the basal to the apical side (Papp B→A), for both isatin **22** and pyrimidoindolone **62**. The experimental set up is shown in Figure **3.18**.

Table 3.8: Permeability of the probes across the caco-2 cells from the apical to the basal side, measured by LCMS (for details see experimental page 226). 2 hour incubation with results mean of n = 3.

	Papp A-B ($x10^{-6}$ cm/sec)	
	Average (n = 3)	**Standard Deviation**
Pyrimido Probe **62**	11	0.6
Isatin Lead **22**	36	2.2
Vinblastine (negative control)	10	0.4

The permeability of isatin **22** and pyrimidoindolone **62** across the caco-2 cells from the apical to the basal side is shown in Table **3.8**. The isatin **22** was shown to be absorbed into the cell through the membrane by more than 3 times the absorption rate of the pyrimidoindolone **62**. However, the standard deviation of 0.6 and 2.2 for the pyrimidoindolone and isatin respectively suggested that the results obtained for the pyrimidoindolone were more reproducible, while the isatin data showed more variation across the three runs of the experiment (n = 3). Vinblastine, a known Pgp-substrate[139] which is actively effluxed from cells following absorption was added as a control compound. The data

shown in Table **3.8** show that both the isatin and pyrimidoindolone are absorbed into the cell. However, if the compounds are secreted faster than they are absorbed, their intracellular concentrations would be altered despite possible high absorption rates.

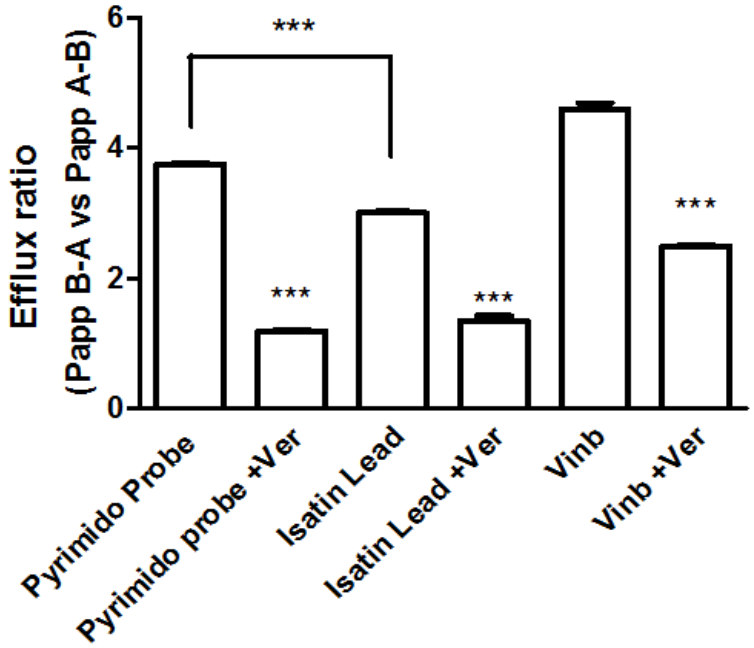


Figure 3.19: Efflux ratio in caco-2 transwell assay as expressed by the ratio between the permeability from the basal to the apical side (Papp A-B) and the permeability from the apical to the basal side (Papp B-A). Results are mean of n = 3. Verapamil was incubated for 1 hour before incubation with the different compounds at 50 µM. The results are mean of n = 3.

It has been established that if a compound exerts a ratio between the secretion (permeability from the basal to the apical side) and the absorption (permeability from the apical to the basal side) of ≥ 3, it can be considered as being actively effluxed.[140] 'Normal' diffusion, where the compound is at equilibrium between the apical and basal side gives a secretion/absorption ratio of approximately one. The isatin sulfonamide **22** and the pyrimidoindolone **62** show an efflux ratio (Papp B→A / Papp A→B) of 3 and 3.74 respectively (Figure **3.19**). This indicated that both the isatin and pyrimidoindolone were actively effluxed, with the pyrimidoindolone effluxed at a higher rate than the isatin. To ascertain that the observed active efflux was due to transport by the ABC transporters, the secretion/absorption ratio was also measured in the presence of the Pgp inhibitor, verapamil (Ver). Upon addition of verapamil, the efflux ratios of the pyrimidoindolone and the isatin were reduced to 1.19 and 1.94 respectively. The efflux ratio of vinblastine[139] which is known to be actively effluxed by the Pgp transporter was also reduced. Efflux of the compounds was not completely blocked because verapamil only blocks the Pgp transporter and not ABCG2 or any other ABC

transporters. It is worth noting that, as indicated by the three 'stars' above the plot in Figure **3.19**, a P-value of <0.0001 statistically indicated that the results obtained were significant and the observation were highly unlikely to be the result of random chance.

Table 3.9: The physicochemical properties of isatin **22** and pyrimidoindolone **62** responsible for Pgp binding

	MW	**No. of N+O atoms**	**Acid pKa***
Isatin **22**	549.5	10	> 4
Pyrimido **62**	530.6	10	> 4

*Acid pKa values of isatin **22** and pyrimidoindolone **62** assumed to be > 4

The Pgp transport is associated with a single flexible binding site that can accommodate several substrates, with substrate specificity shown to be conformation-independent.[141] Pgp substrate specificity is instead defined by a set of simple rules: typical Pgp substrates are large molecules with high H-bond accepting capability, whereas small molecules with low H-bond accepting capability are likely to be non-substrates.[141] Acids are unlikely Pgp substrates but bases have higher chances of being substrates. Pgp substrate specificity has been defined by a set of physicochemical properties estimated by the "rule of fours": compounds with (N + O) ≥ 8; MW > 400; and acid pKa > 4 are likely to be Pgp substrates. Conversely, compounds with (N + O) ≤ 4; MW < 400; and base pK_B < 8 are likely to be non-substrates. Molecular weight was found to play a particularly key role in determining substrate affinity for Pgp.[141] Table **3.9** shows that both the isatin **22** and pyrimidoindolone **62** have the physicochemical properties of typical Pgp substrates (MW > 400 and N+O of > 8), accounting for the fact that both are actively effluxed. Given the presence of the basic amidine group in the pyrimidoindolone structure and a keto-amide group in the isatin heterocycle, the tracers are not considered acidic and are highly likely to have acid pKa values of > 4.

As tumours are known to over-express the ABC transporters, the fact that both the pyrimidoindolone **62** and the isatin **22** appear to be substrates for the transporters would impact on the ability of the probes to permeate and sufficiently accumulate in tumour cells to bind to intracellular caspase-3. It would therefore be necessary to optimise the probes to be poor substrates for the ABC transporters before potential clinical use. Although it is possible to block active efflux by administering substrates that block the transporters alongside the drug molecules, known transporter inhibitors have been shown to be toxic.[142] The inhibitors do not only block the ABC transporters found on tumour cells, they also block those found in cells throughout the body.[142]

Hence, the preferred solution to active efflux of compounds such as the isatin and pyrimidoindolone is optimisation and development of structures that do not bind to the transporters and are specific to caspase-3. This is a key consideration for future work on the continued search for an optimal caspae-3 binding apoptotic PET imaging probe.

III.5. Conclusion

Based on the observations that PET imaging using isatin sulfonamides is hampered by low target-to-background activity,[57] we set out to prepare and investigate the properties of a pyrimidoindolone-based probe with the initial structure modelled on the lead isatin sulfonamide **22**. The initial results reported here show that the pyrimidoindolone **62** and isatin sulfonamide **22** share similar biological characteristics. Despite the reported dual binding of the pyrimidoindolone[87] and the expected reduced electrophilicity of the C-10 carbonyl, the pyrimidoindolone heterocycle **62** generally showed no significant differences from the isatin sulfonamide with regards to caspase-3 potency and selectivity.

Future work on the study of pyrimidoindolones as caspase-3 binding apoptotic radioligands would involve the preparation of a library of derivatives for SAR studies. Similarly to the design of the initial pyrimidoindolone probe **62**, the library compounds would be modelled on the extensively studied isatin sulfonamides. Further studies to optimise the preparation of the pyrimidoindolone scaffold, and the efficiency and yield of radiosynthesis would also be required.

For the purpose of the reported studies, we achieved the aim of synthesising and radiolabelling an initial pyrimidoindolone target for biological evaluation of the heterocycle's utility as a caspase-biding radioligand. As well as the cold, unradiolabelled reference compound, precursors for radiolabelling by both click reaction and direct displacement by [^{18}F]fluoride were prepared and used in the successful radiosynthesis of the pyrimidoindolone target [^{18}F]**62**.

CHAPTER IV:

IMIDAZOLEINDOLONE AND TRIAZOLEINDOLONE SYNTHESIS

IV. IMIDAZOLEINDOLONE AND TRIAZOLEINDOLONE SYNTHESIS

IV.1. Introduction

We sought to develop a new class of potent caspase-3 binding radioligands with increased specificity and reduced non-specific binding interactions relative to the isatin series for use in the PET imaging of apoptosis. With the aim of investigating new heterocycles with structural similarities to the extensively studied isatin sulfonamides, we proposed the unexplored imidazoleindolone (**52**) and triazoleindolone (**53**) heterocycles (Figure **4.1**). Like the isatin sulfonamides, these heterocycles possess an electrophilic ketone carbonyl essential for caspase-3 inhibition through the formation of a thiohemiketal with a cysteine residue in the caspase-3 active site (Chapter **I.4**).[69, 74]

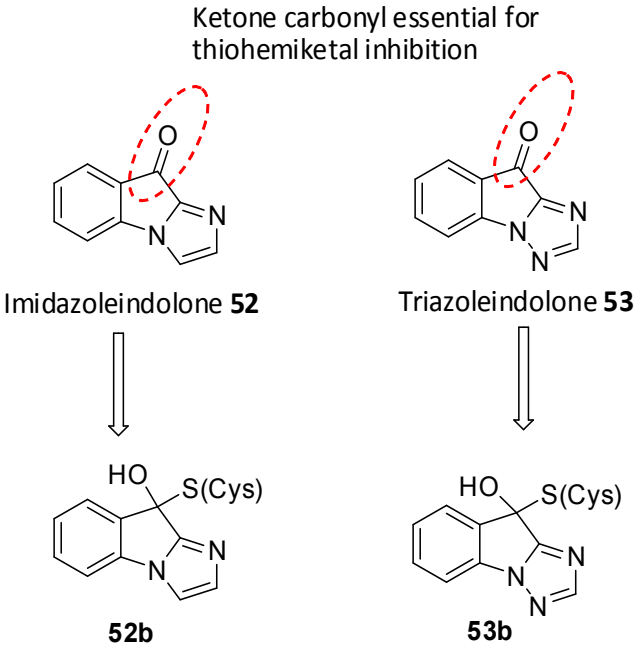


Figure 4.1: Imidazoleindolone and the triazoleindolone heterocycles containing the ketone carbonyl essential for caspase-3 inhibition through the formation of a thiohemiketal with a thiol residue

It was hoped that the extended aromatic system of the imidazoleindolone and triazoleindolone heterocycles would favourably modulate the reactivity of the ketone carbonyl, reducing non-specific interactions in the cytosol which is believed to be responsible for the low target-to-background ratio of PET images using the isatin sulfonamides (Chapter **I.4**).[57, 69, 77] As previously discussed, computational studies were initially employed to model the favourability of thiol addition to the imidazoleindolone **52** and triazoleindolone **53** scaffolds in order to gain a preliminary insight into their potential caspase-3 inhibitory potencies (Chapter **II**). The computational

results suggested that, like the isatin ring, the two heterocycles would favourably react with a thiol group to give the corresponding thiohemiketal products. The order of thiohemiketal formation favourability according to the obtained free energy of reactions was shown to be **isatin > triazoleindolone > imidazoleindolone.** This suggested that the imidazoleindolone **52** and triazoleindolone **53** heterocycles would form a thiohemiketal less readily than the isatin. It is worth noting that the computational calculations using the unsubstituted heterocycles did not consider the spatial distribution of a radiotracer within the target active site cavity. As such, the calculated favourability may not reflect biological binding affinities where the binding interaction of an inhibitor as a whole has a substantial effect on inhibitory activity.

This chapter describes the results of the synthetic routes explored for the preparation of the novel triazoleindolone and imidazoleindolone structures. As well as preparing the core heterocycles, we aimed to synthesise target substituted structures to be used in preliminary experimental characterisations. Similarly to the pyrimidoindolone target **62** (Chapter **III**), these target heterocycles were designed to emulate the structure of the lead isatin sulfonamide **22** (Figure **4.2**). SAR studies of the isatin series showed that a sulfonamide bearing a pyrrolidine ring was highly preferable for potency (Chapter **I.4**). Additionally, the importance of stereochemistry with the (*S)*-configuration at the chiral pyrrolidine was demonstrated by prior SAR studies (Chapter **I.4**).[56 72] As a result, the designed substituted imidazoleindolone and triazoleindolone structures to be synthesised contained the same sulfonyl pyrrolidine moiety as the isatin sulfonamide **22** with the (*S)*-configuration at the chiral pyrrolidine (Figure **4.2**).

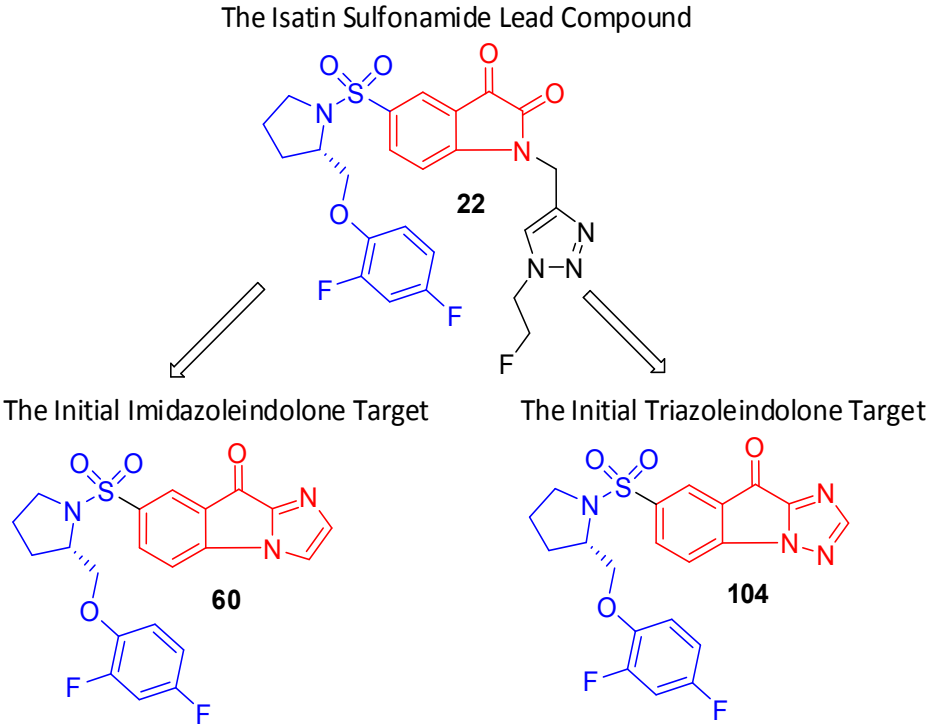


Figure 4.2: Imidazoleindolone and Triazoleindolone target structures, **60** and **104**, modelled on the lead isatin sulfonamide structure

The first set of structures selected were imidazoleindolone **60** and triazoleindolone **104**, substituted with the same sulfonamide group found in the lead isatin structure **22** (Figure **4.2**). The aim was to optimise the synthetic routes to these heterocycles before proceeding to the addition of substituents on the azole side of the heterocycles.

IV.2. Imidazoleindolone and Triazoleindolone Synthesis via Isatin Sulfonamide Intermediates

Synthesis of the sulfonamide substituted imidazoleindolone and triazoleindolone heterocycles from the isatin sulfonamide **109** was initially explored (Figure **4.3**). From the isatin intermediate **109**, functional group interconversion of the isatin amide group to an imidazole or a triazole ring would then give the desired imidazoleindolone and triazoleindolone heterocycle respectively (Figure **4.3**).

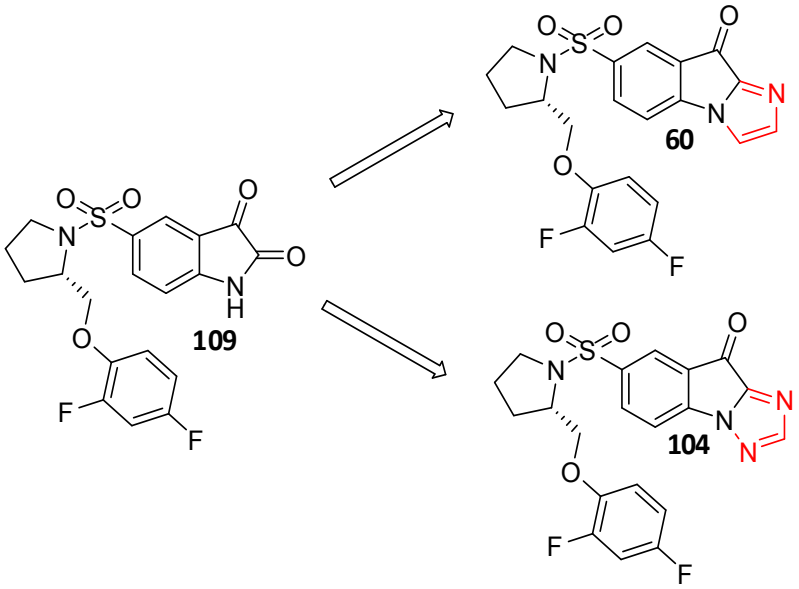
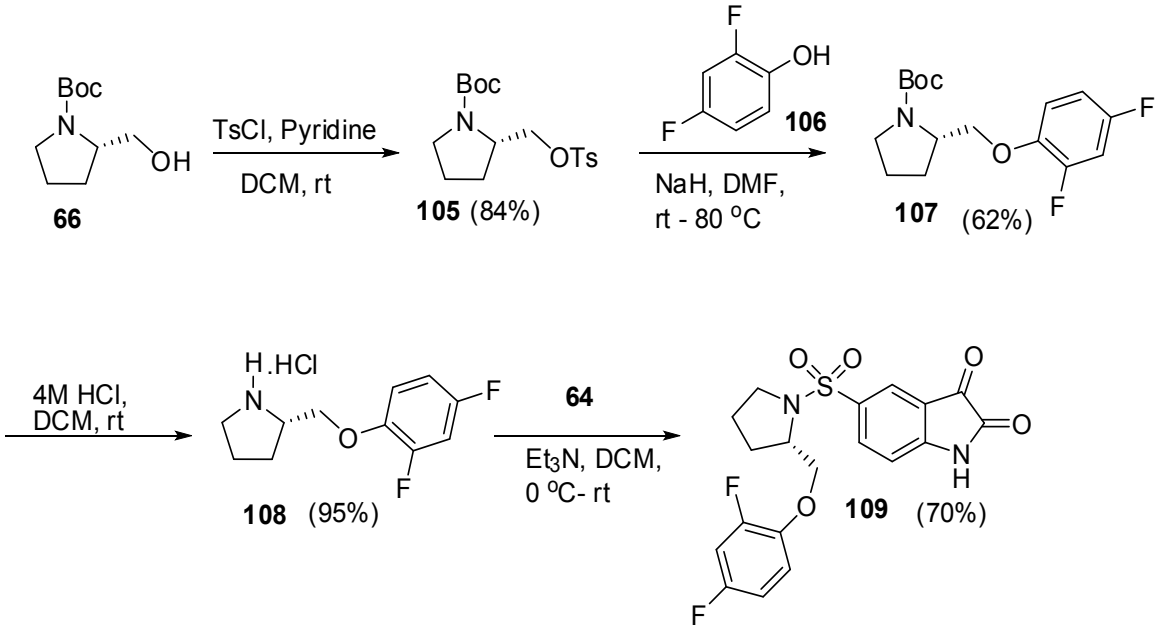


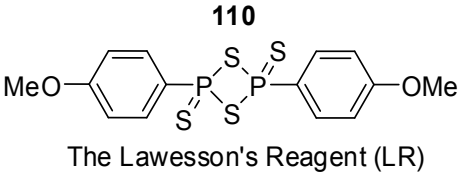
Figure 4.3: Imidazoleindolone and triazoleindolone synthesis via an isatin intermediate

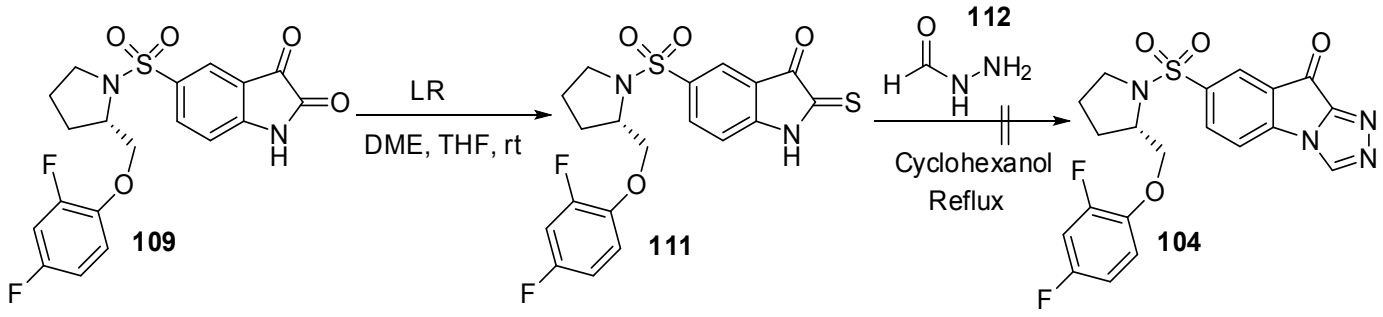
To obtain the target structures **60** and **104**, the sulfonamide substituted isatin **109** was first synthesised, following reported literature procedures and similar steps utilised for the pyrimidoindolone synthesis described in Chapter **III**.[57] Starting from the Boc-protected (*S*)-prolinol **66**, the alcohol group was converted into tosylate **105** in 84 % yield, which was subsequently displaced with 2,4-difluorophenol **106** under basic conditions to give phenoxy ether **107** in 62 % yield. Boc deprotection of ether **107** gave the amine **108** in 95 % yield, followed by the amine coupling with isatin sulfonyl chloride **64** to give the sulfonamide **109** in 70 % yield (Scheme **4.1**).



Scheme 4.1: Preparation of the isatin sulfonamide **109** as a starting material in imidazoleindolone **60** and triazoleindolone **104** synthesis.[57]

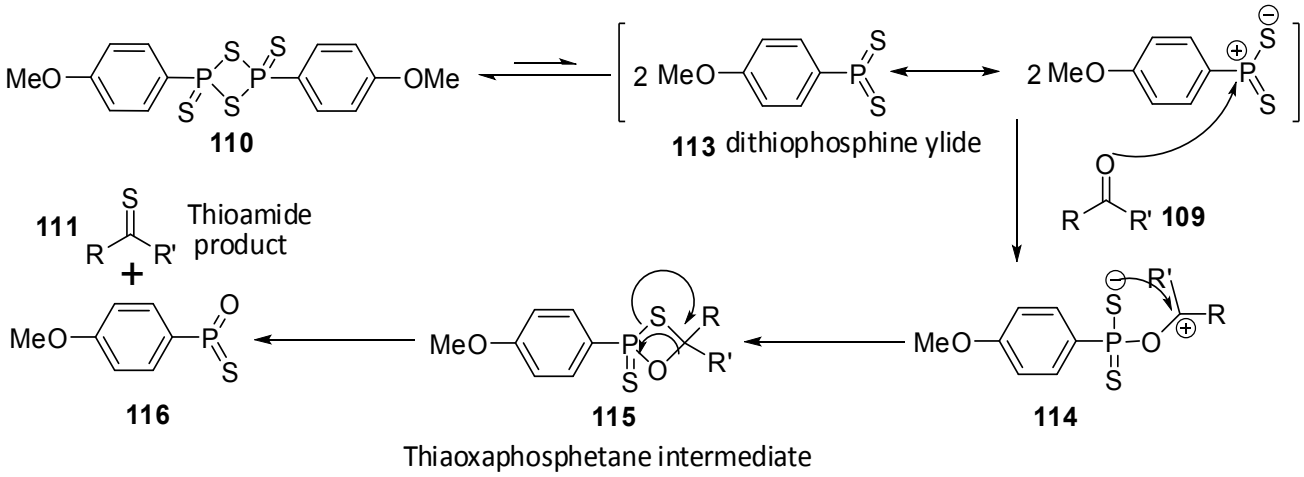
After facile preparation of isatin sulfonamide **109**, a number of synthetic strategies designed to incorporate the imidazole and triazole rings were explored. Firstly, it was hoped that the triazoleindolone target **104** could be achieved through the reaction of formic hydrazide **112** with reactive intermediates of isatin sulfonamide **109**. Such intermediates included the thioamide, imidoyl chloride, carbamate and methyl imidate derivatives of the isatin sulfonamide **109**.





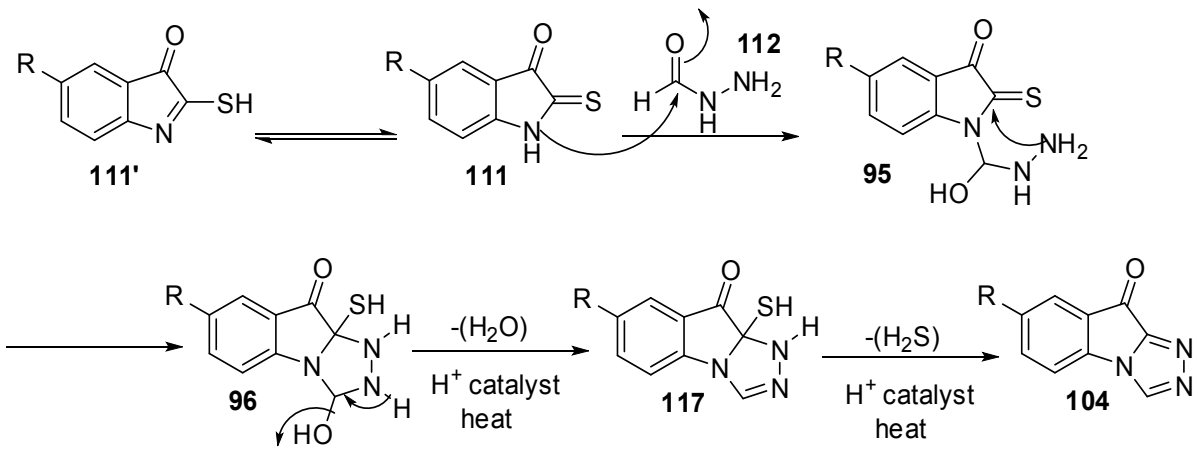
Scheme 4.2: Intended formation of the triazoleindolone heterocycle from thioamide intermediate **111**.[143-146]

The first isatin sulfonamide intermediate explored was the thioamide species **111** (Scheme **4.2**). Preparation of the thioamide **111** involved treatment with Lawesson's reagent (LR) **110** (Scheme **4.2**), a thionating agent used to convert C=O bonds to C=S bonds.[147] In solution, LR is at equilibrium with the more reactive dithiophosphine ylide **113** which reacts with a carbonyl to give rise to a thiaoxaphosphetane intermediate **115** (Scheme **4.3**). The driving force is the formation of a stable P=O bond in a cyclo-reversion step that gives the C=S bond.[147]



Scheme 4.3: Thionating mechanism of the Lawesson's reagent[147]

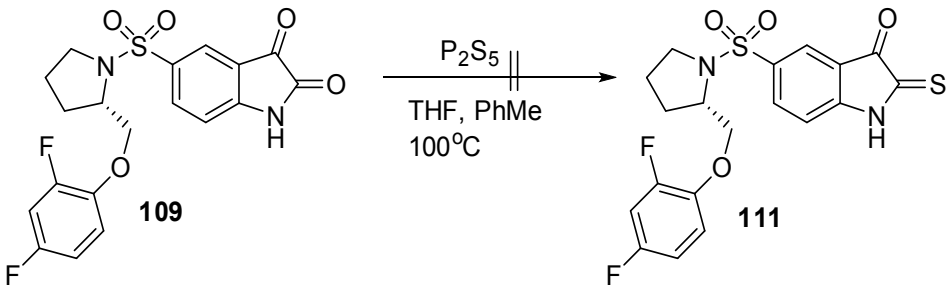
Thioamides (C=S bonds) are known to be much less stable than amides (C=O bonds) and are therefore more reactive.[148] While the incorporation of a triazole ring is not known to occur through the reaction of formic hydrazide with an amide group, formic hydrazide **112** has been reported to successfully react with the more reactive thioamide group to give a 1,2,4-triazole ring (Schemes **4.2**, **4.4**).[143-146]



Scheme **4.4**: Proposed mechanism of formic hydrazide **112** reaction with thioamides

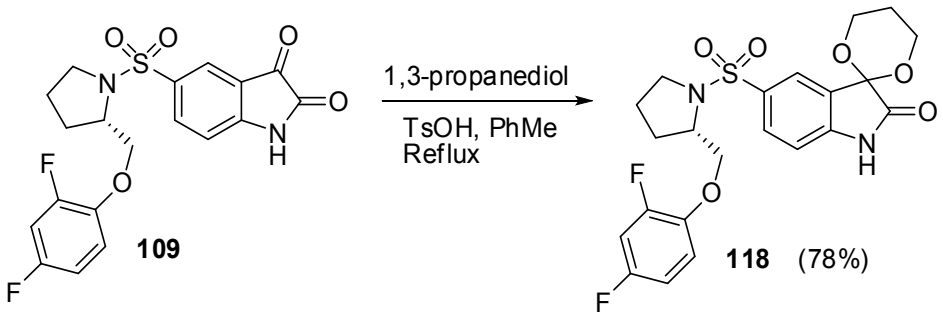
Upon treatment of thioamide **111** with formic hydrazide, the N-H group of the thioamide was expected to attack the aldehyde carbonyl of formic hydrazide **112** to give the corresponding alcohol **95**. Subsequent intramolecular nucleophilic addition of the hydrazide group to the thioamide, followed by dehydration and loss of H_2S would then give the triazole ring of the triazoleindolone structure (Scheme **4.4**). Regioselective formation of thioamide in preference to a thioketone was expected as the amide carbonyl is generally the most easily thionated of the carbonyl groups, owing to the delocalisation of the nitrogen lone pair onto the C=S bond.[149]

Full conversion of sulfonamide **109** in the presence of LR was observed within 2 hrs in DME or THF at room temperature. In both solvents, a TLC of the reaction mixture revealed several spots. Successful conversion of sulfonamide **109** to the corresponding thioamide **111** was confirmed by LCMS, which showed the thioamide product, as well as a number of by-products. The reaction was performed under dilute conditions in an attempt to avoid side product formation. Purification of the crude residue obtained proved challenging as it contained a range of closely eluting components. Instead, the mixture was separated into crude fractions by column chromatography, in an attempt to obtain thioamide **111** in a cleaner mixture. Unfortunately, thioamide **111** appeared to be unstable as the product peak observed by LCMS prior to crude purification was not present in any of the fractions following flash column chromatography. Formation of the thioamide and proceeding to the next step without purification, heating with formic hydrazide in cyclohexanol, failed to give the desired triazoleindolone heterocycle **104** (Scheme **4.2**).



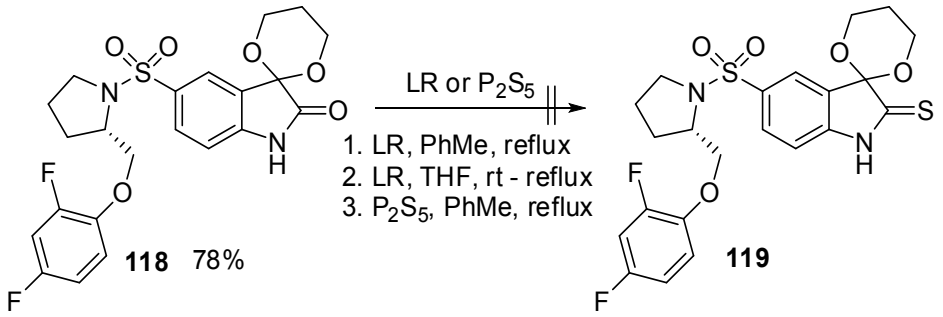
Scheme **4.5:** Unsuccessful P_2S_5 thionation of amide **109**.[149, 150]

In an attempt to successfully isolate thioamide **111**, P_2S_5 was employed as an alternative, milder thionating agent, but the reaction in THF and toluene failed to give any trace of the desired product (Scheme **4.5**).



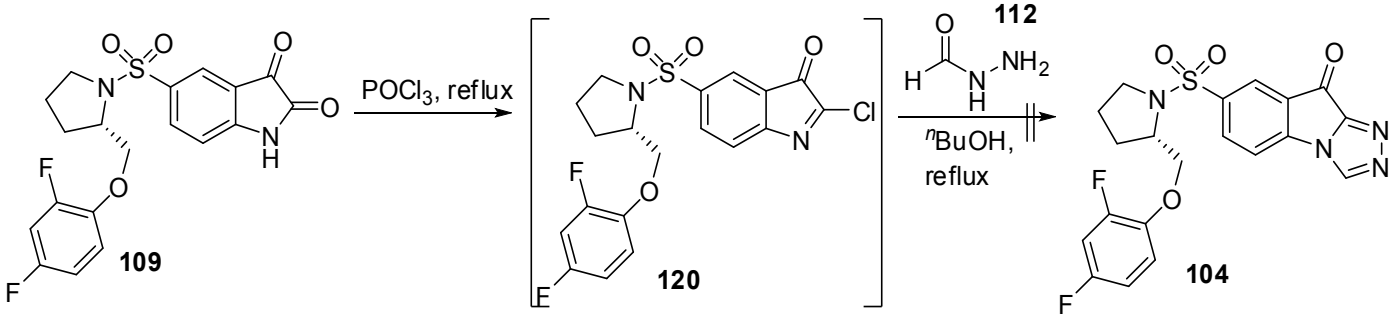
Scheme 4.6: Preparation of ketal protected isatin sulfonamide **118**

It is likely that possible intermolecular reactions of the thioamide group with the electrophilic ketone centre may have been responsible for the numerous by-products observed with LR. Hence, the reaction was repeated with protected ketone **118**, prepared from the acid catalysed condensation of isatin sulfonamide **109** with 1,3-propanediol in toluene in 78 % yield (Scheme **4.6**).



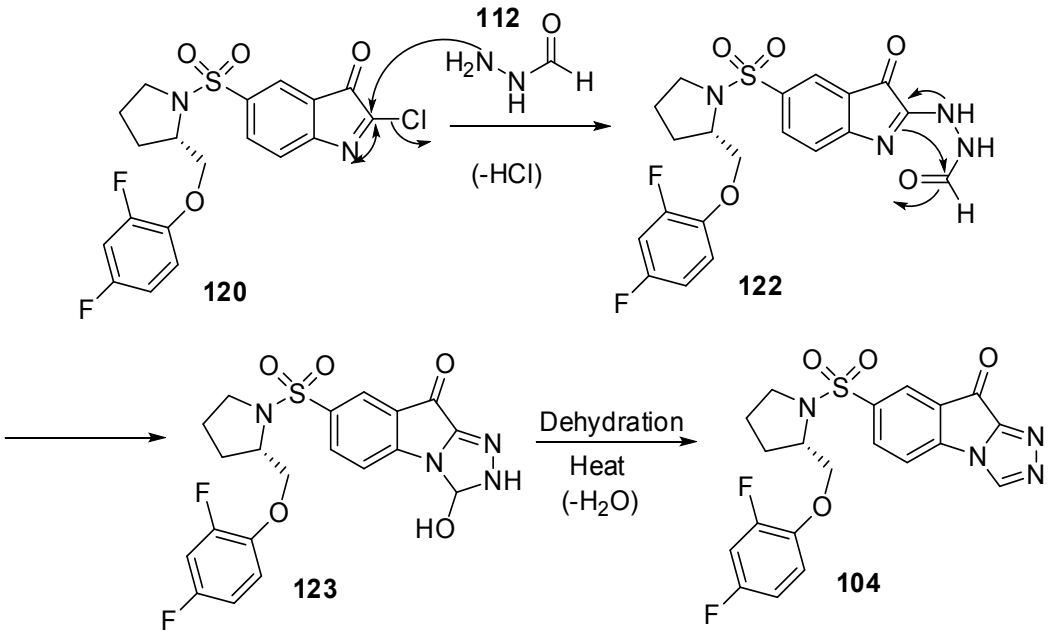
Scheme 4.7: Attempts to prepare the ketal protected thioamide **119**

Unfortunately, no reaction was observed using ketal **118** and LR in THF, at either room temperature or heating to reflux. The same outcome was observed with P_2S_5 (Scheme **4.7**). Unlike the reaction of isatin **109** with LR, no trace of the thioamide product was observed with all attempts to prepare the ketal protected thioamide **119** (Scheme **4.7**). The reason for lack of reaction of ketal **118** with LR or P_2S_5 is not known, though possible steric effects due to the presence of the 6 membered 1,3-dioxolane ring may have hindered reaction with the thionating agents. As a result, triazoleindolone synthesis from a thioamide intermediate was terminated and the imidoyl chloride strategy was explored.



Scheme 4.8: Triazoleindolone synthesis via the imidoyl chloride **120**.[151, 152]

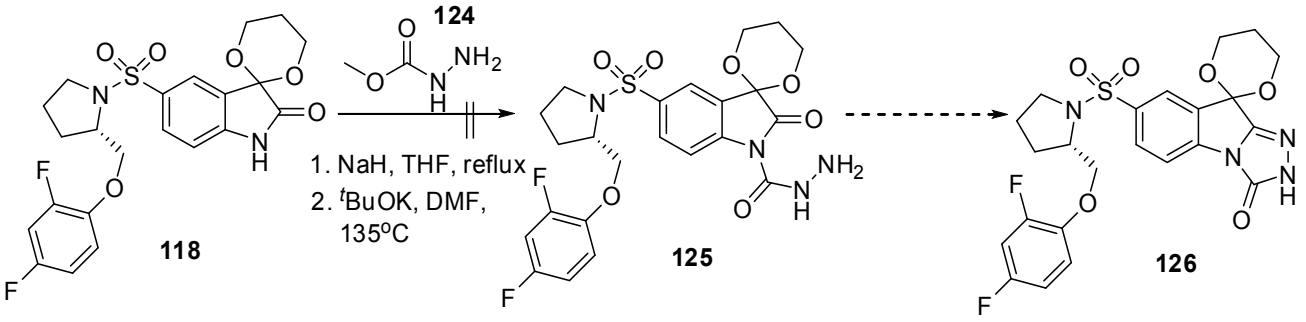
The formation of imidoyl chlorides from isatin rings have been reported in literature by Katritzky *et al*. and Campagna *et al*.[151, 153] Preparation of the imidoyl chloride intermediate **120** involved heating isatin sulfonamide **109** in $POCl_3$ for 2.5 hrs, followed by subsequent removal of excess $POCl_3$ under reduced pressure. The resulting intermediate was used in the next step without workup or purification, in order to avoid the facile hydrolysis of the labile imidoyl chloride group (Scheme **4.8**).[153]



Scheme 4.9: The mechanism of imidoyl chloride reaction with formic hydrazide

It was hoped that imidoyl chloride **120** would react with formic hydrazide **112** to give the triazoleindolone heterocycle **104**. The proposed mechanism of formic hydrazide reaction with imidoyl chloride **120** to give the corresponding triazoleindolone structure is shown in Scheme **4.9**.

TLC of the sulfonamide-$POCl_3$ reaction mixture showed complete consumption of isatin sulfonamide starting **109** after 2.5 hrs, while ^{1}H NMR showed one major product with loss of the amide hydrogen, suggesting successful formation of imidoyl chloride **120**. Following a reported procedure,[152] the residue was heated to reflux with formic hydrazide **112** in ^{n}BuOH. Disappointingly, a complex mixture suggesting complete decomposition was obtained, which may have resulted from side reactions such as formic hydrazide condensation with the ketone group to give formic hydrazone species which could undergo further reactions. It was possible that ketone **109** protection as a ketal **118** would block the formation of by-products and decomposition resulting from unwanted reactions of the isatin ketone group. However, given that the by-product of $POCl_3$ reaction with an amide to form an imidoyl chloride is HCl, a ketal group was expected to undergo hydrolysis under the reaction conditions.

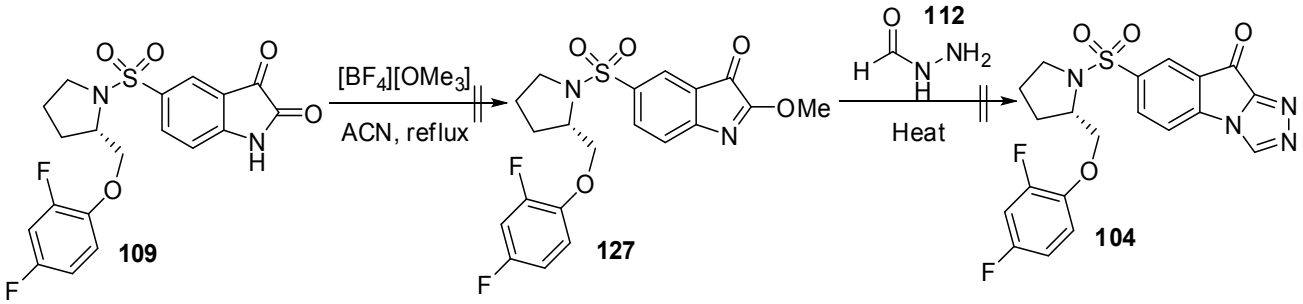


Scheme 4.10: Attempts to prepare triazoleindolone **104** from ketal **118** and hydrazinocarboxylate **124**

Subsequently, hydrazinocarboxylate **124** was used as an electrophile with ketal sulfonamide **118**. This involved treating ketal **118** with a base (NaH or ^{t}BuOK), prior to the addition of hydrazinocarboxylate **124**, in either THF or DMF at 135 ^{o}C (Scheme **4.10**). However, no reaction was observed with either of the two bases and solvents, possibly due to the limited electrophilicity of the carbonyl group of hydrazinocarboxylate **124**.

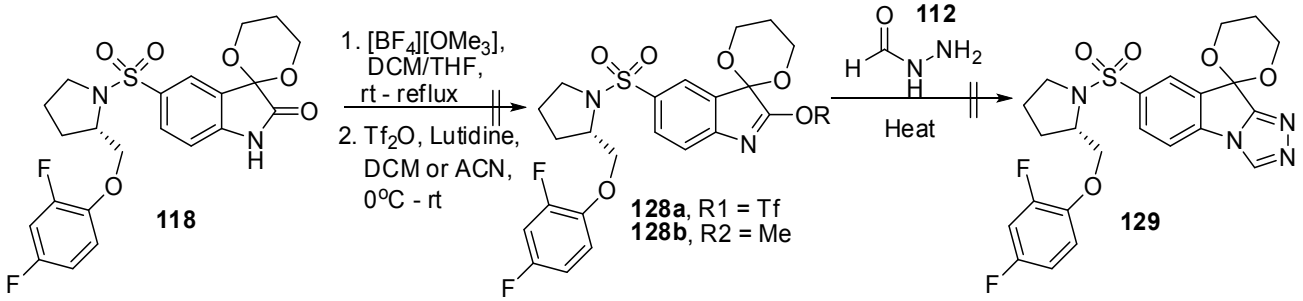
In successive reactions, preparation of the triazoleindolone heterocycle **104** from imidate based intermediates was explored. This route involved the formation of a reactive methyl or triflate imidate from isatin sulfonamide **109**, using powerful alkylating agents such as triflic anhydride and the Meerwein's salt.[154-156] The resulting imidate intermediate would contain a methoxy or a triflate leaving group which could be treated with formic hydrazide **112** to give the triazoleindolone heterocycle **104**. Trialkyloxonium salts such as $[BF_4][OMe_3]$ ("Meerwein salts"),[157, 158] are versatile

reagents for the O-alkylation of amides, lactams and related functional groups in preference to N-alkylation.[155, 159, 160]



Scheme 4.11: Attempts to achieve triazoleindolone **104** from the methyl imidate intermediate **127**.[154-156]

In the initial reaction, the Meerwein's salt, $[BF_4][OMe_3]$ was employed to O-alkylate isatin sulfonamide **109** and give the methyl imidate **127**, following reported procedures.[154, 155] After heating for two days in acetonitrile, only the starting material **109** was isolated from the reaction mixture (Scheme **4.11**). Repeating the reaction in DCM or adding the base, disodium hydrogen phosphate according to other reported conditions,[156] did not change the outcome of the reaction and the methyl imidate intermediate **127** was not obtained (Scheme **4.11**).

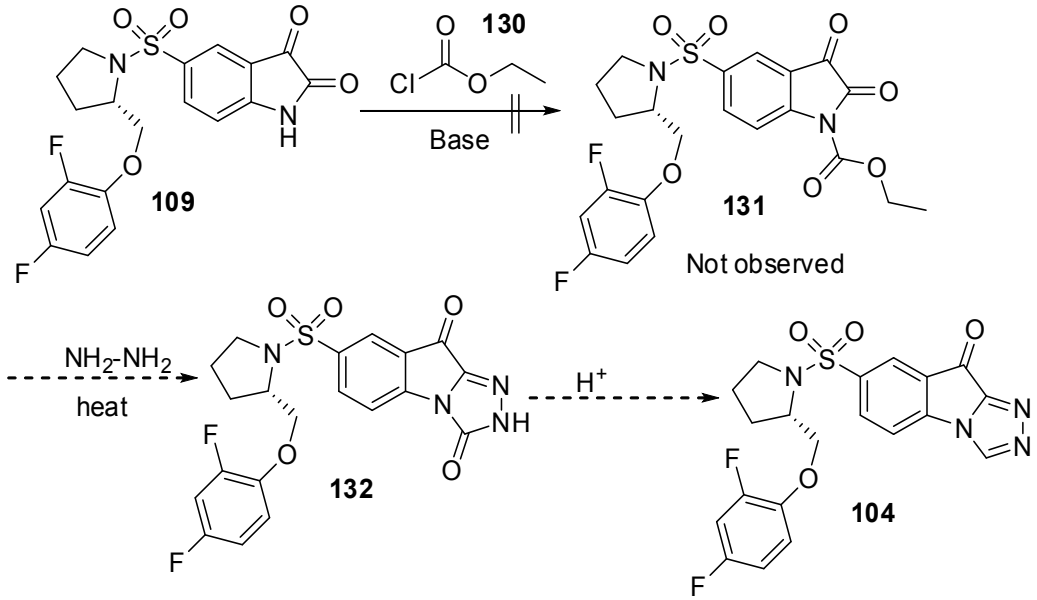


Scheme 4.12: Attempts to achieve triazoleindolone derivative **129** from the reaction of imidate intermediates **128a/b** with formic hydrazide **112**

Methyl imidate formation was subsequently repeated with the ketal protected isatin sulfonamide **118**, using $[BF_4][OMe_3]$ as the alkylating agent (Scheme **4.12**). It was hoped that replacement of the ketone group with a ketal would increase the electron density of the isatin ring, increasing the chances of nucleophilic attack on the alkylating agent. At all temperatures trialled, though the starting material was the major component of the reaction mixture, minor reactions was observed overnight to give a bright yellow compound. Crude ^1H NMR of the reaction mixture showed that the product of the incomplete reaction was not the desired product, but a close derivative of the starting material **118** in which the ketal protecting group was displaced. Given that isatin rings are characterised by a bright yellow/orange colour, turning colourless upon protection/removal of

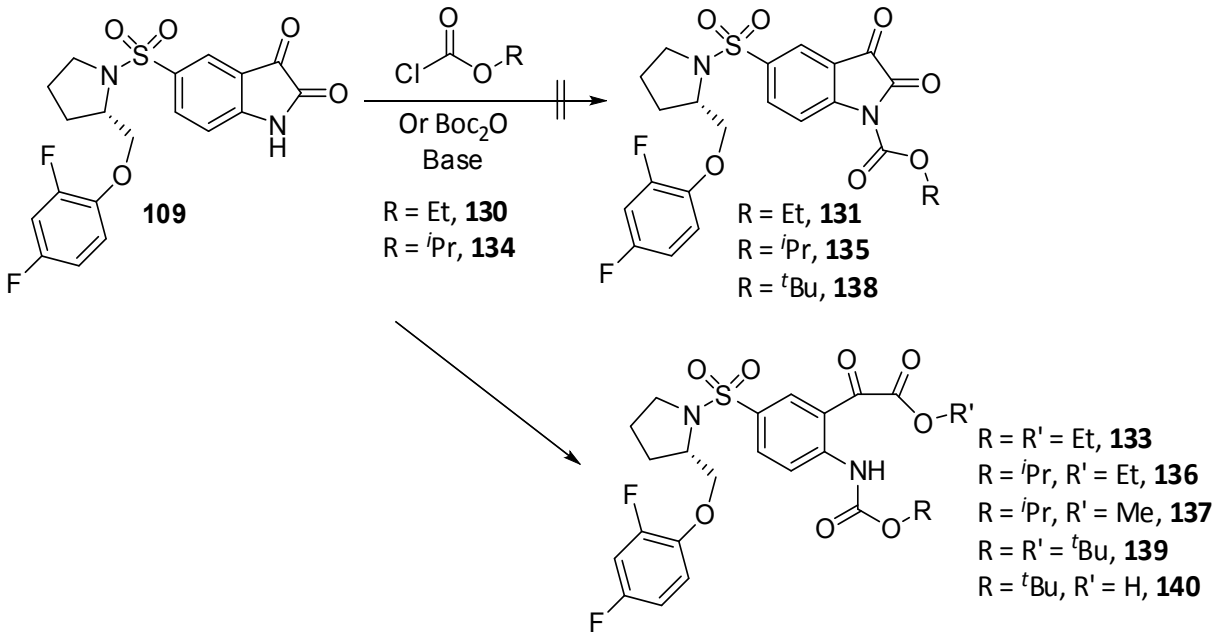
the ketone, it was possible that the strong alkylating agent resulted in hydrolysis of the ketal bond, to give a brightly coloured ketone species. The small amount of a side product could not be isolated for further characterisation. The reaction appeared to halt after a day as there was no significant increase in consumption of the starting material after prolonged stirring for up to 3 days. It is worth noting that the reaction was carried out in anhydrous solvents under argon, as the presence of water was expected to react with any resulting methyl imidate product **127**/**128** to regenerate the starting material.

Triflate anhydride is another strong electrophile used for O-sulfonation.[161-163] This reagent was also used in attempts to prepare the imidate intermediate of the ketal **118** (Scheme **4.12**). Similarly to reactions with $[BF_4][OMe_3]$, an LCMS showed that the major component of the reaction mixture after one day was unreacted starting material **118**. It was thought that the limited solubility of triflate anhydride in DCM, as well as the inherent instability of the triflyl imidate **128a** could account for the fact that no reaction was observed. As a result, another reaction was carried out in the more polar acetonitrile, where instead of attempting to isolate the triflate intermediate **128a**, formic hydrazide **112** was added to the reaction mixture, and after one day, the mixture was heated overnight to force the reaction. It was hoped that the ketal-protected triazoleindolone **129** would be obtained in a one-pot synthesis (Scheme **4.12**). Again, no reaction was observed and only the starting material **118** was isolated. The apparent lack of reactivity of ketal-protected and unprotected isatin sulfonamide **118** and **109** towards triflic anhydride and $[BF_4][OMe_3]$ could be a result of the sulfonamide substituent significantly reducing the nucleophilicity of the amide group. It is also possible that the electron deficiency of the isatin sulfonamide gave rise to imidate intermediates which were highly unstable and easily hydrolysed. As a result of the lack of reaction with triflic anhydride and $[BF_4][OMe_3]$, synthesis via imidate intermediates was abandoned.



Scheme 4.13: Attempted preparation of the triazoleindolone **104** from carbamate **131**

Subsequently, triazoleindolone synthesis via a carbamate intermediate was investigated. The strategy for this route was to prepare the carbamate derivative **131** of isatin sulfonamide **109**, which would be treated with hydrazine to give the species **132**, followed by dehydration to give the triazoleindolone heterocycle **104** (Scheme **4.13**). Such reactions of isatin carbamate derivatives and other heterocycles with hydrazine to give the corresponding triazoloindole-dione **132** have been reported in literature.[164, 165] The first attempt to obtain the carbamate derivative of isatin sulfonamide **109** involved treatment with ethyl chloroformate **130**. Although isatin derivatives have reportedly been successfully N-acyalted,[164, 166] a range of reactions using different bases and solvents failed to give the desired carbamate **131** (Scheme **4.14**, Table **4.1**). Instead, the open ring α-keto ester **133** was obtained (Scheme **4.14**), using a range of bases including, pyridine, triethylamine, potassium *tert*-butoxide and sodium hydride. As well as ethyl chloroformate **130**, the bulkier isobutyl chloroformate **134** and Boc_2O were also utilised as acylating agents, as it was hoped these reagents would sterically hinder isatin ring opening.



Scheme 4.14: Acylation of isatin sulfonamide **109** with chloroformate and Boc_2O

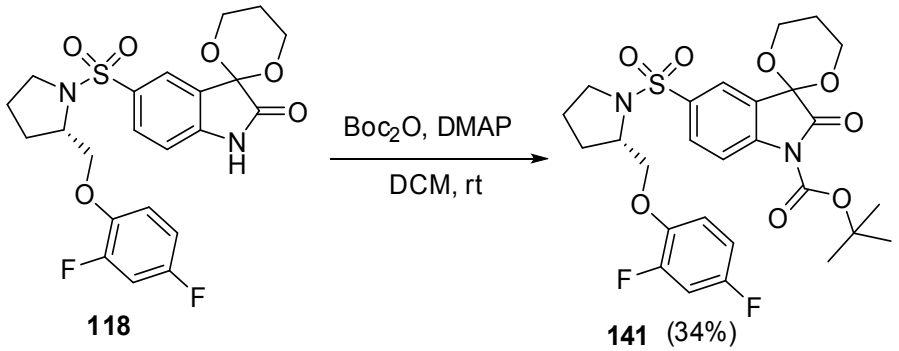
Table 4.1: Acylation reaction conditions and obtained products

Entry	Acylating agent	Base	Solvent	Temp (°C)	Product
1	Ethyl chloroformate	Pyridine	PhMe	rt	**133**
2	Ethyl chloroformate	Et_3N	THF	rt	**133**
3	Ethyl chloroformate	K_2CO_3	DMF	rt	**133**
4	Ethyl chloroformate	^{t}BuOK	DMF	rt	**133**
5	Ethyl chloroformate	NaH	THF	0	**133**
6	Isobutyl chloroformate	NaOEt	MeOH	0	**136** and **137**
7	Isobutyl chloroformate	LiHMDS	THF	0	-
8	Boc_2O	DMAP*	DCM	rt	**139** and **140**

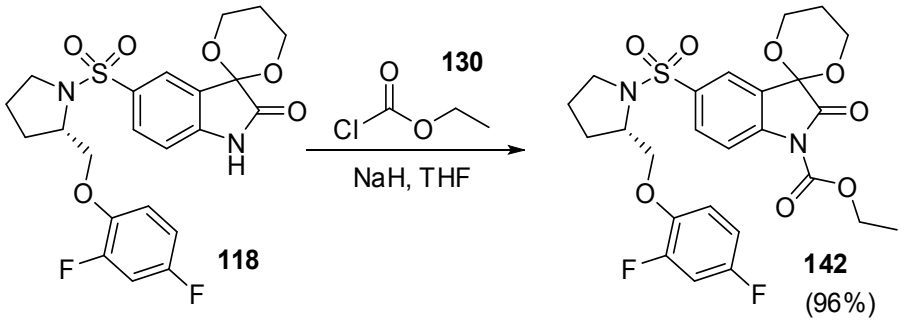
*Catalytic amount of DMAP used

When isobutyl chloroformate **134** was used as the acylating agent with sodium ethoxide as the base in methanol, a mixture of two open ring α-keto esters were obtained, the ethoxy ester **136** and the methoxy ester **137** (Table **4.1**, Entry **6**; Scheme **4.14**). By contrast, the use of LiHMDS as the base with isobutyl chloroformate **134** led to complete decomposition, likely due to the much stronger base promoting multiple side reactions (Table **4.1**, Entry **7**). Likewise, the use of Boc_2O led to open ring structures, giving a mixture of α-keto ester **139** and α-keto carboxylic acid **140** (Table **4.1**, Entry **8**; Scheme **4.14**). It is likely that the acylation reactions generated the alcohol derivatives of the corresponding chloroformate which then acted as a nucleophile, attacking the carbonyl of the initially

formed desired carbamate product, and opening the isatin ring. Ring opening by alcohol derivatives could account for the fact that, a mixture of the open ring methyl and ethyl esters (**136** and **137**) were obtained when the nucleophilic base, NaOEt was used with MeOH as the solvent (Table **4.1**, Entry **6**; and Scheme **4.14**).

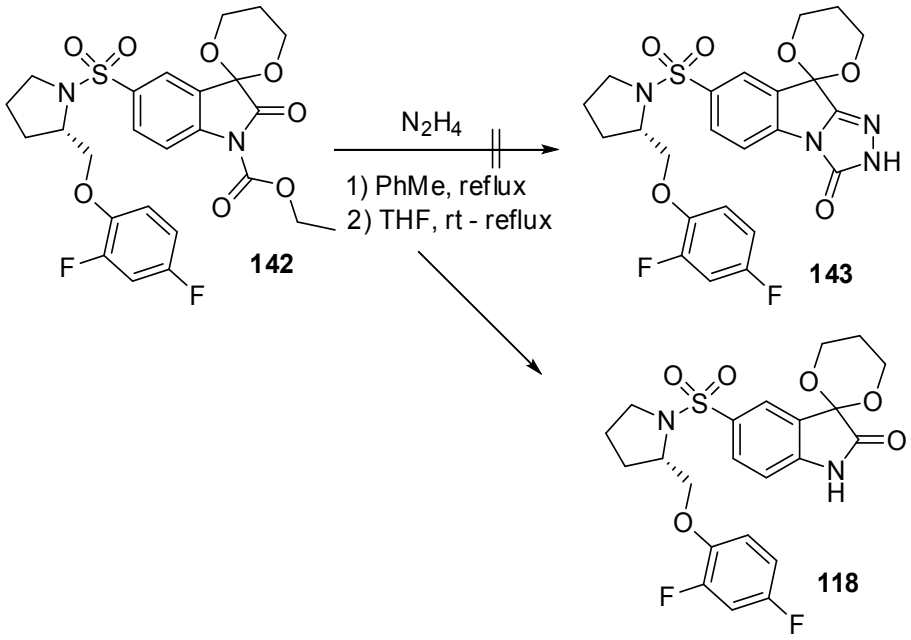


Scheme 4.15: Successful synthesis of carbamate **141**



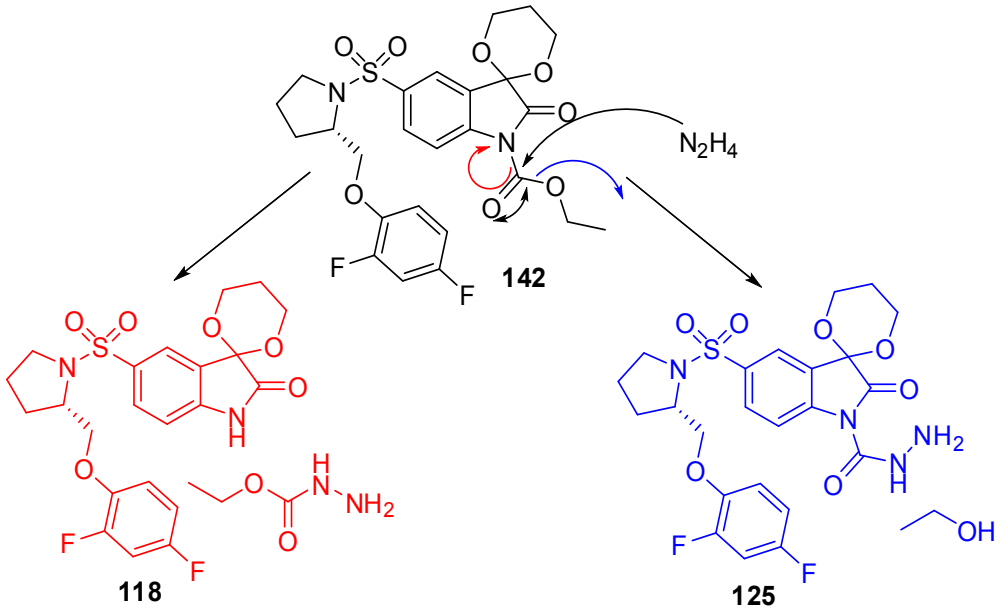
Scheme 4.16: Preparation of the ethoxy carbamate **142** from ketal **118** in 96 % yield

By contrast, acylation reactions with ketal **118** and Boc_2O successfully gave the desired carbamate **141** in 34 % yield (Scheme **4.15**). The ethoxy carbamate **142** was prepared in the higher yield of 96 % from ethyl chloroformate **130** and ketal **118** (Scheme **4.16**). The ethyl carbamate **142** was preferred for the next step instead of the *tert*-butyl carbamate **141** as the ethoxide is less sterically hindered and a better leaving group.



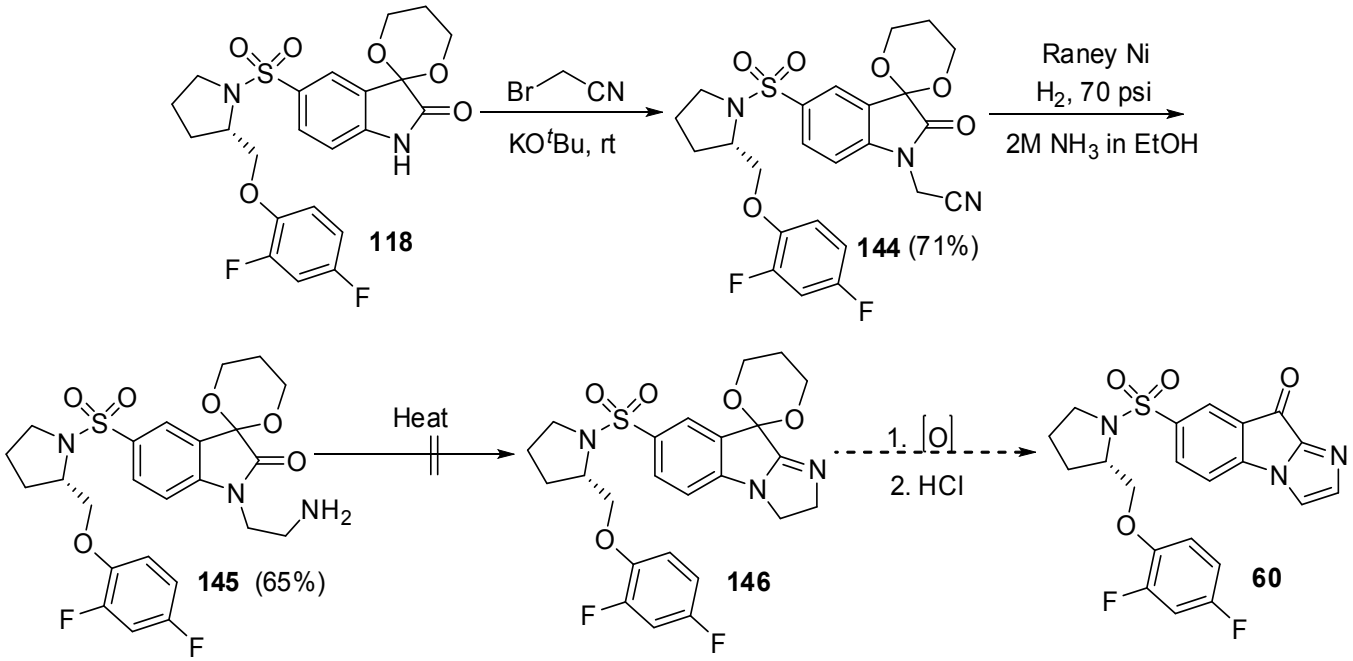
Scheme 4.17: Treatment of carbamate **142** with hydrazine in toluene and THF

Unfortunately, the next step involving the reaction of carbamate **142** with hydrazine failed to give the desired spiro-triazoloindolone **143** (Scheme **4.17**). The disappearance of carbamate **142** within 2 hours in either toluene or THF was observed by TLC. In addition to a mixture of unknown species, the ketal-protected isatin sulfonamide **118** was regenerated and recovered from the reaction mixture. Hydrazine apparently reacted with carbamate **142** to displace the isatin ring rather than the ethoxide as the leaving group (Scheme **4.18**).



Scheme 4.18: Possible reaction leading to the regeneration of ketal **118** upon treatment of carbamate **142** with hydrazine

While hydrazide based reagents, including formic hydrazide **112**, hydrazinocarboxylate **124** and hydrazine were employed for reactions with isatin sulfonamide intermediates with the aim of achieving the triazoleindolone heterocycle **104**, bromoacetonitrile was utilised for the preparation of the imidazoleindolone heterocycle **60** from ketal **118**.



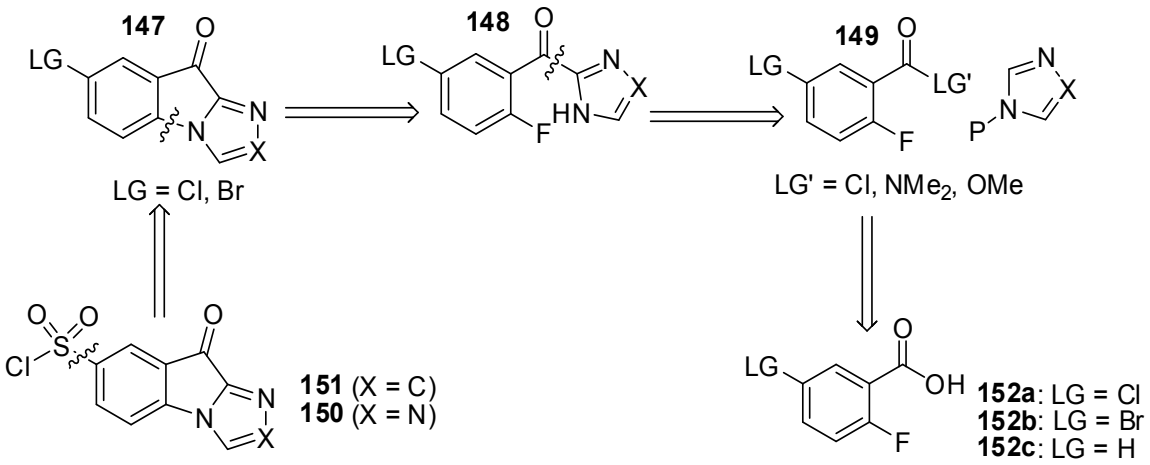
Scheme 4.19: Attempts to prepare the imidazoleindolone heterocycle **60** from ketal **118** and bromoacetonitrile

In an attempt to form the imidazole ring of the imidazoleindolone scaffold, ketal **118** was first N-alkylated with bromoacetonitrile in the presence of potassium *tert*-butoxide to give the nitrile intermediate **144** in 71 % yield (Scheme **4.19**). In an analogous reaction described for the pyrimidoindolone synthesis in Chapter **III**, the next step involved the Raney Ni catalysed nitrile reduction to give primary amine **145** in 65 % yield (Scheme **4.19**). Intramolecular cyclisation/dehydration would then give the amidine ring **146** which would be oxidised to the aromatic imidazole ring, followed by ketal hydrolysis to give the imidazoleindolone heterocycle **60** (Scheme **4.19**). However, unlike the pyrimidoindolone synthesis (Chapter **III**), heating to effect dehydration/cyclisation in order to obtain amidine **146** led to the decomposition of primary amine **145**. For the pyrimidoindolone synthesis, Thorpe-Ingold effect of the bulky cyclopentyl ring could account for the facile dehydration of the amine intermediate **78** to give pyrimidoindolone **79** (Chapter **III**, Scheme **3.6**).[167]

Cyclisation of the primary amine **145** was subsequently attempted using $POCl_3$ as a dehydrating agent but this was also unsuccessful, with no reaction and quantitative isolation of the starting material. Similar dehydration reactions have been achieved using acid catalysts such as TsOH, acetic acid or camphorsulfonic acid, though in the absence of acid sensitive ketal groups.[168-170] However, acid catalysed cyclisation was not attempted with amine **145** as it was believed that ketal hydrolysis would be faster than cyclisation and the resulting ketone could then react with the amine group to give dimeric species leading to decomposition.

IV.3. Imidazoleindolone and Triazoleindolone Synthesis via S_NAr Fluoride displacement

The synthetic results thus far have shown that the preparation of the triazoleindolone **104** and imidazoleindolone **60** heterocycles from isatin sulfonamide intermediates was hampered by problems associated with unexpected reactions or lack of reaction in some cases. As a result, the synthetic route for achieving the indolone heterocycles was re-evaluated and an alternative retrosynthetic approach was devised. Since attempts to incorporate the imidazole or triazole ring onto the intact indolinone ring of isatin sulfonamide intermediates proved problematic, we investigated a route where the entire indolone would be constructed in sequence. The retrosynthetic approach is shown below in Scheme **4.20**.

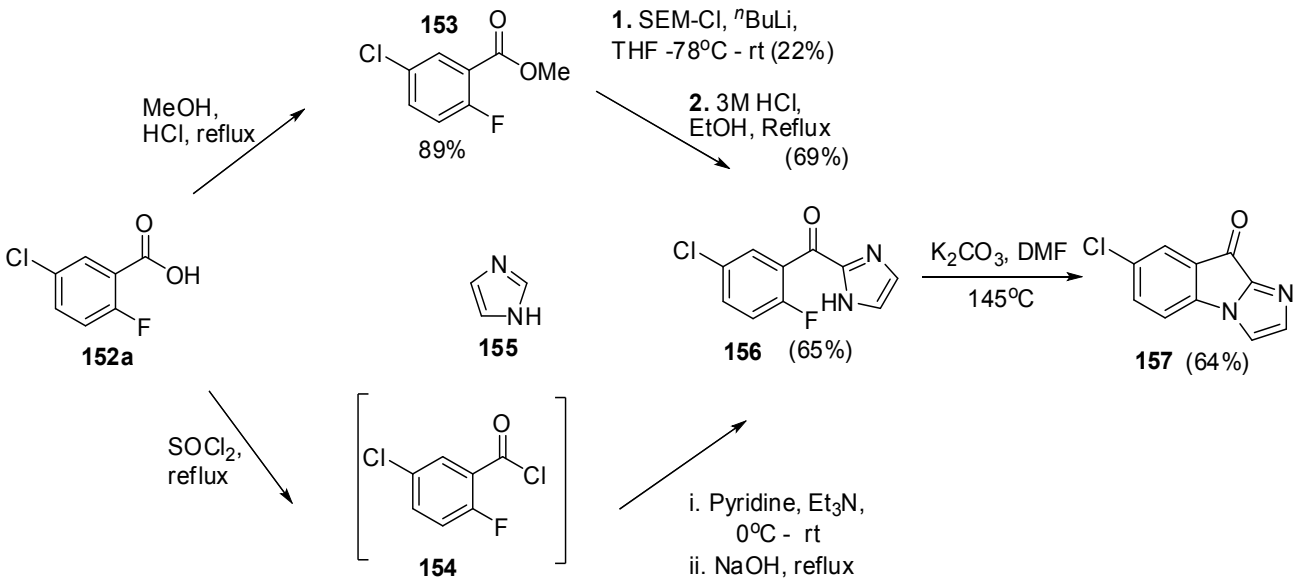


Scheme 4.20: Retrosynthetic analysis of an alternative route to the triazoleindolone and imidazoleindolone heterocycles

The key step in the revised route is the formation of the indolone ring system **147** from an intramolecular S_NAr displacement of an aryl fluoride by the azole nitrogen atom. Fluoride is a stable leaving group with high yielding intermolecular and intramolecular displacement of aromatic

fluorides by amino groups reported in literature.[171-173] Introduction of the sulfonamide substituent was initially reserved for the final steps in order to avoid any problems that may arise from the strong electron withdrawing effects of the sulfonyl group. Halogen substituents were instead employed, with the aim of converting the halogen groups into the sulfonyl chloride following the formation of indolone scaffold. The resulting sulfonyl chloride **150**/**151** would then be treated with the relevant amine to give the corresponding sulfonamide.

IV.3.1. Imidazoleindolone Synthesis

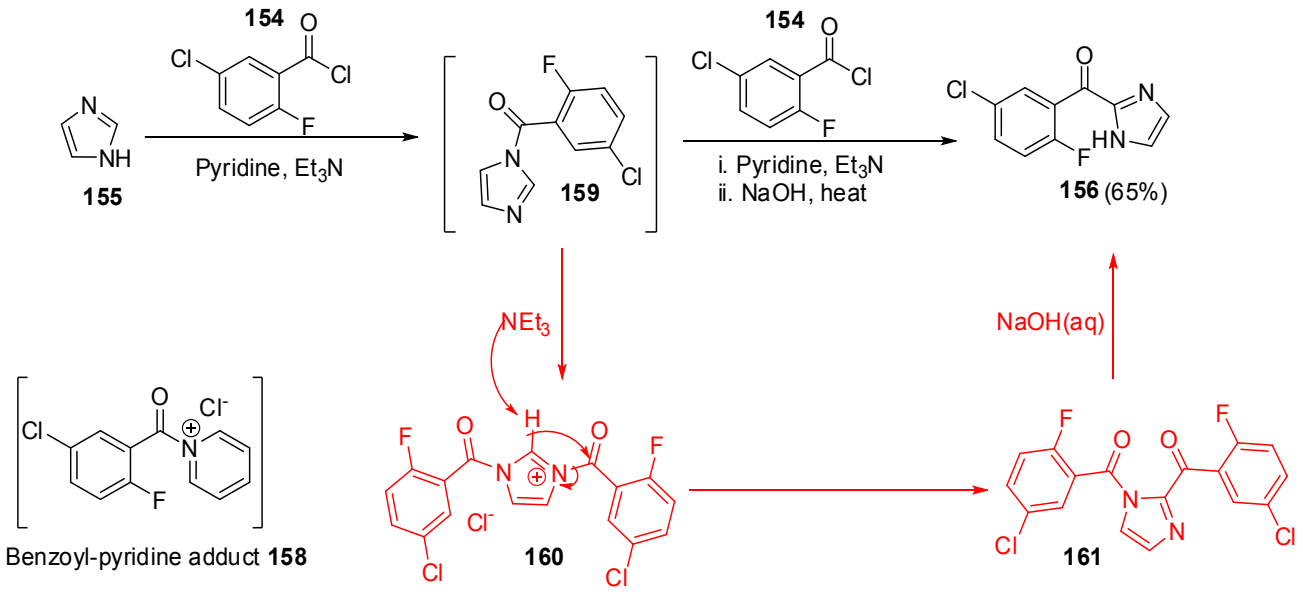


Scheme 4.21: Synthesis of imidazoleindolone **157** from the commercially available benzoic acid **152a** and imidazole **155**

Starting from the commercially available 5-chloro-2-fluorobenzoic acid **152a**, two reaction intermediates were prepared, methyl ester **153** in 89 % yield and the acid chloride **154** in assumed quantitative yield (Scheme **4.21**). At first, phenyl-imidazole ketone **156** was prepared following a reported procedure, which involved the one-pot synthesis of SEM-protected imidazole, and subsequent imidazole C-2 lithiation and nucleophilic substitution of an ester reagent.[174] Following this procedure, imidazole **155** was treated with ^{n}BuLi at -78 ^{o}C and warmed to room temperature prior to the addition of SEM-Cl to generate the SEM-protected imidazole *in situ*. The mixture was then re-cooled to -78 ^{o}C and treated with another equivalent of ^{n}BuLi, followed by quenching with methyl ester **153** to generate the SEM-protected ketone derivative of **156** in 22 % yield (Scheme **2.1**). This was treated with HCl to remove the SEM protecting group, giving the deprotected ketone **156** in

69 % yield (Scheme **4.21**). While the one-pot N-protection-substitution procedure reduced the number of steps, the modest yield of 22 % was not ideal.

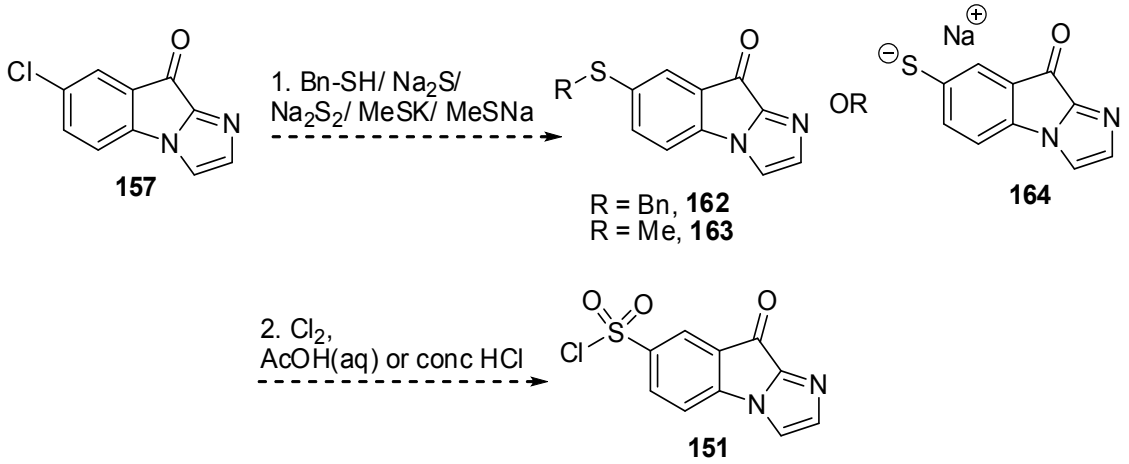
Bastiaansen *et al*. reported that the preparation of phenyl-imidazole ketone derivatives can be achieved without the need for N-protection of imidazole.[175] Following the literature procedure,[175] imidazole was treated with triethylamine and two equivalents and benzoyl chloride **154**, which was prepared by heating the benzoic acid **152a** in thionyl chloride. After stirring in pyridine for 3.5 hours at room temperature, the mixture was treated with 7.5N NaOH and heated to reflux for one hour. Upon cooling, the desired ketone **156** precipitated from the reaction mixture in 65 % yield (Scheme **4.21**).



Scheme 4.22: A single-pot synthesis of 2-benzoylimidazole **156**.[175]

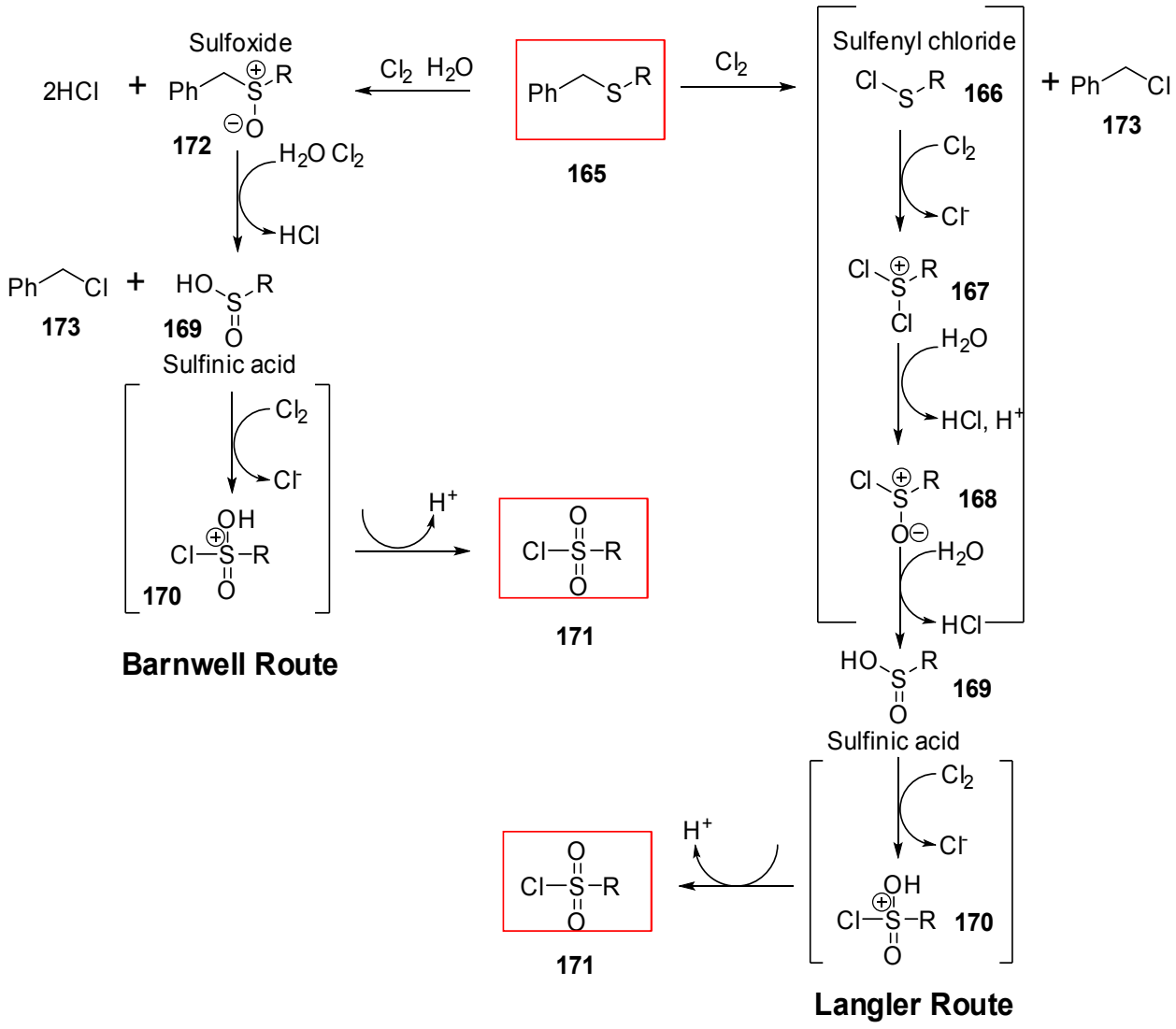
This reaction was reported to proceed via a benzoyl-pyridine adduct **158**, acting as a powerful benzoylating agent to give an N-benzoylimidazole intermediate **159** (Scheme **4.22**).[175] Bastiaansen *et al*. concluded that N-benzoylimidazole **159** reacts with a second equivalent of benzoyl chloride, and upon aqueous workup with NaOH, 2-benzoylimidazole **156** is obtained.[175] We believe that N-benzoylimidazole intermediate (**159**) reacts with a second equivalent of benzoyl chloride to give an *N,N*-dibenzoylimidazole species (**160**), followed by C-2 deprotonation and benzoyl transfer to the imidazole C-2 position to give a 1,2-dibenzoyl intermediate (**161**). This is then cleaved by NaOH on the N-benzoyl bond to give the phenyl-imidazole ketone (**156)** (Scheme **4.22**).

Following the successful formation of phenyl-imidazole ketone **156**, K_2CO_3 was utilised as a base in DMF, stirring at 145 ^oC to achieve the intramolecular S_NAr displacement of the fluoride substituent by the imidazole group. This successfully gave the anticipated imidazoleindolone heterocycle **157** in 64 % yield (Scheme **4.21**).

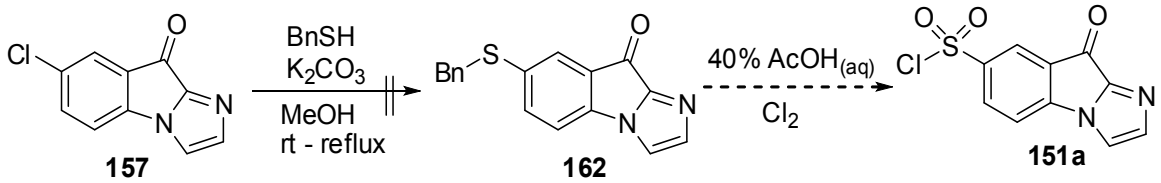


Scheme 4.23: Conversion of aromatic halides to sulfonyl chlorides via nucleophilic substitution and oxidative chlorination.[176-180]

In successive reactions, conditions for the preparation of 7-sulfonyl imidazoleindolone **151** from 7-chloro imidazoleindolone **157** were explored. The functional group interconversion of aromatic chlorides into sulfonyl groups have been reported to occur in a two-step process, involving nucleophilic chloride displacement by a sulfur nucleophile followed by oxidative chlorination to give the corresponding sulfonyl chloride (Scheme **4.23**).[176-179] A range of sulfur nucleophiles can be employed, though benzylthiol is the most commonly used, and oxidative chlorination typically occurs in aqueous acidic media (Scheme **4.23**). Langler proposed that oxidative chlorination occurs via an initial loss of benzyl cation and concomitant formation of a sulfenyl chloride **166**,[181] while Barnwell *et al*. observed that oxidative chlorination proceeded via an initial formation of a sulfoxide **172**.[182] The proposed oxidative chlorination pathways by the two groups are shown in Scheme **4.24**.



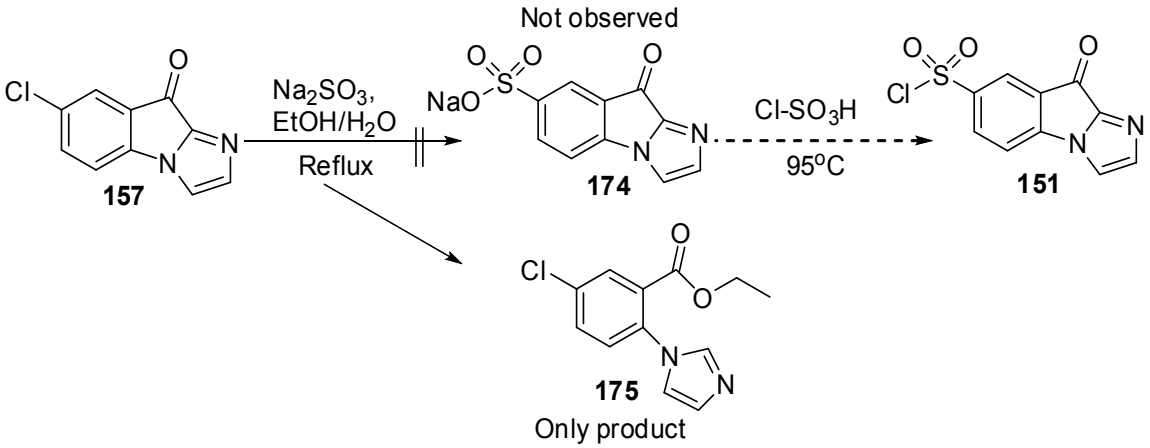
Scheme 4.24: Two proposed mechanisms for the oxidative chlorination of thioether intermediates[181, 182]



Scheme 4.25: An initial attempt to prepare the sulfonyl chloride substituted imidazoleindolone heterocycle **151a**

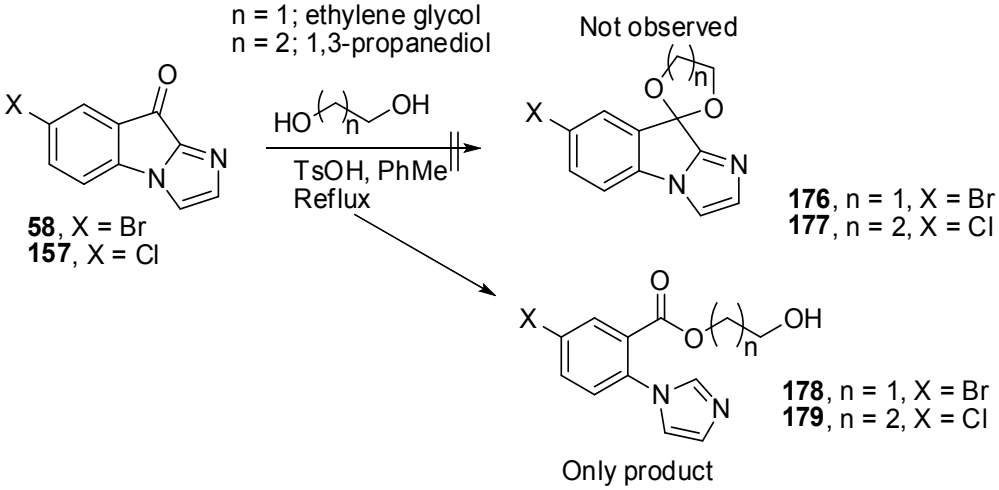
Following a reported procedure,[180] an initial attempt to introduce the sulfonyl group involved treatment of a mixture of 7-chloroimidazoleindolone **157** and benzyl thiol with K_2CO_3, aiming to obtain the benzyl thioether intermediate **162** (Scheme **4.25**). Given that the imidazoleindolone heterocycle was designed to incorporate thiols as a caspase-binding inhibitor, an excess amount of

benzyl thiol was used in order to counteract any trapping of the thiol reagent by the ketone carbonyl. However, the formation of the thioether **162** was unsuccessful, with only unreacted imidazoleindolone **157** isolated from the reaction mixture.



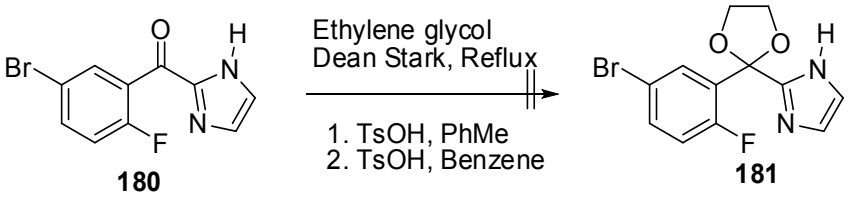
Scheme 4.26: An attempt to prepare sulfonyl chloride **151** via the sodium salt **174** using sodium sulfite

Sodium sulfide (Na_2S)[179, 180] was also utilised for the S_NAr displacement of the aryl chloride **157** in DMSO at room temperature. A TLC and crude ^1H NMR of the resulting reaction mixture suggested complete decomposition of the starting material. In an attempt to achieve the sodium sulfonate salt **174**, sodium sulfite (Na_2SO_3) was utilised, following literature procedures (Scheme **4.26**).[183, 184] In this case, ring opening to give the ethyl benzoate ester **175** was observed (Scheme **4.26**), which was attributed to the reaction of solvent ethanol with the ketone carbonyl of imidazoleindolone **157**. The imidazoleindolone scaffold is known to be stable in ethanol or methanol. Hence, it is likely that sodium sulfite catalysed the nucleophilic addition of ethanol to imidazoleindolone **157** (Scheme **4.14**). The reaction was repeated in DMF, but no reaction occurred, likely due to the limited solubility of sodium sulfite in DMF.



Scheme 4.27: Attempts to prepare the ketal protected derivatives of imidazoleindolone

It was hoped that protection of the ketone carbonyl as a ketal would lead to successful reactions with sulfur nucleophiles. Hence, protection of imidazoleindolone **157** as ketal **177** using 1,3-propanediol and catalytic TsOH was attempted (Scheme **4.27**), but similarly to the reaction resulting in the formation of ethyl benzoate ester **175** (Scheme **4.26**), the open ring ester **179** was obtained. Ring opening was also observed when ethylene glycol was used instead of 1,3-propanediol, so the size of the ketal had no effect on the reaction outcome (Scheme **4.27**).

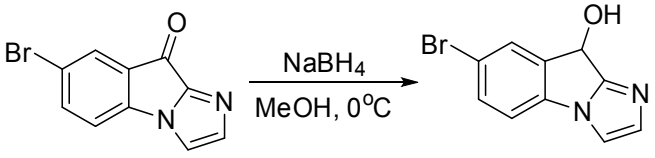


Scheme 4.28: Attempts to prepare ketal **181** from ketone **180**

The bromo-substituted imidazoleindolone **58** was also prepared using the same steps employed for the preparation of the chloro-substituted imidazoleindolone **157** (Scheme **4.21**). Aromatic bromides are reportedly converted to sulfonyl chlorides in a process that involves treatment with ^{n}BuLi, with lithium-halogen exchange giving an anion which is treated with a sulfur electrophile such as sulfuryl chloride (SO_2Cl_2) to give the desired sulfonyl chloride.[185] This procedure required the protection of the ketone carbonyl as a ketal in order to avoid undesired trapping of ^{n}BuLi by the carbonyl group. As treatment of the imidazoleindolone ring with ethylene glycol or propanediol in the presence of an acid catalyst led to ring opening, ketone protection was attempted prior to S_NAr cyclisation with phenyl-imidazole ketone **180**. This involved treatment of ketone **180** with ethylene glycol and TsOH in toluene, heating to reflux (Scheme **4.28**). After 12 hrs, no reaction

was observed. It was initially thought that the lack of reaction could be due to ethylene glycol azeotroping with toluene when heated to reflux, hindering reaction with ketone **180**. However, using benzene as the solvent made no difference to the reaction outcome. It was likely that protonation of the basic imidazole ring prevented protonation of the ketone impeding ketal formation.

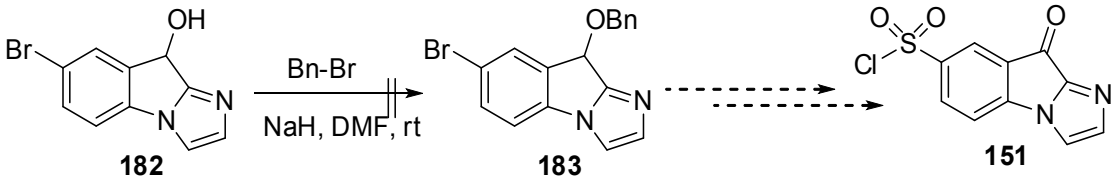
We considered alternative ketone protecting groups such as 1,3-dithioacetals. However, the open ring reactions observed during ketal formation attempts (Scheme **4.27**) stemmed from the nucleophilic displacement of the imidazole ring by the diol reagent. A thiol utilised for dithioacetal formation was expected to behave in a similar way. The alcohol derivative of imidazoleindolone **182** was instead explored as an alternative to ketal-protection of the ketone group (Scheme **4.29**).



58 **182** (92%)

Scheme 4.29: Reduction of imidazoleindolone **58**

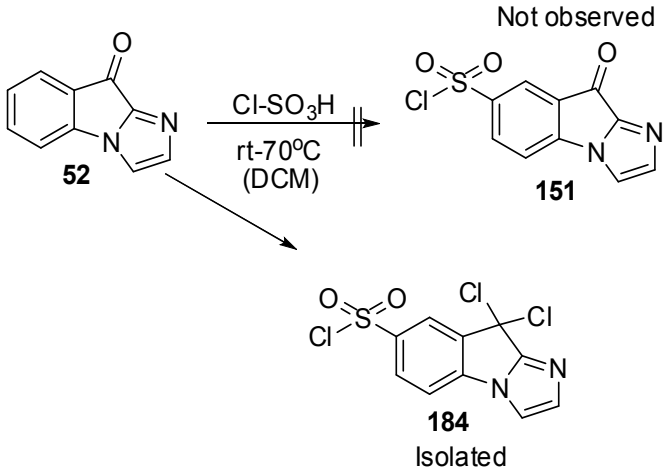
Treatment of ketone **58** with sodium borohydride in methanol gave the alcohol product **182** according to a crude ^{1}H NMR analysis. However, after aqueous work-up and concentration *in vacuo*, an insoluble solid, unable to dissolve in a range of solvents, including hot methanol, DMF, DMSO, water, and DCM/MeOH mixtures was obtained. Ketone reduction was repeated, and without work-up, the polar but soluble alcohol product **182** was obtained in 92 % yield (Scheme **4.29**).



182 **183** **151**

Scheme 4.30: An attempt to protect alcohol **182** as a benzyl ether prior to the introduction of the sulfonyl chloride substituent

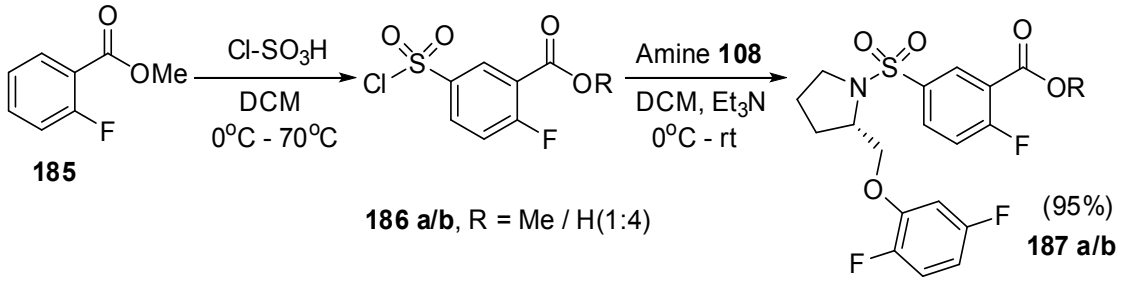
Unfortunately, treatment of alcohol **182** with benzyl bromide and NaH in order to obtain the benzyl ether protected alcohol **183** was unsuccessful, giving a decomposed mixture with no signs of the desired product (Scheme **4.30**).



Scheme 4.31: An attempt to introduce the sulfonyl chloride group to the unsubstituted imidazoleindolone heterocycle **52**

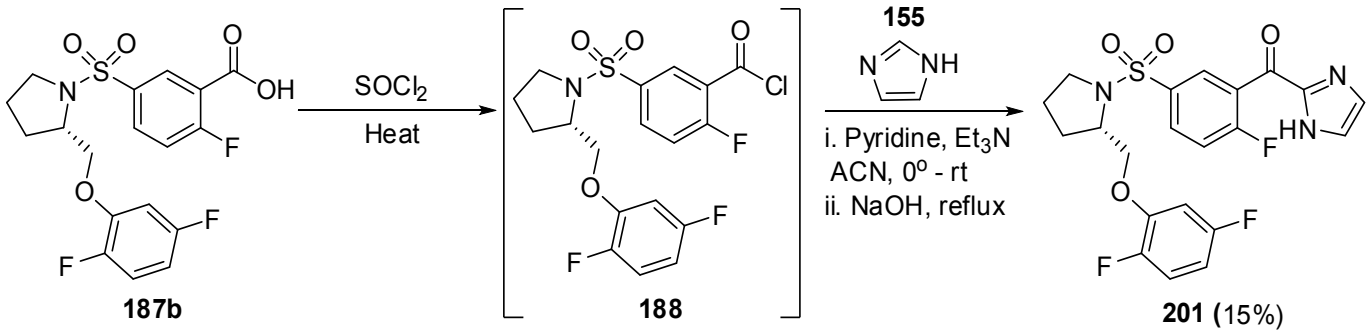
We subsequently investigated the direct sulfonation of the phenyl group of unsubstituted imidazoleindolone **52**. It was hoped that the presence of the electron donating imidazole ring would direct sulfonation to the desired 7-position of the imidazoleindolone heterocycle. No reaction was observed when imidazoleindolone **52** was heated with chlorosulfonic acid in DCM for 12 hours, but stirring in neat chlorosulfonic acid at either room temperature or at 70 ^{o}C resulted in full consumption of the starting material (Scheme **4.31**). A mixture of products was observed by TLC, but the only product isolated was the 5-chlorosulfonyl *gem*-dichloride **184**, in 11 % yield (Scheme **4.31**). Since the sulfonyl chloride was introduced in the desired 7-position, hydrolysis of the *gem*-dichloride group to give a ketone using reported conditions,[186] could give the sulfonyl substituted imidazoleindolone **151**. However, the poor yield of the reaction discouraged further use of *gem*-dichloride **184**.

As a result of the problems encountered with attempts to introduce the sulfonyl substituent following the successful formation of the halogen-substituted and unsubstituted imidazoleindolone heterocycles, the synthetic sequence was reversed to incorporate the sulfonamide substituent in the initial steps prior to the formation of the indolone heterocycle.



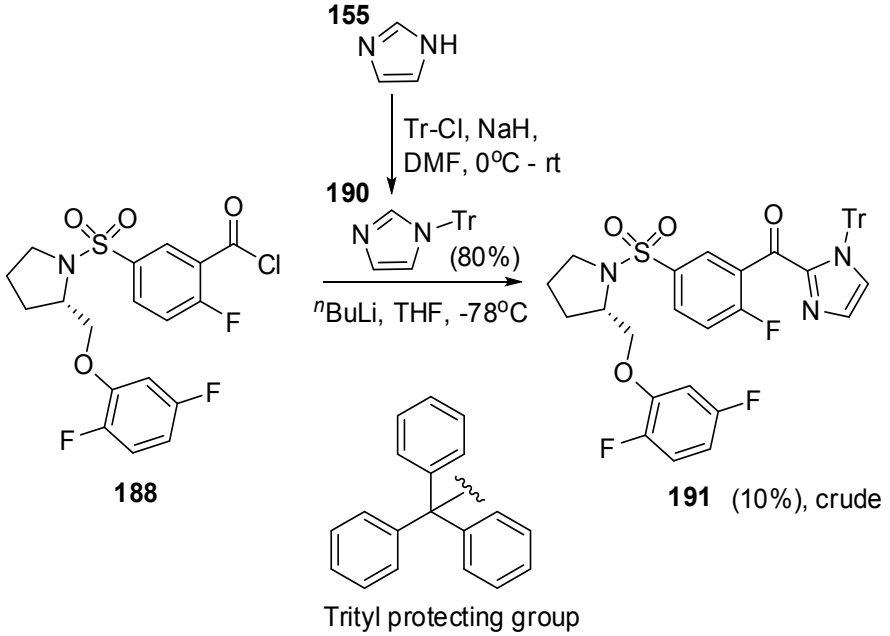
Scheme 4.32: Preparation of 5-sulfonamide-2-fluorobenzoate **187a/b**

The first step in the preparation of the sulfonamide substituted intermediate **187**, involved treatment of methyl 2-fluorobenzoate **185** with chlorosulfonic acid at 70 ^{o}C. This exclusively added the chlorosulfonyl group to the 5-phenyl position to give methyl ester **186a** as the minor product and the ester hydrolysed carboxylic acid **186b** as the major product in a 1:4 ratio (Scheme **4.32**). The acid/ester mixture was used in the next step, treating with the previously described amine **108** (Scheme **4.1**) to give 5-sulfonamide methyl benzoate **187a** and the benzoic acid derivative **187b** in a total yield of 95 % (Scheme **4.32**).



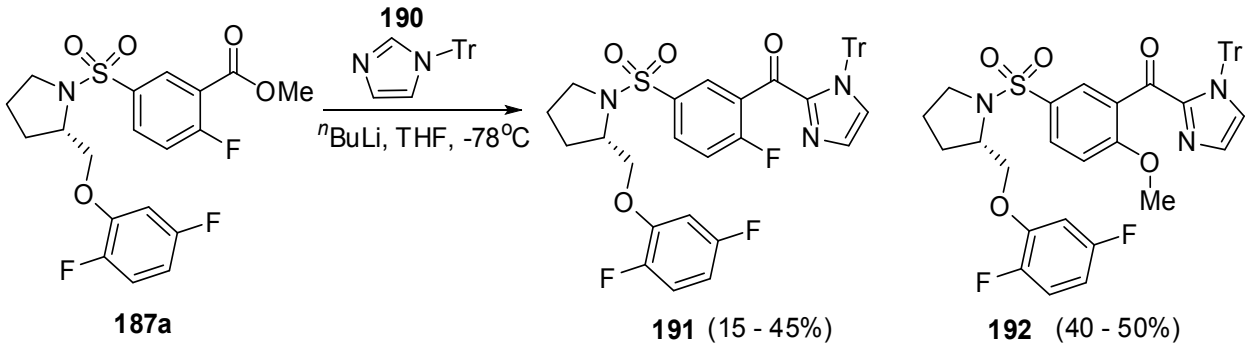
Scheme 4.33: Preparation of sulfonamide substituted phenyl-imidazole ketone **201** using the one-pot synthesis of 2-benzoylimidazoles with unprotected imidazole

In the next step, 5-sulfonamide-benzoic acid **187b** was treated with thionyl chloride, giving benzoyl chloride **188** (Scheme **4.33**). This was used in the one-pot synthesis of 2-benzoylimidazoles with unprotected imidazole, which successfully gave the halogen substituted ketone **157** (Scheme **4.22**). Unfortunately the reaction was less efficient with sulfonamide substituted **188** with only 15 % of the desired ketone **201** isolated and in less than 80 % purity (Scheme **4.33**).



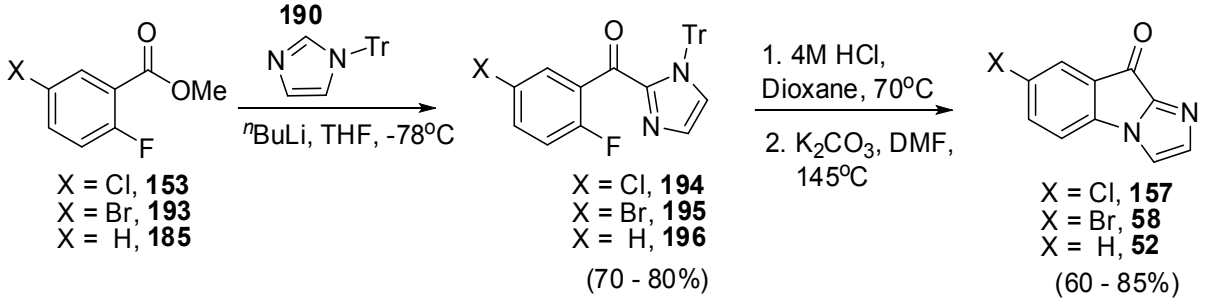
Scheme 4.34: Preparation of N-trityl protected phenyl-imidazole ketone **191** from benzoyl chloride **188**

A more stepwise approach was adopted where imidazole was first protected with a trityl group, a protecting group chosen for its facile synthesis and easy handling of the solid 1-trityl-1*H*-imidazole **190** (Scheme **4.34**).[187] Trityl protected imidazole **190** was prepared in 80 % yield by treatment of imidazole with Tr-Cl and NaH in DMF (Scheme **4.34**). This was then lithiated on the C-2 position using ^{n}BuLi in THF at -78 ^{o}C, prior to quenching with benzoyl chloride **188**. However, there was no improvement in the reaction efficiency, with ketone **191** isolated in only 10 % yield (Scheme **4.34**). As a result, 5-sulfonamide-carboxylate **187a** was employed as an alternative, milder acylating agent.



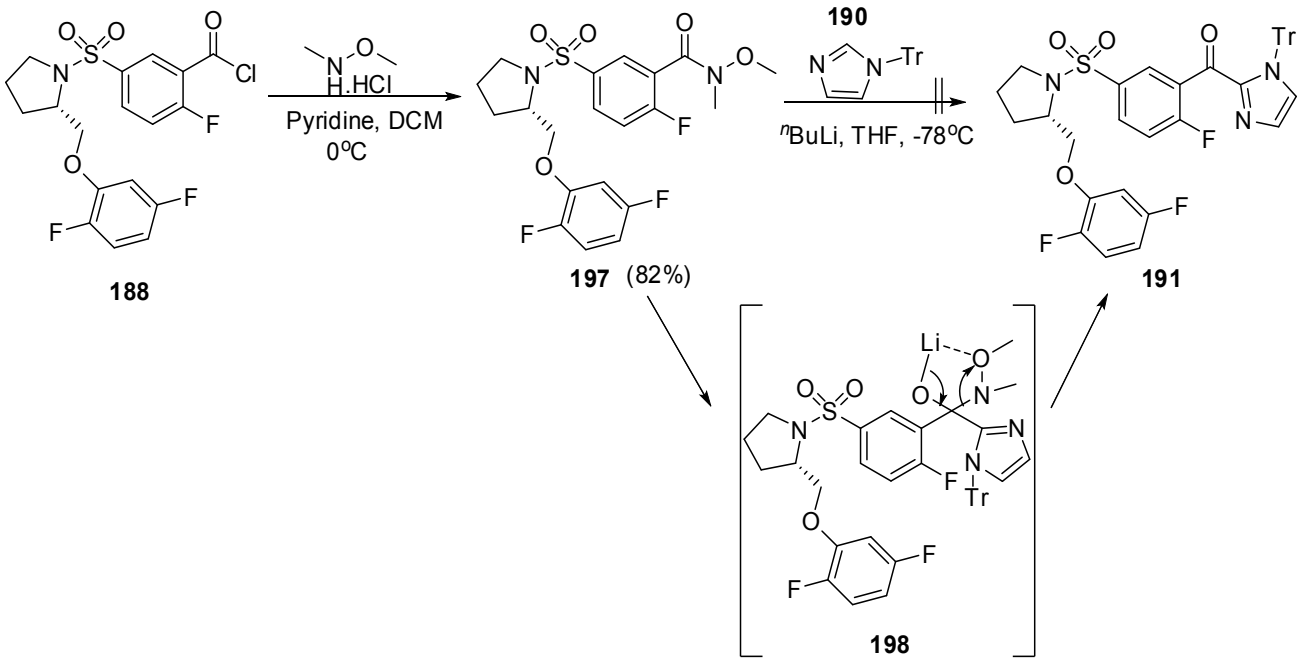
Scheme 4.35: Preparation of N-trityl protected imidazole-ketone **191** from 5-sulfonamide methoxy benzoate **187a**

Treatment of lithiated trityl-imidazole anion **190** with methyl carboxylate **187a** inconsistently gave the desired ketone **191** in 15 – 45 % yield (Scheme **4.35**). The major product of the reaction was the fluoride displaced, methoxide-substituted ketone **192**, presumably formed from further reaction of the desired product **191** with the methoxide leaving group of ester **187a**. Despite the formation of the methoxide substituted species **192** as the major product, nucleophilic substitution using the ester **187a** gave the ketone in higher yield and purity, compared to the use of acid chloride **188**. Efforts were made to increase the percentage yield of ketone **191** formation. Controlling the speed of ester **187a** addition to the lithiated imidazole solution whilst maintaining the temperature at or below -78 ^{o}C; quenching the reaction mixture below -50 ^{o}C; or varying the reaction concentration made very little difference to the reproducibility and yield of ketone **191** formation.



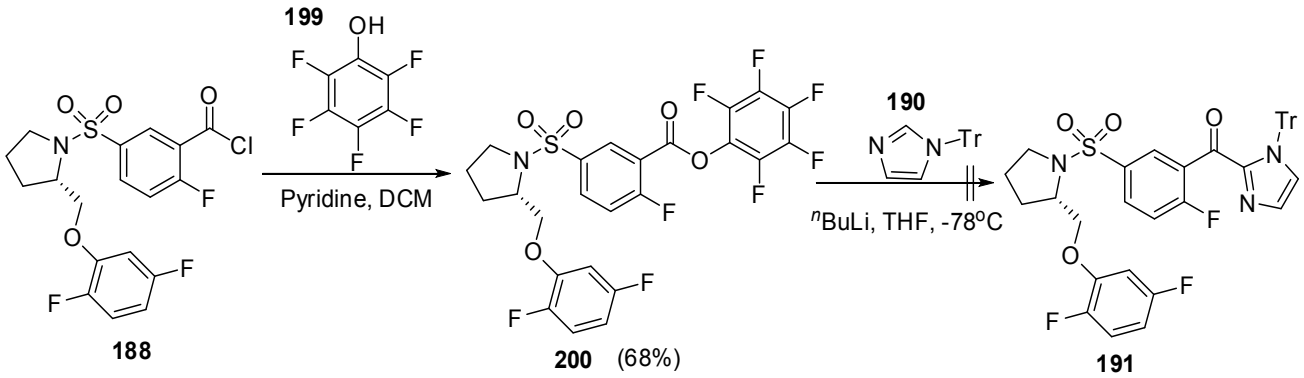
Scheme 4.36: High yielding preparation of trityl protected ketone **194** – **196** from halogen-substituted and unsubstituted ester electrophile, **153**, **185** and **193**

It is worth noting that nucleophilic substitution of 5-bromo-, 5-chloro- and unsubstituted 2-fluoro-methylbenzoate (**194**, **195** and **196**; Scheme **4.36**) with lithiated trityl imidazole **190** proceeded efficiently to give the corresponding ketone products (**52**, **58** and **157**; Scheme **4.36**) in reproducible 70 – 80 % yields, higher than the percentage yields obtained using the one-pot synthesis with unprotected imidazole (Scheme **4.22**). Hence, the poor yield and irreproducibility observed with the nucleophilic substitution using methyl benzoate **187a** was attributed to the strong electron withdrawing effect of the sulfonamide group activating the phenyl ring to side reactions.



Scheme 4.37: Preparation of Weinreb amide **197**[188] and its use in nucleophilic substitution with lithiated imidazole anion **190**

Aiming to optimise the production of ketone **191**, alternative acylating agents were investigated, including Weinreb amide **197** and pentafluorophenoxide ester **200**. Weinreb amide **197** was prepared in 82 % yield from treatment of benzoyl chloride **188** with *N,O*-dimethylhydroxylamine, using pyridine as the base (Scheme **4.37**). The reaction of Weinreb amides with organometallic reagents such as 2-lithum-tritylimidazole **190** is believed to proceed via a tetrahedral intermediate stabilised by chelation with the amide methoxy group as illustrated in Scheme **4.37**.[188] The resulting ketone is subsequently released following reaction workup. It was hoped that this chelation mechanism, which halts the release of a leaving group before work-up, would hinder undesired nucleophilic substitution of the 2-fluoride substituent. However, treatment of Weinreb amide **197** with lithiated trityl-imidazole **190** only gave trace amounts of the desired ketone **191**, observed by LCMS, with isolation of 25 % of unreacted trityl-imidazole **190** and no recovery of Weinreb amide **197**.

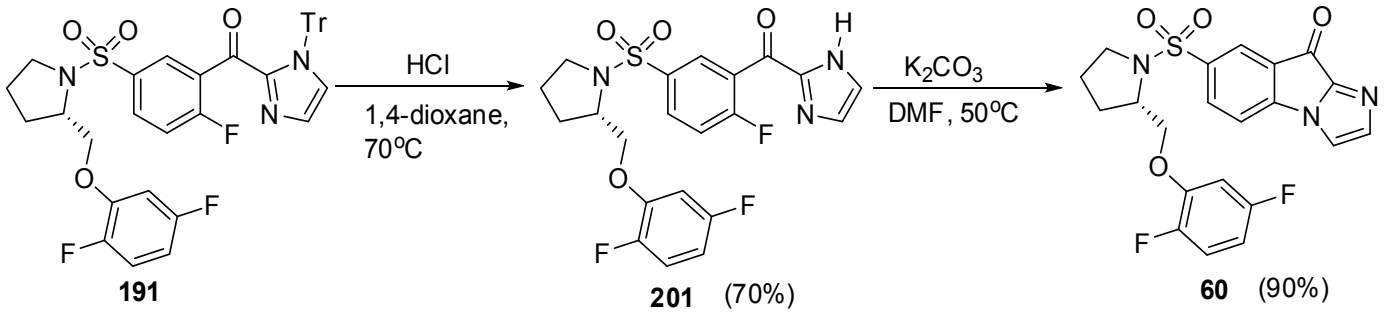


Scheme 4.38: Preparation of pentafluorophenoxy ester **200** and its reaction with 2-lithium-tritylimidazole **190**

Following the disappointing results observed with Weinreb amide **197**, the bulky pentafluorophenoxy ester **200** was prepared from acid chloride **188** and pentafluorophenol **199** in 68 % yield (Scheme **4.38**). We hoped that displacement of the pentafluorophenoxide group following nucleophilic substitution of ester **200** with deprotonated imidazole would give a stable, bulky anion that would be a poor nucleophile for further side reactions involving undesired S_NAr displacement of the phenyl fluoride. Unfortunately, only a small percentage (< 20 %) of unreacted trityl-imidazole **190** was isolated from the reaction mixture with no trace of the desired ketone **191** (Scheme **4.38**).

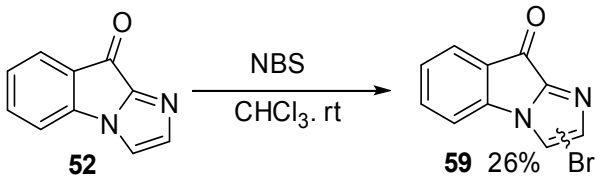
The fact that unreacted trityl-imidazole **190** was isolated from the nucleophilic substitution reactions, with no recovery of Weinreb amide **197** or pentafluorophenoxy ester **200**, suggested possible deprotonation of the electron deficient sulfonamide substituted phenyl ring by the imidazole anion. Such deprotonation could account for the recovery of trityl-imidazole **190**, despite confirmation of full deprotonation by ^{n}BuLi, observed by the incorporation of deuterium in samples of lithiated trityl-imidazole solutions quenched with deuterium oxide. The deprotonated acylating agents could then undergo further reactions leading to decomposition.

To address the inefficient nucleophilic substitution reaction of lithiated trityl-imidazole **190** with the sulfonamide substituted acylating agents, alternative synthetic routes were proposed which are described in the next section. However, a sufficient amount of trityl-protected imidazole-ketone **191** was obtained from nucleophilic substitution reactions using ester **187a**. This was successfully utilised in the preparation the sulfonamide substituted imidazoleindolone target **60** (Scheme **4.39**).



Scheme 4.39: The final steps in the synthesis of target 5-sulfonamide-imidazoleindolone **60**

Trityl deprotection of **191** was achieved using 4M HCl in 1,4-dioxane to give ketone **201** in 70 % yield. Facile intramolecular S_NAr cyclisation was achieved by treatment of ketone **201** with K_2CO_3 in DMF, stirring at 50 °C to give the target 5-sulfonamide substituted imidazoleindolone **60** in 90 % yield (Scheme **4.39**).

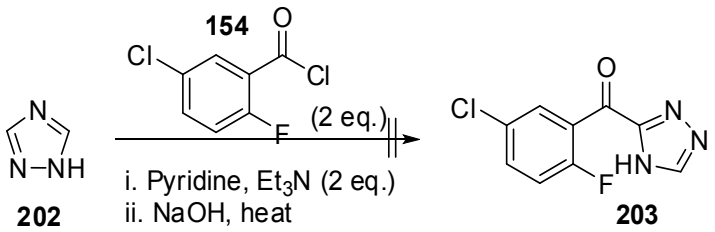


Scheme 4.40: Preparation of bromide substituted imidazoleindolone **59**

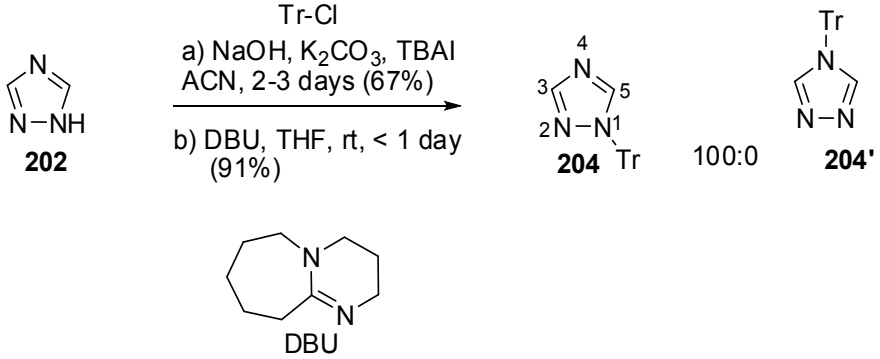
In addition to the target 7-sulfonamide substituted imidazoleindolone **60**, the 2/3-bromo-substituted derivative **59** was prepared for use in the UV-vis titrations detailed in Chapter **II**. This involved treating the core imidazoleindolone **52** with *N*-bromosuccinimide in chloroform at room temperature, which successfully gave the desired product in a moderate 26 % yield (Scheme **4.40**). This was sufficient for use in the UV-vis experiment (Chapter **II**). The bromide substituent on the imidazole ring could also act as handle for future introduction of functional groups. The product **59** was assumed to be a mixture of 2- and 3-bromo-imidazoleindolone regioisomers.

IV.3.2. Triazoleindolone Synthesis

The retrosynthetic approach shown in Scheme **4.20** was devised for the synthesis of both the imidazoleindolone and triazoleindolone heterocycles. In the first step of the forward synthesis, unlike the preparation of phenyl-imidazole ketone **156** (Scheme **4.22**), formation of phenyl-triazole ketone **203** could not be achieved in one-pot using unprotected 1,2,4-triazole and benzoyl chloride **154** (Scheme **4.41**). As a result, the trityl-protected triazole **204** was prepared for use in nucleophilic substitution reactions with acylating agents (Scheme **4.42**).

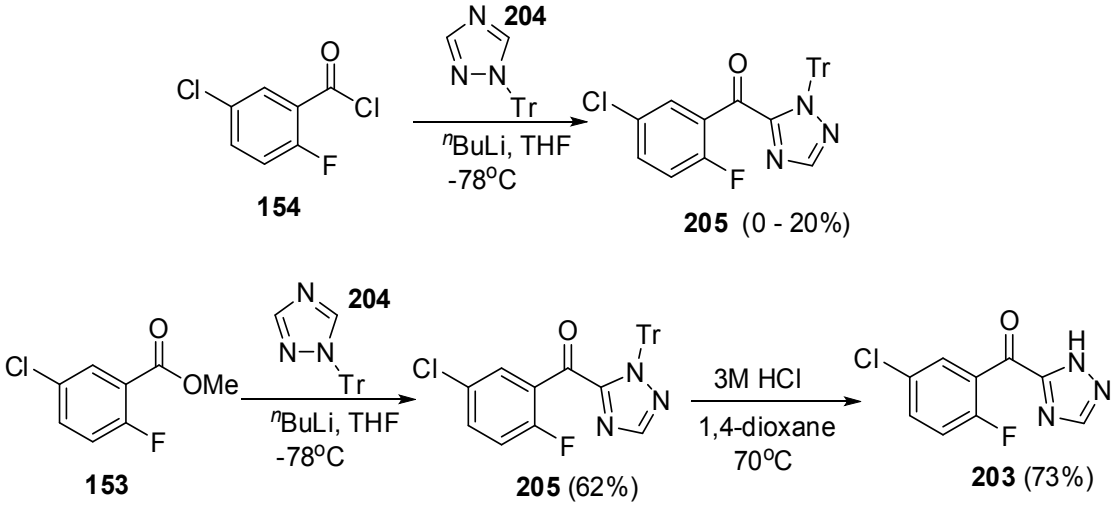


Scheme 4.41: An attempt to prepare phenyl-triazole ketone **203** from unprotected triazole **202**



Scheme 4.42: Preparation of trityl protected triazole **204**

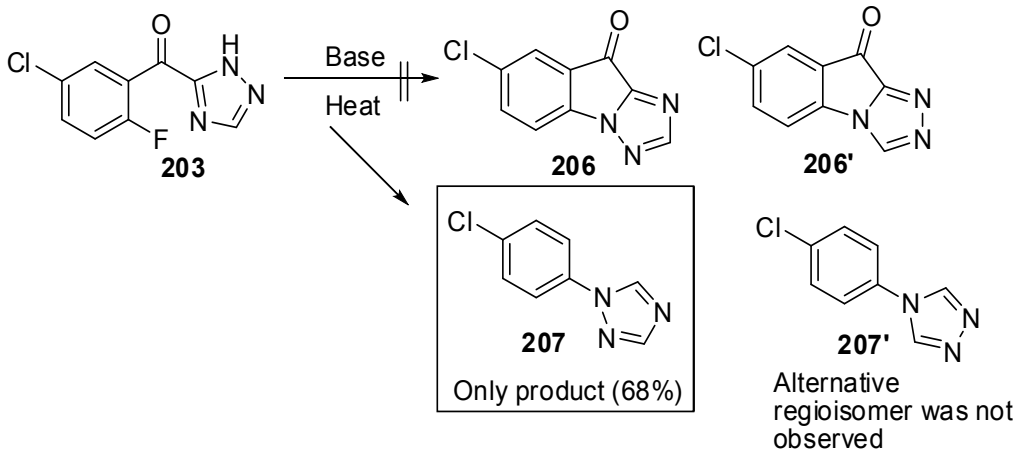
Preparation of N-trityl triazole **204** from Tr-Cl regioselectively gave the isomer **204** in preference to the alternative symmetric **204'** (Scheme **4.42**). Trityl-triazole **204** was initially prepared in ACN using a mixture of K_2CO_3 and NaOH, with TBAI used as a catalyst (Scheme **4.42**).[189] Though giving the product **204** in moderate yield of 67 %, the reaction was relatively slow, taking 2 days to complete. An improved yield of 91 % and faster reaction time of 5 hours was achieved using the weakly nucleophilic base DBU as a proton sponge (Scheme **4.42**).



Scheme 4.43: Preparation of phenyl-triazole ketone **203**

In the next step, trityl-triazole **204** was deprotonated with ^{n}BuLi in THF at -78 ^{o}C. Trapping of triazole anion with acyl chloride **154** at -78 ^{o}C, inconsistently gave ketone **205** in 0 – 20 % yield (Scheme **4.43**). By contrast, trapping the tritytriazole anion with methyl benzoate **153** was more consistent, successfully giving the desired product **205** with an average yield of 62 % (Scheme **4.43**). The trityl protecting group was subsequently removed by acid catalysed hydrolysis to give ketone **203** in 73 % yield.

Unlike the facile S_NAr cyclisation of phenyl-imidazole ketone **156**, initial attempts to achieve triazoleindolone **206** from ketone **203** via the intramolecular S_NAr substitution of the aryl fluoride, resulted in the unexpected formation of 1-pheny-1,2,4-triazole **207** (Scheme **4.44**). The different reaction conditions used in attempts to prepare the triazoleindolone heterocycle **206** are shown in Table **4.3**.



Scheme 4.44: Attempts to prepare the triazoleindolone heterocycle **206**, resulted in the formation of 1-phenyl-1,2,4-triazole **207**

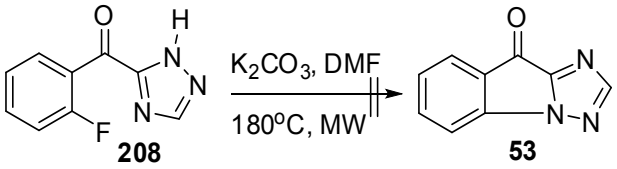
Table 4.2: Reaction conditions and results observed for attempts to prepare the triazoleindolone **206**

Entry	Base	Solvent	Temp (^{o}C)	Time	Result
1	K_2CO_3	DMF	145	18 hrs	**207**
2	Cs_2CO_3	DMF	145	18 hrs	**207**
3	K_2CO_3	DMF	80	18 hrs	No reaction
4	Cs_2CO_3	DMF	50-100	18 hrs	No reaction
5	K_2CO_3	DMF	180*	20 mins	**207**
6	Cs_2CO_3	DMF	180*	20 mins	**207**
7	Cs_2CO_3	DMSO	180*	20 mins	**207**
8	NaOH	DMF	180*	20 mins	Decomposition

*Microwave irradiation

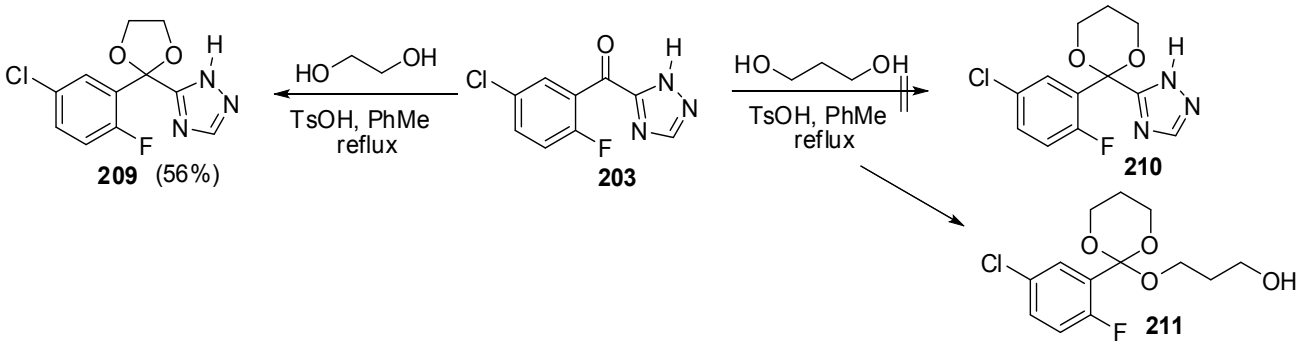
Identical conditions used for the S_NAr cyclisation of phenyl-imidazole ketone **156** (Scheme **4.21**) was initially employed for the equivalent reaction with phenyl-triazole ketone **203** (Scheme **4.44**; Table **4.2**, Entries **1** and **2**). After overnight heating at 145 ^{o}C using either K_2CO_3 or Cs_2CO_3, the starting material had fully reacted, but the only component isolated from the mixture was 1-phenyl-triazole **207** in 68 % yield. The reaction was repeated at lower temperatures in order to limit side reactions. However, no reaction was observed at 80 ^{o}C using K_2CO_3, or at 50 – 100 ^{o}C using Cs_2CO_3, despite overnight heating (Table **4.2**, Entries **3** and **4**). At low temperatures (50 – 100 ^{o}C), no reaction was observed but at a higher temperature (145 ^{o}C), prolonged heating was required to drive the reaction to completion. With the aim of quickly forcing the reaction to limit the formation of side products, microwave irradiation was employed, stirring at 180 ^{o}C for 20 mins with either K_2CO_3 or Cs_2CO_3 (Table **4.2**, Entries **5** and **6**). These conditions also gave 1-phenyl-triazole **207**. DMSO was used

as the solvent instead of DMF in order to eliminate the possibility that reactions with DMF was responsible for the apparent decarbonylation to give the 1-phenyl-triazole **207**, but the same result was observed (Table **4.2**, Entry **7**). The mechanism of phenyl-triazole ketone **203** reaction to give the 1-phenyl-triazole species **207** is not known, though it is possible the reaction proceeded via the desired triazoleindolone **206** which quickly decomposes by a decarbonylation mechanism to give the species **207**.



Scheme 4.45: Intramolecular S_NAr cyclisation attempt with unsubstituted phenyl-triazole ketone **208**

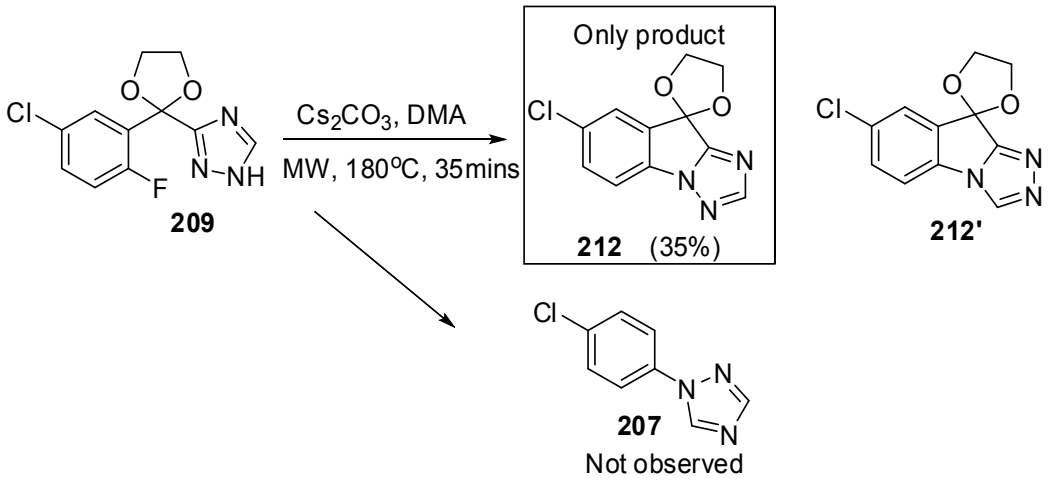
To assess the possibility that the observed decarbonylation could have been driven by the presence of the electron withdrawing chloride substituent, the unsubstituted phenyl-triazole ketone **208** was prepared, using the same conditions described for the formation of chloro-substituted ketone **203** (Scheme **4.43**, **4.45**) and used in in the S_NAr cyclisation reaction. Unfortunately, irradiating ketone **208** in DMF with K_2CO_3 at 180 °C (Scheme **4.45**), resulted in complete decomposition, attributed to the lack of an electron withdrawing substituent activating the phenyl ring to nucleophilic attack which was supported by the fact that no reaction was observed with conventional heating of a mixture of ketone **208** and K_2CO_3 in DMF at 145 °C.



Scheme 4.46: Attempts to prepare the ketal protected derivative of ketone **203**

Since a form of decarbonylation was responsible for the formation of 1-phenyl-triazole **207**, it was hoped that using the ketal protected derivative of ketone **203** would lead to successful S_NAr cyclisation to give the ketal protected derivative of triazoleindolone **206**. Treatment of ketone **203** with 1,3-propanediol and TsOH in toluene, in an attempt to obtain ketal **210**, led to triazole ring

displacement to give the species **211**, while the use of ethylene glycol successfully gave ketal **209** in 56 % yield (Scheme **4.46**). Unlike the unsuccessful reaction of imidazoleindolone derivatives with diols (Schemes **4.27** and **4.28**), the size of the ketal appears to be an important factor for the effective formation of phenyl-triazole ketal **209**. Imidazole (pKa, 1*H*-imidazlole = 14.5) is a much stronger base than 1,2,4-triazole (pKa, 1*H*-1,2,4-triazole = 10.3). It was therefore likely that, unlike 1,2,4-triazole, imidazole acted as a strong proton sponge, hindering ketal formation.



Scheme 4.47: Synthesis of triazole-1,3-dioxolane **212** from ketal **209**

The obtained ketal **209**, was treated with Cs_2CO_3 and irradiated in a microwave in an attempt to achieve S_NAr cyclisation. DMA was found to be give a cleaner reaction than DMF with less by-products, successfully giving the cyclised ketal **212**, albeit with a low yield of 35 % (Scheme **4.47**). 1-Phenyl-triazole **207** obtained from ketone **203** was not observed, suggesting that ketal protection indeed hinders the unwanted decarbonylation reaction. It is worth noting that X-ray crystallography was used to confirm the regiochemistry of the cyclised ketal as exclusively **212** instead of the alternative **212'** (Scheme **4.47**, Figure **4.4** below). This was supported by the obtained regioisomer of 1-phenyl-triazole **207** (Scheme **4.44**), with two singlet chemical shifts observed for the triazole ring by ^1H NMR, instead of the one singlet peak expected from the symmetric regioisomer **207'**. Full crystallography data for the ketal **212** can be found in the appendix.

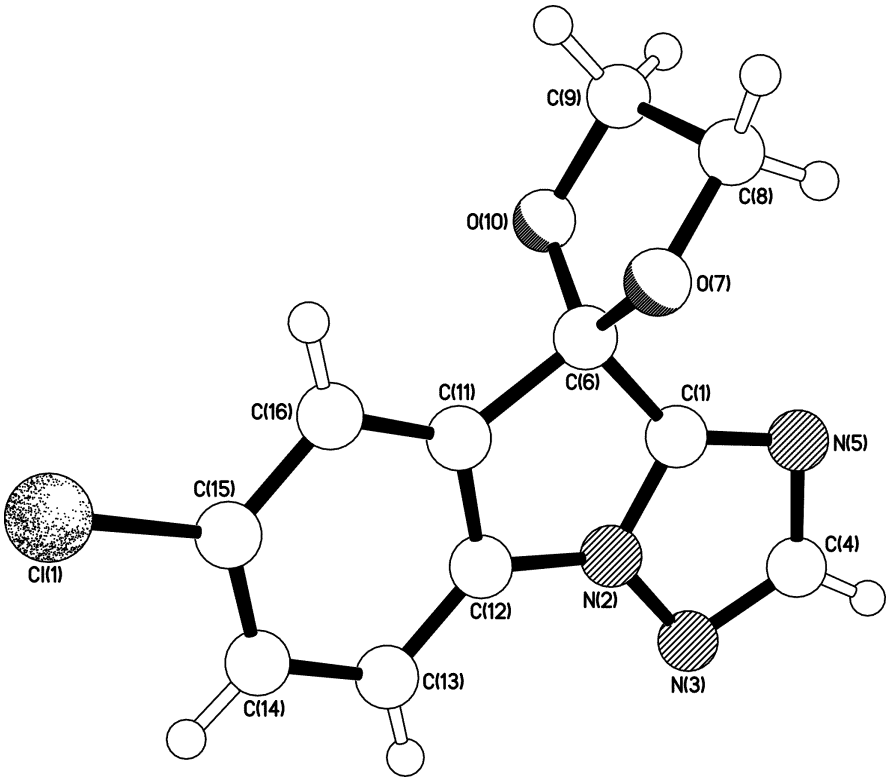
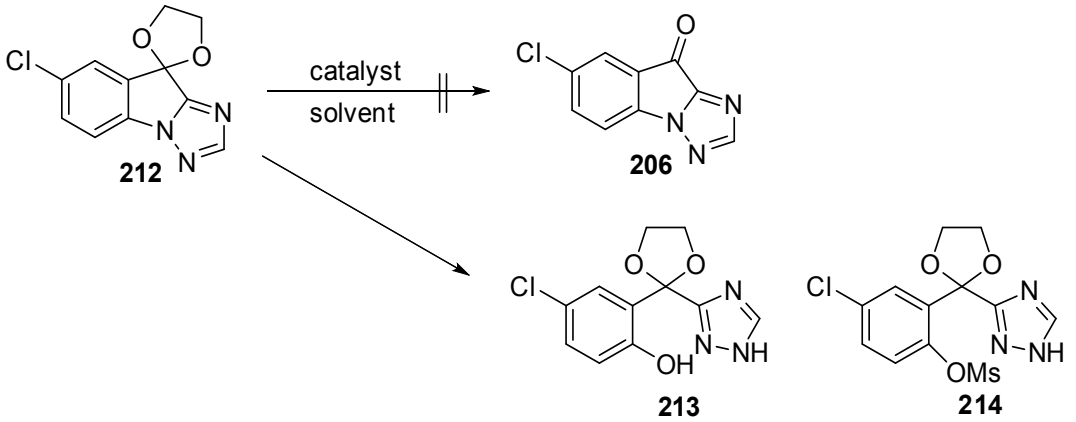


Figure **4.4**: The crystal structure of ketal-protected triazoleindolone **212**

Following the successful formation of the ketal protected triazoleindolone **212**, ketal deprotection would then complete the synthesis of the triazoleindolone heterocycle **206**. Unfortunately, problems with ring opening reactions were encountered when ketal deprotection was attempted (Scheme **4.48**). Table **4.3** summarises the ketal deprotection reaction conditions utilised with the resulting observations.

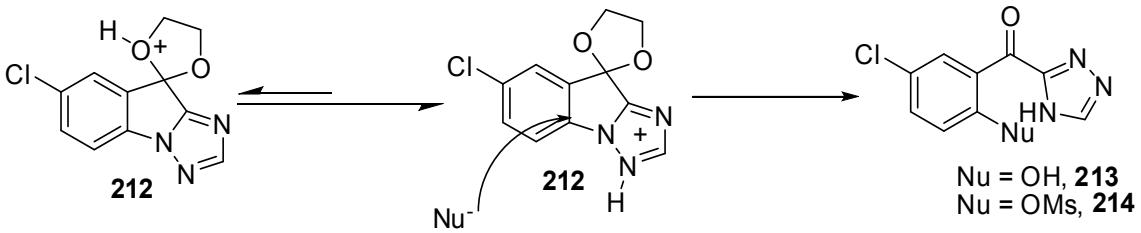


Scheme 4.48: Attempted deprotection of ketal **212**

Table 4.3: The employed ketal deprotection reaction conditions

Entry	Solvent	Catalyst/reagent	Temp ^{O}C	Time (hrs)	Result
1	H_2O/Acetone	TsOH	rt	15	No reaction
2	H_2O/Acetone	TsOH	70 - 90	20	No reaction
3	THF	3M HCl	rt	18	No reaction
4	THF	3M HCl	90	5	**213**
5	MsOH	MsOH	rt	5	**214**
6	H_2O/Acetone	PPTS	reflux	18	No reaction
7	DCM	Ph_3BF_4	rt	24	No reaction

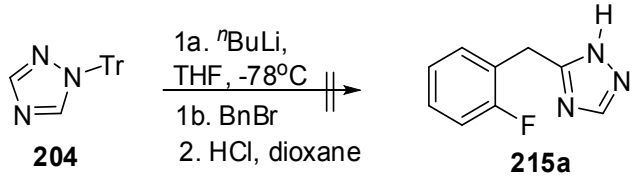
In the first ketal deprotection attempt, TsOH was employed with acetone/water mixture used as the solvent. No reaction was observed at room temperature, or at 70 – 90 ^{O}C (Table **4.3**, Entries **1** and **2**). When aqueous 3M HCl was used as the acid catalyst, no reaction was observed at room temperature (Table **4.3**, Entry **3**), but at 90 ^{O}C, full reaction occurred to give C-N ring hydrolysis, resulting in the open ring phenolic species **213** with the ketal group still intact (Table **4.3**, Entry **4**). Likewise, the use of MsOH led to ring hydrolysis, this time giving mesylate **214** at room temperature (Table **4.3**, Entry **5**).



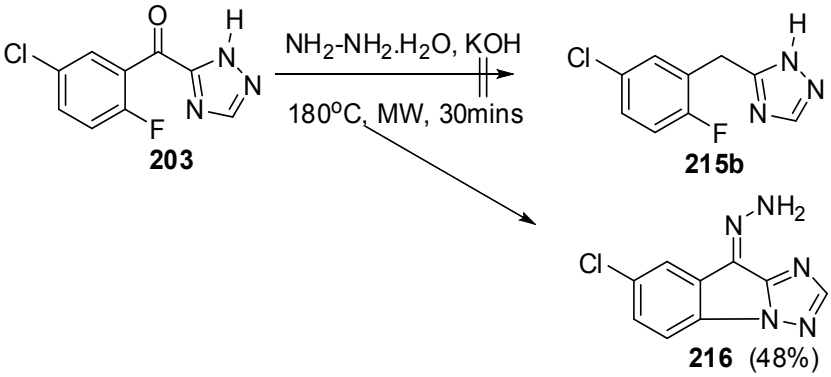
Scheme 4.49: Ring hydrolysis of heterocycle **212** under acidic conditions

It was highly likely that the ring opening reactions were a direct result of triazole ring protonation, catalysing indolone ring hydrolysis in preference to ketal hydrolysis when heated with HCl or at room temperature with the strong acid, MsOH (Scheme **4.49**). Given the acid sensitivity of the heterocycle, mild, non-protic deprotection conditions were employed, involving the use of PPTS[190, 191] and Ph_3BF_4[192] (Table **4.3**, Entries **6** and **7**) which unfortunately proved unsuccessful. Though we came close to obtaining the triazoleindolone heterocycle **206**, deprotection of ketal **212** was ultimately not achieved.

Proceeding via the alcohol derivative of phenyl-triazole ketone **203** was considered, but the problems encountered with the protection of the imidazoleindolone alcohol derivative **182** (Scheme **4.29**) discouraged this approach. We investigated an alternative route involving the fully reduced ketone derivative, **215a** (Scheme **4.50**) and the chloride substituted equivalent, **215b** (Scheme **4.51**), which would then be re-oxidised back to the ketone, following S_NAr ring cyclisation. Initial preparation of benzyl-triazole **215a** from lithiated trityltriazole **204** and benzyl bromide resulted in complete decomposition (Scheme **4.50**). Since ketone **203** could be prepared in facile steps, we focused on obtaining the fluorobenzyl-triazole **215b** by the reduction of ketone **203**, using Wolf Kishner reduction conditions (Scheme **4.51**).[193, 194]

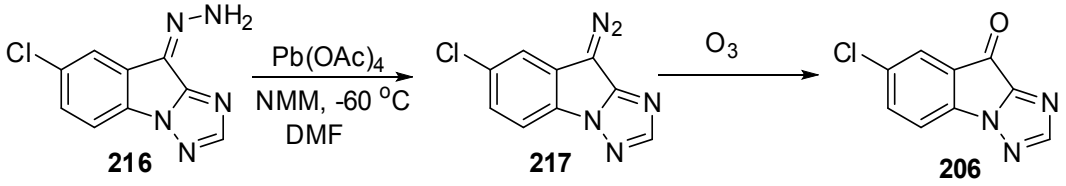


Scheme 4.50: An attempt to prepare fluorobenzyl-triazole **215a** from BnBr



Scheme 4.51: Wolf-Kishner reduction attempt of ketone **203**

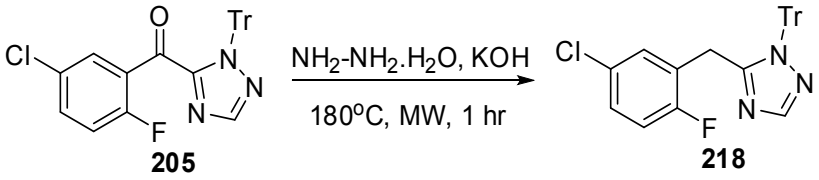
Wolf Kishner reduction is known to proceed via the formation of a hydrazone intermediate and subsequent hydrazone deprotonation to displace nitrogen gas and give the corresponding alkyl group.[193, 194] To obtain the fully reduced compound **215b**, a mixture of ketone **203** and excess KOH in hydrazine was irradiated in a microwave at 180 ^{o}C for 30 minutes. Surprisingly, the precipitate isolated from the reaction mixture was shown to be the cyclised hydrazone **216** in 48 % yield, with only minor traces of the expected fluorobenzyl-triazole **215b** observed from an LCMS of the reaction mixture (Scheme **4.51**). Prolonged heating for up to one hour only served to decompose the hydrazone product, reducing its yield to 10 %, while conventional heating resulted in the slower formation of hydrazone **216** with more side products. Hydrolysis of hydrazone **216** would give the corresponding ketone and therefore the triazoleindolone heterocycle **206**. However, given the problems encountered with hydrolysis attempts of the more labile ketal **212**, hydrolysis of hydrazone **216** was not expected to occur with ease.



216 217 206

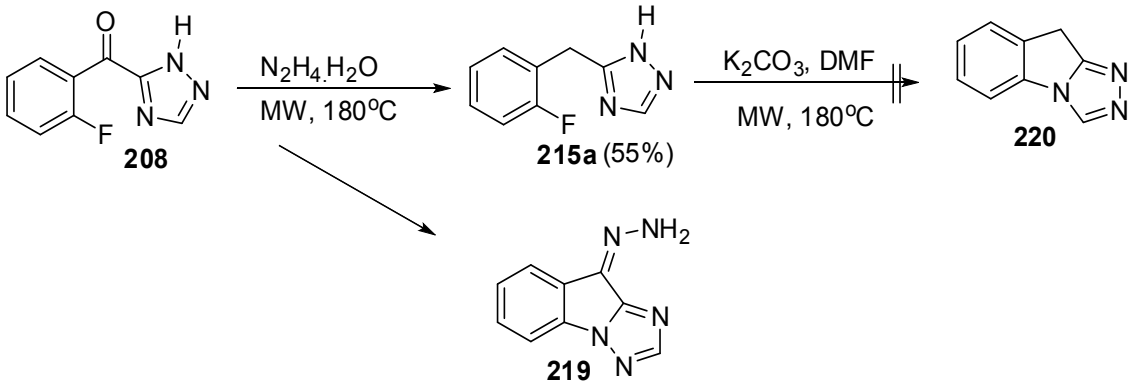
Scheme 4.52: Hydrazone hydrolysis attempt to give ketone **206**[195]

The commonly used acid hydrolysis of hydrazones[196] was not considered an option for hydrazone **216**, given the demonstrated acid sensitivity of the heterocycle. The use of non-acidic conditions was considered essential. The oxidation of hydrazones to diazomethanes is well documented.[197, 198] Ozonation of diazomethanes is then reported to result in ketone equivalents, with the overall reaction being the hydrolysis of a hydrazone in two steps (Scheme **4.52**).[164, 199] Following the reported conditions,[195] a solution of hydrazone **216** and *N*-methylmorpholine in DMF was treated with $Pb(OAc)_4$ at -60 ^{o}C and stirred for 30 minutes. Following aqueous work up at 0 ^{o}C and concentration *in vacuo*, the resulting pale yellow solid was dissolved in a DCM/methanol mixture and bubbled with ozone for 30 minutes to give a colourless precipitate. As indolone heterocycles are characterised with bright colours, the colourless precipitate immediately indicated that the desired ketone **206** was not obtained. This precipitate was found to be highly insoluble, failing to dissolve in solvents ranging from DMF, DMSO, water, DCM, methanol and acetone, and hence could not be characterised. The high insolubility suggested a possible by-product or complex of the lead catalyst used.



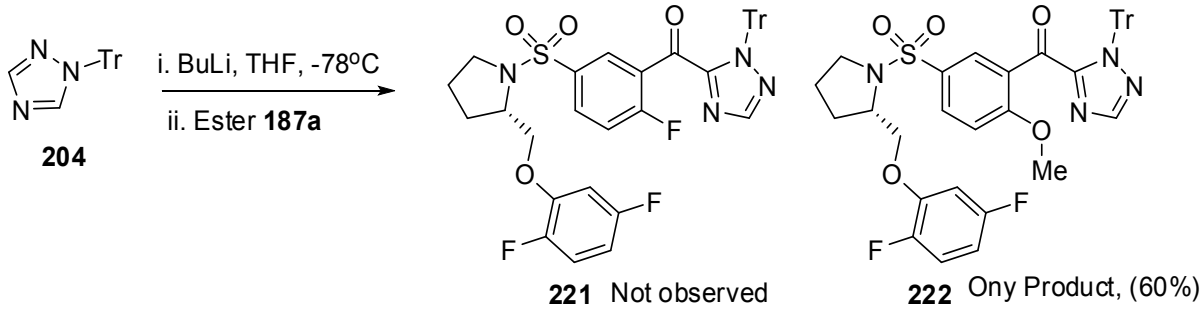
Scheme 4.53: Wolf-Kishner reduction of trityl-protected ketone **205**

Hydrolysis of hydrazone **216** was ultimately not achieved. To block the formation of the cyclised hydrazone **216**, Wolf Kishner reduction was attempted with the *N*-trityl protected ketone **205** (Scheme **4.53**). Though the presence of the desired product **218** was confirmed by LCMS and crude ^{1}H NMR, the reaction contained a mixture of closely eluting components, making purification difficult and product **218** was not isolated (Scheme **4.53**).



Scheme 4.54: Preparation of unsubstituted fluorobenzyl-triazole **215a**

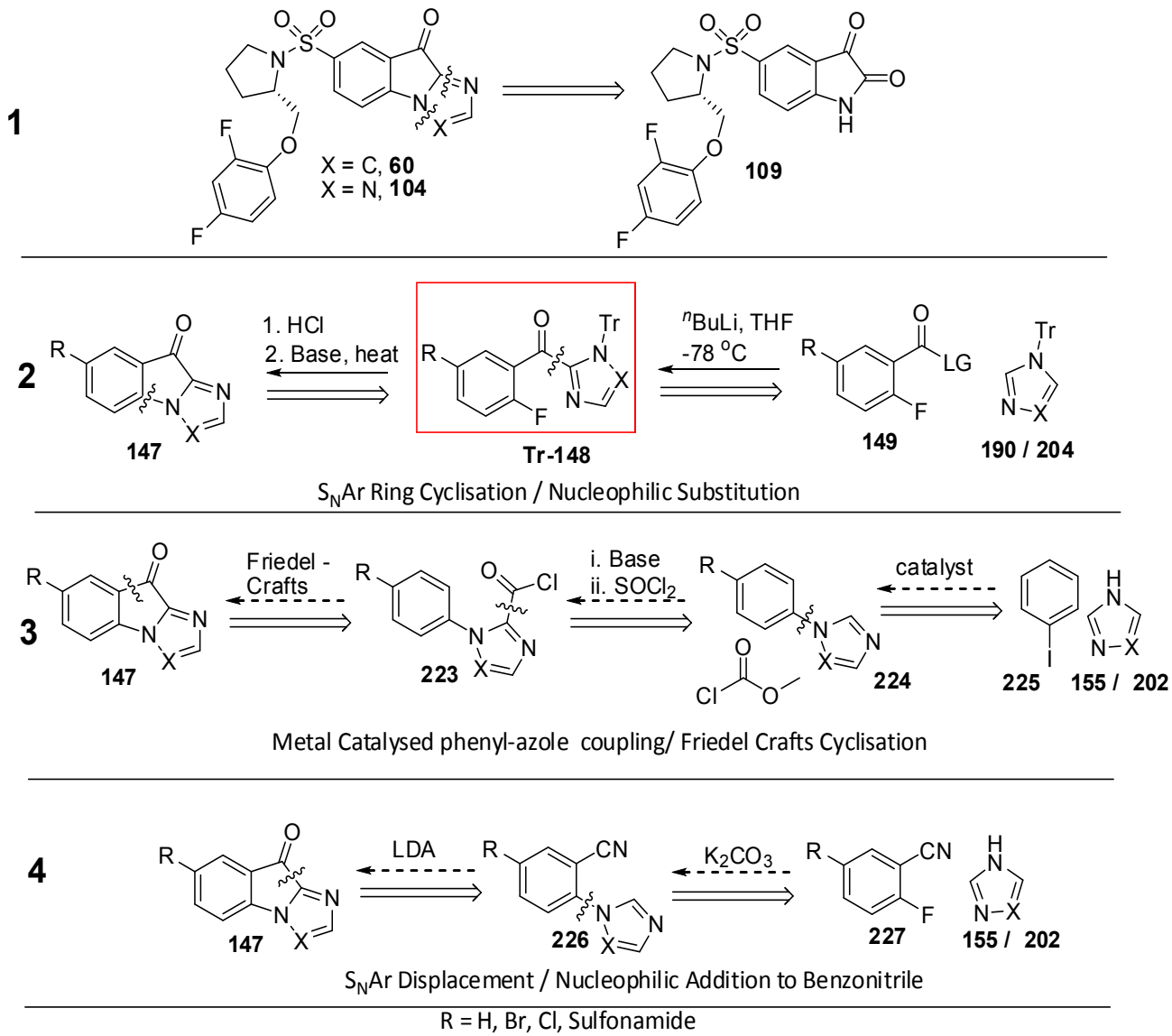
Wolf Kishner reduction was subsequently attempted with the unsubstituted ketone **208** (Scheme **4.54**). In the absence of the electron withdrawing chloride substituent to drive S_NAr cyclisation of a hydrazone intermediate, the fully reduced, unprotected fluorobenzyl-triazole **215a** was isolated as the only product in 55 % yield, with minor traces of the cyclised hydrazone **219** observed from an LCMS of the reaction mixture (Scheme **4.54**). The absence of an electron withdrawing group led to successful Wolf Kishner reduction, but it also hindered S_NAr cyclisation in the next step and the reduced derivative of the triazoleindolone heterocycle **220** was not achieved (Scheme **4.54**). As a result of the apparent importance of an electron withdrawing substituent to activate the phenyl ring to nucleophilic attack and S_NAr cyclisation, we progressed to introduce the sulfonamide substituent of the target triazoleindolone heterocycle, using the 5-sulfonamide methyl benzoate ester **187a** in a nucleophilic substitution reaction with deprotonated trityl-triazole **204**.



Scheme 4.55: An attempt to prepare the sulfonamide substituted phenyl-triazole ketone **221**

The initial attempt to prepare the sulfonamide substituted phenyl-triazole ketone **221** involved treatment of trityl-triazole **204** with ^{n}BuLi in THF at -78 ^{o}C, prior to the addition of 5-sulfonamide-methylbenzoate **187a**. Using trityl-imidazole **190**, this reaction gave a mixture containing the desired ketone **191** and a side product resulting from further reaction of product **191** with the methoxide leaving group of the ester reagent to give the methoxide substituted species **192** (Scheme **4.35**). In the analogous reaction with trityl-triazole **204**, only the fluoride-displaced by-product **222** was isolated from the reaction mixture in 60 % yield (Scheme **4.55**). Given the problems encountered with this S_NAr route to the triazoleindolone heterocycle, alternative robust reaction pathways were investigated.

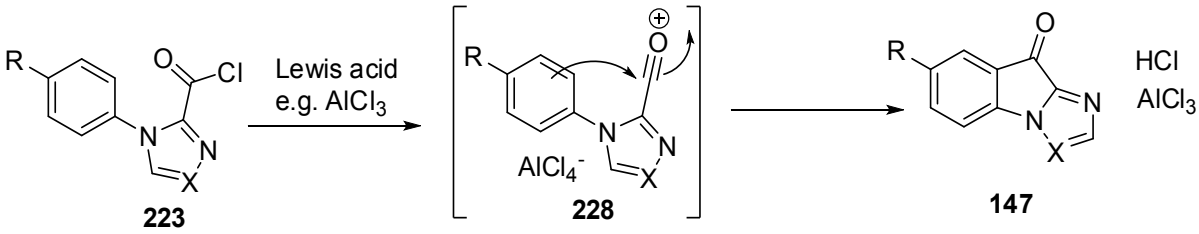
IV.4. Alternative Routes to the Imidazoleindolone and Triazoleindolone Targets



Scheme 4.56: The explored isatin sulfonamide and S_NAr cyclisation routes, and two alternative routes to the triazoleindolone and imidazoleindolone heterocycles

Scheme **4.56** summarises the retrosynthetic analysis for preparation of the triazoleindolone and imidazoleindolone scaffolds, via the explored isatin sulfonamide (section **IV.2**) and the S_NAr cyclisation routes (section **IV.3**), in addition to two proposed alternative reaction pathways. The isatin sulfonamide route **1** was hampered by difficulties with forming the required reactive intermediates (section **IV.2**). For the imidazoleindolone synthesis, the S_NAr cyclisation route **2** was limited by the problematic nucleophilic substitution of trityl-imidazole **190** with sulfonamide substituted acylating agents, though the target imidazoleindolone **60** was successfully synthesised using this route. For the

triazoleindolone synthesis, the S_NAr cyclisation route **2** was fraught with the formation of undesired products, with only the precursors, ketal **212** and hydrazone **216**, successfully prepared.



Scheme 4.57: Friedel-Crafts acylation reaction mechanism[200]

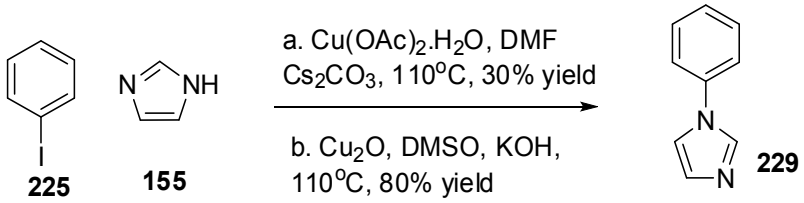
An alternative route to the indolone ring formation involves disconnection of the phenyl-carbonyl bond of the indolone heterocycle, where the synthetic equivalent is a 1-phenyl-2/5-acyl-azole **223**, and the forward reaction would involve an intramolecular Friedel-Crafts acylation reaction (Scheme **4.56**, Route **3**).[200] This route came with the worry that the oxonium ion species **228** (Scheme **4.57**) may undergo decarbonylation to displace CO faster than Friedel –Crafts acylation. There were also concerns that the Lewis acid catalyst required for Friedel-Crafts acylation may coordinate to the azole nitrogen atoms, hindering reaction. The acidic conditions, with HCl as a by-product of the reaction, may also lead to the indolone product ring hydrolysis. Nevertheless, this route was briefly explored as described below, in order to assess its viability for use in imidazoleindolone and triazoleindolone synthesis.

Fewer problems were anticipated with a second alternative route which involves disconnection of the carbonyl-azole bond of the indolone ring (Scheme **4.56**, Route **4**). The deduced forward reaction for this disconnection is an intramolecular nucleophilic addition of an azole ring to a benzonitrile **226**. This would give an iminium ion which would hydrolyse upon aqueous workup to give the corresponding ketone **147**.

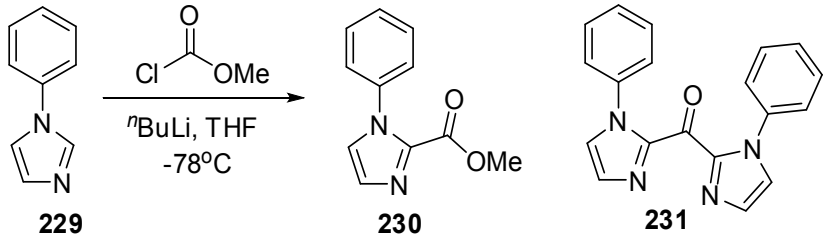
IV.4.1. Investigating the Friedel-Crafts Route

IV.4.1.1. Imidazoleindolone Synthesis

In the first step in the sequence, 1-phenylimidazole **229** was initially prepared from the coupling of iodobenzene and imidazole in the presence of a Cu(II) catalyst and Cs_2CO_3 (Scheme **4.58**). This condition gave 1-phenylimidazole **229** with a maximum yield of 30 %.[201] Huang *et al*. reported the superiority of Cu(I) to Cu(II) in catalysing N-arylation reactions, with KOH giving much higher yields than carbonate bases.[202] Repeating the reaction using these conditions, copper(I) oxide and KOH in DMSO, gave product **229** in a much higher yield of 80 % (Scheme **4.58**).

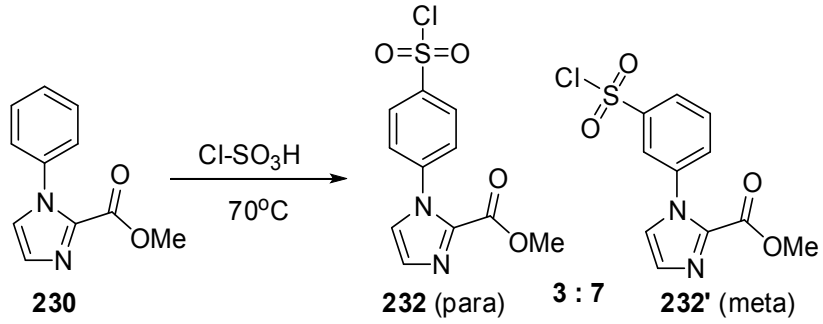


Scheme 4.58: Preparation of 1-Phenyl-1*H*-imidazole **229**[201, 202]



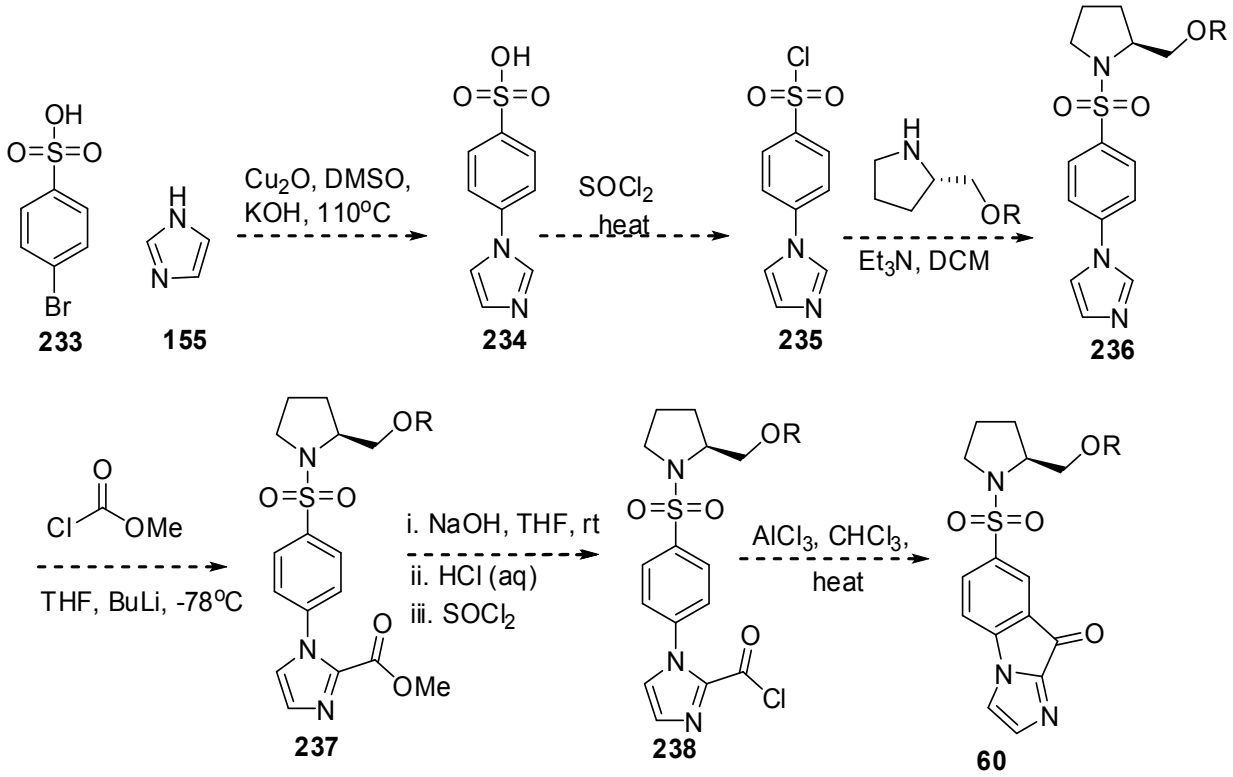
Scheme 4.59: Acylation of 1-phenyl-imidazole **229**

Subsequently, 1-phenylimidazole **229** was lithiated and treated with methyl chloroformate in order to achieve the ester **230** (Scheme **4.59**). As well as the desired ester **230**, which was obtained in only 13 % yield, a dimeric ketone species **231**, resulting from further reaction of the ester product was obtained as the major product in 25 % yield. However, adding a solution of deprotonated **229** to the chloroformate solution (instead of the other way round) gave the desired ester **230** in a significantly improved yield of 60 % (Scheme **4.59**).

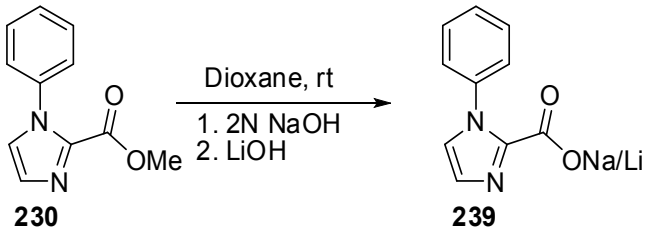


Scheme 4.60: Sulfonation of 1-phenyl-imidazole **230**

To introduce the sulfonyl chloride group, ester **230** was initially treated with chlorosulfonic acid and stirred overnight at room temperate, but no reaction was observed. When stirred at 70 ^{o}C for 3 hrs, the starting material fully reacted to give a crude mixture of two isomers that could not be separated. ^{1}H NMR analysis of the crude product indicated a mixture of the meta and para sulfonyl substituted regioisomers **232** and **232'**, with the unwanted meta-isomer being the major product (Scheme **4.60**). Formation of the meta isomer **232'** was attributed to protonation of the imidazole ring under the strongly acidic conditions, directing addition of the chlorosulfonyl group to the meta position. As well as giving a mixture of isomers, the reaction underwent decomposition and only 15 % of a crude product mixture was obtained. Further reactions to optimise the efficiency of the sulfonation reaction were not carried out as we aimed to first investigate the feasibility of the key Friedel-Crafts cyclisation step before future reaction optimisations. We therefore proceeded with the unsubstituted 1-phenyl-imidazole ester **230**. However, it is worth noting that, a solution to the poor yield and preferential formation of the meta regioisomer would be to introduce the sulfonyl group earlier in the reaction sequence, as illustrated Scheme **4.61** below. It has been reported that *N*-arylation of imidazole is successful using bromobenzenesulfonamide or bromobenzenesulfonic acid based reagents.[203-205]

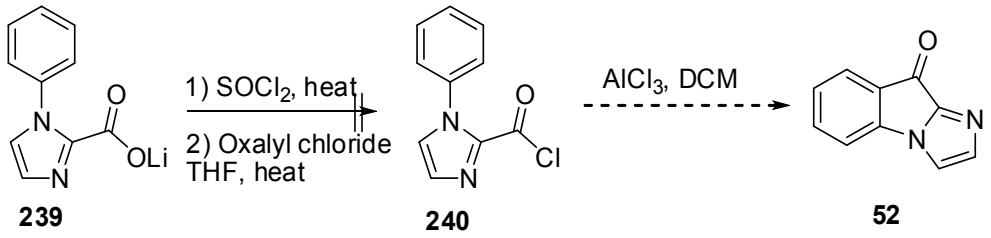


Scheme 4.61: Proposed introduction of the sulfonyl group in the early stages of the Friedel-Crafts synthetic route



Scheme 4.62: Base catalysed hydrolysis of ester **230**

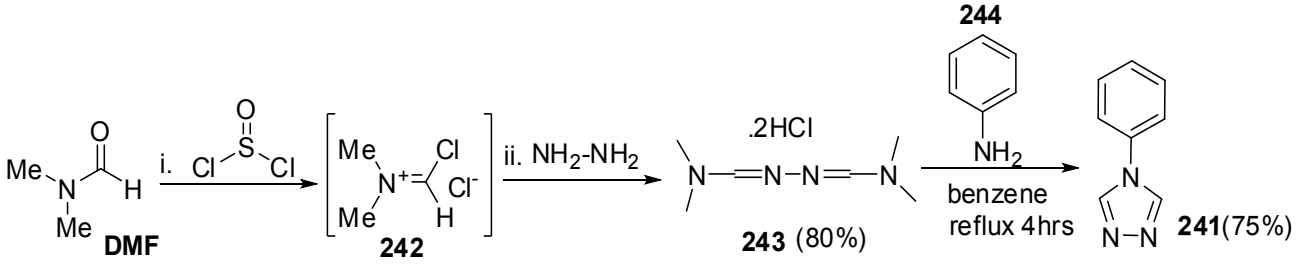
Proceeding with ester **230**, it was treated with 2N NaOH in 1,4-dioxane (Scheme **4.62**) to give the carboxylate **239** which was confirmed by crude ^{1}H NMR and mass spectrometry analysis. However, after aqueous work-up, less than 10 % of the mass before work up was recovered, with the rest presumed to remain in the aqueous solution. Subsequently, ester hydrolysis was repeated using LiOH which is monobasic and therefore could be used in one equivalent, without the need to remove excess LiOH with an aqueous work-up. The resulting lithium carboxylate salt was used in the next step without work-up or purification, aiming to convert lithium carboxylate **239** into acid chloride **240**, the intermediate required for the Friedel-Crafts cyclisation step (Scheme **4.63**).



Scheme 4.63: An attempt to prepare acid chloride **240** from carboxylate salt **239**

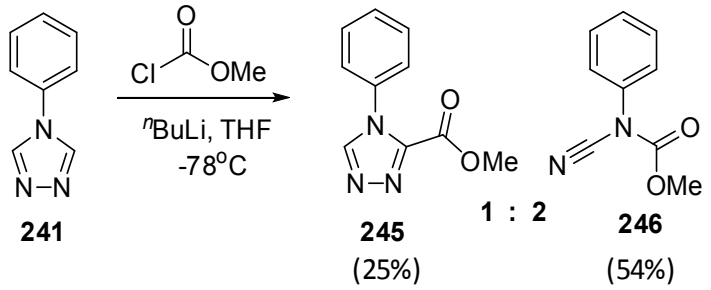
Heating carboxylate **239** in $SOCl_2$ or with excess oxalyly chloride in THF led to complete decomposition (Scheme **4.63**). As facile formation of the acid chloride **240** was not be achieved, investigation of imidazoleindolone synthesis via the Friedel-Crafts route was halted.

IV.4.1.2. Triazoleindolone Synthesis

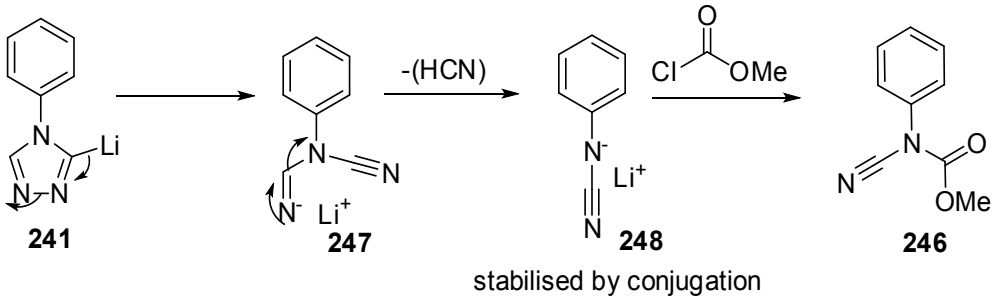


Scheme 4.64: Preparation of 1-phenyl-triazole **241** by transamination[206]

Unlike the formation of 1-phenylimidazole **230**, copper-catalysed *N*-arylation of 1,2,4-triazole was unsuccessful. Naik *et al*. reported the preparation of *N*-aryl 1,2,4-triazoles from transamination of primary amines with dimethylformamide azine dichloride **243** (Scheme **4.64**).[206] Following the reported conditions,[206] azine dichloride **243** was successfully prepared in 80 % yield by stirring a mixture of excess DMF with thionyl chloride to give the reactive intermediate, (chloromethylene)dimethylammoniun chloride **242**. This was treated with hydrazine to give the azine salt **243** (Scheme **4.64**).[206] A suspension of the azine **243** and aniline was then heated to reflux, giving 1-phenyltriazole **241** in 75 % yield (Scheme **4.64**).

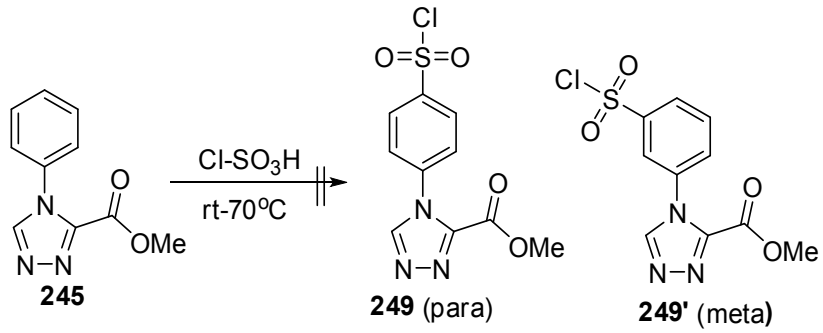


Scheme 4.65: Acylation of 1-phenyl-triazole **241** with methyl chloroformate, leading to a mixture of 2 products



Scheme 4.66: Proposed mechanism for the formation of methyl cyano(phenyl)carbamate **246**

Subsequently, 1-phenyltriazole **241** was treated with ^{n}BuLi at -78 ^{o}C, followed by the addition of methyl chloroformate. Surprisingly this gave the desired ester **245** as the minor product in 25 % yield and the cyano phenylcarbamate species **246** as the major product 54 % yield, a ratio of approximately 1:2 (Scheme **4.65**). We attributed this formation of cyano phenyl carbamate **246** to cleavage of the triazole N-N bond following deprotonation by ^{n}BuLi, leading to the displacement of hydrogen to give a highly stabilised anion **248**, which then reacted with methyl chloroformate to give cyano phenyl carbamate **246** (Scheme **4.66**). In the initial reaction, a solution of 1-phenyltriazole **241** in THF at -78 ^{o}C was stirred for 15 minutes after the addition of ^{n}BuLi and prior to quenching with methyl chloroformate. In a separate reaction, in an attempt to limit the displacement of hydrogen cyanide and trap the triazole anion, methyl chloroformate was added within 2.5 minutes of adding ^{n}BuLi to a solution of 1-phenyltriazole **241**. This made no difference to the proportion of products obtained. Presumably, the displacement of hydrogen cyanide to give the stabilised N-phenylcyanamide anion **248** occurs almost instantly. A sufficient amount of the desired ester **245** was obtained and used in the next step, towards assessment of the Friedel-Crafts route.

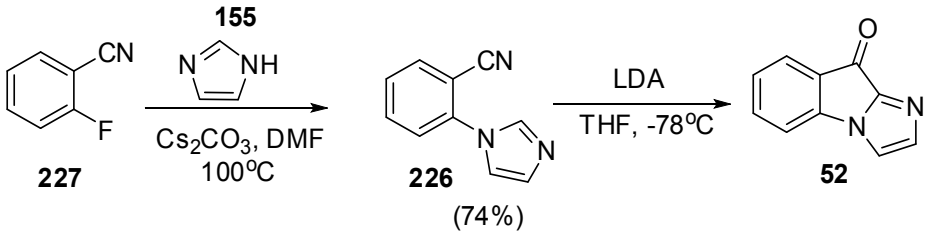


Scheme 4.67: Treatment of ester **245** with chlorosulfonic acid

In an attempt to introduce the *para*-sulfonyl substituent, ester **245** was treated with chlorosulfonic acid (Scheme **4.67**). 1-Phenyltriazole **245** reacted more slowly with chlorosulfonic acid, requiring overnight heating at 70 ^{o}C for complete consumption of the starting material **245**, compared to the full reaction of 1-phenyl-imidazole **230** within 3 hrs at 70 ^{o}C. A TLC and crude ^{1}H NMR suggested complete decomposition of the ester **245** and no product was isolated or clearly identified from the reaction mixture.

At this stage in the triazoleindolone synthetic sequence towards Friedel-Crafts cyclisation, difficulties encountered with the formation of the imidazole acyl chloride species **240**, combined with the poor yield of 1-phenyltriazole-2-carboxylate **245** formation, discouraged further work on this route. However, there is scope for future work on this route, optimising/employing different reaction conditions to potentially achieve efficient reactions.

IV.4.2. Investigating the 'Addition to Benzonitrile' Route



Scheme 4.68: Imidazoleindolone **52** formation via intramolecular imidazole addition to benzonitrile **226**

As discussed above, azole addition to benzonitrile was proposed as an alternative ring closure method to give the indolone ring system. Preliminary experiments to give an overview of the viability of this route was conducted with imidazole only. In the first step, 2-imidazolebenzonitrile **226** was prepared from the base catalysed S_NAr reaction of imidazole with 2-fluorobenzonitrile **227** in 74 % yield (Scheme **4.68**). 2-Imidazolebenzonitrile **226** was subsequently treated with LDA, with the aim

of achieving an intramolecular nucleophilic addition of the imidazole C-2 carbon to the nitrile group. Following work-up and column chromatography, the isolated material appeared to be a crude residue containing the desired imidazoleindolone **52**. LCMS further confirmed the presence of imidazoleindolone **52**, though separation from the unknown co-eluting side product was not achieved by flash column chromatography. Nevertheless, the observed result was encouraging, showing that intramolecular imidazole addition to benzonitrile **226** can be achieved. Future optimisation reactions would explore conditions that would reduce the formation of the co-eluting side-product, in addition to exploring alternative purification methods such as re-crystallisation. The use of 5-sulfonamide substituted benzonitrile as the starting material may also result in a more efficient reaction. The promising results from the initial reactions makes this route top priority for future work on the imidazoleindolone and triazoleindolone synthesis.

IV.5. Conclusion

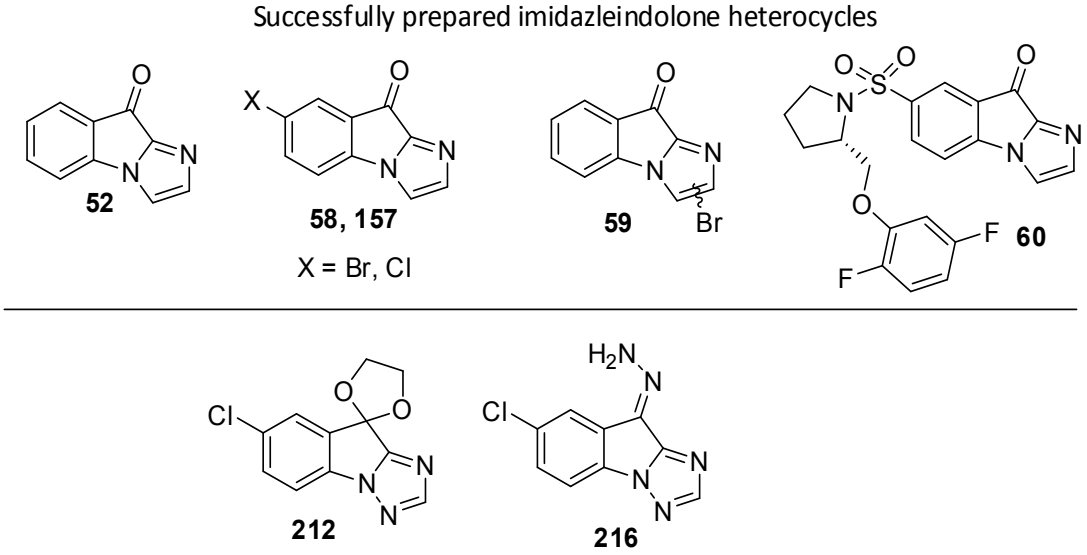


Figure 4.5: Products successfully prepared from the explored triazoleindolone and imidazoleindolone synthetic strategies

Four different routes were explored for the synthesis of the imidazoleindolone and triazoleindolone heterocycles, including the use of isatin sulfonamide intermediates, an intramolecular S_NAr cyclisation route, Friedel-Crafts cyclisation method and cyclisation by nucleophilic addition to benzonitrile. The use of isatin sulfonamide intermediates was impeded by problems associated with unpredictable reactions of the isatin carbonyl centre. Using the S_NAr cyclisation route, where the phenyl-azole bond is formed from the intramolecular nucleophilic

displacement of an aryl fluoride, the substituted and unsubstituted imidazoleindolone heterocycles were successfully achieved (Figure **4.5**). Preparation of the target sulfonamide substituted imidazoleindolone **60** was tempered by a problematic step, involving the nucleophilic substitution of sulfonamide substituted acylating agents with C-2 deprotonated trityl-imidazole. Using the S_NAr route, only the triazoleindolone precursors, hydrazone **216** and ketal **212** were achieved. The Friedel-Crafts cyclisation route was briefly explored and halted when problems were encountered with the preparation the acid chloride intermediate required for the key cyclisation step. Indolone ring formation by the intramolecular addition of the azole ring to benzonitrile was also briefly investigated, and initial results were encouraging, showing the successful formation of the core imidazoleindolone heterocycle **52**, albeit in low purity.

In general, 1,2,4-triazole species appeared to be less reactive than their imidazole equivalents, requiring harsher conditions to force reactions or failing altogether. This was attributed to the higher nucleophilicity of imidazole compared with 1,2,4-triazole. The difference in nucleophilicity was manifested in conditions used for S_NAr cyclisation reactions by nucleophilic attack of the azole nitrogen on the phenyl-fluoride bond. Microwave irradiation or prolonged heating was required for triazole derivatives, compared to the conventional heating of imidazole derivatives for significantly less time and at lower temperatures. Both heterocycles showed sensitivity to acidic conditions, which was attributed to their basic properties, leading to the azole ring protonation which either hindered reactions or catalysed the opening of the indolone scaffolds.

Based on the positive computational modelling results (Chapter **II**), it would be worth dedicating future efforts to further studies aimed at optimising reaction conditions to successfully achieve the triazoleindolone heterocycle. Studies aimed at understanding the mechanism of decarbonylation leading to the formation of the 1-phenyltriazole species **207** may shed some light on the triazoleindolone ring stability. The two alternative synthetic routes briefly explored (Routes **3** and **4**, Scheme **4.56**) could be expanded to evaluate their robustness and efficacy in the synthesis of the triazoleindolone and imidazoleindolone heterocycles. Optimisation of the imidazoleindolone heterocycle synthesis would be necessary for future work, involving the preparation of a library of derivatives for SAR studies.

GENERAL SUMMARY & PERSPECTIVE

GENERAL SUMMARY & PERSPECTIVE

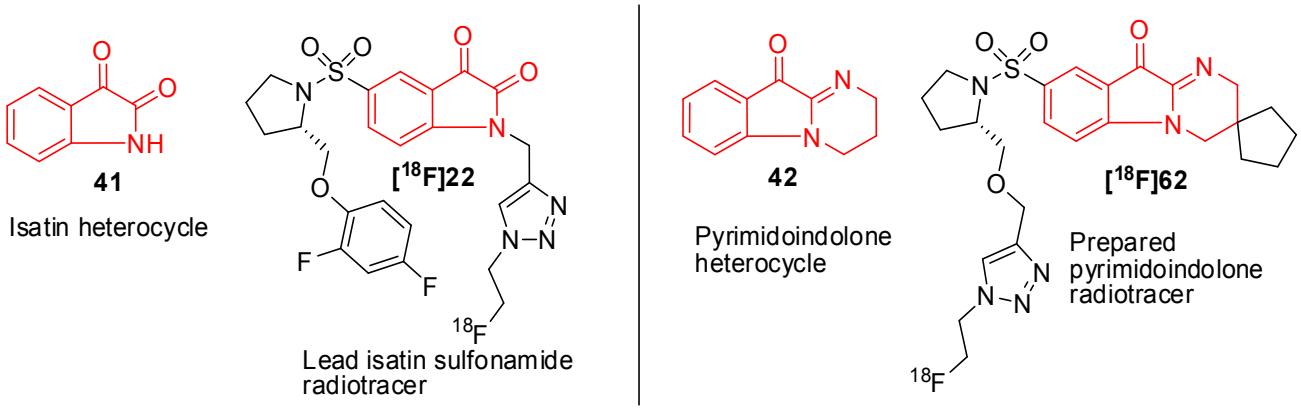
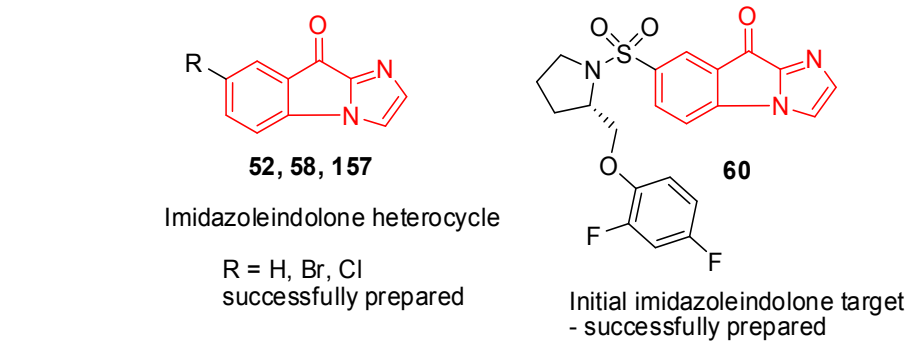


Figure 5.1: Reported isatin sulfonamide and the prepared pyrimidoindolone radiotracer

Imaging attempts using ^{18}F-labelled isatin sulfonamide **22** (Figure **5.1**) have shown elevated background uptake of the radiotracer, attributed to non-specific *in vivo* binding interactions.[57] The research described is part of an ongoing effort to develop caspase-3 binding radioligands with optimal properties for the PET imaging of apoptosis. Three series of heterocycles were proposed as possible alternatives to the isatin sulfonamides, for the selective inhibition of caspase-3, the biomarker of apoptosis for PET imaging. The series based on the pyrimidoindolone **42**, triazoleindolone **53** and imidazoleindolone **52** (Figure **5.1**) heterocycles are structurally similar to the isatin heterocycle, with all containing the crucial ketone responsible for caspase inhibition via the formation of a thiohemiketal in the enzyme active site. The presence of an azole ring in the imidazoleindolone and triazoleindolone heterocycles, and the amidine group of the pyrimidoindolone system, instead of the dicarbonyl function of the isatin ring was expected to modify the reactivity the ketone. It was hoped that this would lead to specific binding interactions with caspase-3, reducing non-specific interactions with cytosolic nucleophilic moieties liable for the low target-to-background ratio of isatin PET images.



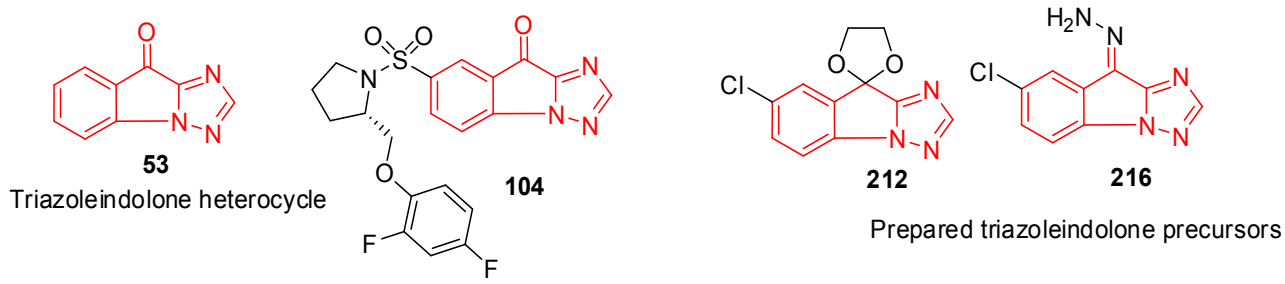


Figure 5.2: Imidazoleindolone and triazoleindolone heterocycles – target and successfully prepared structures

While the imidazoleindolone and triazoleindolone heterocycles were structurally novel, unexplored systems, pyrimidoindolones were previously reported by Havran *et al*. as potent caspase-3 inhibitors.[58] Aiming to investigate radiotracer properties of the pyrimidoindolone heterocycle, an initial target structure [^{18}F]**62** (Figure **5.1**) was designed, synthesised and radiolabelled. The designed target [^{18}F]**62** was modelled on the structure of the lead isatin sulfonamide [^{18}F]**22** to allow direct comparison. Initial biological results, including IC_{50} measurement, cell uptake studies, *in vivo* biodistribution and metabolic profiles, showed that the pyrimidoindolone has a similar biological profile as the isatin sulfonamide though further characterisation and whole body imaging in mice is still required.

We employed computational studies to model the favourability of thiohemiketal formation of the unexplored imidazoleindolone and triazoleindolone structures, in comparison to the pyrimidoindolone and isatin sulfonamide systems. Values obtained included free energies of reactions, equilibrium constants and intramolecular hydrogen bonding distances. Computational results suggested that, like the isatin ring, the pyrimidoindolone, imidazoleindolone and triazoleindolone heterocycles would favourably incorporate a thiol group to give the corresponding thiohemiketal products. The order of thiohemiketal favourability according to the obtained Gibbs free energy was shown to be **isatin > triazoleindolone > pyrimidoindolone > imidazoleindolone**. As

the research was aimed at developing potent caspase inhibitors with increased specific binding interactions, possibly through the modulation of ketone reactivity, the computational results were considered encouraging, despite the alternative heterocycles showing lower favourabilities than the isatin system.

Following the encouraging computational modelling results, initial imidazoleindolone and triazoleindolone heterocycles were designed for synthesis and experimental characterisation. The target structures **60** and **104** (Figure **5.2**) incorporated the same sulfonamide substituent as the lead isatin **22**, shown to be highly favourable by reported isatin SAR studies. Four different synthetic strategies were investigated for the syntheses of the imidazoleindolone and triazoleindolone heterocycles including, the use of isatin sulfonamide intermediates, an intramolecular S_NAr cyclisation route, Friedel-Crafts cyclisation method and cyclisation by nucleophilic addition to a benzonitrile. The preparation of the unsubstituted, halogen-substituted and sulfonamide-substituted imidazoleindolone heterocycles (Figure **5.2**) were achieved using S_NAr cyclisation route.

Although the imidazoleindolone and triazoleindolone differ by only one nitrogen atom, their different properties and reactivities were highlighted during the synthetic studies. Preparation of the triazoleindolone heterocycle proved challenging with only the core heterocyclic precursors, hydrazone **216** and ketal **212** (Figure **5.2**) currently achieved, using the S_NAr cyclisation route. Hydrolysis of the hydrazone and ketal groups would give the core triazoleindolone heterocycle. However, sensitivity of the ring system led to side reactions that destroyed the heterocycle.

Both the imidazoleindolone and triazoleindolone heterocycles demonstrated sensitivity to acidic conditions, attributed to protonation of the basic azole rings, which led to indolone ring hydrolysis or the inhibition of reactions at the ketone or ketal-protected centre. The apparent acid sensitivity raised concerns for the *in vivo* aqueous stability of the heterocycles, as well as their potential selectivity in interactions with nucleophilic moieties in the cytosol, a problem believed to be responsible for the sub-optimal imaging properties of isatin sulfonamides. However, the acid sensitivity of the heterocycle was only manifested when heated under acidic conditions or when a very strong acid such as MsOH was used. Tumour cells are typically more acidic than normal cells, but with a median pH value of approximately 7.0 compared to 7.5 in normal tissues, excluding the more acidic stomach pH.[207] Given the pH range of body tissues, the acid sensitivity of the heterocycles

is not expected to impede potential *in vivo* applications of radiotracers based on the imidazoleindolone and triazoleindolone structures.

Future work would involve continued optimisation reactions designed to successfully give the triazoleindolone ring system, as well as improving the efficiency of the imidazoleindolone formation, prior to biological characterisation in cell based models. Further biological characterisation, including whole body PET imaging in mice would be carried out with the pyrimidoindolone radiotracer [^{18}F]**62** with encouraging results leading to the preparation of a library for SAR studies and radiotracer optimisation.

EXPERIMENTAL

EXPERIMENTAL

General Methods

Reagents were used as commercially supplied without further purification. All reactions and manipulations of air or moisture sensitive materials were conducted in oven dried glassware under an atmosphere of dry nitrogen or argon. Reaction solvents were distilled from CaH_2 (dichloromethane, triethylamine, pyridine), Na (toluene), Na-Ph_2CO (tetrahydrofuran) and Mg turnings-I_2 (methanol). Petroleum ether refers to the fraction distilled at 40-60 ^oC. Manual flash column chromatography were carried out using neutral silica gel. Thin Layer Chromatography (TLC) were developed on pre-coated aluminium backed plates and visualised under UV light (254 nm lamp) or by staining with potassium permanganate, vanillin or phosphomolybdic acid stains as appropriate.

^1H NMR spectra were recorded using a 400 MHz Bruker DRX-400 spectrometer. ^{13}C NMR spectra were recorded using a 101 MHz or 126 MHz Bruker DRX-400 spectrometer. All spectra were recorded under the supervision of the Imperial College London Department of Chemistry NMR Service. Chemical shifts (δ) are quoted in parts per million (ppm) and are referenced to the residual solvent peaks, $CDCl_3$ (δ_H: 7.26, δ_C: 77.0) and DMSO-d_6 (δ_H: 2.50, δ_C: 39.4). Coupling constants (*J*) are quoted to the nearest 0.5 Hz. Low and high resolution mass spectrometry were recorded by the Imperial College London Department of Chemistry Mass Spectrometry Service, using a Micromass Platform II or a Micromass AutoSpec-Q spectrometer.

UV-vis spectra were recorded with a Perkin Elmer Lambda 25 spectrometer, using 3.5 mL stoppered ES Quartz cuvettes and, IR spectra were measured on a Perkin Elmer Spectrum Express, version 1.01.00. Microwave reactions were conducted in a CEM Discover S Class microwave in Dynamic mode setting with a fixed hold time and IR temperature probe. All microwave reactions were conducted in DMF or DMA at 180 ^oC with a default pressure of 1 – 5 bar.

For computational calculations, geometry optimisations were performed using the wB97xD and M062X functionals, and the 6-31G (2d,2p) basis set. Frequency calculations were performed to identify energy minima (no imaginary frequencies) and transition states (one imaginary frequency). Thermal corrections for Gibbs free energy were calculated at 298K. For conversions of Gaussian computational data output in Hartree to kJ/mol, a factor of 2625.5 was used.

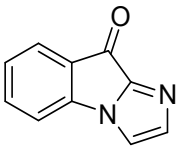
Purity analysis for compounds used in radiochemistry was evaluated by analytical and preparatory HPLC. [^{18}F]Fluoride was produced by a cyclotron (GE PETrace), utilising the [^{18}O(*p,n*)^{18}F] nuclear reaction with 16.4 MeV proton irradiation of an enriched [(^{18}O)H_2O] target.

HPLC Methods

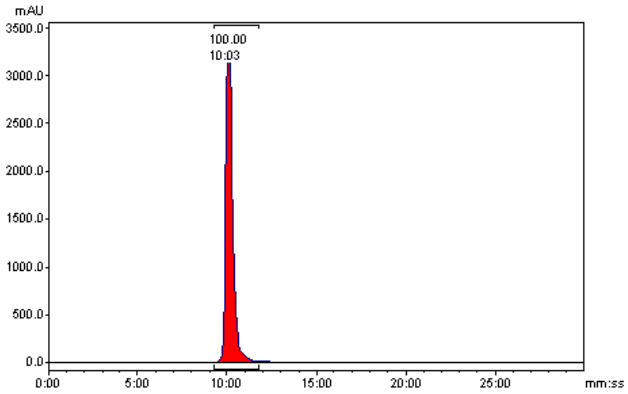
Analytical and preparatory HPLC methods of non-radioactive compounds were developed on an Agilent 1100 series system with Laura 3 software and linear UV detector recording absorption at 254 nm. Preparatory and analytical radio-HPLC were carried out on a Beckman System Gold machine fitted with a Bioscan Flowcount FC-3400 PIN diode detector (Lablogic) and a linear UV-200 detector recording at 254 nm.

For analytical HPLC, a Phenomenex 4.6 x 50 mm C18 (2) column was used in 15 min running time and 1ml/min flow rate. For preparatory HPLC, a Phenomenex 10 x 250 mm C18 (2) column was used in 30 min running time and 3ml/min flow rate. Isocratic elution methods were used which composed of a mobile phase of ethanol and 0.1 M ammonium formate. 60 % and 35 % or 45 % of ethanol was used for analytical and preparatory isocratic elution respectively.

9*H*-Imidazo[1,2-a]indol-9-one **52**

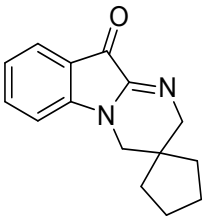


A mixture of the trityl-deprotected 2-fluorophenyl-imidazomethanone **196** (0.54 g, 2.85 mmol) and K_2CO_3 (1.18 g, 8.55 mmol) in DMF (60 mL) was stirred at 145 ^{o}C for 10 hours. The reaction mixture was allowed to cool to room temperature before diluting with ethyl acetate (50 mL), and washing with water (50 mL) and brine (3 x 150 mL). The organic layer was dried over $MgSO_4$ and concentrated *in vacuo*. Purification by flash column chromatography, eluting with 1:1 – 1:0 ethyl acetate/ petroleum ether gave the imidazoleindolone heterocycle **52** as an orange solid (0.34 g, 69 % yield): ^{1}H NMR (400 MHz, $CDCl_3$) δ 7.19 (d, *J* = 7.8 Hz, 1H), 7.30 (m, 2 H), 7.44 (br m, 1H), 7.56 (td, *J* = 1.0 Hz, 7.8 Hz, 1H), 7.68 (d, *J* = 6.9 Hz, 1H); ^{13}C NMR (101 MHz, $CDCl_3$) δ 111.5, 115.0, 125.4, 127.3, 128.4, 135.5, 137.5, 141.5, 146.1, 177.7; ν_{max}/cm^{-1} 1719 (C=O), 1618, 1504, 1469, 1346; HRMS (ES) *m/z* = 171.0550 $[M+H]^+$ found, $C_{10}H_7N_2O$ needs 171.0553.

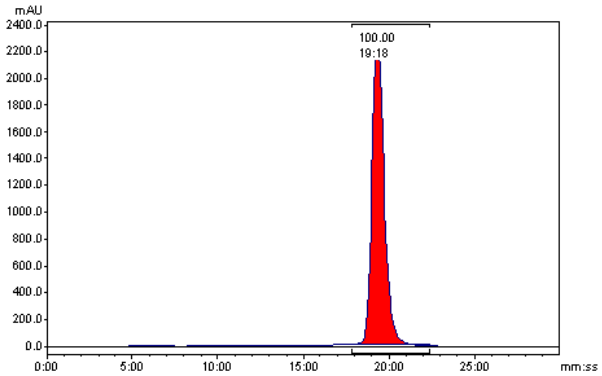


Reverse phase prep HPLC chromatogram of the imidazoleindolone **52**, eluting with a mobile phase of 35 % ethanol

2'*H*-Spiro[cyclopentane-1,3'-pyrimido[1,2-a]indol]-10'(4'*H*)-one **57**

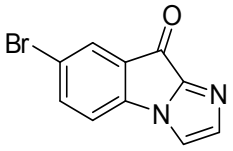


The ketal-protected pyrimidoindolone **94** (0.025 g, 0.08 mmol) was treated with methanesulfonic acid (0.3 mL) and the resulting yellow solution was stirred at room temperature for 2 hours. The mixture was then treated with saturated aqueous Na_2CO_3 solution until a pH of ~9 was reached. The aqueous solution was extracted with DCM (4 x 10 mL) with the combined organic extracts dried over $MgSO_4$ and concentrated *in vacuo*. The crude material was purified by flash column chromatography, eluting with 1:4 – 1:1 ethyl acetate/ petroleum ether to give the pyrimidoindolone heterocycle **57** as a yellow foam (0.017 g, 89 % yield); ^{1}H NMR (400 MHz, $CDCl_3$) δ 1.55 (m, 2H), 1.77 (m, 6H), 3.38 (s, 2H), 3.67 (s, 2H), 6.78 (d, *J* = 8.3 Hz, 1H), 7.00 (br td, *J* = 8.0 Hz, 1H), 7.55 (m, 1H), 7.67 (m, 1H); ^{13}C NMR (101 MHz, $CDCl_3$) δ 25.1, 36.2, 39.9, 49.8, 57.4, 107.8, 119.4, 121.1, 125.2, 137.7, 148.5, 152.3, 184.4; ν_{max}/cm^{-1} 1714 (C=O), 1653, 1606 (C=N), 1473, 1370, 1122; HRMS (ES) *m/z* = 241.1341 $[M+H]^+$ found, $C_{15}H_{17}N_2O$ needs 241.1341; R_f = 0.29 (1:1 ethyl acetate/petroleum ether).

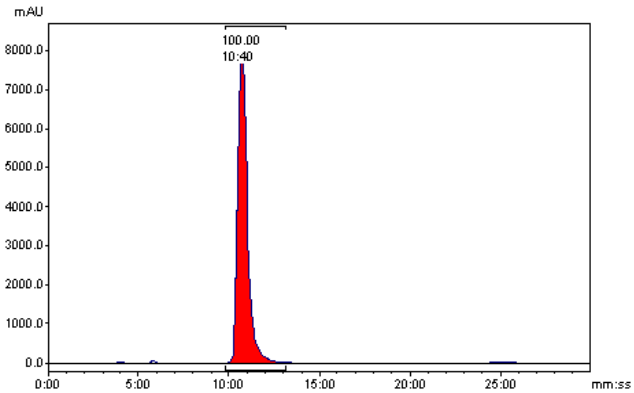


Reverse phase prep HPLC chromatogram of the pyrimidoindolone **57**, eluting with a mobile phase of 35 % ethanol

7-Bromo-9*H*-imidazo[1,2-a]indol-9-one **58**

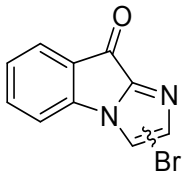


A solution of 5-bromo-2-fluorophenyl-imidazomethanone **180** (0.50 g, 1.86 mmol) and Cs_2CO_3 (1.81 g, 5.57 mmol) in DMF (30 mL) was stirred at 140 ^oC for 1.5 hours. After cooling to room temperature, the mixture was diluted with ethyl acetate (50 mL) and washed with water (2 x 20 mL) and brine (3 x 100 mL). The organic layer was dried over $MgSO_4$ and concentrated *in vacuo*, prior to purification by flash column chromatography, eluting with 1:1 ethyl acetate/ petroleum ether to give the imidazoleindolone **58** as a yellow solid (0.29 g, 63 % yield): ^1H NMR (400 MHz, $CDCl_3$) δ 7.08 (d, *J* = 7.8 Hz, 1H), 7.26 (m, 1H), 7.45 (m, 1H), 7.68 (dd, *J* = 2.0 Hz, 7.8 Hz, 1H), 7.77 (d, *J* = 2.0 Hz, 1H); ^{13}C NMR (101 MHz, $CDCl_3$) δ 113.0, 115.3, 120.3, 128.6, 129.8, 137.8, 137.9, 140.1, 145.8, 176.1; ν_{max}/cm^{-1} 1699 (C=O), 1612 (C=N), 1476, 1390, 1262; HRMS (ES) *m/z* = 248.9651 $[M+H]^+$ found, $C_{10}H_6BrN_2O$ needs 248.9658.

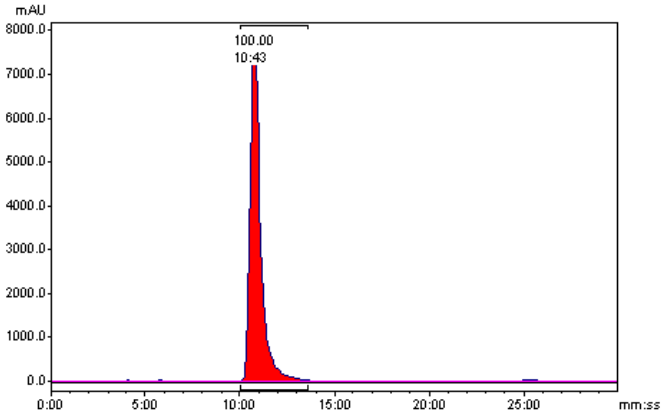


Reverse phase prep HPLC chromatogram of the bromo-substituted imidazoleindolone **58**, eluting with a mobile phase of 35 % ethanol

2/3-Bromo-9*H*-imidazo[1,2-a]indol-9-one **59**

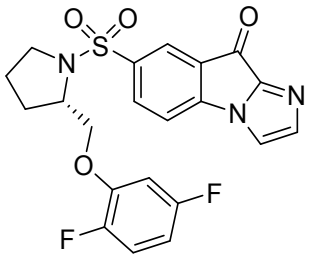


To a solution of imidazoleindolone **52** (0.05 g, 0.39 mmol) in chloroform (1.5 mL), was added NBS (0.10 g, 0.58 mmol) and the mixture was stirred at room temperature for 15 hours. DCM (10 mL) was subsequently added, prior to washing with water (5 mL) and brine (5 mL). The organic layer was dried over $MgSO_4$ and concentrated *in vacuo*, followed by purification by flash column chromatography, eluting with 1:4 – 1:1 ethyl acetate/ petroleum ether to give the bromo-substituted imidazoleindolone **59** as an orange solid (0.019 g, 26 % yield): ^{1}H NMR (400 MHz, $CDCl_3$) δ 7.17 (d, *J* = 7.8 Hz, 1H), 7.34 (m 2H), 7.60 (td, *J* = 1.5 Hz, 7.8 Hz, 1H), 7.70 (br d, *J* = 8.0 Hz, 1H); ^{13}C NMR (126 MHz, $CDCl_3$) δ 111.7, 114.9, 123.2, 125.7, 126.9, 127.9, 135.7, 141.1, 144.2, 176.4; ν_{max}/cm^{-1} 3120, 1715 (C=O), 1617 (C=N), 1471, 1427, 1349; HRMS (ES) *m/z* = 248.9657 $[M+H]^+$ found, $C_{10}H_6BrN_2O$ needs 248.9658; R_f = 0.12 (1:4 ethyl acetate/ petroleum ether).

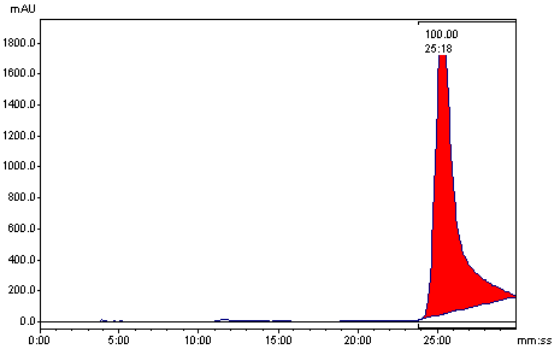


Reverse phase prep HPLC chromatogram of the bromo-substituted imidazoleindolone **59**, eluting with a mobile phase of 35 % ethanol

(*S*)-7-(2-((2,5-Difluorophenoxy)methyl)pyrrolidin-1-ylsulfonyl)-9*H*-imidazo[1,2-a]indol-9-one **60**

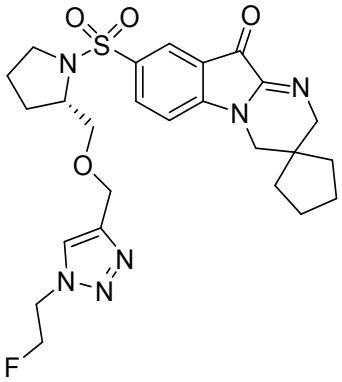


A mixture of 5-sulfonamide-2-fluorophenyl-imidazomethanone **201** (0.04 g, 0.09 mmol) and K_2CO_3 (0.04 g, 0.27 mmol) in DMF (3 mL) was stirred at 120 ^oC for 1 hour. Then, the reaction mixture was allowed to cool to room temperature, before diluting with ethyl acetate (5 mL), and washing with water (5 mL) and brine (3 x 10 mL). The organic layer was dried over $MgSO_4$ and concentrated *in vacuo*. Purification by flash column chromatography, eluting with 1:1 – 1:0 ethyl acetate/ petroleum ether gave the imidazoleindolone target **60** as an orange solid (0.037 g, 92 % yield): ^1H NMR (400 MHz, $CDCl_3$) δ 1.79 (m, 2H), 2.05 (m, 2H), 3.20 (m, 1H), 3.52 (m, 1H), 4.00 (m, 2H), 4.18 (m, 1H), 6.77 (m, 2H), 6.91 (m, 1H), 7.26 (m, 2H), 7.46 (s, 1H), 8.03 (m, 2H); ^{13}C NMR (126 MHz, $CDCl_3$) δ 24.2, 29.0, 49.5, 58.7, 71.5, 104.8 (dd, *J* = 21.8 Hz, 27.2 Hz), 110.4 (dd, *J* = 4.4 Hz, 22.9 Hz), 111.9, 115.4, 115.4 (m), 124.2, 128.9, 135.1, 137.3, 138.6, 142.9 (dd, *J* = 3.3 Hz, 10.9 Hz), 143.9, 146.3, 152.3 (dd, *J* = 12.0 Hz, 248.5 Hz), 156.5 (dd, *J* = 9.8 Hz, 242.0 Hz), 175.6; ν_{max}/cm^{-1} 1719 (C=O), 1614, 1508 (C=N), 1476, 1337, 1146; HRMS (ES) *m/z* = 446.0986 $[M+H]^+$ found, $C_{21}H_{18}F_2N_3O_4S$ needs 446.0986; R_f = 0.34 (ethyl acetate).



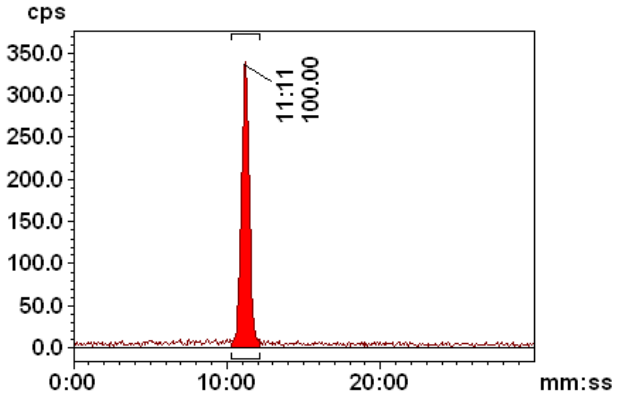
Reverse phase prep HPLC chromatogram of the imidazoleindolone target **60**, eluting with a mobile phase of 35 % ethanol

(*S*)-8'-(2-(((1-(2-Fluoroethyl)-1*H*-1,2,3-triazol-4-yl)methoxy)methyl)pyrrolidin-1-ylsulfonyl)-2'*H*-spiro[cyclopentane-1,3'-pyrimido[1,2-a]indol]-10'(4'*H*)-one, **62**



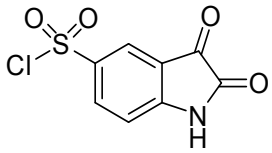
Part 1: To a solution of 1-fluoroethyltosylate **75** (0.10 g, 0.46 mmol) in DMF (2 mL) was added NaN_3 (0.09 g, 1.40 mmol) and the mixture was stirred at room temperature for 15 hours. A TLC showed the full disappearance of the 1-fluoroethyltosylate **75** and a new polar product, indicating conversion to 1-fluoroethylazide **37**.

Part 2: $CuSO_4$ (0.006 g, 0.025 mmol) and L-ascorbic acid (0.009 g, 0.05 mmol) were added to a separate reaction flask, followed by the addition of the alkyne precursor **81** (0.022 g, 0.05 mmol) in DMF (1.5 mL). The mixture was stirred to give a dark brown solution. Then, fluoroethylazide **37** (0.26 mL, 0.06 mmol of the filtered solution from *part 1*) was added and stirring was continued at room temperature for 1 hour. This was followed by quenching with 10 % aqueous NH_4Cl solution (10 mL) and extraction with ethyl acetate (2 x 10 mL). The combined organic extracts was washed with brine (2 x 15 mL) and water (2 x 5 mL), dried over $MgSO_4$ and concentrated *in vacuo*. Purification by flash column chromatography, eluting with 1:1 – 1:0 ethyl acetate/ petroleum ether gave the pyrimidoindolone target **62** as a yellow foam (0.013 g, 50 % yield); ^{1}H NMR (400 MHz, $CDCl_3$) δ 1.55 (m, 12H), 3.15 (m, 1H), 3.42 (m, 3H), 3.54 (m, 1H), 3.76 (m, 4H), 4.67 (m, 3H), 4.75 (m, 2H), 4.89 (m, 1H), 6.88 (d, *J* = 8.5 Hz, 1H), 7.73 (s, 1H), 8.02 (dd, *J* = 8.5 Hz, 1.8 Hz, 1H), 8.04 (d, *J* = 1.8 Hz, 1H); ^{13}C NMR (126 MHz, $CDCl_3$) δ 24.1, 25.1, 28.9, 36.1, 39.9, 49.3, 50.0, 50.5 (d, *J* = 20.7 Hz), 57.5, 59.1, 64.6, 72.7, 81.0 (d, *J* = 173.3 Hz), 108.1, 119.1, 123.6, 124.7, 130.8, 137.0, 145.2, 147.9, 154.2, 183.3; ν_{max}/cm^{-1} 1728 (C=O), 1660, 1603 (C=N), 1484, 1461, 1334 (-SO_2-N), 1276, 1151, 1127 (C-F), 1075 (C-O-C); HRMS (ES) *m/z* = 531.2183 $[M+H]^+$ found, $C_{25}H_{32}FN_6O_4S$ needs 531.2184; $[\alpha_D]^{20}$ = -50.4 (c 0.004, $CHCl_3$); R_f = 0.11 (ethyl acetate).



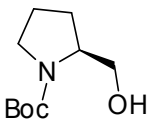
Reverse phase prep HPLC chromatogram of the pyrimidoindolone target **62**, eluting with a mobile phase of 45 % ethanol

5-Chlorosulfonylisatin **64**[69]



To a suspension of sodium-5-isatinsulfonate **63** (10.00 g, 35.10 mmol) in sulfolane (50 mL) was added $POCl_3$ (16 mL, 176.50 mmol) and the mixture was stirred at 60 ^oC for 3 hours. The dark-brown solution was cooled to 0 ^oC and ice-cold water (150 mL) was cautiously added. The resulting precipitate was filtered and washed with water (100 mL). The solid was then dissolved in ethyl acetate (100 mL) and further washed with water (50 mL). This was followed by drying over $MgSO_4$ and concentration *in vacuo* to give a solid residue which was recrystallised from an ethyl acetate/hexane mixture to give the sulfonyl chloride **64** as an orange solid (3.72 g, 43 % yield): ^1H NMR (400 MHz, DMSO) δ 6.86 (d, *J* = 7.8 Hz, 1H), 7.58 (d, *J* = 1.5 Hz, 1H), 7.80 (dd, *J* = 1.5 Hz, 7.8 Hz, 1H), 11.11 (s, 1H); ^{13}C NMR (126 MHz, DMSO) δ 111.5, 117.0, 121.4, 135.5, 143.2, 150.7, 159.7, 184.3; MS – a molecular ion was not observed.

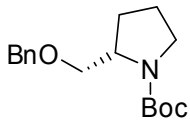
(*S*)-*tert*-Butyl 2-(hydroxymethyl)pyrrolidine-1-carboxylate **66**[208]



To a solution of 2-pyrrolidinemethanol **65** (5 mL, 51.00 mmol) in anhydrous DCM (100 mL) was added Et_3N (21.2 mL, 152.00 mmol), followed by the addition of Boc_2O (13.30 g, 60.84 mmol). The mixture was stirred under argon at room temperature for 1 hour. Then, the pale yellow reaction mixture was washed with water (100 mL) and the organic extract was dried over $MgSO_4$ and concentrated *in*

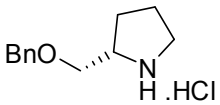
vacuo. The crude product was purified by flash column chromatography, eluting with 1:1 - 1:0 ethyl acetate/ petroleum ether to give the Boc-protected prolinol **66** as a colourless solid (9.08 g, 89 % yield): ^{1}H NMR (400 MHz, $CDCl_3$) δ 1.48 (s, 9H), 1.81 (m, 2H), 2.01 (m, 1H), 3.31 (m, 1H), 3.46 (m 1H), 3.61 (m, 3H), 3.98 (br m, 1H), 4.77 (br m, 1H); ^{13}C NMR (101 MHz, $CDCl_3$) δ 24.1, 28.5, 28.7, 47.6, 60.2, 67.8, 80.2, 157.2; HRMS (ES) *m/z* = 224.1256 $[M+Na]^+$ found, $C_{10}H_{19}NNaO_3$ needs 224.1257; R_f = 0.31 (1:1 ethyl acetate/ petroleum ether).

(*S*)-*tert*-Butyl 2-(benzyloxymethyl)pyrrolidine-1-carboxylate, **67**[58]



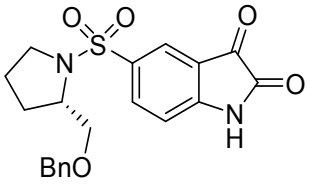
To a solution of N-Boc-prolinol **66** (6.00 g, 30.00 mmol) and NaH (60 % in mineral oil, 2.40 g, 60.00 mmol) in anhydrous THF (70 mL) at 0 ^{o}C, was added BnBr (4.3 mL, 36.00 mmol) and the mixture was stirred at 0 ^{o}C for 30 minutes and then at room temperature for 16 hours. This was followed by washing with water (100 mL), drying over $MgSO_4$ and concentration *in vacuo*. The crude residue was purified by flash column chromatography, eluting with 1:9 ethyl acetate/ petroleum ether to give the benzyl ether **67** as a colourless oil (8.03 g, 92 % yield): ^{1}H NMR (400 MHz, $CDCl_3$) δ 1.44 (s, 9H), 1.88 (m, 4H), 3.40 (m, 3H), 3.63 (br m, 1H), 3.95 (br m, 1H), 4.54 (m, 2H), 7.30 (m, 5H); ^{13}C NMR (101 MHz, $CDCl_3$) δ 23.35 (d, *J* = 91.6 Hz), 28.5, 46.4 (br d), 56.5, 60.3, 70.9 (br d), 73.2, 79.2, 127.5, 127.5, 128.4, 138.4, 154.6; HRMS (ES) *m/z* = 314.1732 $[M+Na]^+$, $C_{17}H_{25}NNaO_3$ needs 314.1732; R_f = 0.20 (1:9 ethyl acetate/ petroleum ether).

(*S*)-2-(Benzyloxymethyl)pyrrolidine **68**[58]



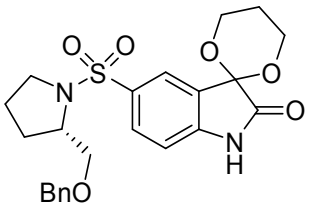
A solution of the Boc-protected amine **67** (7.70 g, 26.50 mmol) in 4M HCl in dioxane (65 mL) and DCM (50 mL) was stirred at room temperature for 12 hours. Then, the reaction mixture was concentrated *in vacuo* to give the HCl salt of the amine **68** as a colourless solid (5.85 g, 97 % yield): ^{1}H NMR (400 MHz, $CDCl_3$) δ 1.96 (m, 4H), 3.30 (s, 2H), 3.77 (m, 3H), 4.63 (q, *J* = 35.2 Hz, 11.7 Hz, 2H), 7.35 (m, 5H), 9.27 (s, 1H), 10.14 (s, 1H); ^{13}C NMR (101 MHz, $CDCl_3$) δ 24.2, 27.2, 45.7, 58.5, 68.8, 73.4, 127.9, 128.1, 128.4, 137.5; ν_{max}/cm^{-1} 2873 - 2657 (br -NH_2^+), 1575, 1497, 1390, 1088; HRMS (ES) *m/z* = 192.1387 $[M+H]^+$ found, $C_{12}H_{18}NO$ needs 192.1388.

(*S*)-5-(2-(Benzyloxymethyl)pyrrolidin-1-ylsulfonyl)indoline-2,3-dione **69**[58]



To a solution of 2-benzyloxymethyl pyrrolidine **68** (HCl salt, 3.79 g, 16.70 mmol) and Et_3N (7.40 mL, 53.13 mmol) in 1:1 mixture of THF and DCM (300 mL) at 0 ^oC, was added a solution of isatin-5-sulfonyl chloride **64** (3.72 g, 15.18 mmol) in THF (50 mL) over 30 minutes, maintaining the temperature at 0 ^oC. The mixture was stirred at room temperature for 1 hour and concentrated *in vacuo*. Purification of the resulting residue by flash column chromatography, eluting with 1:1 ethyl acetate/ petroleum ether gave the sulfonamide **69** as an orange solid (5.05 g, 83 % yield): ^1H NMR (400 MHz, DMSO) δ 1.53 (m, 2H), 1.79 (m, 3H), 3.09 (m, 1H), 3.43 (m, 1H), 3.58 (m, 1H), 3.72 (m, 1H), 4.51 (s, 2H), 7.07 (d, *J* = 8.3 Hz, 1H), 7.33 (m, 5H), 7.76 (d, *J* = 2.0 Hz, 1H), 8.01 (dd, *J* = 2.0 Hz, 8.3 Hz, 1H), 11.44 (s, 1H); ^{13}C NMR (101 MHz, DMSO) δ 24.1, 28.8, 49.5, 59.3, 72.7, 72.8, 113.2, 118.6, 123.6, 127.9, 127.9, 128.7, 131.4, 137.3, 138.8, 154.1, 160.0, 183.5; ν_{max}/cm^{-1} 3240 (N-H), 1730 (C=O ketone), 1615 (C=O amide), 1344, 1467; HRMS (ES) *m/z* = 401.1165 $[M+H]^+$ found, $C_{20}H_{21}N_2O_5S$ needs 401.1166; R_f = 0.15 (1:1 ethyl acetate/ petroleum ether).

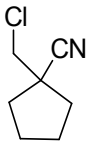
(*S*)-5'-(2-(Benzyloxymethyl)pyrrolidin-1-ylsulfonyl)spiro[[1,3]dioxane-2,3'-indolin]-2'-one **70**[58]



To a solution of isatin sulfonamide **69** (2.42 g, 6.00 mmol) and 1,3-propanediol (4.3 mL, 60.00 mmol) in toluene (100 mL), was added toluenesulfonic acid (0.29 g, 1.50 mmol) and the mixture was refluxed for 12 hours, collecting water with a Dean Stark trap. The mixture was subsequently allowed to cool to room temperature, washed with saturated aqueous Na_2CO_3 solution (70 mL), water (100 mL) and brine (100 mL), before drying over $MgSO_4$. After concentration *in vacuo*, the crude product was purified by flash column chromatography, eluting with 1:4 – 1:1 ethyl acetate/ petroleum ether to give the ketal protected sulfonamide **70** as a colourless foam (2.39 g, 87 % yield): ^1H NMR (400 MHz, $CDCl_3$) δ 1.64 (m, 3H), 1.92 (m, 2H), 2.39 (m, 1H), 3.08 (m, 1H), 3.48 (m, 2H), 3.82 (m, 2H), 4.00 (m, 2H), 4.57 (m, 2H), 4.94 (m, 2H), 6.88 (d, *J* = 8.3 Hz, 1H), 7.35 (m, 5H), 7.80 (m, 2H), 7.91 (d, *J* = 2.0 Hz,

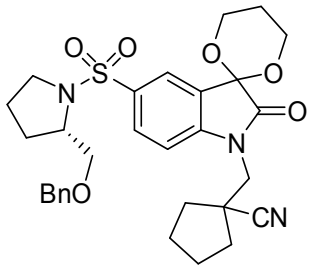
1H); ^{13}C NMR (126 MHz, $CDCl_3$) δ 24.0, 25.1, 28.8, 49.3, 59.2, 61.2, 72.8, 73.5, 93.0, 110.0, 124.4, 127.7, 127.7, 128.4, 128.6, 131.1, 132.3, 138.2, 143.9, 173.0; ν_{max}/cm^{-1} 3280 (N-H), 1620 (C=O), 1473, 1335 (-SO2-N), 1201 (O-C-O); HRMS (ES) *m/z* = 459.1583 $[M+H]^+$ found, $C_{23}H_{27}N_2O_6S$ needs 459.1584; R_f = 0.32 (1:1 ethyl acetate/ petroleum ether).

1-(Chloromethyl)cyclopentanecarbonitrile **72**[117]



A mixture of cyclopentanecarbonitrile **71** (6.6 mL, 63.00 mmol) and bromochloromethane (14.4 mL, 221.00 mmol) in THF (100 mL) was cooled to -78 °C. A solution of LDA, prepared by the addition of ^{n}BuLi (1.6 M in hexane, 59 mL, 94.50 mmol) to diisopropylamine (13.26 mL, 94.50 mmol) in THF (50 mL) at 0 °C, was cooled to -78 °C in a separate flask. The two solutions were quickly mixed and stirred at -78 °C for 3 hours, before allowing to stand at room temperature overnight. This was followed by quenching with water (150 mL) and washing with brine (50 mL). The organic extract was dried over $MgSO_4$ and concentrated *in vacuo*. Purification by flash column chromatography, eluting with 1:19 ethyl acetate/ petroleum ether gave the 1-chloromethyl cyclopentanecarbonitrile **72** as a pale yellow oil (2.16 g, 24 % yield): ^{1}H NMR (400 MHz, $CDCl_3$) δ 1.85 (m, 6H), 2.24 (m, 2H), 3.61 (s, 2H)); ^{13}C NMR (101 MHz, $CDCl_3$) δ 24.7, 36.7, 45.4, 48.5, 123.1; HRMS (CI) *m/z* = 161.0846 $[M+NH_4]^+$ found, $C_7H_{14}ClN_2$ needs 161.0846; R_f = 0.30 (1:5 ethyl acetate/ petroleum ether).

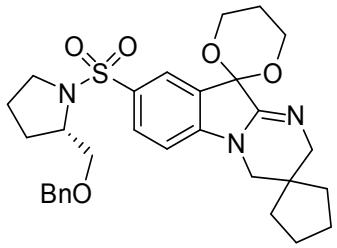
(*S*)-1-((5'-(2-(Benzyloxymethyl)pyrrolidin-1-ylsulfonyl)-2'-oxospiro[[1,3]dioxane-2,3'-indoline]-1'-yl)methyl)cyclopentanecarbonitrile **77**[58]



A mixture of ketal-protected isatin sulfonamide **70** (1.60 g, 3.50 mmol) and ^{t}BuOK (0.98 g, 8.75 mmol) in DMF (10 mL) was stirred at room temperature for 1 hour. The alkylating agent, 1-chloromethyl cyclopentanecarbonitrile **72** (1.50 g, 10.50 mmol) was added and stirring was continued at 140 °C for 2 days. The reaction mixture was subsequently concentrated *in vacuo* and purified by flash column

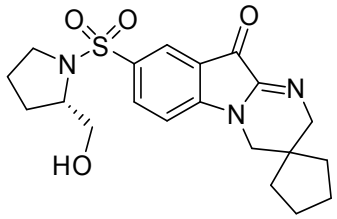
chromatography, eluting with 1:4 – 1:1 ethyl acetate/ petroleum ether to give the nitrile **77** as a colourless foam (1.40 g, 71 % yield): ^{1}H NMR (400 MHz, $CDCl_3$) δ 1.91 (m, 8H), 2.17 (m, 3H), 2.42 (m, 1H), 3.09 (m, 1H), 3.49 (m, 3H), 3.66 (m, 1H), 3.77 (m, 1H), 3.86 (m, 3H), 4.01 (m, 2H), 4.57 (m, 2H), 4.92 (m, 2H), 7.20 (d, *J* = 8.3 Hz, 1H), 7.36 (m, 5H), 7.86 (dd, *J* = 2.0 Hz, 8.3 Hz, 1H), 7.93 (d, *J* = 2.0 Hz, 1H); ^{13}C NMR (126 MHz, $CDCl_3$) δ 23.8, 24.0, 25.1, 28.8, 36.5, 43.9, 45.5, 49.2, 59.2, 61.3, 72.8, 73.4, 92.7, 109.7, 124.0, 127.7, 127.7, 128.0, 128.4, 131.1, 132.8, 132.8, 138.2, 145.9, 172.7; ν_{max}/cm^{-1} 2235 (C≡N), 1721 (C=O), 1661 (C=N), 1342 (-SO2-N), 1055 (O-C-O); HRMS (ES) *m/z* = 566.2325 $[M+H]^+$ found, $C_{30}H_{36}N_3O_6S$ needs 566.2325; R_f = 0.52 (1:1 ethyl acetate/ petroleum ether).

(*S*)-8'-(2-(Benzyloxymethyl)pyrrolidin-1-ylsulfonyl)-2'*H*-spiro[cyclopentane-1,3'-pyrimido[1,2-a]indole]-10',10'-(1,3-dioxolane) **79**[58]



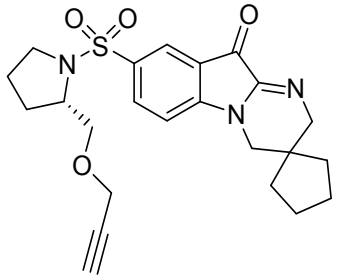
A mixture of the nitrile **77** (0.113 g, 0.20 mmol) and a spatula of wet Raney Ni in 2M methalonic ammonia (5 mL) was hydrogenated in an autoclave at a hydrogen pressure of ~70 psi for 7 hours. The suspension was filtered through Celite® and the filtrate was refluxed for a further 5 hours. After cooling to room temperature and concentration *in vacuo*, the crude product was purified by flash column chromatography, eluting with 1:4 – 1:1 ethyl acetate/ petroleum ether to give the amidine **79** as a colourless foam (0.091 g, 83 % yield): ^{1}H NMR (400 MHz, $CDCl_3$) δ 1.48 (m, 2H), 1.59 (m, 4H), 1.75 (m, 5H), 1.90 (m, 2H), 2.27 (m, 1H), 3.07 (m, 1H), 3.30 (s, 2H), 3.45 (m, 4H), 3.79 (m, 2H), 3.97 (m, 2H), 4.57 (m, 2H), 5.07 (m, 2H), 6.62 (d, *J* = 8.4 Hz, 1H), 7.36 (m, 5H), 7.80 (dd, *J* = 1.8 Hz, 8.4 Hz, 1H), 7.92 (d, *J* = 1.8 Hz, 1H); ^{13}C NMR (126 MHz, $CDCl_3$) δ 24.0, 25.0, 25.5, 28.8, 35.9, 38.5, 49.2, 50.2, 55.9, 59.0, 60.2, 73.0, 73.4, 96.0, 105.5, 124.0, 127.6, 127.7, 128.4, 128.5, 129.1, 131.4, 138.3, 147.6, 156.2; ν_{max}/cm^{-1} 2954, 1611 (C=N), 1494, 1466, 1335, 1264, 1153; HRMS (ES) *m/z* = 552.2532 $[M+H]^+$ found, $C_{30}H_{38}N_3O_5S$ needs 552.2532; R_f = 0.34 (1:1 ethyl acetate/ petroleum ether).

(*S*)-8'-(2-(Hydroxymethyl)pyrrolidin-1-ylsulfonyl)-2'*H*-spiro[cyclopentane-1,3'-pyrimido[1,2-a]indol]-10'(4'*H*)-one **80**[58]



The ketal/benzyl protected pyrimidoindolone **79** (0.22 g, 0.40 mmol) was dissolved in methanesulfonic acid (3 mL) and the resulting yellow solution was stirred at room temperature for 5 hours. The mixture was then cooled to 0 ^{o}C and treated with saturated aqueous Na_2CO_3 solution until a pH of ~8 was reached. This was followed by extraction with DCM (4 x 10 mL). The combined organic extracts was dried over $MgSO_4$ and concentrated *in vacuo*. Purification by flash column chromatography, eluting with ethyl acetate gave the fully deprotected pyrimidoindolone **80** as a yellow foam (0.13 g, 81 % yield); ^{1}H NMR (400 MHz, $CDCl_3$) δ 1.57 (m, 5H), 1.78 (m, 7H), 2.64 (s, 1H), 3.26 (m, 1H), 3.49 (m, 3H), 3.72 (m, 5H), 6.90 (d, *J* = 8.5 Hz, 1H), 8.05 (dd, *J* = 8.4 Hz, 1.8 Hz, 1H), 8.12 (d, *J* = 1.8 Hz, 1H); ^{13}C NMR (126 MHz, $CDCl_3$) δ 24.3, 25.1, 29.0, 29.7, 36.1, 39.9, 50.1, 57.5, 61.9, 65.8, 108.2, 119.3, 124.9, 130.0, 137.1, 147.9, 154.4, 183.2; HRMS (ES) *m/z* = 404.1644 $[M+H]^+$ found, $C_{20}H_{26}N_3O_4S$ needs 404.1644; R_f = 0.12 (ethyl acetate).

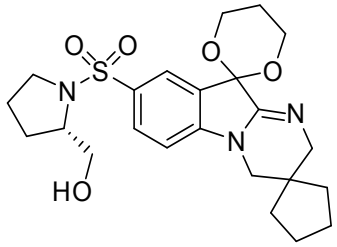
(*S*)-8'-(2-((Prop-2-ynyloxy)methyl)pyrrolidin-1-ylsulfonyl)-2'H-spiro[cyclopentane-1,3'-pyrimido[1,2-a]indol]-10'(4'*H*)-one, **81**



A solution of the ketal-protected alkyne **83** (0.18 g, 0.36 mmol) in methanesulfonic acid (2 mL) was stirred at room temperature for 12 hours. The mixture was slowly quenched with saturated aqueous Na_2CO_3 solution until a pH of ~8 was reached, before extracting with DCM (3 x 15 mL). This was followed by drying over $MgSO_4$ and concentration *in vacuo*. Purification by flash column chromatography, eluting with 1:1 – 1:0 ethyl acetate/ petroleum ether, gave deprotected alkyne **81** as a yellow foam (0.091 g, 58 % yield); ^{1}H NMR (400 MHz, $CDCl_3$) δ 1.65 (m, 10H), 1.93 (m, 2H), 2.49

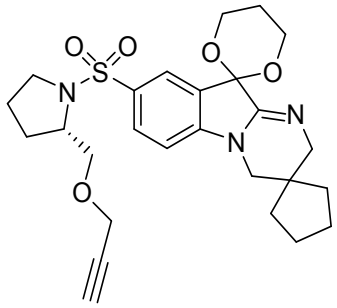
(t, *J* = 2.4 Hz, 1H), 3.13 (m, 1H), 3.44 (m, 3H), 3.54 (m, 1H), 3.71 (s, 2H), 3.77 (m, 2H), 4.19 (d, *J* = 2.4 Hz, 2H), 6.89 (d, *J* = 8.4 Hz, 1H), 8.04 (dd, *J* = 8.4 Hz, 1.8 Hz, 1H), 8.11 (d, *J* = 1.8 Hz, 1H); ^{13}C NMR (101 MHz, $CDCl_3$) δ 24.0, 25.1, 28.9, 36.1, 39.9, 49.4, 50.0, 57.5, 58.6, 59.0, 72.4, 74.7, 79.6, 108.2, 119.2, 124.9, 130.5, 137.0, 147.9, 154.3, 183.3; ν_{max}/cm^{-1} 2924 (C≡C), 1727 (C=O), 1605 (C=N), 1464, 1334, 1151, 1093; HRMS (ES) *m/z* = 442.1801 $[M+H]^+$ found, $C_{23}H_{28}N_3O_4S$ needs 442.1801; $[\alpha_D]^{20}$ = -60.3(c 0.003, $CDCl_3$); R_f = 0.37 (ethyl acetate).

(*S*)-8'-(2-(Hydroxymethyl)pyrrolidin-1-ylsulfonyl)-2'*H*-spiro[cyclopentane-1,3'-pyrimido[1,2-a]indole]-10',10'(1,3)-dioxolane **82**[58]



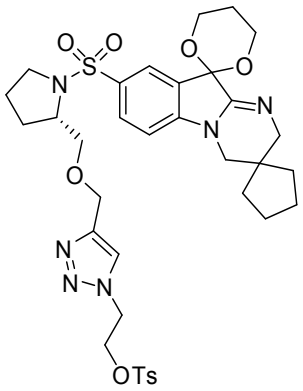
A mixture of ketal/benzyl protected pyrimidoindolone **79** (0.50 g, 0.91 mmol) and 10 % Pd/C (0.05 g) in EtOH (2 mL) was degassed for 20 minutes. 1,4-Cyclohexadiene (15 mL) was added and the mixture was refluxed for 2 days. After cooling to room temperature, the suspension was filtered through Celite® and the resulting filtrate was concentrated *in vacuo*. Purification by flash column chromatography, eluting with 3:7 acetone/ petroleum ether gave the benzyl deprotected ketal **82** as a colourless foam (0.27 g, 64 % yield); ^{1}H NMR (400 MHz, $CDCl_3$) δ 1.56 (m, 5H), 1.75 (m, 8H), 2.31 (m, 1H), 2.84 (m, 1H), 3.28 (m, 3H), 3.46 (m, 3H), 3.69 (m, 3H), 3.97 (m, 2H), 5.09 (br td, *J* = 11.2 Hz, 2.7 Hz, 2H), 6.65 (d, *J* = 8.3 Hz, 1H), 7.81 (dd, *J* = 8.3 Hz, 1.8 Hz, 1H), 7.92 (d, *J* = 1.8 Hz, 1H); ^{13}C NMR (126 MHz, $CDCl_3$) δ 24.3, 25.0, 25.4, 28.9, 29.2, 35.9, 38.6, 50.2, 55.9, 60.2, 61.8, 66.0, 97.0, 105.6, 124.1, 128.4, 128.7, 131.5, 147.9, 155.9; ν_{max}/cm^{-1} 3427 (O-H), 1671, 1611 (C=N), 1266, 1152 (O-C-O); HRMS (ES) *m/z* = 462.2063 $[M+H]^+$ found, $C_{23}H_{32}N_3O_5S$ needs 462.2063; R_f = 0.26 (ethyl acetate).

(*S*)-10',10'-(1,3)Dioxolane-8'-(2-((prop-2-ynyloxy)methyl)pyrrolidin-1-ylsulfonyl)-4',10'-dihydro-2'*H*-spiro[cyclopentane-1,3'-pyrimido[1,2-a]indole] **83**



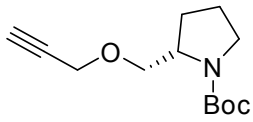
To a solution of alcohol **82** (0.016 g, 0.03 mmol) in THF (0.5 mL) was added NaH (60 % in mineral oil, 1.00 mg, 0.07 mmol) and the mixture was stirred at room temperature for 10 minutes. Propargyl bromide (80 % in toluene, 0.01 mL, 0.14 mmol) was added and stirring was continued at room temperature for 12 hours. Then, the reaction mixture was poured into 1M NaOH solution (3 mL) and partitioned between water (5 mL) and DCM (5 mL). The organic layer was dried over $MgSO_4$ and concentrated *in vacuo*. Purification of the crude material by flash column chromatography, eluting with 1:4 – 1:0 ethyl acetate/ petroleum ether gave the alkyne **83** as a colourless foam (0.009 g, 60 % yield): ^{1}H NMR (400 MHz, $CDCl_3$) δ 1.50 (m, 2H), 1.61 (m, 4H), 1.74 (m, 5H), 1.90 (m, 2H), 2.31 (m, 1H), 2.48 (t, *J* = 2.3 Hz, 1H), 3.09 (m, 1H), 3.30 (s, 2H), 3.47 (m, 4H), 3.81 (m, 2H), 3.98 (m, 2H), 4.21 (d, *J* = 2.3 Hz, 2H), 5.07 (m, 2H), 6.64 (d, *J* = 8.3 Hz, 1H), 7.81 (dd, *J* = 8.3 Hz, 1.8 Hz, 1H), 7.93 (d, *J* = 1.8 Hz, 1H); ^{13}C NMR (101 MHz, $CDCl_3$) δ 24.0, 25.1, 25.5, 28.8, 35.9, 38.6, 49.3, 50.3, 56.0, 58.6, 58.8, 60.2, 72.7, 74.6, 79.7, 96.0, 105.6, 124.0, 128.6, 129.0, 131.5, 147.7, 156.2; ν_{max}/cm^{-1} 3279 (C≡C), 1670, 1612 (C=N), 1464, 1335 (-SO_2-N), 1263 (C-O-C), 1155, 1018; HRMS (ES) *m/z* = 500.2219 $[M+H]^+$ found, $C_{26}H_{34}N_3O_5S$ needs 500.2219; $[\alpha_D]^{20}$ = -65.6 (c 0.0025, $CDCl_3$); R_f = 0.40 (ethyl acetate).

(*S*)-2-(4-(((1-(10',10'-(1,3)Dioxolane-4',10'-dihydro-2'*H*-spiro[cyclopentane-1,3'-pyrimido[1,2-a]indole]-8'-ylsulfonyl)pyrrolidin-2-yl)methoxy)methyl)-1*H*-1,2,3-triazol-1-yl)ethyl 4-methylbenzenesulfonate **84**



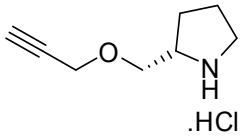
A mixture of $CuSO_4$ (0.011 g, 0.045 mmol), L-ascorbic acid (0.016 g, 0.09 mmol) and the alkyne **83** (0.045 g, 0.09 mmol) in DMF (1.0 mL) was stirred at room temperature for 10 minutes to give a pale yellow solution. Tosylethylazide **36** (0.027 g, 0.11 mmol) in DMF (0.5 mL) was added and stirring was continued at room temperature for 1 hour. This was followed by quenching with 10 % NH_4Cl aqueous solution (10 mL) and extraction with ethyl acetate (2 x 10 mL). The combined organic extracts was washed with brine (2 x 15 mL) and water (2 x 15 mL), dried over $MgSO_4$ and concentrated *in vacuo*. The crude mixture was purified by flash column chromatography, eluting with 1:1 – 1:0 ethyl acetate/ petroleum ether to give the tosylate **84** as a colourless foam (0.036 g, 54 % yield); ^{1}H NMR (400 MHz, $CDCl_3$) δ 1.50 (m, 2H), 1.61 (m, 4H), 1.75 (m, 5H), 1.89 (m, 2H), 2.31 (m, 1H), 2.47 (s, 3H), 3.09 (m, 1H), 3.31 (s, 2H), 3.44 (br s, 3H), 3.54 (m, 1H), 3.79 (m, 2H), 3.96 (m, 2H), 4.44 (t, *J* = 5.1 Hz, 2H), 4.68 (m, 4H), 5.08 (m, 2H), 6.65 (d, *J* = 8.3 Hz, 1H), 7.36 (d, *J* = 8.3 Hz, 2H), 7.66 (s, 1H), 7.72 (d, *J* = 8.3 Hz, 2H), 7.80 (dd, *J* = 8.3 Hz, 1.7 Hz, 1H), 7.91 (d, *J* = 1.7 Hz, 1H); ^{13}C NMR (101 MHz, $CDCl_3$) δ 21.7, 24.0, 25.1, 25.5, 28.8, 35.9, 38.6, 49.0, 49.3, 50.3, 56.0, 59.0, 60.2, 64.6, 67.6, 73.1, 96.0, 105.6, 123.7, 124.0, 127.9, 128.6, 129.0, 130.1, 131.4, 132.1, 145.3, 145.5, 147.7, 156.2; ν_{max}/cm^{-1} 1674, 1612 (C=N), 1465, 1335 (-SO_2-N), 1152 (C-O-C), 1117, 1032 (O-C-O); HRMS (ES) *m/z* = 741.2740 $[M+H]^+$ found, $C_{35}H_{45}N_6O_8S_2$ needs 741.2740; $[\alpha_D]^{20}$ = -50.4 (c 0.004, $CDCl_3$); R_f = 0.16 (ethyl acetate).

(*S*)-*tert*-Butyl 2-((prop-2-ynyloxy)methyl)pyrrolidine-1-carboxylate **85**[57]



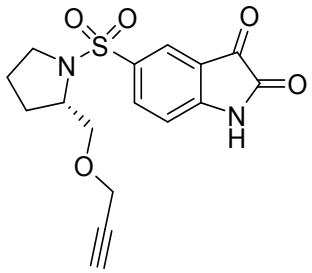
To a mixture of *N*-Boc-prolinol **66** (4.20 g, 20.90 mmol) and NaH (60 % in mineral oil, 4.18 g, 104.50 mmol) in anhydrous THF (100 mL) at 0 ^{o}C, was added propargyl bromide **74** (80 % in toluene, 23.29 mL, 326.60 mmol) and the mixture was stirred at room temperature for 18 hours. The mixture was then poured into 1M NaOH solution (50 mL) and extracted with DCM (100 mL). The organic layer was washed with water (100 mL) and brine (50 mL), dried over $MgSO_4$ and concentrated *in vacuo*. The crude product was purified by flash column chromatography, eluting with 1:19 – 1:4 ethyl acetate/ petroleum ether to give the alkyne **85** as a pale yellow oil (3.42 g, 65 % yield): ^{1}H NMR (400 MHz, $CDCl_3$) δ 1.47 (s, 9H), 1.86 (m, 4H), 2.43 (s, 1H), 3.35 (m, 3H), 3.66 (dd, *J* = 9.0 Hz, 3.4 Hz, 1H), 3.94 (m, 1H), 4.16 (s, 2H); ^{13}C NMR (101 MHz, $CDCl_3$) δ 22.9, 23.8, 28.5, 46.4, 56.3, 58.4, 70.8, 74.3, 79.4, 79.9, 154.7; HRMS (ES) *m/z* = 262.1419 $[M+Na]^+$ found, $C_{13}H_{21}NNaO_3$ needs 262.1419; R_f = 0.29 (1:4 ethyl acetate/ petroleum ether).

(*S*)-2-((Prop-2-ynyloxy)methyl)pyrrolidine hydrochloride **86**



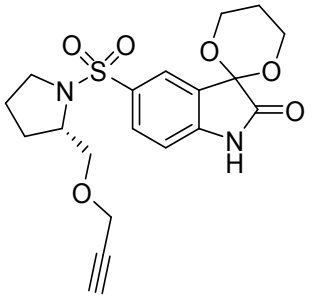
A solution of the Boc-protected alkyne **85** (3.42 g, 13.56 mmol) in 4M HCl in dioxane (34 mL, 135.60 mmol) and DCM (30 mL) was stirred at room temperature for 12 hours. The mixture was subsequently concentrated *in vacuo* to give the HCl salt of the deprotected amine **86** as a colourless solid (2.26 g, 97 % yield): ^{1}H NMR (400 MHz, $CDCl_3$) δ 1.89 (m, 1H), 2.13 (m, 3H), 2.49 (s, 1H), 3.42 (br s, 2H), 3.92 (m, 3H), 4.35 (br s, 2H), 9.24 (s, 1H), 10.13 (s, 1H); ^{13}C NMR (101 MHz, $CDCl_3$) δ 24.2, 27.2, 45.8, 58.5, 58.7, 68.3, 75.3, 79.0; ν_{max}/cm^{-1} 3230 (C≡C), 3162, 2907 - 2737 (-NH_2^+), 2503, 2441, 2106 (C≡C), 1605, 1397, 1355, 1096; HRMS (ES) *m/z* = 140.1075 $[M+H]^+$ found, $C_8H_{14}NO$ needs 140.1075.

(*S*)-5-(2-((Prop-2-ynyloxy)methyl)pyrrolidin-1-ylsulfonyl)indoline-2,3-dione **87**[57]



To a solution of the amine **86** (HCl salt, 3.28 g, 18.72 mmol) and Et_3N (8.29 mL, 59.57 mmol) in a 1:1 mixture of THF and DCM (300 mL) at 0 ^oC was added dropwise, a solution of 5-chlorosulfonylisatin **64** (4.17 g, 17.02 mmol) in THF (50 mL), maintaining the temperature at 0 ^oC. The mixture was allowed to warm to room temperature with further stirring for an hour. After concentration *in vacuo*, the crude product was purified by flash column chromatography, eluting with 1:1 ethyl acetate/ petroleum ether to give the sulfonamide **87** as an orange solid (5.07 g, 85.6 % yield); ^1H NMR (400 MHz, DMSO) δ 1.52 (m, 2H), 1.76 (m, 2H), 3.07 (m, 1H), 3.48 (m, 3H), 3.65 (m, 2H), 4.18 (m, 2H), 7.10 (d, *J* = 8.3 Hz, 1H), 7.79 (s, 1H), 8.04 (br d, *J* = 8.1 Hz, 1H), 11.47 (s, 1H); ^{13}C NMR (126 MHz, DMSO) δ 23.5, 28.3, 49.0, 57.8, 58.5, 71.7, 77.2, 80.2, 112.8, 118.1, 123.1, 130.8, 136.8, 153.6, 159.4, 183.0; HRMS (ES) *m/z* = 349.0843 $[M+H]^+$ found, $C_{16}H_{17}N_2O_5S$ needs 349.0843.

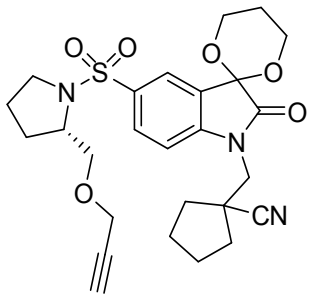
(*S*)-5'-(2-((Prop-2-ynyloxy)methyl)pyrrolidin-1-ylsulfonyl)spiro[[1,3]dioxane-2,3'-indolin]-2'-one **88**



A mixture of isatin sulfonamide **87** (4.87 g, 13.99 mmol), 1,3-propanediol (10.1 mL, 139.90 mmol) and p-toluenesulfonic acid (0.67 g, 3.50 mmol) in toluene (150 mL) was refluxed for 15 hours, collecting water with a Dean Stark trap. The mixture was subsequently allowed to cool to room temperature, washed with saturated aqueous Na_2CO_3 solution (70 mL), water (100 mL), and brine (100 mL), before drying over $MgSO_4$. Concentration *in vacuo* gave a crude product which was purified by flash column chromatography, eluting with 1:4 – 1:1 ethyl acetate/ petroleum ether to give the ketal-protected isatin sulfonamide **88** as a colourless foam (3.60 g, 64 % yield): ^1H NMR (400 MHz, $CDCl_3$) δ 1.67 (m, 1H), 1.92 (m, 3H), 2.48 (m, 2H), 3.09 (m, 1H), 3.50 (m, 2H), 3.77 (m, 3H), 4.01 (m, 2H), 4.20 (m, 2H),

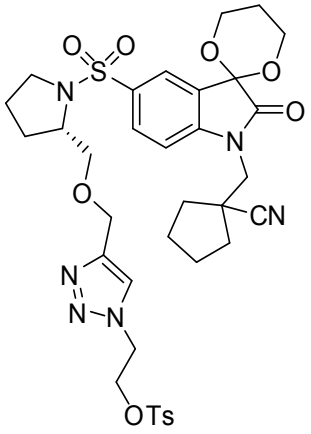
4.94 (m, 2H), 6.95 (d, *J* = 8.2 Hz, 1H), 7.82 (dd, *J* = 8.2 Hz, 1.9 Hz, 1H), 7.90 (d, *J* = 1.9 Hz, 1H), 8.31 (s, 1H); ^{13}C NMR (101 MHz, $CDCl_3$) δ 24.0, 25.2, 28.8, 49.3, 58.6, 58.9, 61.2, 72.5, 74.7, 79.6, 93.0, 110.1, 124.4, 128.7, 131.2, 132.1, 144.0, 173.0; HRMS (ES) *m/z* = 407.1272 $[M+H]^+$ found, $C_{19}H_{23}N_2O_6S$ needs 407.1271; R_f = 0.36 (1:1 ethyl acetate/ petroleum ether).

(*S*)-1-((2'-Oxo-5'-(2-((prop-2-ynyloxy)methyl)pyrrolidin-1-ylsulfonyl)spiro[[1,3]dioxane-2,3'-indoline]-1'-yl)methyl)cyclopentanecarbonitrile **89**



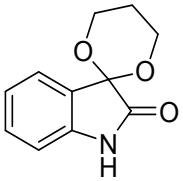
A mixture of isatin sulfonamide **88** (0.10 g, 0.25 mmol) and ^{t}BuOK (0.08 g, 0.75 mmol) in DMF (0.5 mL) was stirred under argon at room temperature for 30 minutes. 1-Chloromethylcarbonitrile **72** (0.11 g, 0.75 mmol) in DMF (0.5 mL) was added and stirring was continued at 140 ^{o}C for 2 days. After cooling to room temperature, the reaction mixture was concentrated *in vacuo* and purified by flash chromatography, eluting with 1:5 – 1:1 ethyl acetate/ petroleum ether to give the nitrile **89** as a colourless foam (0.076 g, 59 % yield); ^{1}H NMR (400 MHz, $CDCl_3$) δ 1.67 (m, 3H), 1.91 (m, 7H), 2.18 (m, 2H), 2.43 (m, 2H), 2.97 (m, 2H), 3.50 (m, 2H), 3.81 (m, 2H), 3.90 (s, 2H), 4.00 (m, 2H), 4.19 (d, *J* = 2.3 Hz, 2H), 4.91 (m, 2H), 7.24 (d, *J* = 8.3 Hz, 1H), 7.89 (m, 2H), 7.94; ^{13}C NMR (101 MHz, $CDCl_3$) δ 23.8, 24.0, 25.1, 28.8, 36.5, 43.9, 45.6, 49.3, 58.6, 58.9, 61.4, 66.8, 72.5, 74.7, 79.6, 92.7, 109.8, 124.1, 128.0, 131.1, 132.7, 146.0, 172.7; ν_{max}/cm^{-1} 3276 (C≡C), 2235 (C≡N), 1729 (C=O), 1615, 1441, 1340 (-SO_2-N), 1151, 1036; HRMS (ES) *m/z* = 514.2005 $[M+H]^+$ found, $C_{26}H_{32}N_3O_6S$ needs 514.2006; R_f = 0.55 (1:1 ethyl acetate/ petroleum ether).

(*S*)-2-(4-(((1-(1'-((1-Cyanocyclopentyl)methyl)-2'-oxospiro[[1,3]dioxane-2,3'-indoline]-5'-ylsulfonyl)pyrrolidin-2-yl)methoxy)methyl)-1*H*-1,2,3-triazol-1-yl)ethyl-4-methylbenzenesulfonate **91**



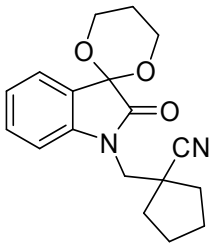
A mixture of $CuSO_4$ (0.036 g, 0.145 mmol), L-ascorbic acid (0.051 g, 0.29 mmol) and alkyne **89** (0.150 g, 0.29 mmol) in DMF (3 mL) was stirred at room temperature for 10 minutes, prior to the addition of a solution of tosylethylazide **36** (0.084 g, 0.35 mmol) in DMF (1.5 ml) with stirring for 1 hour. The reaction mixture was poured into 10 % aqueous NH_4Cl solution (15 mL) and extracted with DCM (3 x 15 mL). The combined organic extract was dried over $MgSO_4$ and concentrated *in vacuo*, followed by purification by flash column chromatography, eluting with 1:1 – 1:0 ethyl acetate/ petroleum ether to give the triazole **91** as a colourless foam (0.132 g, 50 % yield); ^{1}H NMR (400 MHz, $CDCl_3$) δ 1.66 (m, 3H), 1.90 (m, 8H), 2.16 (m, 2H), 2.45 (m, 4H), 3.08 (m, 1H), 3.43 (m, 1H), 3.53 (m, 1H), 3.78 (m, 2H), 3.90 (s, 2H), 4.00 (m, 2H), 4.42 (t, *J* = 5.2 Hz, 2H), 4.65 (m, 4H), 4.91 (m, 2H), 7.22 (d, *J* = 8.3 Hz, 1H), 7.34 (d, *J* = 8.3 Hz, 2H), 7.64 (s, 1H), 7.70 (d, *J* = 8.3 Hz, 2H), 7.86 (dd, *J* = 8.3 Hz, 1.9 Hz, 1H), 7.90 (d, *J* = 1.9 Hz, 1H); ^{13}C NMR (101 MHz, $CDCl_3$) δ 21.7, 23.8, 24.0, 25.1, 28.8, 36.5, 43.9, 45.5, 49.0, 49.3, 59.1, 61.3, 64.6, 67.6, 73.0, 92.7, 109.8, 123.8, 124.0, 124.0, 127.9, 128.0, 130.1, 131.1, 132.0, 132.7, 145.1, 145.5, 146.0, 172.7; HRMS (ES) *m/z* = 755.2533 $[M+H]^+$ found, $C_{35}H_{43}N_6O_9S_2$ needs 755.2533; R_f = 0.34 (ethyl acetate).

Spiro[[1,3]dioxane-2,3'-indolin]-2'-one **92**[209]



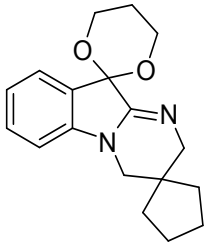
To a solution of isatin **61** (1.00 g, 6.80 mmol) and 1,3-propanediol (4.9 mL, 68 mmol) in toluene (40 mL) was added p-toluenesulfonic acid (0.32 g, 1.70 mmol) and the mixture was refluxed for 12 hours, collecting water with a Dean Stark trap. This was followed by cooling to room temperature, prior to washing with water (100 mL) and brine (100 mL). Subsequent drying over $MgSO_4$ and concentration *in vacuo* gave a crude residue which was purified by flash column chromatography, eluting with 1:9 – 1:1 ethyl acetate/ petroleum ether to give the corresponding ketal **92** as a colourless solid (0.70 g, 50 % yield): ^{1}H NMR (400 MHz, $CDCl_3$) δ 1.68 (m, 1H), 2.42 (m, 1H), 4.01 (m, 2H), 5.02 (m, 2H), 6.81 (d, *J* = 7.8 Hz, 1H), 7.10 (m, 1H), 7.31 (m, 1H), 7.45 (br m, 2H); ^{13}C NMR (101 MHz, $CDCl_3$) δ 25.3, 61.2, 93.6, 109.9, 123.3, 124.4, 127.8, 130.9, 139.9, 173.2; ν_{max}/cm^{-1} 3139 (N-H), 1705 (C=O), 1622, 1470, 1212 (O-C-O), 1024; HRMS (CI) *m/z* = 206.0817 $[M+H]^+$ found, $C_{11}H_{12}NO_3$ needs 206.0817.

1-((2'-Oxospiro[[1,3]dioxane-2,3'-indoline]-1'-yl)methyl)cyclopentanecarbonitrile **93**



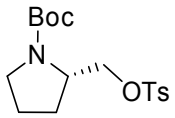
A mixture of ketal-protected isatin **92** (0.50 g, 2.44 mmol) and ^{t}BuOK (0.68 g, 6.10 mmol) in DMSO (7 mL) was stirred at room temperature for 1 hour. Then, carbonitrile **72** (0.70 g, 4.88 mmol) was added and stirring was continued at 130 ^{o}C for 12 hours. Additional carbonitrile reagent **72** was added to the mixture with further stirring at 140 ^{o}C for 24 hours. This was followed by cooling to room temperature, diluting with ethyl acetate (30 mL) and washing with water (50 mL) and brine (100 mL). The organic layer was dried over $MgSO_4$ and concentrated *in vacuo*. The crude residue was purified by flash column chromatography, eluting with 1:4 – 3:7 ethyl acetate/ petroleum ether to give the nitrile **93** as pale yellow foam (0.11 g, ~ 80% purity). The crude product was used in the next reaction step, to prepare the amidine **94** without further purification: HRMS (ES) *m/z* = 313.1545 $[M+H]^+$ found, $C_{18}H_{21}N_2O_3$ needs 313.1547.

Pyrimidoindole-1,3-dioxolane **94**



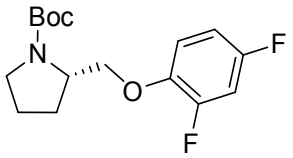
A solution of the crude nitrile **93** (0.10 g, 0.32 mmol) and a spatula of wet Raney Ni in 2M methalonic ammonia (5 mL) was hydrogenated in an autoclave at a pressure of ~130 psi for 12 hours. The mixture was filtered through Celite® with the resulting filtrate refluxed for 12 hours. This was followed by cooling to room temperature and concentration *in vacuo*. The residue was purified by flash column chromatography, eluting with 1:4 ethyl acetate/ petroleum ether to give the amidine **94** as colourless foam (0.025 g): ^{1}H NMR (400 MHz, $CDCl_3$) δ 1.65 (m, 4H), 1.76 (m, 5H), 2.25 (m, 1H), 3.38 (s, 2H), 3.42 (s, 2H), 4.02 (m, 2H), 5.08 (m, 2H), 6.60 (d, *J* = 7.8 Hz, 1H), 6.96 (t, *J* = 7.6 Hz, 1H), 7.29 (m, 1H), 7.51 (m, 1H); ^{13}C NMR (101 MHz, $CDCl_3$) δ 25.1, 25.6, 36.0, 38.6, 50.1, 56.0, 60.2, 96.9, 105.9, 120.8, 124.0, 127.8, 130.7, 144.2, 157.1; HRMS (ES) *m/z* = 299.1755 $[M+H]^+$ found, $C_{18}H_{23}N_2O_2$ needs 299.1754.

(*S*)-*tert*-Butyl 2-(tosyloxymethyl)pyrrolidine-1-carboxylate **105**[73]



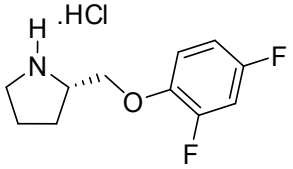
To a solution of N-Boc-prolinol **66** (6.20 g, 31.00 mmol) and pyridine (20 mL) in DCM (40 mL) at 0 ^{o}C, was added p-toluenesulfonyl chloride (7.44 g, 39.00 mmol) and the mixture was stirred at 0 ^{o}C for 15 minutes, and then at room temperature for 12 hours. This was followed by quenching with water (100 mL) and extracting with DCM (50 mL). The organic extract was washed with 10 % aqueous citric acid solution (100 mL), brine (50 mL), saturated aqueous $NaHCO_3$ solution (50 mL). Subsequent drying over $MgSO_4$ and concentration *in vacuo* gave a crude product which was purified by flash column chromatography, eluting with 1:9 – 1:4 ethyl acetate/ petroleum ether to give the tosylate **105** as a pale yellow oil (9.28 g, 84 % yield); ^{1}H NMR (400 MHz, $CDCl_3$) δ 1.40 (br d, *J* = 14 Hz, 9H), 1.90 (br m, 4H), 2.46 (s, 3H), 3.29 (m, 2H), 4.09 (br m, 3H), 7.35 (br m, 2H), 7.79 (d, *J* = 7.8 Hz, 2H); ^{13}C NMR (101 MHz, $CDCl_3$) δ 21.6, 22.8, 23.8, 28.4, 46.5, 55.6, 70.0, 79.9, 127.9, 129.9, 132.9, 144.8, 154.3; HRMS (ES) *m/z* = 378.1351 $[M+Na]^+$ found, $C_{17}H_{25}NNaO_5S$ needs 378.1351; R_f = 0.22 (1:4 ethyl acetate/ petroleum ether).

(*S*)-*tert*-Butyl 2-((2,4-difluorophenoxy)methyl)pyrrolidine-1-carboxylate **107**[57]



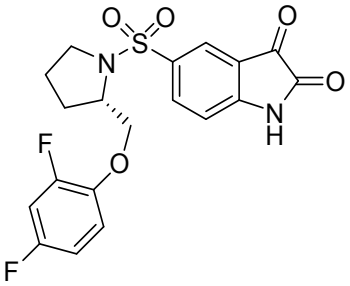
To a solution of 2,4-difluorophenol (3.22 g, 24.80 mmol) in anhydrous DMF (60 mL) was added NaH (60 % dispersion in mineral oil, 1.24 g, 31.00 mmol) and the mixture was stirred at room temperature for 30 minutes. This was followed by the addition of tosylate **105** (7.00 g, 20.60 mmol) and stirring was continued at 80 ^{o}C for 8 hours. After cooling to room temperature, the mixture was poured into 1M aqueous NaOH (100 mL) and extracted with DCM (2 x 60 mL). The combined organic extract was dried over $MgSO_4$ and concentrated *in vacuo*. Purification by flash column chromatography, eluting with 1:9 ethyl acetate/ petroleum ether gave the phenyl ether **107** as a colourless oil (4.00 g, 62 % yield); ^{1}H NMR (400 MHz, $CDCl_3$) δ 1.49 (s, 9H), 2.00 (br m, 4H), 3.41 (br s, 2H), 4.15 (br m, 3H), 6.79 (m, 1H), 6.89 (m, 1H), 7.01 (br s, 1H); ^{13}C NMR (126 MHz, $CDCl_3$) δ 22.8, 23.8, 28.5, 46.6 (d, *J* = 53.4 Hz), 55.9, 70.3 (d, *J* = 122.1 Hz), 79.6 (d, *J* = 44.7 Hz), 104.7 (m), 110.3 (dd, *J* = 3.3 Hz, 22.9 Hz), 115.8 (m), 143.5 (m), 154.5 (m), 155.7, 157.5 (m); HRMS (ES) *m/z* = 336.1387 $[M+Na]^+$ found, $C_{16}H_{21}F_2NNaO_3$ needs 336.1387; R_f = 0.17 (1:9 ethyl acetate/ petroleum ether).

(*S*)-2-((2,4-Difluorophenoxy)methyl)pyrrolidine hydrochloride **108**[57]



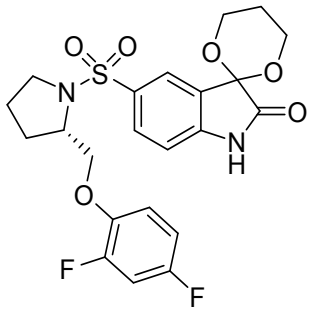
To a solution of Boc-protected amine **107** (3.70 g, 11.80 mmol) in DCM (50 mL), was added 4M HCl in dioxane (29.5 mL) and the mixture was stirred at room temperature for 18 hours. Subsequent concentration *in vacuo* gave the HCl salt of the amine **108** as a colourless solid (2.80 g, 95 % yield); ^{1}H NMR (400 MHz, $CDCl_3$) δ 2.05 (m, 2H), 2.21 (m, 2H), 3.45 (m, 2H), 4.06 (m, 1H), 4.35 (m, 2H), 6.81 (m, 2H), 7.24 (m, 1H), 9.73 (s, 1H), 10.30 (s, 1H); ^{13}C NMR (101 MHz, $CDCl_3$) δ 24.0, 27.2, 45.8, 58.1, 69.8, 104.9 (dd, *J* = 22.5 Hz, 27.7 Hz), 110.8 (dd, *J* = 3.5 Hz, 22.5 Hz), 118.6 (m), 142.2 (dd, *J* = 3.5 Hz, 10.4 Hz), 153.0 (dd, *J* = 12.1 Hz, 248.7 Hz), 157.7 (dd, *J* = 10.4 Hz, 244.5 Hz); ν_{max}/cm^{-1} 3026 – 2722 (N-H), 1509, 1453 (C-F), 1400, 1260 (C-O-C), 1209; HRMS (ES) *m/z* = 214.1043 $[M+H]^+$ found, $C_{11}H_{14}F_2NO$ needs 214.1043.

(*S*)-5-(2-((2,4-Difluorophenoxy)methyl)pyrrolidin-1-ylsulfonyl)indoline-2,3-dione **109**[57]



A solution of amine **108** (HCl salt, 0.10 g, 0.41 mmol) in DCM (2 mL) was slowly added to a solution of 5-chlorosulfonylisatin **64** (0.10 g, 0.41 mmol) and Et_3N (0.17 mL, 1.23 mmol) in THF (2 mL) at 0 ^oC. The mixture was stirred at 0 ^oC for 30 minutes and then at room temperature for 1 hour. Subsequent concentration *in vacuo* and purification by flash column chromatography, eluting with 1:1 ethyl acetate/ petroleum ether gave the sulfonamide **109** as an orange solid (0.12 g, 70 % yield); ^1H NMR (400 MHz, DMSO) δ 1.66 (m, 2H), 1.90 (m, 2H), 3.14 (m, 1H), 3.37 (m, 1H), 3.93 (m, 1H), 4.10 (m, 2H), 7.05 (m, 2H), 7.27 (m, 2H), 7.79 (d, *J* = 2.0 Hz, 1H), 8.05 (dd, *J* = 2.0 Hz, 8.3 Hz, 1H), 11.46 (s, 1H); ^{13}C NMR (126 MHz, DMSO) δ 23.6, 28.4, 49.2, 58.2, 71.4, 104.8 (dd, *J* = 22.9 Hz, 27.8 Hz), 110.8 (dd, *J* = 3.3 Hz, 22.3 Hz), 112.8, 115.6 (dd, *J* = 2.2 Hz, 9.3 Hz), 118.1, 123.1, 130.7, 136.8, 142.9 (dd, *J* = 2.7 Hz, 10.4 Hz), 151.0 (dd, *J* = 12.0 Hz, 246.9 Hz), 153.8, 155.6 (dd, *J* = 10.4 Hz, 239.8 Hz), 159.4, 182.9; ν_{max}/cm^{-1} 3263 (N-H), 1747 (C=O ketone), 1618 (C=O amide), 1510, 1470 (C-F), 1347 (-SO_2-N); HRMS (ES) *m/z* = 423.0821 $[M+H]^+$ found, $C_{19}H_{17}F_2N_2O_5S$ needs 423.0821; R_f = 0.45 (ethyl acetate).

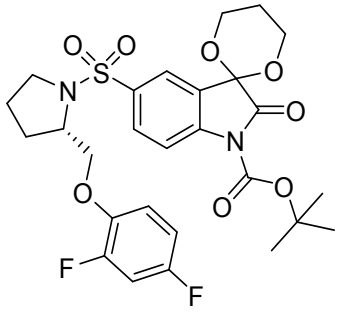
(*S*)-5'-(2-((2,4-Difluorophenoxy)methyl)pyrrolidin-1-ylsulfonyl)spiro[[1,3]dioxane-2,3'-indolin]-2'-one **118**[123]



To a solution of isatin sulfonamide **109** (1.12 g, 2.65 mmol) and 1,3-propanediol (3.05 mL, 42.3 mmol) in toluene (60 mL) was added p-toluenesulfonic acid (0.20 g, 1.05 mmol) and the mixture was refluxed for 18 hours, collecting water with a Dean Stark trap. After cooling to room temperature, saturated aqueous Na_2CO_3 solution (40 mL) was added, followed by washing with water (60 mL) and brine (60

mL). The organic extract was dried over $MgSO_4$ and concentrated *in vacuo*. Purification by flash column chromatography, eluting with 1:4 – 1:1 ethyl acetate/ petroleum ether gave the ketal protected isatin sulfonamide **118** as a colourless foam (1.00 g, 78 % yield); ^{1}H NMR (400 MHz, $CDCl_3$) δ 1.74 (m, 3H), 2.04 (m, 2H), 2.42 (m, 1H), 3.13 (m, 1H), 3.55 (m, 1H), 3.99 (m, 4H), 4.32 (m, 1H), 4.96 (m, 2H), 6.92 (m, 3H), 7.03 (td, *J* = 9.1 Hz, 5.3 Hz, 1H), 7.65 (s, 1H), 7.83 (dd, *J* = 8.2 Hz, 1.8 Hz, 1H), 7.92 (d, *J* = 1.8 Hz, 1H); ^{13}C NMR (126 MHz, $CDCl_3$) δ 24.0, 25.1, 28.9, 49.4, 58.3, 61.2, 71.9, 92.9, 104.9 (dd, *J* = 22.0 Hz, 26.9 Hz), 110.4, 110.6 (dd, *J* = 3.7 Hz, 22.4 Hz), 115.5 (m), 124.4, 128.7, 131.1, 131.9, 143.1 (dd, *J* = 3.2 Hz, 10.8 Hz), 144.0, 152.3 (dd, *J* = 12.0 Hz, 248.0 Hz), 156.5 (dd, *J* = 10.4 Hz, 241.0 Hz), 173.0; ν_{max}/cm^{-1} 3329 (N-H), 1771 (C=O), 1611, 1512, 1328, 1144, 1034; HRMS (ES) *m/z* = 481.1245 $[M+H]^+$ found, $C_{22}H_{23}F_2N_2O_6S$ needs 481.1245; R_f = 0.34 (1:1 ethyl acetate/ petroleum ether).

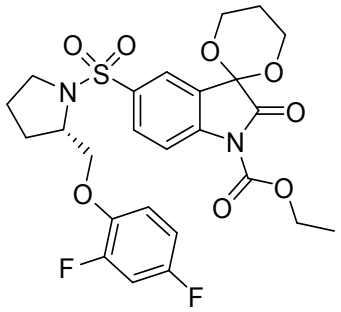
(*S*)-*tert*-Butyl-5'-(2-((2,4-difluorophenoxy)methyl)pyrrolidin-1-ylsulfonyl)-2'-oxospiro[[1,3]dioxane-2,3'-indoline]-1'-carboxylate **141**



Boc_2O (0.026 g, 0.12 mmol) was added to a solution of ketal-protected isatin sulfonamide **118** (0.050 g, 0.10 mmol) in DCM (1 mL) with stirring at room temperature. A TLC showed that no reaction had occurred after 6 hours. DMAP (0.002 g, 0.02 mmol) was added and stirring was continued at room temperature for 16 hours. The reaction mixture was then partitioned between DCM (5 mL) and water (5 mL) and the organic layer was dried over $MgSO_4$ and concentrated *in vacuo*. Subsequent purification by flash column chromatography, eluting with 1:9 – 1:1 ethyl acetate in petroleum ether, gave the carbamate **141** as a colourless foam (0.021 g, 34 % yield); ^{1}H NMR (400 MHz, $CDCl_3$) δ 1.68 (m, 12H), 2.03 (m, 2H), 2.43 (m, 1H), 3.15 (m, 1H), 3.56 (m, 1H), 4.00 (m, 4H), 4.32 (m, 1H), 4.92 (m, 2H), 6.86 (m, 2H), 7.02 (td, *J* = 9.1 Hz, 5.2 Hz, 1H), 7.90 (dd, *J* = 8.6 Hz, 2.0 Hz, 1H), 7.97 (d, *J* = 2.0 Hz, 1H), 8.00 (d, *J* = 8.6 Hz, 1H); ^{13}C NMR (101 MHz, $CDCl_3$) δ 24.0, 25.0, 28.1, 28.9, 49.5, 58.4, 61.5, 71.8, 85.5, 91.8, 104.9 (m), 110.4 (m), 115.5 (m), 115.6, 123.9, 127.7, 130.8, 133.6, 142.9, 143.2 (m), 148.7, 154.6 (m), 156.8 (m), 168.7; ν_{max}/cm^{-1} 3090 (O-^{t}Bu), 1775, (C=O amide), 1732 (C=O carbamate), 1615,

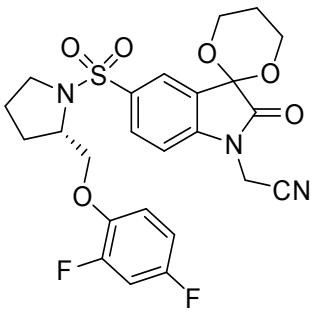
1514, 1476, 1337 (-SO_2-N), 1300, 1254, 1124; HRMS (ES) *m/z* = 581.1764 $[M+H]^+$ found, $C_{27}H_{31}F_2N_2O_8S$ needs 581.1764; R_f = 0.26 (1:4 ethyl acetate/ petroleum ether).

(*S*)-Ethyl-5'-(2-((2,4-difluorophenoxy)methyl)pyrrolidin-1-ylsulfonyl)-2'-oxospiro[[1,3]dioxane-2,3'-indoline]-1'-carboxylate, **142**



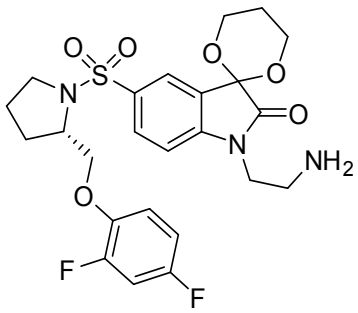
To a solution of ketal-protected isatin sulfonamide **118** (0.20 g, 0.42 mmol) in anhydrous THF (1.5 mL) was added NaH (60 % in mineral oil, 0.034 g, 0.84 mmol) and the mixture was stirred at room temperature for 10 minutes. Ethyl chloroformate (0.05 mL, 0.50 mmol) was added and stirring was continued at room temperature for 30 minutes. The reaction mixture was diluted with DCM (10 mL) and washed with water (5 mL) and brine (5 mL). The organic layer was dried over $MgSO_4$ and concentrated *in vacuo* to give the carbamate **142** as a colourless foam (0.22 g, 96 % yield); ^{1}H NMR (400 MHz, $CDCl_3$) δ 1.49 (t, *J* = 7.1 Hz, 3H), 1.74 (m, 3H), 2.04 (m, 2H), 2.43 (m, 1H), 3.15 (m, 1H), 3.55 (m, 1H), 3.99 (m, 4H), 4.31 (m, 1H), 4.51 (q, *J* = 7.1 Hz, 2H), 4.90 (m, 2H), 6.85 (m, 2H), 7.02 (td, *J* = 9.1 Hz, 5.2 Hz, 1H), 7.91 (dd, *J* = 8.6 Hz, 1.9 Hz, 1H), 7.97 (d, *J* = 1.9 Hz, 1H), 8.04 (d, *J* = 8.6 Hz, 1H); ^{13}C NMR (126 MHz, $CDCl_3$) δ 14.2, 24.0, 25.0, 28.9, 49.4, 58.4, 61.5, 64.1, 71.8, 91.9, 104.9 (dd, *J* = 21.8 Hz, 24.0 Hz), 110.5 (dd, *J* = 3.3 Hz, 21.8 Hz), 115.5 (dd, *J* = 2.2 Hz, 9.8 Hz), 115.7, 124.0, 127.8, 130.9, 134.1, 142.5, 143.1 (dd, *J* = 3.3 Hz, 10.9 Hz), 150.4, 152.3 (dd, *J* = 13.1 Hz, 249.6 Hz), 156.6 (dd, *J* = 10.9 Hz, 242.0 Hz), 168.5; ν_{max}/cm^{-1} 1776 (C=O amide), 1743 (C=O carbamate), 1618, 1516, 1468, 1355 (-SO_2-N), 1292; HRMS (ES) *m/z* = 553.1451 $[M+H]^+$ found, $C_{25}H_{27}F_2N_2O_8S$ needs 553.1451; R_f = 0.42 (1:1 ethyl acetate/ petroleum ether).

(*S*)-2-(5'-(2-((2,4-Difluorophenoxy)methyl)pyrrolidin-1-ylsulfonyl)-2'-oxospiro[[1,3]dioxane-2,3'-indoline]-1'-yl)acetonitrile **144**



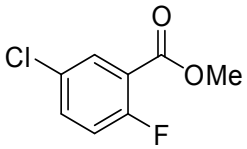
A mixture of ketal-protected isatin sulfonamide **118** (0.78 g, 1.63 mmol) and ^{t}BuOK (0.91 g, 8.15 mmol) in anhydrous THF (25 mL) was stirred at room temperature for 10 minutes. Bromoacetonitrile (0.34 mL, 4.90 mmol) was added and stirring was continued at room temperature for 4 hours. The reaction mixture was then partitioned between DCM (15 mL) and water (30 mL). The organic layer was washed with brine (20 mL), dried over $MgSO_4$ and concentrated *in vacuo*. Purification by flash column chromatography, eluting with 1:4 – 1:1 ethyl acetate/ petroleum ether gave the nitrile **144** as a colourless foam (0.60 g, 71 % yield); ^{1}H NMR (400 MHz, $CDCl_3$) δ 1.76 (m, 3H), 2.05 (m, 2H), 2.44 (m, 1H), 3.13 (m, 1H), 3.56 (m, 1H), 4.01 (m, 4H), 4.31 (m, 1H), 4.63 (m, 2H), 4.90 (m, 2H), 6.87 (m, 2H), 7.04 (m, 2H), 7.96 (m, 2H); ^{13}C NMR (101 MHz, $CDCl_3$) δ 24.0, 25.0, 27.2, 28.9, 49.5, 58.5, 61.6, 71.8, 93.0, 104.9 (m), 108.8, 110.4 (dd, *J* = 3.5 Hz, 22.5 Hz), 113.0, 115.6 (m), 124.4, 128.1, 131.4, 133.4, 143.1 (m), 143.5, 152.4 (dd, *J* = 12.1 Hz, 249.7 Hz), 156.7 (dd, *J* = 10.4 Hz, 241.0 Hz), 170.0; ν_{max}/cm^{-1} 1738 (C=O), 1617, 1512, 1334 (-SO_2-N), 1266, 1138; HRMS (ES) *m/z* = 520.1347 $[M+H]^+$ found, $C_{24}H_{24}F_2N_3O_6S$ needs 520.1348; R_f = 0.40 (1:1 ethyl acetate/ petroleum ether).

(*S*)-1'-(2-Aminoethyl)-5'-(2-((2,4-difluorophenoxy)methyl)pyrrolidin-1-ylsulfonyl)spiro[[1,3]dioxane-2,3'-indolin]-2'-one, **145**



A mixture of nitrile **144** (0.10 g, 0.19 mmol) and a spatula of wet Raney Ni in 0.25M methalonic ammonia (5 mL) was hydrogenated in an autoclave at a pressure of ~70 psi for 12 hours. The reaction was filtered through Celite® and the resulting filtrate was concentrated *in vacuo*. The crude product was purified by flash column chromatography, eluting with 0:1 – 1:4 MeOH/ ethyl acetate to give the primary amine **145** as a colourless foam (0.065 g, 65 % yield): ^{1}H NMR (400 MHz, $CDCl_3$) δ 1.74 (m, 4H), 2.60 (m, 2H), 2.42 (m, 1H), 3.05 (m, 3H), 3.53 (m, 1H), 3.75 (t, *J* = 6.4 Hz, 2H), 3.98 (m, 5H), 4.32 (m, 1H), 4.97 (m, 2H), 6.86 (m, 2H), 6.96 (d, *J* = 8.3 Hz, 1H), 7.04 (m, 1H), 7.86, (dd, *J* = 2.0 Hz, 8.3 Hz, 1H), 7.90 (br s, 1H); ^{13}C NMR (101 MHz, $CDCl_3$) δ 24.0, 25.2, 28.9, 39.7, 43.0, 49.4, 58.3, 61.3, 71.9, 92.9, 104.8 (dd, *J* = 22.5 Hz, 26.0 Hz), 108.7, 110.4 (dd, *J* = 3.5 Hz, 22.5 Hz), 115.6 (m), 124.0, 128.3, 131.3, 131.7, 143.1 (m), 146.6, 152.3 (dd, *J* = 12.1 Hz, 248.0 Hz), 156.5 (dd, *J* = 10.4 Hz, 241.0 Hz), 172.1; ν_{max}/cm^{-1} 3370 (N-H), 1725 (C=O), 1615, 1512 (C-N, amine), 1338 ($-SO_2-$N), 1297, 1146, 1027; HRMS (ES) *m/z* = 524.1660 $[M+H]^+$ found, $C_{24}H_{28}F_2N_3O_6S$ needs 524.1661; R_f = 0.10 (1:4 MeOH/ ethyl acetate).

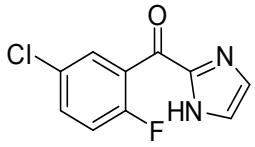
Methyl 5-chloro-2-fluorobenzoate **153**[210]



A solution of 2-fluoro-5-chlorobenzoic acid **152a** (1.52 g, 8.71 mmol) in MeOH (20 mL) and concentrated HCl (1 mL) was refluxed for 3.5 hours. The mixture was concentrated *in vacuo* and the resulting residue was dissolved in DCM (20 mL) and washed with water (2 x 15 mL). The organic extract was dried over $MgSO_4$ and concentrated *in vacuo* to give methyl 5-chloro-2-fluorobenzoate **153** as a colourless oil (1.46 g, 89 % yield): ^{1}H NMR (400 MHz, $CDCl_3$) δ 3.94 (s, 3H), 7.10 (dd, *J* = 8.8 Hz, 9.8 Hz, 1H), 7.47 (m, 1H), 7.91 (dd, *J* = 2.5 Hz, 5.9 Hz, 1H); ^{13}C NMR (101 MHz, $CDCl_3$) δ 52.6, 118.5

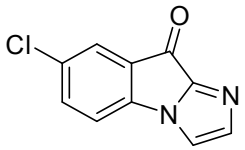
(d, *J* = 24.3 Hz), 119.9 (d, *J* = 10.4 Hz), 129.2 (m), 131.8, 134.3 (d, *J* = 8.7 Hz), 160.4 (d, *J* = 260.1 Hz), 163.7; HRMS (EI) *m/z* = 188.0040 $[M]^+$ found, $C_8H_6ClFO_2$ needs 188.0040; R_f = 0.60 (1:1 ethyl acetate/ petroleum ether).

(5-Chloro-2-fluorophenyl)(1*H*-imidazol-2-yl)methanone **156**



A solution of benzoic acid **152a** (2.30 g, 13.18 mmol) in thionyl chloride (10 mL) was refluxed for 2 hours. Excess thionyl chloride was azeotroped with toluene and removed *in vacuo* to give the corresponding acid chloride **154**, which was then dissolved in pyridine (0.50 mL). The resulting solution was added dropwise to a solution of imidazole **155** (0.45 g, 6.59 mmol) and Et_3N (1.83 mL, 13.18 mmol) in pyridine (1.5 mL) at 0 ^oC, before warming to room temperature and stirring for 3.5 hours. This was followed by the addition of aqueous NaOH (7.5N, 1.3 mL) and heating to reflux for 1 hour. The mixture was then diluted with water (6 mL) and allowed to cool to room temperature. The resulting precipitate was filtered and washed with water (20 mL) and diethyl ether (20 mL). The precipitate was further purified by flash column chromatography, eluting with 1:3 - 1:1 ethyl acetate/ petroleum ether to give 2-acylimidazole **156** as a colourless solid (0.96 g, 65 % yield): ^1H NMR (400 MHz, $CDCl_3$) δ 7.15 (m, 1H), 7.34 (br s, 1H), 7.40 (br s, 1H), 7.50 (m, 1H), 8.04 (dd, *J* = 2.9 Hz, 5.9 Hz, 1H), 10.46 (s, 1H); ^{13}C NMR (101 MHz, $CDCl_3$) δ 118.0 (d, *J* = 24.1 Hz), 120.9, 126.1 (d, *J* = 13.8 Hz), 129.2 (d, *J* = 4.3 Hz), 131.6 (br m), 132.5 (br m), 133.5 (d, *J* = 8.6 Hz), 144.6, 159.5 (d, *J* = 256.0 Hz), 179.7; ν_{max}/cm^{-1} 1659 (C=O), 1606, 1482, 1392, 1198, 792; HRMS (ES) *m/z* = 225.0224 $[M+H]^+$ found, $C_{10}H_7ClFN_2O$ needs 225.0225; R_f = 0.45 (1:1 ethyl acetate/ petroleum ether).

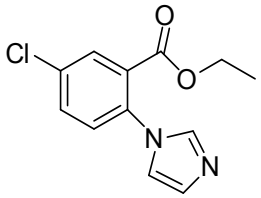
7-Chloro-9*H*-imidazo[1,2-a]indol-9-one **157**



A mixture of 2-acylimidazole **156** (0.56 g, 2.50 mmol) and K_2CO_3 (1.03 g, 7.46 mmol) in DMF (5 mL) was stirred at 140 ^oC for 2.5 hours. After cooling to room temperature, the mixture was diluted with ethyl acetate (10 mL) and washed with water (2 x 10 mL) and brine (3 x 20 mL). The organic extract was dried over $MgSO_4$ and concentrated *in vacuo*. Then, the crude residue was purified by flash

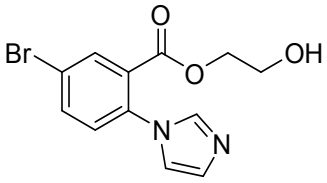
column chromatography, eluting with 1:3 – 1:1 ethyl acetate/ petroleum ether to give imidazoleindolone **157** as a yellow solid (0.33 g, 65 % yield): ^{1}H NMR (400 MHz, $CDCl_3$) δ 7.11 (d, *J* = 8.3 Hz, 1H), 7.24 (br m, 1H), 7.43 (br m, 1H), 7.50 (dd, *J* = 2.0 Hz, 8.3 Hz, 1H), 7.61 (d, *J* = 2.0 Hz, 1H); ^{13}C NMR (101 MHz, $CDCl_3$) δ 112.6, 112.6, 115.3, 125.8, 129.7, 133.1, 134.8, 137.9, 139.6, 176.2; ν_{max}/cm^{-1} 3135, 1702 (C=O), 1613, 1476 (C=N), 1428, 1390, 1262, 1180, 828; HRMS (ES) *m/z* = 205.0169 $[M+H]^+$ found, $C_{10}H_6ClN_2O$ needs 205.0169; R_f = 0.20 (1:1 ethyl acetate/ petroleum ether).

Ethyl 5-chloro-2-(1*H*-imidazol-1-yl)benzoate **175**



To a solution of imidazoleindolone **157** (0.05 g, 0.245 mmol) in EtOH (1.00 mL) was added a solution of Na_2SO_3 (0.04 g, 0.32 mmol) in water (0.2 mL) and the mixture was refluxed for 2.5 hours. Ethanol was removed by concentration *in vacuo*, followed by partitioning between water (3 mL) and DCM (5 mL). The organic extract was dried over $MgSO_4$ and concentrated *in vacuo* to give a colourless product, **175** (0.045 g, 73 % yield): ^{1}H NMR (400 MHz, $CDCl_3$) δ 1.16 (t, *J* = 7.1 Hz, 3H), 4.18 (q, *J* = 7.1 Hz, 2H), 7.06 (s, 1H), 7.18 (s, 1H), 7.32 (d, *J* = 8.4 Hz, 1H), 7.60 (m, 2H), 7.94 (d, *J* = 2.4 Hz, 1H); ^{13}C NMR (101 MHz, $CDCl_3$) δ 13.8, 62.2, 120.9, 128.9, 129.4, 129.8, 131.2, 132.6, 134.9, 135.0, 137.6, 164.5; HRMS (ES) *m/z* = 251.0585 $[M+H]^+$ found $C_{12}H_{12}ClN_2O_2$ needs 251.0582.

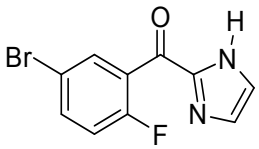
2-Hydroxyethyl 5-bromo-2-(1*H*-imidazol-1-yl)benzoate **178**



A mixture of imidazoleindolone **58** (0.05 g, 0.20 mmol), ethylene glycol (0.11 mL, 2.00 mmol) and p-toluenesulfonic acid (0.01 g, 0.05 mmol) in toluene (1.00 mL) was refluxed for 12 hours. After cooling to room temperature, the reaction mixture was diluted with ethyl acetate (3 mL) and washed with water (5 mL). The organic extract was dried over $MgSO_4$ and concentrated *in vacuo*. Purification by flash column chromatography, eluting with 1:1 – 1:0 ethyl acetate/ petroleum ether gave the hydroxyl benzoate **178** as a colourless solid (0.028 g, 45 % yield): ^{1}H NMR (400 MHz, $CDCl_3$) δ 3.65 (m 2H), 3.76 (s, 1H), 4.24 (m, 2H), 7.12 (s, 1H), 7.22 (s, 1H), 7.29 (m, 1H), 7.66 (s, 1H), 7.79 (dd, *J* = 8.4 Hz,

2.2 Hz, 1H), 8.21 (d, *J* = 2.2 Hz, 1H); ^{13}C NMR (101 MHz, $CDCl_3$) δ 60.2, 67.9, 121.2, 123.1, 129.3, 129.5, 129.6, 134.8, 135.4, 136.1, 138.4, 164.4; ν_{max}/cm^{-1} 3500 (O-H), 1721 (C=O), 1499 (C=N), 1246 (C-O ester); HRMS (ES) *m/z* = 311.0031 $[M+H]^+$ found, $C_{12}H_{12}BrN_2O_3$ needs 311.0031.

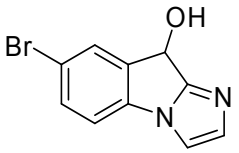
(5-Bromo-2-fluorophenyl)(1*H*-imidazol-2-yl)methanone **180**



To a solution of 1-trityl imidazole **190** (2.66 g, 8.58 mmol) in THF (75 mL) at -78 °C was added ^{n}BuLi (1.6 M in hexane, 5.90 mL, 9.44 mmol) and the mixture was stirred for 15 minutes. A precooled solution of the ester **193** (2.00 g, 8.58 mmol) in THF (5 mL) at -78 °C was added and stirring was continued for 30 minutes before warming to room temperature. The reaction mixture was then washed with water (30 mL) and brine (20 mL), dried over $MgSO_4$ and concentrated *in vacuo*. The crude mixture was recrystallised from ethyl acetate/petroleum ether mixture to give the trityl-protected ketone **195** as a colourless solid (3.12 g, 71 % yield).

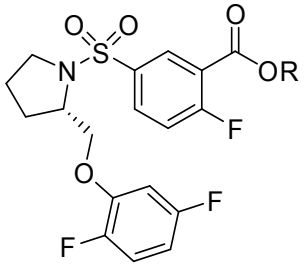
The resulting N-trityl ketone **195** (3.12 g, 6.10 mmol) was dissolved in a mixture of 1,4-dioxane (35 mL) and 10 % aqueous HCl (15 mL) and allowed to stir at 70 °C for 18 hours. After cooling to room temperature, the reaction mixture was made basic with saturated aqueous $NaHCO_3$ solution (pH ~ 8), re-acidified with solid citric acid (pH ~5) and extracted with ethyl acetate (3 x 60 mL). The combined organic extract was dried over $MgSO_4$ and concentrated *in vacuo*. Recrystallisation from ethyl acetate/petroleum ether mixture gave the deprotected ketone **180** as a colourless solid (1.40 g, 85 % yield): ^{1}H NMR (400 MHz, $CDCl_3$) δ 7.12 (t, *J* = 9.8 Hz, 1H), 7.36 (s, 1H), 7.43 (s, 1H), 7.67 (m, 1H), 8.20 (dd, *J* = 2.4 Hz, 5.9 Hz, 1H), 10.70 (s, 1H); ^{13}C NMR (101 MHz, $CDCl_3$) δ 116.4 (d, *J* = 3.4 Hz), 118.4 (d, *J* = 23.3 Hz), 121.1 (br s), 126.5 (d, *J* = 12.9 Hz), 132.5 (br s), 134.5, 136.4 (d, *J* = 7.8 Hz), 144.6, 160.0 (d, *J* = 256.9 Hz), 179.6; ν_{max}/cm^{-1} 3015 (N-H), 1649 (C=O), 1601 (C=N), 1476, 1395, 1196, 1129; HRMS (ES) *m/z* = 268.9726 $[M+H]^+$ found, $C_{10}H_7BrFN_2O$ needs 268.9726.

7-Bromo-9*H*-imidazo[1,2-a]indol-9-ol **182**



To a solution of imidazoleindolone **58** (0.030 g, 0.12 mmol) in MeOH (0.5 mL) and 3 drops of water, was added $NaBH_4$ (0.002 g, 0.06 mmol), with stirring at room temperature for 1 hour. The mixture was subsequently concentrated *in vacuo* to give the alcohol **182** as a colourless solid (0.028 g, 92 % yield): ^{1}H NMR (400 MHz, DMSO) δ 5.57 (s, 1H), 6.34 (s, 1H), 7.14 (s, 1H), 7.53 (d, *J* = 8.2 Hz, 1H), 7.67 (m, 2H), 7.75 (m, 1H); ^{13}C NMR (126 MHz, DMSO) δ 65.0, 112.3, 113.2, 117.0, 129.1, 132.1, 133.1, 136.8, 140.8, 154.7; HRMS (ES) *m/z* = 250.9820 $[M+H]^+$ found, $C_{10}H_8BrN_2O$ needs 250.9820.

(*S*)-Methyl 5-(2-((2,5-difluorophenoxy)methyl)pyrrolidin-1-ylsulfonyl)-2-fluorobenzoate **187a** and (*S*)-5-(2-((2,5-Difluorophenoxy)methyl)pyrrolidin-1-ylsulfonyl)-2-fluorobenzoic acid **187b**



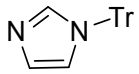
Part 1: To a solution of methyl 2-fluorobenzoate **185** (0.38 mL, 3.00 mmol) in DCM (5 mL) was added chlorosulfonic acid (1.20 mL, 18.00 mmol), followed by stirring at 70 ^{o}C for 12 hours. The reaction mixture was cooled to 0 ^{o}C, slowly diluted with ice cold water (20 mL) and extracted with DCM (2 x 10 mL). The organic extract was dried over $MgSO_4$ and concentrated *in vacuo* to give a mixture of the ester and carboxylic acid sulfonyl chloride derivatives **186a/b** as a colourless solid. The mixture of acid and ester products **186a/b** was used in the next step without further purification.

Part 2: To a solution of amine **108** (HCl salt, 1.14 g, 4.58 mmol) and Et_3N (2.02 mL, 14.53 mmol) in DCM (40 mL) at 0 ^{o}C, was slowly added, a solution of the sulfonyl chloride mixture **186a/b** (1.00 g, 4.10 mmol) in DCM (5 mL). The resulting solution was stirred at room temperature for 1 hour, before washing with water (50 mL), drying over $MgSO_4$ and concentrating *in vacuo*. The residue was purified by flash column chromatography, eluting with 1:3 – 1:0 ethyl acetate/ petroleum ether and then with 0:1 – 1:49 acetic acid/ ethyl acetate to give the ester **187a** as a colourless solid (0.41 g, 95% yield) and the carboxylic acid **187b** as a colourless solid (1.23 g, 95% yield).

Ester **187a**: ^{1}H NMR (400 MHz, $CDCl_3$) δ 1.75 (m, 2H), 2.06 (m, 2H), 3.17 (m, 1H), 3.54 (m, 1H), 3.96 (s, 3H), 4.00 (m, 2H), 4.24 (m, 1H), 6.83 (m, 2H), 6.97 (m, 1H), 7.29 (m, 1H), 8.00 (m, 1H), 8.42 (dd, *J* = 2.45 Hz, 6.36 Hz, 1H); ^{13}C NMR (126 MHz, $CDCl_3$) δ 24.1, 28.9, 49.5, 52.8, 58.6, 71.6, 104.9 (dd, *J* = 21.8 Hz, 26.2 Hz), 110.5 (dd, *J* = 3.3 Hz, 21.8 Hz), 115.5 (m), 118.3 (d, *J* = 22.9 Hz), 119.7 (d, *J* = 10.9 Hz), 131.9 (br s), 133.5 (d, *J* = 9.8 Hz), 133.8 (d, *J* = 3.3 Hz), 143.0 (dd, *J* = 3.3 Hz, 10.9 Hz), 152.3 (dd, *J* = 12.0 Hz, 249.6 Hz), 156.6 (dd, *J* = 10.9 Hz, 243.1 Hz), 163.1 (d, *J* = 4.4 Hz), 164.2 (d, *J* = 268.1 Hz); ν_{max}/cm^{-1} 2959, 1728 (C=O), 1608, 1514, 1343 (SO_2-N), 1258 (C-O), 1105, 839; HRMS (ES) *m/z* = 430.0936 $[M+H]^+$ found, $C_{19}H_{19}F_3NO_5S$ needs 430.0936; R_f = 0.23 (1:4 ethyl acetate/ petroleum ether).

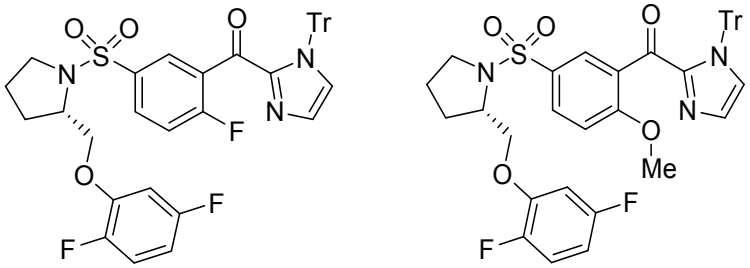
Acid **187b**: ^{1}H NMR (400 MHz, DMSO) δ 1.59 (m, 1H), 1.70 (m, 1H), 1.90 (m, 2H), 3.15 (m, 1H), 3.40 (m, 1H), 3.94 (m, 1H), 4.07 (m, 1H), 4.13 (m, 1H), 7.01 (m, 1H), 7.26 (m, 2H), 7.55 (dd, *J* = 8.8 Hz, 10.3 Hz, 1H), 8.12 (m, 1H), 8.23 (br m, 1H), 13.76 (br s, 1H); ^{13}C NMR (126 MHz, DMSO) δ 23.5, 28.3, 49.1, 58.3, 71.3, 104.7 (dd, *J* = 22.9 Hz, 27.2 Hz), 110.8 (dd, *J* = 3.3 Hz, 22.9Hz), 115.6 (br m), 118.7 (d, *J* = 24.0 Hz), 120.5 (br m), 131.2 (br s), 133.0 (d, *J* = 3.3 Hz), 133.3 (d, *J* = 10.9 Hz), 142.8 (dd, *J* = 3.3 Hz, 10.9 Hz), 151.2 (dd, *J* = 12.0 Hz, 246.3 Hz), 155.6 (dd, *J* = 10.9 Hz, 239.8 Hz), 163.2 (d, *J* = 263.8 Hz), 163.7 (br m); ν_{max}/cm^{-1} 3000 (O-H), 1706 (C=O), 1604, 1512, 1343, 1167, 837; HRMS (ES) *m/z* = 414.0623 $[M-H]^-$ found, $C_{18}H_{15}F_3NO_5S$ needs 414.0623; R_f = 0.56 (1:49 acetic acid/ ethyl acetate)

1-Trityl-1*H*-imidazole **190**[187]



To a solution of imidazole (1.00 g, 14.71 mmol) in DMF (30 mL) at 0 °C was added NaH (60 % in mineral oil, 0.71 g, 17.65 mmol), with stirring at 0 °C for 15 minutes. Trityl chloride (5.33 g, 19.12 mmol) was subsequently added, followed by warming to room temperature and continued stirring for 15 hours. The reaction mixture was diluted with ethyl acetate (100 mL), and washed with water (100 mL) and brine (3x 100 mL). The organic extract was dried over $MgSO_4$, concentrated *in vacuo* and purified by flash column chromatography, eluting with 1:4 – 1:0 ethyl acetate/ petroleum ether to give 1-trityl imidazole **190** as a colourless solid (3.65 g, 80 % yield): ^{1}H NMR (400 MHz, $CDCl_3$) δ 6.83 (s, 1H), 7.07 (s, 1H), 7.14 (m, 6H), 7.33 (m, 9H), 7.46 (s, 1H); ^{13}C NMR (126 MHz, DMSO) δ 75.2, 121.7, 128.0, 128.0, 128.3, 129.8, 139.0, 142.5; HRMS (ES) *m/z* = 311.1548 $[M+H]^+$ found, $C_{22}H_{19}N_2$ needs 311.1548; R_f = 0.22 (1:1 ethyl acetate/ petroleum ether).

(*S*)-(5-(2-((2,5-Difluorophenoxy)methyl)pyrrolidin-1-ylsulfonyl)-2-fluorophenyl)(1-trityl-1*H*-imidazol-2-yl)methanone **191** and (*S*)-(5-(2-((2,5-Difluorophenoxy)methyl)pyrrolidin-1-ylsulfonyl)-2-methoxyphenyl)(1-trityl-1*H*-imidazol-2-yl)methanone **192**



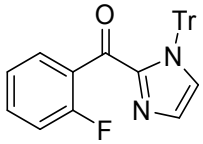
To a solution of N-trityl-imidazole **190** (1.00 g, 3.23 mmol) in THF (30 mL) at -78 ^{o}C was added ^{n}BuLi (2.06 M in hexane, 1.88 mL, 3.88 mmol). After stirring for 10 minutes, a solution of the ester **187a** (1.38 g, 3.22 mmol) in THF (5 mL) was added and stirring was continued at -78 ^{o}C for 15 minutes, before allowing to warm to room temperature. The mixture was then diluted with ethyl acetate (20 mL) and washed with water (30 mL) and brine (10 mL). This was followed by drying over $MgSO_4$ and concentration *in vacuo*. The crude material was purified by flash column chromatography, eluting with 1:4 – 2:3 ethyl acetate/ petroleum ether to give the ketone **191** as a colourless foam (0.46 g, 20 % yield) and the ketone **192** also as a colourless foam (1.25 g, 54 % yield, ~90% pure).

Ketone **191**: ^{1}H NMR (400 MHz, $CDCl_3$) δ 1.72 (m, 2H), 1.97 (m, 2H), 3.08 (m, 1H), 3.52 (m, 1H), 3.95 (m, 2H), 4.27 (m, 1H), 6.84 (m, 2H), 6.98 (m, 1H), 7.19 (m, 9H), 7.34 (m, 9H), 7.82 (m, 1H), 7.88 (m, 1H); ^{13}C NMR (126 MHz, $CDCl_3$) δ 24.0, 28.9, 49.5, 58.6, 71.7, 82.0, 104.8 (dd, *J* = 22.1 Hz, 26.6 Hz), 110.5 (dd, *J* = 3.8 Hz, 22.5 Hz), 115.5 (d, *J* = 9.6 Hz), 117.6 (d, *J* = 23.0 Hz), 121.3, 125.6 (d, *J* = 12.9 Hz), 127.3, 127.9, 128.6, 132.4 (m), 132.6, 132.8 (d, *J* = 10.0 Hz), 133.2 (m), 143.1 (m), 144.5, 146.8, 152.3 (dd, *J* = 11.9 Hz, 249 Hz), 156.5 (dd, *J* = 10.3 H, 231.7 Hz), 163.3 (d, *J* = 265.3 Hz), 179.0; HRMS (ES) *m/z* = 730.1979 $[M+Na]^+$ found, $C_{40}H_{32}F_3N_3NaO_4S$ needs 730.1963; R_f = 0.28 (2:3 ethyl acetate/ petroleum ether).

Ketone **192**: HRMS (ES) *m/z* = 742.2156 $[M+Na]^+$ found, $C_{41}H_{35}F_2N_3O_5S$ needs 742.2158. For further characterisation, the trityl group was removed, following the procedure outlined below for the deprotection of ketone **191** to give **201**. For the deprotected derivative of ketone **192**: ^{1}H NMR (400 MHz, $CDCl_3$) δ 1.81 (m, 3H), 2.05 (m, 2H), 3.22 (m, 1H), 3.56 (m, 1H), 3.94 (s, 3H), 4.05 (m, 2H), 6.83 (m, 2H), 7.03 (m, 1H), 7.13 (d, *J* = 8.8 Hz, 1H), 7.31 (br s, 2H), 8.00 (dd, *J* = 8.8 Hz, 2.4 Hz, 1H), 8.31 (d, *J* = 2.4 Hz, 1H), 10.72 (s, 1H); ^{13}C NMR (101 MHz, $CDCl_3$) δ 24.0, 28.8, 49.5, 56.3, 58.4, 71.8, 104.7 (m),

108.9, 110.4 (dd, *J* = 22.4 Hz, 3.7 Hz), 111.9, 115.3 (m), 126.6, 128.3, 131.3, 132.3, 143.0 (dd, *J* = 236.7 Hz, 10.6 Hz), 144.9, 152.2 (dd, *J* = 236.7 Hz, 12.0 Hz), 156.4 (dd, *J* = 231.4 Hz), 161.4, 162.6, 182.1; ν_{max}/cm^{-1} 1655 (C=O), 1596, 1511 (C=N), 1411, 1260 (C-O-C), 1140; HRMS (ES) *m/z* = 478.1243 $[M+H]^+$ found, $C_{22}H_{22}F_2N_3O_5S$ needs 478.1243.

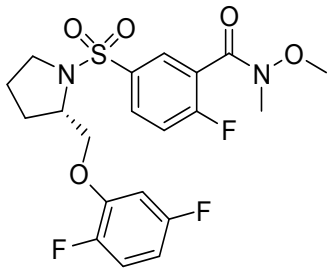
(2-Fluorophenyl)(1-trityl-1*H*-imidazol-2-yl)methanone **196**



To a solution of 1-trityl imidazole **190** (2.03 g, 6.55 mmol) in THF (150 mL) at -78 ^oC was added ^nBuLi (2.06 M in hexane, 3.50 mL, 7.21 mmol) with stirring for 15 minutes. A solution of the ester **185** (1.00 mL, 7.86 mmol) in THF (10 mL) was added dropwise, maintaining the temperature at -78 ^oC. Stirring was continued at -78 ^oC for 30 minutes before warming to room temperature. The mixture was washed with water (100 mL) and brine (50 mL), dried over $MgSO_4$ and concentrated *in vacuo*. Purification by flash column chromatography, eluting with 1:4 ethyl acetate/ petroleum ether gave the corresponding N-trityl protected ketone product **196** as a colourless foam (1.89 g, 67 % yield); ^1H NMR (400 MHz, $CDCl_3$) δ 7.01 (m, 1H), 7.11 (m, 1H), 7.18 (m, 1H), 7.28 (m, 16H), 7.40 (m, 2H); ^{13}C NMR (101 MHz, $CDCl_3$) δ 77.7, 116.0, 123.6 (m), 127.4, 127.6, 127.8, 127.8, 128.1, 130.0, 130.6 (m), 132.7 (d, *J* = 8.6 Hz), 142.5, 145.3, 160.0 (d, *J* = 252.6 Hz), 180.3.

The resulting N-trityl ketone **196** (1.50 g, 3.47 mmol) was dissolved in 1,4-dioxane (10 mL), treated with 10 % aqueous HCl solution (1 mL) and stirred at 70 ^oC for 4 hours. The mixture was then made basic with saturated aqueous $NaHCO_3$ solution (pH ~8), re-acidified with solid citric acid (pH ~5) and extracted with DCM (2 x 200 mL). The combined organic extract was dried over $MgSO_4$ and concentrated *in vacuo*. Purification by flash column chromatography, eluting with 1:4 – 1:1 ethyl acetate/ petroleum ether gave the deprotected ketone as a colourless solid (0.64 g, 97 % yield): ^1H NMR (400 MHz, $CDCl_3$) δ 7.22 (m, 1H), 7.33 (m, 2H), 7.42 (br s, 1H), 7.57 (m, 1H), 8.10 (td, *J* = 1.5 Hz, 7.3 Hz, 1H), 10.93 (s, 1H); ^{13}C NMR (101 MHz, $CDCl_3$) δ 116.5 (d, *J* = 21.4 Hz), 120.7, 123.9 (m), 125.0 (d, *J* = 11.8 Hz), 132.0 (br s), 132.3 (br s), 133.9 (d, *J* = 8.8 Hz), 145.0, 161.0 (d, *J* = 256.5 Hz), 181.3; ν_{max}/cm^{-1} 1653 (C=O), 1608 (C=N), 1452, 1394, 899; HRMS (ES) *m/z* = 191.0621 $[M+H]^+$ found, $C_{10}H_8FN_2O$ needs 191.0621.

(*S*)-5-(2-((2,5-Difluorophenoxy)methyl)pyrrolidin-1-ylsulfonyl)-2-fluoro-N-methoxy-N-methylbenzamide **197**

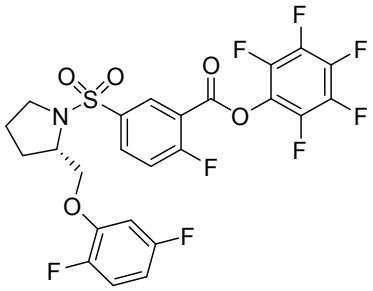


The acid chloride **188** was initially prepared by the treatment of 2-fluorobenzoic acid **187a** (0.15 g, 0.36 mmol) with thionyl chloride (2 mL) and refluxing for 3 hours. Subsequent concentration *in vacuo*, azeotroping with toluene gave the acid chloride **188**.

To a solution of the resulting acid chloride **188** in DCM (2 mL), was added N,O-dimethylhydroxylamine hydrochloride (0.033 g, 0.34 mmol) and the mixture was cooled to 0 ^{o}C. This was followed by the dropwise addition of pyridine (0.06 mL, 0.72 mmol), before warming to room temperature and stirring for a further 30 minutes. The reaction mixture was then diluted with DCM (10 mL) and washed with water (10 mL) and 10 % aqueous citric acid solution (3 x 20 mL). After drying over $MgSO_4$ and concentrating *in vacuo*, the resulting residue was purified by flash column chromatography, eluting with 1:9 – 1:1 ethyl acetate/ petroleum ether to give the Weinreb amide **197** as colourless oil (0.135 g, 82 % yield): ^{1}H NMR (400 MHz, $CDCl_3$) δ 1.76 (m, 2H), 2.06 (m, 2H), 2.39 (br s, 1H), 3.17 (m, 1H), 3.40 (br s, 3H), 3.54 (br m, 3H), 4.01 (m, 2H), 4.29 (m, 1H), 6.86 (m, 2H), 7.01 (m, 1H), 7.22 (m, 1H), 7.94 (m, 1H), 7.98 (m, 1H); ^{13}C NMR (101 MHz, $CDCl_3$) δ 21.5, 24.0, 28.9, 49.5, 58.6, 61.5, 71.8, 105.1 (dd, *J* = 22.4, 26.7 Hz), 110.6 (m), 115.6 (m), 116.8 (d, *J* = 22.4 Hz), 124.6 (d, *J* = 19.0 Hz), 125.3, 128.2, 129.0 (m), 130.9 (br m), 143.1 (m), 152.3 (dd, *J* = 11.2, 250.0 Hz), 156.5 (dd, *J* = 10.3, 241.4 Hz), 161.3 (d, *J* = 257.8 Hz); HRMS (ES) *m/z* = 459.1195 $[M+H]^+$ found, $C_{20}H_{22}F_3N_2O_5S$ needs 459.1196.

(*S*)-Perfluorophenyl 5-(2-((2,5-difluorophenoxy)methyl)pyrrolidin-1-ylsulfonyl)-2-fluorobenzoate

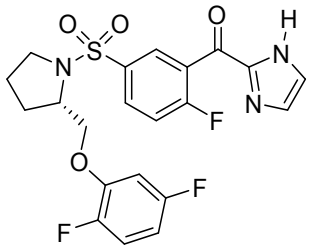
200



The acid chloride **188** was initially prepared by the treatment of 2-fluorobenzoic acid **187a** (0.12 g, 0.29 mmol) with thionyl chloride (2 mL) and refluxing for 3 hours. Subsequent concentration *in vacuo*, azeotroping with toluene gave the acid chloride **188**.

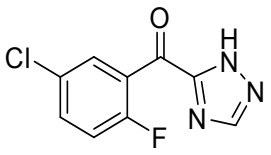
To a solution of the acid chloride **188** in DCM (2 mL) was added pentafluorophenol (0.053 g, 0.29 mmol) and pyridine (0.03 mL, 0.38 mmol), with stirring at room temperature for 1 hour. The reaction mixture was then diluted with DCM (10 mL), washed with water (10 mL) and dried over $MgSO_4$. After concentration *in vacuo*, the crude material was purified by flash column chromatography, eluting with 1:4 ethyl acetate/ petroleum ether to give the pentafluorophenyl ester **200** as pale yellow oil (0.115 g, 68 % yield): ^{1}H NMR (400 MHz, $CDCl_3$) δ 1.85 (m, 2H), 2.12 (m, 2H), 3.25 (m, 1H), 3.56 (m, 1H), 4.06 (m, 2H), 4.24 (m, 1H), 6.81 (m, 2H), 6.96 (m, 1H), 7.41 (t, *J* = 9.8 Hz, 1H), 8.17 (m, 1H), 8.61 (dd, *J* = 2.4 Hz, 6.4 Hz, 1H); ^{13}C NMR (101 MHz, $CDCl_3$) δ 24.2, 29.0, 49.5, 58.7, 71.4, 104.9 (dd, *J* = 21.7 Hz, 26.3 Hz), 110.5 (dd, *J* = 4.0 Hz, 22.5 Hz), 115.4 (m), 116.5 (d, *J* = 10.5 Hz), 118.8 (d, *J* = 23.1 Hz), 124.6 (m), 132.4, 135.0 (d, *J* = 3.7 Hz), 135.3 (d, *J* = 10.1 Hz), 138.0 (m), 139.9 (m), 141.2 (m), 142.9 (dd, *J* = 3.0 Hz, 11.1 Hz), 152.3 (dd, *J* = 10.1 Hz, 249.5 Hz), 156.7 (dd, *J* = 11.1 Hz, 243.4 Hz), 158.5 (m), 164.6 (d, *J* = 272. 7 Hz); ^{19}F NMR (471 MHZ, $CDCl_3$) δ -161.9, -157.0, -152.3, -130.1, -119.7, -99.1; ν_{max}/cm^{-1} 1756 (C=O), 1611, 1516 (C-F), 1351 (C-O ester); HRMS (ES) *m/z* = 582.0621 $[M+H]^+$ found, $C_{24}H_{16}F_8NO_5S$ needs 582.0621.

(*S*)-(5-(2-((2,5-Difluorophenoxy)methyl)pyrrolidin-1-ylsulfonyl)-2-fluorophenyl)(1*H*-imidazol-2-yl)methanone **201**



To a solution of N-trityl protected ketone **191** (0.22 g, 0.31 mmol) in 1,4-dioxane (1.0 mL) was added 10 % aqueous HCl (1 mL) and the solution was stirred at 70 ^{o}C for 2 hours. After cooling to room temperature, the reaction mixture was made basic with saturated aqueous $NaHCO_3$ solution (~pH 8), re-acidified with solid citric acid (pH ~5) and extracted with DCM (2 x 10 mL). The combined organic extract was dried over $MgSO_4$ and concentrated *in vacuo*. The crude mixture was recrystallised from ethyl acetate/ petroleum ether mixture to give the deprotected ketone **201** as a colourless solid (0.10 g, 70 % yield): ^{1}H NMR (400 MHz, $CDCl_3$) δ 1.92 (m, 2H), 2.10 (m, 2H), 3.25 (m, 1H), 3.60 (m, 1H), 4.03 (m, 1H), 4.11 (m, 1H), 4.33 (dd, *J* = 2.9 Hz, 9.3 Hz, 1H), 6.79 (m, 1H), 6.87 (m, 1H), 7.02 (m, 1H), 7.36 (m, 3H), 8.06 (m, 1H), 8.67 (dd, *J* = 2.4 Hz, 6.4 Hz, 1H), 10.57 (s, 1H); ^{13}C NMR (126 MHz, $CDCl_3$) δ 24.0, 28.9, 49.5, 58.6, 71.8, 104.8 (dd, *J* = 21.8 Hz, 26.2 Hz), 110.4 (dd, *J* = 4.4 Hz, 22.9 Hz), 115.5 (m), 117.6 (d, *J* = 22.9 Hz), 121.2, 125.5 (d, *J* = 13.1 Hz), 127.9, 132.4 (m), 132.9 (d, *J* = 10.9 Hz), 133.2 (br m), 143.0 (dd, *J* = 3.3 Hz, 10.9 Hz), 144.5, 152.6 (dd, *J* = 12.0 Hz, 248.5 Hz), 156.5 (dd, *J* = 9.8 Hz, 242.0 Hz) 163.5 (d, *J* = 266.0 Hz), 179.0; ν_{max}/cm^{-1} 3114 (N-H), 1668 (C=O), 1606 (C=N), 1514, 1394, 1260, 1211 (C-O), 1148; HRMS (ES) *m/z* = 466.1048 $[M+H]^+$ found, $C_{21}H_{19}F_3N_3O_4S$ needs 466.1048; R_f = 0.33 (1:1 ethyl acetate/ petroleum ether).

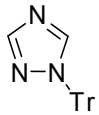
(5-Chloro-2-fluorophenyl)(1*H*-1,2,4-triazol-5-yl)methanone **203**



To a solution of N-trityl protected ketone **205** (1.00 g, 2.14 mmol) in 1,4-dioxane (20 mL) was added 10 % aqueous HCl (5 mL) and the resulting solution was stirred at 70 ^{o}C for 4 hours. After cooling to room temperature, the mixture was made basic with saturated aqueous $NaHCO_3$ solution (pH ~8), re-acidified with solid citric acid (pH 4) and extracted with ethyl acetate (3 x 20 mL). The combined organic extract was dried over $MgSO_4$ and concentrated *in vacuo*. The crude mixture was

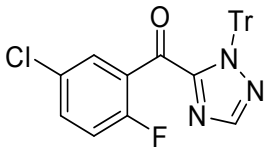
recrystallised from ethyl acetate/ petroleum ether mixture to give the product **203** as a colourless foam (0.35 g, 73 % yield): ^{1}H NMR (400 MHz, DMSO) δ 7.44 (t, *J* = 9.3 Hz, 1H), 7.73 (m, 1H), 7.87 (m, 1H), 8.75 (s, 1H), 14.91 (s, 1H); ^{13}C NMR (126 MHz, DMSO) δ 118.2 (d, *J* = 24.0 Hz), 127.7 (d, *J* = 15.6 Hz), 128.0 (d, *J* = 3.3 Hz), 130.5, 133.4 (d, *J* = 8.7 Hz), 146.3, 158.0 (d, *J* = 254.0 Hz), 158.3, 182.1; ν_{max}/cm^{-1} 1680 (C=O), 1489, 1431, 1240, 1197; HRMS (CI) *m/z* = 243.0449 $[M+NH_4]^+$ found, $C_9H_9ClFN_4O$needs 243.0449; R_f = 0.12 (1:1 ethyl acetate/ petroleum ether).

1-Trityl-1*H*-1,2,4-triazole **204**[211]



To a solution of 1,2,4-triazole (1.00 g, 14.49 mmol) and trityl chloride (5.66 g, 20.29 mmol) in THF (50 mL) was added DBU (2.6 mL, 17.39 mmol) and the mixture was stirred at room temperature for 5 hours. The resulting suspension was dissolved in DCM (80 mL) and washed with water (100 mL) and brine (50 mL). The organic extract was subsequently dried over $MgSO_4$ and concentrated *in vacuo*. Purification of the resulting residue by flash column chromatography, eluting with 1:4 – 1:1 ethyl acetate/ petroleum ether gave N-trityl triazole **204** as a colourless solid (3.17 g, 91 % yield): ^{1}H NMR (400 MHz, $CDCl_3$) δ 7.15 (m 6H), 7.35 (m, 9H), 8.03 (s, 1H), 8.08 (s, 1H); ^{13}C NMR (101 MHz, $CDCl_3$) δ 78.1, 128.0, 128.3, 129.9, 141.9, 145.7, 151.8; HRMS (CI) *m/z* = 311.1422 $[M]^+$ found, $C_{21}H_{17}N_3$ needs 311.1422; R_f = 0.10 (1:4 ethyl acetate/ petroleum ether).

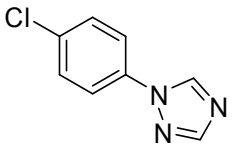
(5-Chloro-2-fluorophenyl)(1-trityl-1*H*-1,2,4-triazol-5-yl)methanone **205**



To a solution of 1-trityl triazole **204** (1.50 g, 4.82 mmol) in THF (50 mL) at -78 ^{o}C was added ^{n}BuLi (2.08 M in hexane, 3.00 mL, 6.27 mmol) and the mixture was stirred for 15 minutes. A solution of the ester **153** (1.09 g, 5.78 mmol) in THF (5 mL) was added and stirring was continued at -78 ^{o}C for 30 minutes. After warming to room temperature, the reaction mixture was washed with water (30 mL) and brine (15 mL), dried over $MgSO_4$ and concentrated *in vacuo*. The residue was recrystallised from ethyl acetate/ petroleum ether mixture to give the N-trityl ketone **205** as a colourless solid (1.40 g, 62 % yield): ^{1}H NMR (400 MHz, $CDCl_3$) δ 7.03 (m, 1H), 7.23 (m, 6H), 7.29 (m, 9H). 7.48 (m, 2H), 8.05

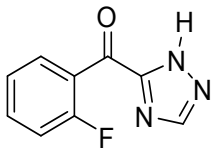
(s, 1H); ^{13}C NMR (101 MHz, $CDCl_3$) δ 80.4, 118.0 (d, *J* = 25.0 Hz), 125.6 (d, *J* = 12.1 Hz), 127.7, 128.1, 129.7 (d, *J* = 2.6 Hz), 130.5, 130.7, 135.0 (d, *J* = 8.6 Hz), 141.7, 149.1, 152.6, 159.8 (d, *J* = 258.6 Hz), 179.1; ν_{max}/cm^{-1} 1673 (C=O), 1600, 1479, 1443, 1256, 1224, 748; HRMS (CI) *m/z* = 467.1201 $[M]^+$ found, $C_{28}H_{19}ClFN_3O$ needs 467.1201; R_f = 0.30 (1:4 ethyl acetate/ petroleum ether).

1-(4-Chlorophenyl)-1*H*-1,2,4-triazole **207**



A mixture of phenyl-triazole ketone **203** (0.03 g, 0.13 mmol) and K_2CO_3 (0.03 g, 0.22 mmol) in DMF (2 mL) was irradiated in a microwave at 180 °C for 20 minutes. After cooling to room temperature, the mixture was diluted with ethyl acetate (5 mL) and, washed with water (2 x 5 mL) and brine (3 x 5 mL). The organic extract was dried over $MgSO_4$ and concentrated *in vacuo*. Purification of the residue by flash column chromatography, eluting with 1:1 – 7:3 ethyl acetate/ petroleum ether gave the 1-phenyl triazole **207** as a colourless solid (0.016 g, 68 % yield): ^{1}H NMR (400 MHz, $CDCl_3$) δ 7.52 (m, 2H), 7.67 (m, 2H), 8.14 (s, 1H), 8.57 (s, 1H); ^{13}C NMR (101 MHz, $CDCl_3$) δ 121.3, 130.0, 134.0, 135.5, 140.8, 152.8; ν_{max}/cm^{-1} 3130, 1512, 1274, 1154, 1094, 823; MS (CI) *m/z* = 180 $[M+H]^+$.

(2-Fluorophenyl)(1*H*-1,2,4-triazol-5-yl)methanone **208**

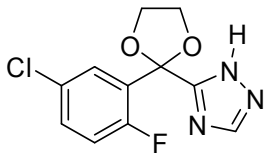


To a solution of 1-trityl triazole **204** (5.00 g, 16.08 mmol) in THF (100 mL) at -78 °C was added ^{n}BuLi (2.06 M in hexane, 8.58 mL, 17.68 mmol) and the mixture was stirred for 15 minutes. This was followed by the dropwise addition of a solution of the ester **185** (2.46 ml, 19.29 mmol) in THF (10 mL), maintaining the temperature below -70 °C. Stirring was continued at -78 °C for 30 minutes before warming to room temperature. The mixture was subsequently washed with water (30 mL) and brine (20 mL), dried over $MgSO_4$ and concentrated *in vacuo*. Purification by flash column chromatography, eluting with 1:5 – 1:1 ethyl acetate/ petroleum ether gave the corresponding N-trityl protected ketone as a colourless solid (5.20 g, 75 % yield): ^{1}H NMR (400 MHz, $CDCl_3$) δ 7.05 (m, 1H), 7.14 (t, *J* = 8.0 Hz, 1H), 7.26 (m, 15H), 7.55 (m, 2H), 8.05 (s, 1H); ^{13}C NMR (126 MHz, $CDCl_3$) δ 80.3, 116.5 (d, *J* = 20.7 Hz), 124.1 (br m), 124.4 (d, *J* = 9.8 Hz), 127.7, 128.0, 130.6, 131.2, 135.4 (d, *J* =

8.7 Hz), 141.9, 149.1, 153.3, 161.5 (d, *J* = 257.2 Hz), 180.5; HRMS (CI) *m/z* = 433.1590 $[M]^+$ found, $C_{28}H_{20}FN_3O$ needs 433.1590; R_f = 0.21 (1:5 ethyl acetate/ petroleum ether).

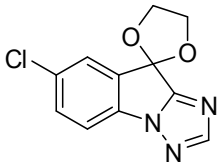
The resulting N-trityl protected ketone (0.56 g, 1.29 mmol) was dissolved in 1,4-dioxane (10 mL), treated with 10 % aqueous HCl (3 mL) and stirred at 70 ^oC for 4 hours. After cooling to room temperature, the mixture was made basic with saturated aqueous $NaHCO_3$ solution (pH ~8), re-acidified with solid citric acid (pH ~5) and extracted with ethyl acetate (3 x 10 mL). The combined organic extract was dried over $MgSO_4$ and concentrated *in vacuo*. Recrystallisation from ethyl acetate/ petroleum ether mixture gave the deprotected ketone **208** as a colourless solid (0.19 g, 77 % yield): ^1H NMR (400 MHz, DMSO) δ 7.37 (m, 2H), 7.70 (m, 1H), 7.79 (m, 1H), 8.75 (s, 1H), 14.85 (s, 1H); ^{13}C NMR (126 MHz, DMSO) δ 116.3 (d, *J* = 20.7 Hz), 124.4 (d, *J* =2.5 Hz), 126.4 (d, *J* = 13.1 Hz), 131.2, 134.3 (d, *J* = 8.7 Hz), 146.3, 158.6, 160.1 (d, *J* = 251.8 Hz), 183.9; ν_{max}/cm^{-1} 1723 (C=O), 1624, 1458, 1340, 1199, 1154; HRMS (CI) *m/z* = 192.0573 $[M+H]^+$ found, $C_9H_7FN_3O$ needs 192.0573; R_f = 0.15 (1:1 ethyl acetate/ petroleum ether).

5-(2-(5-Chloro-2-fluorophenyl)-1,3-dioxolan-2-yl)-1*H*-1,2,4-triazole **209**



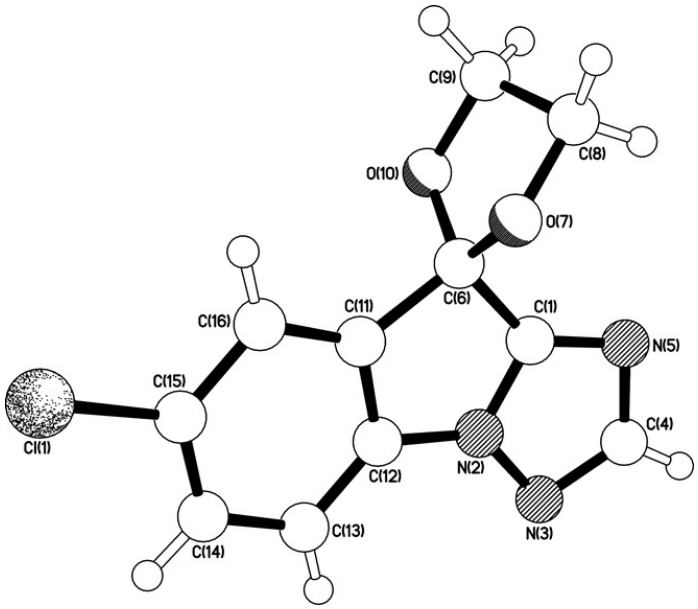
To a suspension of the phenyl-triazole ketone **203** (0.52 g, 2.32 mmol) and ethylene glycol (1.29 mL, 23.20 mmol) in toluene (20 mL) was added p-toluenesulfonic acid (0.05 g, 0.58 mmol) and the mixture was refluxed for 12 hours, collecting water with a Dean Stark trap. After cooling to room temperature, the mixture was washed with water (20 mL), dried over $MgSO_4$ and concentration *in vacuo*. The crude residue was purified by flash column chromatography, eluting with 1:49 MeOH/ DCM to give the ketal **209** as a colourless solid (0.35 g, 50 % yield): ^1H NMR (400 MHz, DMSO) δ 4.08 (m, 2H), 4.25 (m, 2H), 7.23 (t, *J* = 9.3 Hz, 1H), 7.52 (m, 1H), 7.63 (m, 1H), 8.43 (s, 1H), 14.05 (s, 1H); ^{13}C NMR (101 MHz, $CDCl_3$) δ 66.0, 102.9, 117.7 (d, *J* = 23.2 Hz), 127.6 (d, *J* = 4.0 Hz), 128.2 (m), 129.3 (m), 131.0 (d, *J* = 8.1 Hz), 157.9, 158.7, 158.8 (d, *J* = 251.5 Hz); ν_{max}/cm^{-1} 3088 (N-H), 1480 (C=N), 1371, 1207 (O-C-O), 1133, 1182; HRMS (ES) *m/z* = 270.0446 $[M+H]^+$ found, $C_{11}H_{10}ClFN_3O_2$ needs 270.0446; R_f = 0.12 (1:1 ethyl acetate/ petroleum ether).

7-Chlorospiro[[1,2,4]triazolo[1,5-a]indole-9,2'-[1,3]dioxolane] **212**



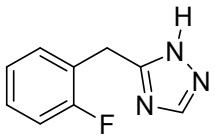
To a solution of the ketal **209** (0.10 g, 0.37 mmol) in DMA (30 mL) was added Cs_2CO_3 (0.37 g, 1.12 mmol) and the suspension was irradiated in a microwave at 180 ^oC for 35 minutes. The mixture was allowed to cool to room temperature before diluting with ethyl acetate (50 mL) and washing with water (50 mL) and brine (3 x 80 mL). The combined organic extract was dried over $MgSO_4$ and concentrated *in vacuo*. The resulting residue was purified by reverse phase prep HPLC, using a Waters 600 controller binary pump; phenomenex Luna 5µ C18 (2), 100Å, 75 x 30 mm column and a waters 2487 detector, measuring absorption at 254 nm. A mobile phase of 70 % aqueous formic acid (0.1 M) and 30 % acetonitrile with a flow rate of 9 mL/min and 50 minute run time were utilised. The cyclised product **212** was obtained as a colourless solid (0.032 g, 35 % yield): ^1H NMR (400 MHz, $CDCl_3$) δ 4.45 (m, 2H), 4.57 (m, 2H), 7.46 (d, *J* = 8.3 Hz, 1H), 7.50 (dd, *J* = 2.0, 8.3 Hz, 1H), 7.54 (d, *J* = 2.0 Hz, 1 H), 8.07 (s, 1H); ^{13}C NMR (101 MHz, $CDCl_3$) δ 66.0, 102.2, 112.4, 126.4, 131.7, 132.7, 135.5, 136.1, 156.1, 160.2; HRMS (ES) *m/z* = 250.0383 $[M+H]^+$ found, $C_{11}H_9ClN_3O_2$ needs 250.0383.

Crystal structure was used to determine the regiochemistry of the ketal **212** as the regioisomer drawn above, and shown below in the image generated from crystal structure analysis. Crystals used for the study was prepared by dissolving the ketal **212** in ethyl acetate with slow solvent evaporation over 4 days. All crystal data and structure refinement data can be found in the appendix.



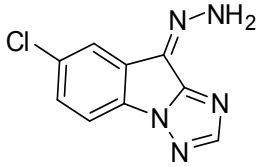
The crystal structure of ketal-protected triazoleindolone **212**

5-(2-Fluorobenzyl)-1*H*-1,2,4-triazole **215a**



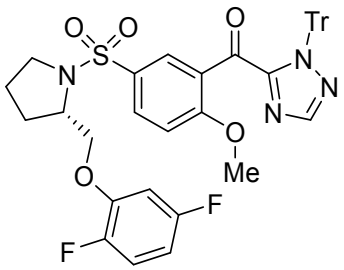
A solution of the phenyl-triazole ketone **208** (0.05 g, 0.22 mmol) in hydrazine monohydrate (1 mL) was irradiated in a microwave at 180 ^{o}C for 1 hour. The mixture was allowed to cool to room temperature, diluted with ethyl acetate (5 mL) and washed with water (5 mL). The organic layer was dried over $MgSO_4$ and concentrated *in vacuo*, followed by purification by flash column chromatography, eluting with 1:1 ethyl acetate/ petroleum ether to give the product **215a** as a colourless solid (0.021 g, 55 %): ^{1}H NMR (400 MHz, $CDCl_3$) δ 4.24 (s, 2H), 7.15 (m, 3H), 7.35 (m, 2H), 8.05 (s, 1H); ^{13}C NMR (101 MHz, $CDCl_3$) δ 26.9, 115.6 (d, *J* = 22.5 Hz), 123.6 (d, *J* = 15.6 Hz), 124.5 (d, *J* = 3.5 Hz), 129.1 (d, *J* = 8.7 Hz), 131.1 (m), 147.8, 157.8, 161.0 (d, *J* = 246.2 Hz); MS (CI) *m/z* = 178 $[M+H]^{+}$; R_f = 0.12 (1:4 ethyl acetate/ petroleum ether).

7-Chloro-9-hydrazono-9*H*-[1,2,4]triazolo[4,3-a]indole **216**



A solution of the phenyl-triazole ketone **205** (0.05 g, 0.22 mmol) and KOH (0.04 g, 0.66 mmol) in hydrazine monohydrate (1 mL) was irradiated in a microwave at 180 ^{o}C for 30 minutes. After cooling to room temperature, the mixture was diluted with water (1 mL) and extracted with DCM (2 x 5 mL). The aqueous layer was left to stand overnight and the resulting precipitated was collected by filtration. The precipitate was then washed with water (5 mL) and ethyl acetate (5 mL) to give the hydrazone **216** as a pale yellow solid (0.023 g, 48 % yield): ^{1}H NMR (400 MHz, DMSO) δ 7.46 (dd, *J* = 2.0 Hz, 8.8 Hz, 1H), 7.68 (d, *J* = 8.8 Hz, 1H), 8.31 (d, *J* = 2.0 Hz, 1H), 8.48 (s, 1H), 13.67 (s, 2H); ^{13}C NMR (101 MHz, $CDCl_3$) δ 112.5, 120.4, 121.5, 125.8, 128.9, 134.8, 139.5, 147.5, 153.1; HRMS (ES) *m/z* = 220.0390 $[M+H]^+$ found, $C_9H_7ClN_5$ needs 220.0390.

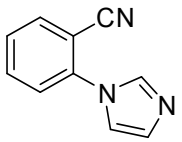
(*S*)-(5-(2-((2,5-Difluorophenoxy)methyl)pyrrolidin-1-ylsulfonyl)-2-methoxyphenyl)(1-trityl-1*H*-1,2,4-triazol-5-yl)methanone **222**



To a solution of N-trityltriazole **204** (0.09 g, 0.29 mmol) in THF (3 mL) at -78 ^{o}C, was added ^{n}BuLi (2.06 M in hexane, 0.14 mL, 0.29 mmol) and the mixture was stirred for 10 minutes. A precooled solution of ester **187a** (0.15 g, 0.35 mmol) in THF (0.5 mL) was added and stirring was continued at -78 ^{o}C for 15 minutes. This was followed by warming to room temperature and diluting with ethyl acetate (10 mL), washing with water (5 mL) and brine (5 mL). Subsequent drying over $MgSO_4$ and concentration *in vacuo* gave a residue which was purified by flash column chromatography, eluting with 1:4 – 2:3 ethyl acetate/ petroleum ether to give ketone **222** as a colourless solid (0.13 g, 62 % yield): ^{1}H NMR (400 MHz, DMSO) δ 1.7 (m, 2H), 2.03 (m, 2H), 3.07 (m, 1H), 3.51 (m, 1H), 3.81 (s, 3H), 3.92 (m, 2H), 4.27 (m, 1H), 6.84 (m, 2H), 7.01 (m, 2H), 7.27 (m, 15H), 7.94 (m, 2H), 8.01 (s, 1H); ^{13}C NMR (101 MHz, $CDCl_3$) δ 24.0, 28.9, 49.5, 56.2, 58.4, 71.8, 80.4, 104.9 (dd, *J* = 27.0 Hz, 22.1 Hz), 110.5 (m), 112.5,

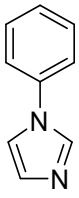
115.5 (d, *J* = 10.8 Hz), 126.0, 127.7, 128.0, 129.3, 130.5, 130.9, 133.7, 141.9, 143.2 (m), 149.0, 152.2 (m), 153.6, 156.3 (dd, *J* = 145 Hz, 9.6 Hz), 161.8, 180.9; ν_{max}/cm^{-1} 2923, 1682 (C=O), 1595, 1511 (C=N), 1443, 1260 (C-O-C), 1140; HRMS (ES) *m/z* = 743.2110 $[M+Na]^+$ found, $C_{40}H_{34}F_2N_4O_5S$ needs 743.2110; R_f = 0.24 (1:1 ethyl acetate/ petroleum ether).

2-(1*H*-Imidazol-1-yl)benzonitrile **226**[212]



To a solution of imidazole (0.25 g, 3.68 mmol) and Cs_2CO_3 (3.00 g, 9.20 mmol) in anhydrous DMF (30 mL) at room temperature, was added 2-fluorobenzonitrile (0.40 mL, 3.68 mmol) and the mixture was stirred at 100 ^oC for 3 hours. After cooling to room temperature, the reaction mixture was diluted with ethyl acetate (30 mL), and washed with water (2 x 20 mL) and brine (3 x 60 mL). The combined organic extract was dried over $MgSO_4$ and concentrated *in vacuo*. Purification by flash column chromatography, eluting with ethyl acetate gave product **226** as a colourless solid (0.46 g, 74 % yield): ^1H NMR (400 MHz, $CDCl_3$): 7.31 (br m, 1H), 7.40 (br m, 1H), 7.51 (br d, *J* = 7.5 Hz, 1H), 7.57 (br td, *J* = 1.0 Hz, 7.5 Hz, 1H), 7.78 (br td, *J* = 1.6 Hz, 8.0 Hz 1H), 7.86 (br dd, *J* = 1.4 Hz, 7.8 Hz, 1H), 7.90 (s, 1H); ^{13}C NMR (101 MHz, $CDCl_3$) δ 108.1, 115.9, 119.7, 125.7, 128.5, 130.8, 134.4, 134.6, 136.7, 139.4; ν_{max}/cm^{-1} 2230 (C≡N), 1600, 1506 (C=N), 1304, 1256; HRMS (CI) *m/z* = 170.0718 $[M+H]^+$ found, $C_{10}H_8N_3$ needs 170.0718.

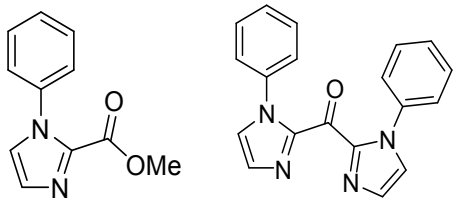
1-Phenyl-1*H*-imidazole **229**[202]



A mixture of imidazole (1.08 g, 10.59 mmol), iodobenzene **225** (1.18 mL, 10.59 mmol), Cu(I) oxide (0.15 g, 1.06 mmol) and KOH (1.19 g, 21.18 mmol) in DMSO (20 mL) was stirred at 110 ^oC for 24 hours. This was followed by cooling to room temperature and filtration through Celite®. The filtrate was diluted with ethyl acetate (40 mL), and washed with water (20 mL) and brine (3 x 60 mL), with subsequent drying over $MgSO_4$ and concentration *in vacuo*. Purification by flash column chromatography, eluting with ethyl acetate gave the 1-phenylimidazole **229** as a pale yellow oil (1.22

g, 80 % yield): ^{1}H NMR (400 MHz, $CDCl_3$) δ 7.24 (s, 1H), 7.32 (s, 1H), 7.40 (m, 3H), 7.51 (m, 2H), 7.89 (s, 1H); ^{13}C NMR (101 MHz, $CDCl_3$) δ 118.3, 121.5, 127.5, 129.9, 130.4, 135.6, 137.4; ν_{max}/cm^{-1} 3355, 3115, 1598, 1505 (C=N), 1303, 1247, 1056; HRMS (EI) *m/z* = 144.0687 $[M]^+$ found, $C_9H_8N_2$ needs 144.0687; R_f = 0.20 (1:49 MeOH/ ethyl acetate).

Methyl 1-phenyl-1*H*-imidazole-2-carboxylate **230** and Bis(1-phenyl-1*H*-imidazol-2-yl)methanone **231**

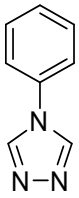


To a solution of 1-phenylimidazole **229** (0.50 g, 3.47 mmol) in THF (7 mL) at -78 °C was added ^{n}BuLi (1.6 M in hexane, 2.39 mL, 3.82 mmol). After stirring for 10 minutes, the resulting solution of deprotonated 1-phenylimidazole **229** was added to a precooled solution of methyl chloroformate (0.30 mL, 3.82 mmol) at -78 °C, with stirring continued for 30 minutes before warming to room temperature. The mixture was washed with water (5 mL) and brine (5 mL), dried over $MgSO_4$ and concentrated *in vacuo*. The obtained residue was purified by flash column chromatography, eluting with 0:1 – 1:49 MeOH/ ethyl acetate to give the ester **230** as a colourless solid (0.42 g, 60 % yield), and ketone **231** as a colourless solid (0.01 g, 9 % yield).

Ester **230**: ^{1}H NMR (400 MHz, $CDCl_3$) δ 3.87 (s, 3H), 7.23 (d, *J* = 1.0 Hz, 1H), 7.31 (d, *J* = 1.0 Hz, 1H), 7.36 (m, 2H), 7.51 (m, 3H); ^{13}C NMR (101 MHz, $CDCl_3$) δ 52.3, 126.1, 126.6, 129.0, 129.1, 130.0, 136.8, 138.0, 158.8; HRMS (CI) *m/z* = 203.0821 $[M+H]^+$ found, $C_{11}H_{11}N_2O_2$ needs 203.0812; R_f = 0.30 (ethyl acetate).

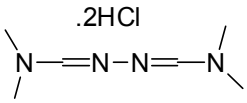
Ketone **231**: ^{1}H NMR (400 MHz, $CDCl_3$) δ 7.33 (m, 2H), 7.40 (m, 4H), 7.45 (br s, 1H); ^{13}C NMR (101 MHz, $CDCl_3$) δ 125.3, 126.4, 128.5, 129.2, 130.8, 137.9, 143.3, 173.0; ν_{max}/cm^{-1} 3092, 1647 (C=O), 1494, 1412 (C=N), 1309; HRMS, (EI) *m/z* = 314.1168 $[M]^+$ found, $C_{19}H_{14}N_4O$ needs 314.1168.

4-Phenyl-4*H*-1,2,4-triazole **241**[206]



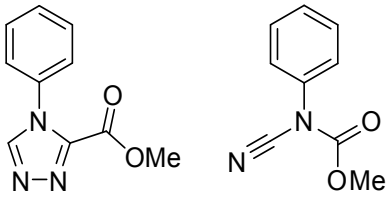
A mixture of aniline (0.44 g, 4.77 mmol) and azine salt **243** (1.00 g, 4.77 mmol) in benzene (10 mL) was heated to reflux for 5.5 hours, followed by cooling to room temperature and concentration *in vacuo*. The resulting residue was dissolved in 3:1 chloroform/ iso-propanol mixture (30 mL) and washed with water (10 mL). The organic layer was dried over $MgSO_4$ and concentrated *in vacuo*. Purification of the residue by flash column chromatography, eluting with ethyl acetate gave the product **241** as a colourless solid (0.50 g, 74 % yield): ^{1}H NMR (400 MHz, $CDCl_3$) δ 7.43 (m, 2H), 7.52 (m, 1H), 7.59 (m, 2H), 8.51 (s, 2H); ^{13}C NMR (101 MHz, $CDCl_3$) δ 122.3, 129.1, 130.4, 133.9, 141.5; ν_{max}/cm^{-1} 3120 (C=N), 1658, 1592, 1519 (C=N), 1222, 1093; HRMS (EI) *m/z* = 145.0640 $[M]^+$ found, $C_8H_7N_3$ needs 145.0640; R_f = 0.22 (ethyl acetate).

N'-((Dimethylamino)methylene)-N,N-dimethylformohydrazonamide **243**[206]



Thionyl chloride (9.53 mL, 133.00 mmol) was added, with stirring to anhydrous DMF (50 mL) at 0 ^{o}C. The mixture was allowed to warm to room temperature and stirred for 24 hours. Then, aqueous hydrazine (1.67 mL, 33.00 mmol) was added and stirring was continued at room temperature for 2 days. The resulting precipitate was collected by filtration and washed with DMF (5 mL) and diethyl ether (20 mL) to give the azine **243** as a colourless solid (2HCl salt, 6.03 g, 85 % yield, ~90 % purity): ^{1}H NMR (400 MHz, DMSO) δ 3.02 (s, 12H), 8.35 (s, 2H); ^{13}C NMR (101 MHz, DMSO) δ 34.4, 163.5; ν_{max}/cm^{-1} 2939 – 2459 (-NH_2^+), 1702 (C=N), 1503, 1298; HRMS (ES) *m/z* = 143.1297 $[M+H]^+$ found, $C_6H_{15}N_4$ needs 143.1297.

Methyl 4-phenyl-4*H*-1,2,4-triazole-3-carboxylate **245**[213] and Methyl cyano(phenyl)carbamate **246**



To a solution of 1-phenyltriazole **241** (0.20 g, 1.38 mmol) in THF (3 mL) at -78 ^{o}C was added ^{n}BuLi (1.6 M in hexane, 0.86 mL, 1.38 mmol). After stirring for 15 minutes, methyl chloroformate (0.11 mL, 1.38 mmol) was added and stirring was continued at -78 ^{o}C for 30 minutes, before warming to room temperature. The mixture was diluted with ethyl acetate (10 mL) and washed with water (5 mL) and brine (5 mL). The organic extract was dried over $MgSO_4$ and concentrated *in vacuo*. The resulting residue was purified by flash column chromatography, eluting with ethyl acetate to give ester **245** as colourless solid (0.07 g, 25 % yield) and carbamate **246** as a colourless solid (0.13 g, 54 % yield).

Ester **245**: ^{1}H NMR (400 MHz, $CDCl_3$) δ 3.96 (s, 3H), 7.37 (m, 2H), 7.58 (m, 3H), 8.38 (s, 1H); ^{13}C NMR (101 MHz, $CDCl_3$) δ 53.0, 125.9, 129.5, 130.1, 133.8, 145.0, 146.4, 157.5; ν_{max}/cm^{-1} 1729 (C=O), 1598, 1510, 1471, 1268, 1146; HRMS (CI) *m/z* = 204.0766 $[M+H]^+$ found, $C_{10}H_{10}N_3O_2$ needs 204.0768.

Carbamate **246**: ^{1}H NMR (400 MHz, $CDCl_3$) δ 4.01 (s, 3H), 7.48 (m, 5H); ^{13}C NMR (101 MHz, $CDCl_3$) δ 53.3, 126.5, 129.2, 130.3, 134.1, 147.5, 156.9; ν_{max}/cm^{-1} 2247 (C≡N), 1761 (C=O), 1493, 1493, 1257 (C-O ester); HRMS (CI) *m/z* = 194.0930 $[M+NH_4]^+$ found, $C_9H_8N_2O_2$ needs 194.0930.

UV-Vis Equilibria Studies

10 mL of 1mM or 2 mM of ketone stock solutions in dry DMSO were prepared in flasks, degassed and stored under nitrogen. 2 mL of 300 mM and 600 mM of PMBSH solutions in dry DMSO were prepared in stoppered vials, degassed and stored under nitrogen.

3 mL of 1 mM or 2 mM ketone stock solution was syringed into a stoppered cuvette under nitrogen. This was titrated with 10 µL aliquots of 300 mM PMBSH stock solution for 1 mM ketone solution or 600 mM PMBSH solution for 2 mM ketone solutions. After each 10 µL aliquot injection, the cuvette was shaken to mix and allowed to stand for 15 minutes, before measuring and recording the UV-vis absorption.

General Radiochemistry

Click Radiolabelling Procedure

Part 1: To a Wheaton vial containing an aqueous solution of K_2CO_3 (50 µL, 1.00 mg), K_{222} (5.00 mg) and acetonitrile (600 µL), was added an aqueous solution of [^{18}F]fluoride (50 -100 µL, < 20 mCi). The mixture was dried by azeotropic distillation using acetonitrile (3 x 600 µL). Then, a solution of tosylethylazide (1.5 µL) in acetonitrile (250 µL) was added to the vial and the resulting mixture was stirred at 80 ^{o}C for 15 minutes. The product [^{18}F]fluoroethylazide **37** was then purified by distillation using a thermospray.

Part 2: A buffered solution (sodium phosphate buffer, pH 6.0, 250 mM) of sodium L-ascorbate (25 µL, pH 6.0, 2.53 mg, 12.79 µmol) was added to a Wheaton vial containing an aqueous solution of $CuSO_4$ (25 µL, 0.51 mg, 2.06 µmol). Then, a solution of the relevant alkyne precursor **81** or **83** (1.00 – 1.30 mg) in DMF or DMSO (50 µL) was added, followed by the addition of the distilled [^{18}F]-2-fluoroethylazide (< 20 mCi) in acetonitrile (30 – 100 µL). The mixture was stirred at room temperature or heated as appropriate. In reactions using BPDS ligand, a solution of BPDS (25 µL, 2.22 mg, 4.13 µmol) in acetate buffer (250 mM, pH 5.0) was added to the Wheaton vial along with $CuSO_4$ and sodium L-ascorbate solution.

Reaction optimisation studies by analytical radio-HPLC: 10 µL samples of the reaction mixture were taken at time intervals, diluted with acetonitrile/water (1:1, 300 µL) and analysed by HPLC.

Radio-product isolation and formulation by SPE: The reaction mixture was diluted with acetonitrile/water (1:1, 1.5 mL) and the resulting mixture was purified by prep radio-HPLC. The isolated HPLC fraction was diluted with water (5 mL) and loaded onto a SepPak C-18 cartridge, pre-conditioned with ethanol (5 mL) and water (10 mL). The loaded cartridge was flushed with water (5 mL) and the product was eluted with ethanol (4 x 100 µL fractions).

Direct radiolabelling with [^{18}F]fluoride

To a Wheaton vial containing K_{222} (~ 7.0 mg), K_2CO_3 (0.05 mL aqueous solution, 1.0 mg) and acetonitrile (0.6 mL), was added an aqueous solution of [^{18}F]fluoride (50 – 100 µL, < 20 mCi). The mixture was dried by azeotropic distillation using acetonitrile (3 x 0.6 mL). Subsequently, a solution of tosylate **84** (1.0 - 1.3 mg) in acetonitrile (0.2 mL) was added to the vial and the resulting mixture was heated at 110 - 120 ^{o}C for 15 minutes to give the intermediate [^{18}F]**97**. Acetonitrile was then removed by distillation, followed by the addition of HCl (5M, 0.3 mL) and heating at 110 - 120 ^{o}C for

a further 20 minutes. The reaction mixture was then transferred into a vial containing aqueous PBS buffer (0.4 mL) and diluted with 3M aqueous NaOAc solution (0.6 mL). Then, the mixture was further diluted with water (10 mL) and loaded onto a SepPak C18 cartridge conditioned with ethanol (5 mL) and water (10 mL). The cartridge was washed with water (20 mL) and eluted with ethanol (0.6 mL). The crude mixture was subsequently diluted with water (0.6 mL) prior to HPLC prep purification to give the radio product [^{18}F]**62**.

Biological Characterisations

a) Caspase Enzyme Inhibition Assay[f]

The affinities of pyrimidoindolone **62** and isatin sulfonamide **22** for activated caspases 3 and 8 were measured by a fluorimetric *in vitro* caspase inhibition assay. Inhibition of recombinant human caspases was assessed by measuring the accumulation of a fluorogenic product, 7-amino-4-methylcoumarin (7-AMC). The results are summarized in Table **3.12** (Chapter **III**). The data are the average for two runs, each done in duplicate at 9 concentrations ranging from 5 pM to 500 µM and at 4 time intervals (15 min, 30 min, 60 min and 90 min). The drug concentration required to inhibit each enzyme by 50 % (IC_{50}) was obtained from nonlinear regression analysis of the inhibition profiles.

b) *In Vitro* Cell Uptake of [^{18}F]-Pyrimidoindolone 62 and Caspase Activation Assay[g]

38C13 Cells were plated in triplicate in 12-well plates, 2 or 3 days before the experiments and treated with either 4-HC (3 µg/mL), PAC-1 (10 µM) or vehicle (0.1 % DMSO) for 24 hrs to induce apoptosis. On the day of the experiment, ~10 µCi/well of [^{18}F]-pyrimidoindolone **62** was added and allowed to accumulate into cells for 60 mins at 37 ^{o}C. Cells were collected, washed, and re-suspended in 400 µL of PBS. Then 260 µL of each sample was transferred into counting tubes and [^{18}F]fluoride radioactivity was immediately determined using a Packard Cobra II gamma counter (Perkin-Elmer, UK). BCA Protein assay (Pierce, UK) was performed for all samples and data were normalized and expressed as counts/mg of protein.

[f] Caspase enzyme inhibition assay was conducted by Dr. Quang-De Nguyen

[g] *In vitro* cell uptake of [^{18}F]-Pyrimidoindolone **62** and caspase activation assay were conducted by Dr. Quang-De Nguyen

c) *In Vivo* Biodistribution[h] and Metabolism Studies

The radiation-induced murine fibrosarcoma (RIF-1) tumour cells were maintained in RPMI 1640 medium (Invitrogen Ltd., Paisley, UK), supplemented with 10 % fetal calf serum (BioWhittaker Europe Ltd., Verviers, Belgium), 2 mM L-glutamine, 100 U/mL penicillin, 100 µg/mL streptomycin, and 0.25 µg/mL fungizone (Gibco, UK) at 37 ^{o}C in a humidified incubator with 5 % CO_2. All animal work was done by licensed investigators in accordance with the United Kingdom's "Guidance on the Operation of Animals (Scientific Procedures) Act 1986" (HMSO, London, United Kingdom, 1990) and in full compliance with government regulations and guidelines on the welfare of animals in experimental neoplasia. Tumours were established in mice by subcutaneous injection of 5 × 105 cells on the back of male C3H/hej mice (Harlan, Bicester, Oxfordshire, UK). Tumour growth was monitored every two days using electronic calipers, and tumour volume, estimated using the equation (π/6) × L × W × D; (L) length, (W) width and (D) depth. Animals were selected for biodistribution studies of [^{18}F]-pyrimidoindolone **62** when the tumours reached ~100 - 150 mm^3. Mice were injected intravenously via the lateral vein with 0.08 - 0.13 mL of radioactivity dissolved in phosphate buffered saline. At 60 minutes after injection, mice were sacrificed by exsanguination via cardiac puncture under general anaesthesia (isofluorane inhalation). Aliquots of heparinized blood were rapidly centrifuged (2000 g for 5 mins) to obtain plasma. The radioactivity contained in tissues was determined by gamma counting on a Cobra II Auto-Gamma counter (Packard Instruments, Meriden, CTA) and expressed as a percentage of injected dose per gram of tissue (% ID/g). A minimum of two mice were used for each time point. All animals were treatment-naıve.

HPLC Analysis of Metabolism. Plasma, liver, and urine samples from the animals were snap frozen in liquid nitrogen and kept in pre-weighed scintillation counting tubes on dry ice. Immediately prior to extraction, the samples were thawed and placed on ice. For extraction, ice cold acetonitrile (1.5 mL) was added to each sample. Each mixture was centrifuged (4 ^{o}C, 3 min) and the resulting supernatant was evaporated *in vacuo* at 40 ^{o}C. Liver samples were homogenized with ice cold acetonitrile (1.5 mL) using an IKA Ultra-Turrax T-25 homogenizer prior to centrifugation. The residues, following rotary evaporation were then re-suspended in HPLC mobile phase (1.2 mL) and filtered through a Minisart hydrophilic syringe filter (0.2 µm) (Sartorius, Goettingen, Germany). Urine samples were diluted with

[h] *In vivo* biodistribution studies were conducted by Dr Quang-De Nguyen

HPLC mobile phase and filtered as above. The plasma, urine and liver samples (1 mL) were then analysed by radio-HPLC on an Agilent 1100 series HPLC system (Agilent Technologies, Stockport, UK) equipped with a γ-RAM model 3 gamma-detector (IN/US Systems Inc., Florida) and the Laura software. The stationary phase comprised of a of a Phenomenex C18 reverse-phase column (250 mm × 10 mm), using a mobile phase comprising of 0.1 M ammonium formate /ethanol (45:55) running in isocratic mode at a flow rate of 3 mL/min.

d) Transwell Assay[i, 136]

Caco-2 cells were seeded on to cell culture chambers (transwells) for 21 days, with the media changed every other day. The transepithelial electric resistance was measured using an epithelial voltohmmeter equipped with an STX2 electrode (World Precision Instruments, Sarasota, Florida), and it was verified to be >300 Ω/cm^2 prior to all experiments.

The assay was started by replacing the culture medium with HBSS containing 1 µM of probe under study. The plates were placed on an orbital shaker (60 rpm) during the experiment. After 2 hrs, a volume of 10 µL of each chamber was collected for analysis by LCMS. The permeability of a test compound was defined by the following equation:

$$Papp = (dQ/dt)/ AC_0$$

Where *A* is the surface area of the transwell membrane; C_0 is the molar drug concentration in the donor chamber at time, and *dQ/dt* is the rate of transfer of the compound to the receiver chamber, determined from the slope of the graph concentration (*dQ*) versus time (*dt*).

It has been established that if a compound exerts a ratio between the secretion (permeability from the basal to the apical side (Papp B→A)) and the absorption (permeability from the apical to the basal side (Papp A→B)) of greater than 3, it can be considered as being actively effluxed.[140] 'Normal' diffusion, where the compound is at equilibrium between the apical and basal side gives a secretion/absorption ratio of approximately one.[140]

At the end of the assay, the integrity of the monolayer was verified by measuring the amount of lucifer yellow, a fluorophore which passes through the membrane, measured using a plate reader

[i] Transwell assay conducted by Dr Maciej Kaliszczak

(Wallac EnVision reader, PerkinElmer, Massachusetts) and verified to be < 2 % of the concentration in the donor chamber.[214] The integrity of the monolayer was assessed post-drug transport as lucifer yellow may interfere with LCMS analysis.

Statistical Analysis: The significance of comparison between two data sets for isatin **22** and pyrimidoindolone **62** was determined using Student's *t* test (Prism v5.0 software, Graph Pad), defined as significant (*, $0.01 < P < 0.05$), very significant (**, $0.001 < P < 0.01$), and extremely significant (***, $P < 0.001$).

REFERENCES

References

1. Saraste, A.; Nekolla, S. G.; Schwaiger, M., *Cardiovasc. Res.* **2009,** *83*, 643-652.
2. Laxman, B.; Hall, D. E.; Bhojani, M. S.; Hamstra, D. A.; Chenevert, T. L.; Ross, B. D.; Rehemtulla, A., *Proc. Natl. Acad. Sci. USA* **2002,** *99*, 16551-16555.
3. Weissleder, R., *Science* **2006,** *312*, 1168-1171.
4. McLarty, K.; Reilly, R. M., *Clin. Pharmacol. Ther.* **2007,** *81*, 420-424.
5. El-Deiry, W. S.; Sigman, C. C.; Kelloff, G. J., *J. Clin. Oncol.* **2006,** *24*, 3261-3273.
6. Reed, J. C., *Nat. Rev. Drug Discov.* **2002,** *1*, 111-121.
7. Otsuki, Y.; Li, Z.; Shibata, M. A., *Prog. Histochem. Cyto.* **2003,** *38*, 275-339.
8. Hakumaki, J. M.; Liimatainen, T., *Eur. J. Radiol* **2005,** *56*, 143-153.
9. Hakumaki, J. M.; Brindle, K. M., *Trends Pharmacol. Sci.* **2003,** *24*, 146-149.
10. Blankenberg, F. G.; Tait, J. F.; Strauss, H. W., *Eur. J. Nucl. Med.* **2000,** *27*, 359-367.
11. Bremer, C.; Ntziachristos, V.; Weissleder, R., *Eur. Radiol.* **2003,** *13*, 231-243.
12. Czarnota, G. J.; Kolios, M. C.; Abraham, J.; Portnoy, M.; Ottensmeyer, F. P.; Hunt, J. W.; Sherar, M. D., *Brit. J. Cancer* **1999,** *81*, 520-527.
13. Hnatowich, D. J., *J. Cell. Biochem. Suppl.* **2002,** *39*, 18-24.
14. Spinks, T. J., PET Theory, *Academic Press*; San Diego, 1999 p 1782-1791
15. Fass, L., *Mol. Oncol.* **2008,** *2*, 115-152.
16. Schutt, E. G.; Klein, D. H.; Mattrey, R. M.; Riess, J. G., *Angew. Chem. Int. Ed.* **2003,** *42*, 3218-3235.
17. Workman, P.; Aboagye, E. O.; Chung, Y.-L.; Griffiths, J. R.; Hart, R.; Leach, M. O.; Maxwell, R. J.; McSheehy, P. M. J.; Price, P. M.; Zweit, J., *J. Natl. Cancer Inst.* **2006,** *98*, 580-598.
18. Schneider, G.; Uder, M., *Top. Magn. Reson. Imag.* **2003,** *14*, 403-425.
19. Schellenberger, E. A.; Bogdanov, J. A.; Hogeemann, D.; Tait, J.; Weissleder, R.; Josephson, L., *Mol. Imaging.* **2002,** *1*, 102-107.
20. Zhao, M.; Bearegard, D. A.; Loizou, L.; Davletov, B.; Brindle, K. M., *Nat. Med.* **2001,** *7*, 1241-1244.
21. Gee, A. D., *Brit. Med. Bull.* **2003,** *65*, 169-177.
22. Willmann, J. K.; Bruggen, N. v.; Dinkelborh, L. M.; Gambnir, S. S., *Nat. Rev. Drug Discov.* **2008,** *7*, 591-607.
23. Elsinga, P. H., *Methods.* **2002,** *27*, 208-217.
24. Gee, A. D., *Amer. Pharm. Rev.* **2006,** *9*, 39-41.
25. Kenny, L.; Coombes, R. C.; Vigushin, D. M.; Al-Nahhas, A.; Shousha, S.; Aboagye, E. O., *Eur. J. Nucl. Med. Mol. Imaging* **2007,** *34*, 1339-1347.

26. Serdons, K.; Verbruggen, A.; Bormans, G. M., *Methods.* **2009,** *48*, 104-111.
27. Cook, G. J. R., *Brit. J. Radiol.* **2003,** *76*, S152-S158.
28. Jennings, L. E.; Long, N. J., *Chem. Commun.* **2009**, 3511-3524.
29. Eckelman, W. C., *Nucl. Med. Biol.* **1994,** *21*, 759-769.
30. Eckelman, W. C., *Nucl. Med. Biol.* **1998,** *25*, 169-173.
31. Cunningham, V. J.; Parker, C. A.; Rabiner, E. A.; Gee, A. D.; Gunn, R. N., *Drug Discov. Today* **2005,** *2*, 311-315.
32. Vallabhajosula, S., *Semin. Nucl. Med.* **2007,** *37*, 400-419.
33. Welch, M. J.; Redvanly, C. S., *Handbook of Radiopharmaceuticals, Radiochemistry and Applications*. John Wiley & Sons Ltd, Chichester: 2003.
34. Bolton, R., *J. Labelled Compd. Rad.* **2002,** *45*, 485-528.
35. Hoz, A. d. l.; Diaz-Ortiz, A.; Moreno, A., *Chem. Soc. Rev.* **2005,** *34*, 164-178.
36. Elander, N.; Jones, J. R.; Lu, S.-Y.; Stone-Elander, S., *Chem. Soc. Rev.* **2000,** *29*, 239-249.
37. Cai, L.; Lu, S.; Pike, V. W., *Eur. J. Org. Chem.* **2008**, 2853-2873.
38. Smith, G.; Carroll, L.; Aboagye, E. O., *Mol. Imaging Biol.* **2012,** *14*, 653-666.
39. Baskin, J.; Prescher, J. A.; Laughlin, S. T.; Agard, N. J.; Chang, P. V.; Miller, I. A.; Lo, A.; Codelli, J. A.; Bertozzi, C. R., *Proc. Nat. Acad. Sci. USA* **2007,** *104*, 16793-16797.
40. Evans, H.; Slade, R. L.; Carroll, L.; Smith, G.; Q.-D.Nguyen; Iddon, L.; Kamaly, N.; Stoeckmann, H.; Leeper, F. J.; Aboagye, E. O.; Spivey, A. C., *Chem. Commun.* **2012,** *48*, 991-993.
41. Bouvet, V.; Wuest, M.; Wuest, F., *Org. Biomol. Chem.* **2011,** *9*, 7393-7399.
42. Campbell-Verduyn, L.; Mirfeizi, L.; Schoonen, A. K.; Dierckx, R. A.; Elsinga, P. H.; Feringa, B. L., *Angew. Chem. Int. Ed.* **2011,** *50*, 11117-11120.
43. Carpenter, R.; Hausner, S. H.; Sutcliffe, J. L., *ACS Med. Chem. Lett.* **2011,** *2*, 885-889.
44. Denault, J. B.; Salvesen, G. S., *Chem. Rev.* **2002,** *102*, 4489-4499.
45. Siegel, R. M., *Nat. Rev. Immunol.* **2006,** *6*, 308-317.
46. Taylor, R. C.; Cullen, S. P.; Martin, S. J., *Nat. Rev. Mol. Cell. Biol.* **2008,** *9*, 231-241.
47. Wyllie, A. H.; Kerr, J. F. R.; Curie, A. R., *Int. Rev. Cytol.* **1980,** *68*, 251-305.
48. Robertson, A. M.; Bird, C.; Waddell, A. W.; Curie, A. R., *J. Pathol.* **1978,** *126*, 181-187.
49. Martin, S. J.; Bradley, J. G.; Cotter, T. G., *Clin. Exp. Immunol* **1990,** *79*, 448-453.
50. Hanahan, D.; Weinberg, R. A., *Cell.* **2000,** *100*, 57-70.
51. Blankenberg, F. G.; Katsikis, P. D.; Tait, J. F.; Davis, E. R.; Naumovski, L.; Ohtsuki, K.; Kopiwoda, S.; Abrams, M. J.; Darkes, M.; Robbins, R. C.; Maecker, H.; Strauss, H. W., *Proc. Nat. Acad. Sci. USA* **1998,** *95*, 6349-6354.

52. Cohe, A.; Shirvan, A.; Levin, G.; Grimberg, H.; Reshef, A.; Ziv., I., *Cell Res.* **2009,** *19*, 625-637.
53. Reshef, A.; Shirvan, A.; Waterhouse, R. N.; Grimberg, H.; Levin, G.; Cohen, A.; Ulysse, L. G.; Friedman, G.; Antoni, G.; Ziv, I., *J. Nucl. Med.* **2008,** *49*, 1520-1528.
54. Damianovich, M.; Ziv, I.; Heyman, S. N.; Rosen, S.; Shina, A.; Kidron, D.; Aloya, T.; Grimberg, H.; Levin, G.; Reshef, A.; Bentolila, A.; Cohen, A.; Shirvan, A., *Eur. J. Nucl. Med. Mol. Imaging* **2006,** *33*, 281-291.
55. Aloya, R.; Shirvan, A.; Grimberg, H.; Reshef, A.; Levin, G.; **D, K.**; **Cohen, A.**; **Ziv, I.**, *Apoptosis.* **2006,** *11*, 2089-2101.
56. Lee, D.; Long, S. A.; Murray, J. H.; Adams, J. L.; Nuttall, M. E.; Nadeau, D. P.; Kikly, K.; Winkler, J. D.; Sung, C.-M.; Ryan, D. M.; Levy, M. A.; Keller, P. M.; DeWolf, W. E., *J. Med. Chem.* **2001,** *44*, 2015-2026.
57. Smith, G.; Glaser, M.; Perumal, M.; Nguyen, Q.-D.; Shan, B.; Arstad, E.; Aboagye, E. O., *J. Med. Chem.* **2008,** *51*, 8057-8067.
58. Havran, L.; Chong, D. C.; Childers, W. E.; Dollings, P. J.; Dietrich, A.; Harrison, B. L.; Marathias, V.; Tawa, G.; Aulabaugh, A.; Cowling, R.; Kapoor, B.; Xu, W.; Mosyak, L.; Moy, F.; Hum, W.-T.; Wood, A.; Robichaud, A. J., *Bioorg. Med. Chem.* **2009,** *17*, 7755-7768.
59. Emoto, K.; Toyama-Sorimachi, N.; Karasuyama, H.; Inoue, K.; Umeda, M., *Exp. Cell. Res.* **1997,** *232*, 430-434.
60. Fadok, V. A.; Voelker, D. R.; Campbell, P. A.; Cohen, J. J.; Bratton, D. L.; Henson, P. M., *J. Immunol.* **1992,** *148*, 2207-2216.
61. Saint-Hubert, M. D.; Prinsen, K.; Mortelmans, L.; Verbruggen, A.; Mottaghy, F. M., *Methods* **2009,** *48*, 178-187.
62. Reshef, A.; Shirvan, A.; Akselrod-Ballin, A.; Wall, A.; Ziv, I., *J. Nucl. Med.* **2010,** *51*, 837-840.
63. Grimberg, H.; Levin, G.; Shirvan, A.; Cohen, A.; Yogev-Falach, M.; Reshef, A.; Ziv, I., *Apoptosis* **2009,** *14*, 257-267.
64. Johanna, H.; Shirvan, A.; Antoni, G.; Gustavsson, S.-Å.; Langstrom, B.; Ringheim, A.; Sorensen, J.; Ben-Ami, M.; Ziv, I., *J. Nucl. Med.* **2011,** *52*, 720-725.
65. Hill, M. M.; Adrian, C.; Martin, S. J., *Mol. Interv.* **2003,** *3*, 19-26.
66. Baliga, B. C.; Read, S. H.; Kumar, S., *Cell Death Differ.* **2004,** *11*, 1234-1241.
67. Pop, C.; Timmer, J.; Sperandio, S.; Salvesen, G. S., *Mol. Cell.* **2006,** *22*, 269-275.
68. Yin, G.; Park, H. H.; Chung, J. Y.; Lin, S.-C.; Lo, Y. C.; Graca, L. S. d.; Jiang, X.; Wu, H., *Mol. Cell.* **2006,** *22*, 259-275.
69. Lee, D.; long, S. A.; Adams, J. L.; Chan, G.; Vaidya, K. S.; Francis, T. A.; Kikly, K.; Winkler, J. D.; Sung, C.-M.; Debouck, C.; Richardson, S.; Levy, M. A.; DeWolf, W. E. J.; Keller, P. M.; Tomaszek, T.; Head, M. S.; Ryan, D. M.; Haltiwanger, C. H.; Liang, P.-H.; Janson, C. A.; McDevitt, P. J.; Johanson, K.; Concha, N. O.;

Chan, W.; Abdel-Meguid, S. S.; Badger, A. M.; Lark, M. W.; Nadeau, D. P.; Suva, L. J.; Gowen, M.; Nuttall, M. E., *J. Biol. Chem.* **2000,** *275*, 16007-16014.

70. Garcia-Calvo, M.; Peterson, E. P.; Leiting, B.; Ruel, R.; Nicholson, D. W.; Thornberry, N. A., *J. Biol. Chem.* **1998,** *273*, 32608-32613.
71. Schotte, P.; Declercq, W.; Huffel, S. v.; Vandenabeele, P.; Beyaert, R., *FEBS Lett.* **1999,** *442*, 117-121.
72. Kravchenko, D. V.; Kysil, V. M.; Tkachenko, S. E.; Maliarchouk, S.; Okun, I. M.; Ivachtchenko, A. V., *Eur. J. Med. Chem.* **2005,** *40*, 1377-1383.
73. Chu, W.; Zhang, J.; Zeng, C.; Rothfuss, J.; Tu, Z.; Chu, Y.; Reichert, D. E.; Welch, M. J.; Mach, R. H., *J. Med. Chem.* **2005,** *48*, 7637-7647.
74. Wang, Q.; Mach, R. H.; Reichert, D. E., *J. Chem. Inf. Model.* **2009,** *49*, 1963-1973.
75. Agniswamy, J.; Fang, B.; Weber, I. T., *Apoptosis.* **2009,** *14*, 1135-1144.
76. Wei, Y.; Fox, T.; Chambers, S. P.; Sintchak, J.; Coll, J. T.; Golec, J. M. C.; Swenson, L.; Wilson, K. P.; Charifson, P. S., *Chem. Biol.* **2000,** *7*, 423-432.
77. Kopka, K.; Faust, A.; Keul, P.; Wagner, S.; Breyholz, H.-J.; Hoeltke, C.; Schober, O.; Schaefers, M.; Levkau, B., *J. Med. Chem.* **2006,** *49*, 6704-6715.
78. Zhou, D.; Chu, W.; Rothfuss, J.; Zeng, C.; Xu, J.; Jones, L.; Welch, M. J.; Mach, R. H., *Bioorg. Med. Chem. Lett.* **2006,** *16*, 5041-5046.
79. Chu, W.; Rothfuss, J.; Avignon, A. d.; Zeng, C.; Zhou, D.; Hotchkiss, R. S.; Mach, R. H., *J. Med. Chem.* **2007,** *50*, 3751-3755.
80. Nguyen, Q.-D.; Smith, G.; Glaser, M.; Perumal, M.; Arstad, E.; Aboagye, E., *Proc. Nat. Acad. Sci. USA* **2009,** *106*, 16375-16380.
81. Fortt, R.; Smith, G.; Awais, R. O.; Luthra, S. K.; Aboagye, E. O., *Nucl. Med. Biol.* **2012,** *39*, 1000-1005.
82. Chen, D. L.; Zhou, D.; Chu, W.; Herrbrich, P. E.; Jones, L. A.; Rothfuss, J. M.; Engle, J. T.; Geraci, M.; Welch, M. J.; Mach, R. H., *Nucl. Med. Biol.* **2009,** *36*, 651-658.
83. Zhou, D.; Chu, W.; Chen, D. L.; Wang, Q.; Reichert, D. E.; Rothfuss, J.; D'Avignon, A.; Welch, M. J.; Mach, R. H., *Org. Biomol. Chem.* **2009,** *7*, 1337-1348.
84. Faust, A.; Wagner, S.; Law, M. P.; Hermann, S.; Schnockel, U.; Keul, P.; Schober, O.; Schafers, M.; Levkau, B.; Kopka, K., *Q. J. Nucl. Med. Mol. Imaging.* **2007,** *51*, 67-73.
85. Marik, J.; Sutcliffe, J. L., *Tetrahedron Lett.* **2006,** *47*, 6681-6684.
86. Nguyen, Q.-D.; Challapalli, A.; Smith, G.; Fortt, R.; Aboagye, E. O., *Eur. J. Cancer* **2012,** *48*, 432-440.
87. Aulabaugh, A.; Kapoor, B.; Huang, X.; Dollings, P.; Hum, W.-T.; Banker, A.; Wood, A.; Ellestad, G., *Biochem.* **2007,** *46*, 9462-9471.
88. Cartier, A.; Rivail, J. L., *Chemometr Intell. Lab.* **1987,** *1*, 335-347.

89. Leo, A.; Hansch, C.; Elkins, D., *Chem. Rev.* **1971,** *71*, 525-616.
90. Ray, S.; Basak, S. C.; Chandhury, C. R.; Ray, A. D.; Ghosh, J. J., *Acta Ciencia Indica* **1981,** *4,* 187-192.
91. Gupta, S.; Singh, P.; Bindal, M. C., *Med. Chem.* **1981,** *16*, 446-448.
92. Lien, E.; Guo, Z. R.; Li, R. L.; Su, C. T., *J. Pharm. Sci.* **1982,** *71*, 641-655.
93. Hall, L.; Kier, L. B., *Med. Chem.* **1981,** *16*, 399-407.
94. Karelson, M.; Lobanov, V. S.; Katritzky, A. R., *Chem. Rev.* **1996,** *96*, 1027-1043.
95. Gomez-Bombarelli, R.; Gonzalez-Perez, M.; Perez-Prior, M. T.; Calle, E.; Casado, J., *J. Phys. Chem. A.* **2009,** *113*, 11423–11428.
96. Parr, R. G., *Annu. Rev. Phys. Chem* **1983,** *34*, 631-656.
97. Zhao, Y.; Truhlar, D. G., *Theor. Chem. Acc.* **2008,** *120*, 215-241.
98. Chai, J.-D.; Head-Gordon, M., *Phys. Chem. Chem. Phys.* **2008,** *10*, 6615-6620.
99. Hariharan, P. C.; Pople, J. A., *Theoretica Chimica Acta* **1973,** *28*, 213-222.
100. Francl, M. M.; Pietro, W. J.; Hehre, W. J.; Binkley, S. J.; Gordon, M. S.; DeFrees, D. J.; Pople, J. A., *J. Chem. Phys.* **1982** *77*, 3654-3665.
101. Davidson, E. R.; Feller, D., *Chem.Rev.* **1986,** *86*, 681-696.
102. Hehre, W. J.; Ditchfield, R.; Pople, J. A., *J. Chem. Phys.* **1972,** *56*, 2257-2261.
103. Tomasi, J.; Mennucci, B.; Cammi, R., *Chem. Rev.* **2005,** *105*, 2999–3093.
104. Onsager, L., *J. Am. Chem. Soc.* **1936** *58*, 1486-1493.
105. Frisch, M. J.; Trucks, G. W.; Schlegel, H. B.; Scuseria, G. E.; Robb, M. A.; Cheeseman, J. R.; Scalmani, G.; Barone, V.; Mennucci, B.; Petersson, G. A.; Nakatsuji, H.; Caricato, M.; Li, X.; Hratchian, H. P.; Izmaylov, A. F.; Bloino, J.; Zheng, G.; Sonnenberg, J. L.; Hada, M.; Ehara, M.; Toyota, K.; Fukuda, R.; Hasegawa, J.; Ishida, M.; Nakajima, T.; Honda, Y.; Kitao, O.; Nakai, H.; Vreven, T.; Montgomery, J. A.; Peralta, J. E.; Ogliaro, F.; Bearpark, M.; Heyd, J. J.; Brothers, E.; Kudin, K. N.; Staroverov, V. N.; Kobayashi, R.; Normand, J.; Raghavachari, K.; Rendell, A.; Burant, J. C.; Iyengar, S. S.; Tomasi, J.; Cossi, M.; Rega, N.; Millam, J. M.; Klene, M.; Knox, J. E.; Cross, J. B.; Bakken, V.; Adamo, C.; Jaramillo, J.; Gomperts, R.; Stratmann, R. E.; Yazyev, O.; Austin, A. J.; Cammi, R.; Pomelli, C.; Ochterski, J. W.; Martin, R. L.; Morokuma, K.; Zakrzewski, V. G.; Voth, G. A.; Salvador, P.; Dannenberg, J. J.; Dapprich, S.; Daniels, A. D.; Farkas, Ö.; Foresman, J. B.; Ortiz, J. V.; Cioslowski, J.; Fox, D. J., In *Gaussian, Inc., Wallingford CT, http://www.gaussian.com/*, 2009.
106. Singh, C. U.; Kollman, P. A., *J. Comput. Chem.* **1984,** *5*, 129-145.
107. Wang, B.; Ford, G. P., *J. Comput. Chem.* **1994,** *15*, 200-207.
108. Mulliken, R. S., *J. Chem. Phys.* **1955,** *23*, 1833-1840.
109. Gross, K. C.; Seybold, P. G.; Hadad, C., *Int. J. Quant. Chem.* **2002,** *90*, 445-458.

110. Grueber, C.; Buss, V., *Chemosphere* **1989,** *19*, 1595-1609.
111. Jeffrey, G. A., *An introduction to hydrogen bonding*. Oxford University Press: Oxford 1997.
112. Martz, E. Help, Index & Glossary for Protein Explorer. http://biomodel.uah.es/en/water/hbonds.htm.
113. Benesi, H.; Hildebrand, J. H., *J. Am. Chem. Soc.* **1949,** *71*, 2703 - 2707.
114. Tao, W.; Barra, M., *J. Chem. Soc., Perkin Trans.* **1998**, 1957-1960.
115. Burkey, T.; Fahey, R. C., *J. Am. Chem. Soc.* **1983,** *105*, 868-871.
116. Jencks, W. P., *Adv. Enzymol. Relat. Areas Mol. Biol.* **1975,** *43*, 219-410.
117. Cliffe, I. A.; Todd, R. S.; White, A. C., *Synth. Comm.* **1990,** *20*, 1757-1767.
118. Koebrich, G., *Angew. Chem. Int. Ed.* **1967,** *6*, 41-52.
119. Brown, H.; Singh, S. M.; Rangaishenvi, M. V., *J. Org. Chem.* **1986,** *51*, 3150-3155.
120. Kowalski, C. L.; Haque, H. S.; Fields, K. W., *J. Am. Chem. Soc.* **1985,** *107*, 1429-1430.
121. Himo, F.; Lovell, T.; Hilgraf, R.; Rostovtsev, V. V.; Noodleman, L.; Sharpless, K. B.; Fokin, V. V., *J. Am. Chem. Soc.* **2005,** *127*, 210-216.
122. Galante, E.; Schoultz, B. W.; Koepp, M.; Arstad, E., *Molecules* **2013,** *18*, 5335-5347.
123. Glaser, M.; Goggi, J.; Smith, G.; Morrison, M.; Luthra, S. K.; Robins, E.; Aboagye, E. O., *Bioorg. Med. Chem. Lett.* **2011,** *21*, 6945-6949.
124. Putt, K.; Chen, G. W.; Pearson, J. M.; Sandhorst, J. S.; Hoagland, M. S.; Kwon, J.-T.; Hwang, S.-K.; Jin, H.; Churchwell, M. I.; Cho, M.-H.; Doerge, D. R.; Helferich, W. G.; Hergenrother, P. J., *Nat. Chem. Biol.* **2006,** *2*, 543-550.
125. Osawa, T.; Davies, D.; Hartley, J. A., *Cell Death & Disease* **2011,** *2* e187.
126. Chen, T.-L.; Kennedy, M. J.; Anderson, L. W.; Kiraly, S. B.; Black, K. C.; Colvin, O. M.; Grochow, L. B., *Drug Metab. Dispos.* **1997,** *25*, 544-551.
127. Dong, Q.; Bullock, N.; Ali-Osman, F.; Colvin, O. M.; Bigner, D. D.; Friedman, H. S., *Cancer Chemother. Pharm.* **1996,** *37*, 242-246.
128. Hilton, J., *Biochem. Pharmacol.* **1984,** *33*, 1867-1872.
129. Bladeren, P. J. v., *Chem-Biol. Interact.* **2000,** *129*, 61-76.
130. King, C. D.; Rios, G. R.; Green, M. D.; Tephly, T. R., *Curr. Drug Metab.* **2000,** *1*, 143-161.
131. Gillette, J. R.; Davis, D. C.; Sasame, H. A., *Annu. Rev. Pharmacol.* **1972,** *12*, 57-84.
132. Park, B. K.; Kitteringham, N. R.; O'Neill, P. M., *Annu. Rev. Pharmacol. Toxicol.* **2001,** *41*, 443-470.
133. Rietjens, I. M. C. M.; Soffers, A. E. M. F.; Veeger, C.; Vervoort, J., *Biochemistry* **1993,** *32*, 4801-4812.
134. Ambudkar, S. V.; Dey, S.; Hrycyna, C. A.; Ramachandra, M.; Pastan, I.; Gottesman, M. M., *Annu. Rev. Pharmacol. Toxicol.* **1999,** *39*, 361-398.
135. Silverman, J. A., *Pharm. Biotechnol.* **1999,** *12*, 353-386.

136. Kaliszczak, M.; Antonow, D.; Patel, K. I.; Howard, P.; Jodrell, D. I.; Thurston, D. E.; Guichard, S. M., *AAPS J.* **2010,** *12*, 617-627.
137. Jones, P. M.; George, A. M., *Cell. Mol. Life Sci.* **2004,** *61*, 682-699.
138. Davidson, A. L.; Dassa, E.; Orelle, C.; Chen, J., *Microbiol. Mol. Biol. Rev.* **2008,** *72*, 317-364.
139. Bruggemann, E. P.; Currier, S. J.; Gottesman, M. M.; Pastan, I., *J. Bio. Chem.* **1992,** *267*, 21020-21026.
140. Szakacs, G.; Paterson, J. K.; Ludwig, J. A.; Booth-Genthe, C.; Gottesman, M. M., *Nat. Rev.* **2006,** *5*, 219-234.
141. Didziapetris, R.; Japertas, P.; Avdeef, A.; Petrauskas, A., *J. Drug Target* **2003,** *11*, 391-406.
142. Thomas, H.; Coley, H. M., *Cancer Control* **2003,** *10*, 159-165.
143. Hitotsuyanagi, Y.; Motegi, S.; Hasuda, T.; Takeya, K., *Org. Lett.* **2004,** *6*, 1111-1114.
144. Hitotsuyanagi, Y.; Motegi, S.; Fukaya, H.; Takeya, K., *J. Org. Chem.* **2002,** *67*, 3266-3271.
145. Wuhong, C.; Zhaohu, L.; Mengmeng, N.; Chunhao, Y.; Xueming, Y.; Xie, Y.; Shen, X.; Wang, M.-W., *Bioorg. Med. Chem.* **2007,** *15*, 5828-5836.
146. Du, X.; Lizarzaburu, M.; Turcotte, S.; Lee, T.; Greenberg, J.; Shan, B.; Fan, P.; Ling, Y.; Medina, J. C.; Houze, J., *Bioorg. Med. Chem. Lett.* **2011,** *21*, 3774-3779.
147. Jesberger, M.; Davis, T. P.; Barner, L., *Synthesis* **2003**, 1929-1958
148. Hadad, C. M.; Rablen, P. R.; Wiberg, K. B., *J. Org. Chem* **1998,** *63*, 8668-8681.
149. Curphey, T. J., *J. Org. Chem.* **2002,** *67*, 6461-6473.
150. Xie, Z.-F.; Chai, K.-Y.; Piao, H.-R.; Kwak, K.-C.; Quan, Z.-S., *Bioorg. Med. Chem. Lett.* **2005,** *15* 4803-4805.
151. Campagna, F.; Palluotto, F.; Mascia, M. P.; Maciocco, E.; Marra, C.; Carotti, A.; Carrieri, A., *Farmaco* **2003,** *58*, 129-140.
152. Guo, L.-J.; Wei, C.-X.; Jia, J.-H.; Zhao, L.-M.; Quan, Z.-S., *Eur. J. Med. Chem.* **2009,** *44*, 954-958.
153. Katritzky, A. R.; Fan, W. Q.; Koziol, A. E.; Palenik, G. J., *J. Heterocyclic Chem.* **1989,** *26*, 821-828.
154. Cheng, A.; Hendel, J. L.; Colangelo, K.; Bonin, M.; Auzanneau, F.-I., *J. Org. Chem.* **2008,** *73*, 7574-7579.
155. Edmondson, S. D.; Mastracchio, A.; Cox, J. M.; Eiermann, G. J.; He, H.; Lyons, K. A.; Patel, R. A.; Patel, S. B.; Petrov, A.; Scapin, G.; Wu, J. K.; Xu, S.; Zhu, B.; Thornberry, N. A.; Roy, R. S.; Weber, A. E., *Bioorg. Med. Chem. Lett.* **2009,** *19*, 4097-4101.
156. Kiessling, A. J.; McClure, C. K., *Synth. Comm.* **1997,** *27*, 923-937.
157. Meerwein, H.; Hofmann, G. H. P.; Kroning, E.; Pfeil, E., *J. Prakt. Chem.* **1937,** *147*, 257 -285.
158. Meerwein, H., *Org. Synth* **1966,** *46*, 120-121.
159. Kaloustian, M. K.; Khouri, F., *Tetrahedron Lett.* **1981,** *22*, 413-416.
160. Ritter, A.; Poschenrieder, H.; Bracher, F., *Z. Naturforsch* **2009,** *64*, 427-433.

161. Gensini, M.; Altamura, M.; Dimoulas, T.; Fedi, V.; Giannotti, D.; Giuliani, S.; Guidi, A.; Harmat, N. J. S.; Meini, S.; Nannicini, R.; Pasqui, F.; Tramontana, M.; Triolo, A.; Maggi, C. A., *ChemMedChem* **2010,** *5*, 65-78.

162. Seganish, M. W.; DeShong, P., *J. Org. Chem.* **2004,** *69*, 1137-1143.

163. Aster, S. D.; Graham, D. W.; Kharbanda, D.; Patel, G.; Ponpipom, M.; Santorelli, G. M.; Szymonifka, M. J.; Mundt, S. S.; Shah, S.; Springer, M. S.; Thieringer, R.; Hermanowski-Vosatka, A.; Wright, S. D.; Xiao, J.; Zokian, H.; Balkovec, J. M., *Bioorg. Med. Chem. Lett.* **2008,** *18*, 2799-2804.

164. Abdel-Rahman, R. M.; Abdel-Halim, A. M.; Ibrahim, S. S.; Mohamed, E. A., *J. Chem. Soc. Pakistan* **1987,** *9*, 523-537.

165. Awas, M. A. A., *Org. Chem. Indian J.* **2008,** *4*, 16-21.

166. Chiyanzu, I.; Hansell, E.; Gut, J.; Rosenthal, P. J.; McKerrow, J. H.; Chibale, K., *Bioorg. Med. Chem. Lett.* **2003,** *13*, 3527-3530.

167. Jung, M. E.; Gervay, J., *J. Am. Chem. Soc.* **1991,** *113*, 224-232.

168. Heidelberger, C.; Guggisberg, A.; Stephanou, E.; Hesse, M., *Helvetica Chimica Acta* **1981,** *64*, 399-406.

169. Aziza, M. A.; Nassar, M. W.; Abdel-Hamide, S. G.; El-Hakim, A. E.; El-Azab, A. S., *Indian J. Heterocyclic Chem* **1996,** *6*, 25-30.

170. Basha, F. Z.; DeBernardis, J. F., *J. Heterocyclic Chem.* **1987,** *24*, 789-791.

171. Tan, D. Q.; Atherton, A. L.; Smith, A. J.; Soldi, C.; Hurley, K. A.; Fettinger, J. C.; Shaw, J. T., *ACS Comb. Sci.* **2012,** *14*, 218-223.

172. Ren, P.; Vechorkin, O.; Csok, Z.; Salihu, I.; Scopelliti, R.; Hu, X., *Dalton Trans.* **2011,** *40*, 8906-8911.

173. Ojima, I.; Okabe, M.; Kato, K.; Kwon, H. B.; Horvath, I. T., *J. Am. Chem. Soc.* **1988,** *110*, 150-157.

174. Lipshutz, B. H.; Huff, B.; Hagen, W., *Tetrahedron Lett.* **1988,** *29*, 3411-3414.

175. Bastiaansen, L. A. M.; Godefroi, E. F., *Synthesis* **1978**, 675-676.

176. RajanBabu, T. V.; Chenard, B. L.; Petti, M. A., *J. Org. Chem* **1986,** *51*, 1704-1712.

177. Andrews, S. P.; Ladlow, M., *J. Org. Chem.* **2003,** *68*, 5525-5533.

178. Maslankiewicz, A.; Marciniec, K.; Pawlowski, M.; Zajdel, P., *Heterocycles* **2007,** *71*, 1975-1990.

179. Congreve, M. S.; Kay, C.; Scicinski, J. J.; Ley, S. V.; Williams, G.; Murray, P. J.; McKeown, S. C.; Watson, S. P., *Tetrahedron Lett.* **2003,** *44*, 4153-4156.

180. Pattarawarapan, M.; Chen, J.; Steffensen, M.; Burgess, K., *J. Combinatorial Chem.* **2001,** *3*, 102-116.

181. Langler, R. F., *Canadian J. Chem.* **1976,** *54*, 498-499.

182. Barnwell, N.; Cornwall, P.; Horner, D.; Knott, J.; Liddon, J., *Org. Proc. Res. Dev.* **2010,** *14*, 278-288.

183. Janota, H.; Alov, E. M.; Moskvichev, Y. A.; Mironov, G. S., *Zhurnal Organicheskoi Khimii* **1985,** *21*, 365-368.

184. Kiprianov, A.; Tolmachev, A. I., *Zhurnal Obshchei Khimii* **1959,** *29*, 2868-2874.
185. Hamada, T.; Yonemitsu, O., *Synthesis* **1986**, 852-854.
186. Verhe, R.; Courtheyn, D.; de Kimpe, N.; de Buyck, L.; Schamp, N., *Synthesis* **1982**, 667-670.
187. Ramirez, S. M.; Layman, J. M.; Bissel, P.; Long, T. E., *Macromolecules* **2009,** *42*, 8010-8012.
188. Nahm, S.; Weinreb, S. M., *Tetrahedron Lett.* **1981,** *22*, 3815-3818.
189. Rezaei, Z.; Khabnadideh, S.; Pakshir, K.; Hossaini, Z.; Amiri, F.; Assadpour, E., *Eur. J. Med. Chem.* **2009,** *44*, 3064-3067.
190. Smith, A. B.; Nolen, E. G.; Shirai, R.; Blase, F. R.; Ohta, M.; Chida, N.; Hartz, R. A.; Fitch, D. M.; Clark, W. M.; Sprengeler, P. A., *J. Org. Chem.* **1995,** *60*, 7837-7848.
191. Smith, A. B.; Kanoh, N.; Ishiyama, H.; Minakawa, N.; Rainier, J. D.; Hartz, R. A.; Cho, Y. S.; Cui, H.; Moser, W. H., *J. Am. Chem. Soc.* **2003,** *125*, 8228-8237.
192. Varin, M.; Barre, E.; Lorga, B.; Guillou, C., *Eur. J.* **2008,** *14*, 6606-6608.
193. Paquette, L. A.; Wright, J.; Drtina, G. J.; Roberts, R. A., *J. Org. Chem.* **1987,** *52*, 2960-2962.
194. Gates, M.; Tschudi, G., *J. Am. Chem. Soc.* **1952,** *74*, 1109-1110.
195. Reader, A. M.; Bailey, P. S.; White, H. M., *J. Org. Chem.* **1965,** *30*, 784-788.
196. Vaisburg, A. F.; Etzlstorfer, C.; Falk, H., *Monatshefte Fur Chemie* **1994,** *125*, 1121-1127.
197. Holton, T. L.; Schechter, H., *J. Org. Chem.* **1995,** *60*, 4725-4729.
198. Wommack, A. J.; Moebius, D. C.; Travis, A. L.; Kingsbury, J. S., *Org. Lett.* **2009,** *11*, 3202-3205.
199. Gonczi, C.; Swistun, Z.; Plas, H. C. V. d., *J. Org. Chem.* **1981,** *46*, 608-610.
200. Clayden, J.; Greeves, N.; Warren, S.; Wothers, P., *Organic Chemistry*. Oxford University Press: 2001.
201. Xu, Z.-L.; Li, H.-X.; Ren, Z.-G.; Du, W.-Y.; Xu, W.-C.; Lang, J.-P., *Tetrahedron* **2011,** *67*, 5282-5288.
202. Huang, Y.-Z.; Miao, H.; Zhang, Q.-H.; Chen, C.; Xu, J., *Catal. Lett.* **2008,** *122*, 344-348.
203. Xiang, J.; Wan, Z.-K.; Li, H.-Q.; Ipek, M.; Binnun, E.; Nunez, J.; Chen, L.; McKew, J. C.; Mansour, T. S.; Xu, X.; Suri, V.; Tam, M.; Xing, Y.; Li, X.; Hahm, S.; Tobin, J.; Saiah, E., *J. Med. Chem.* **2008,** *51*, 4068-4071.
204. Patel, N. B.; Patel, A. L., *Oriental J. Chem.* **2008,** *24*, 551-558.
205. Barnes, D.; Bebernitz, G. R.; Cohen, S. L.; Damon, R. E.; Day, R. F.; Jain, M.; Karki, R. G.; Kirman, L. C.; Patel, T. J.; Raymer, B. K.; Schuster, H. F.; Zhang, W. Preparation of cyclohexane derivatives as inhibitors of acetyl-CoA carboxylase (ACC). PCT Int. Appl., WO 2011067306, 2011.
206. Naik, A. D.; J. Marchand-Brynaert; Garcia, Y., *Synthesis* **2008**, 149-154.
207. Tannock, I. F.; Rotin, D., *Cancer Res.* **1989,** *49*, 4373-4384.
208. Reed, P. E.; Katzenellenbogen, J. A., *J.Org. Chem.* **1991,** *56*, 2624-2634.
209. Rajopadhye, M.; Popp, F. D., *J. Med. Chem.* **1988,** *31*, 1001-1005.

210. Edwards, L.; Isaac, M.; Johansson, M.; Kers, A.; Malmberg, J.; McLeod, D.; Mindis, A.; Staaf, K.; Slassi, A.; Stefanac, T.; Stormann, T.; Wensbo, D.; Xin, T.; Arora, J. Preparation of heteropolycyclic compounds and their use as metabotropic glutamate receptor antagonists. U.S. Pat. Appl. Publ., US 20050272779, 2005.

211. Ohta, S.; Kawasaki, I.; Fukuno, A.; Yamashita, M.; Tada, T.; Kawabata, T., *Chem. Pharm. Bull.* **1993,** *41*, 1226-1231.

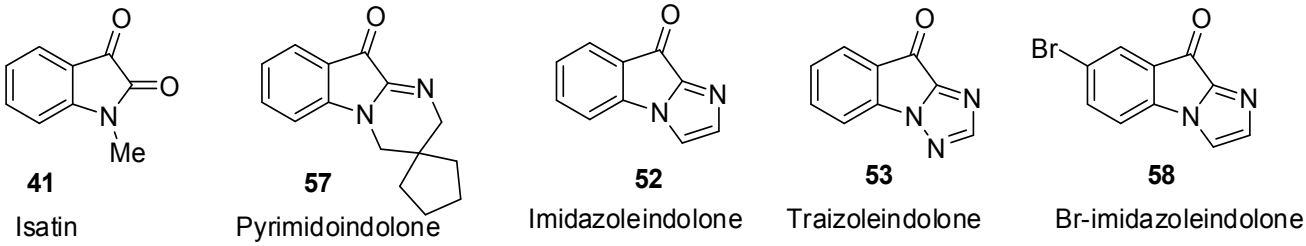
212. Ren, L.; Chen, A. C.; Decken, A.; Crudden, C. M., *Canadian J. Chem.* **2004,** *82*, 1781-1787.

213. Dallacker, F.; Minn, K., *Chemiker-Zeitung* **1986,** *110*, 275-281.

214. Hidalgo, I. J.; Raub, T. J.; Borchardt, R. T., *Gastroenterology* **1989,** *96*, 736-749.

APPENDIX

Appendix 1: Gaussian Data Output from Computational Modelling of the Heterocycles



The heterocycles used for computational studies

wB97xD

	Energies (Hartree)			Energies (kJ/mol)			
	Reactants	TS	Product	G(TS) - G(React)	ΔG	G(TS) - G(Prod)	H-bonding Distance (Å)
41	-951.495666	-951.437916	-951.497073	151.622625	-3.6940785	155.3167	2.668
57	-1243.465737	-1243.40365	-1243.462976	163.0094185	7.2490055	155.7604	2.334
52	-1007.771542	-1007.709685	-1007.768559	162.4055535	7.8318665	154.5737	2.866
53	-1023.804593	-1023.739291	-1023.804206	171.450401	1.0160685	170.4343	3.097
58	-3579.080569	-3579.01554	-3579.076638	170.7336395	10.3208405	160.4128	2.854

M062X

	Energies (Hartree)			Energies (kJ/mol)			
	Reactants	TS	Product	G(TS) - G(React)	ΔG	G(TS) - G(Prod)	H-bonding Distance (Å)
41	-951.428277	-951.374542	-951.435412	141.0812425	-18.7329425	159.8142	2.506
57	-1243.339854	-1243.286934	-1243.343562	138.94146	-9.735354	148.6768	2.315
52	-1007.70608	-1007.647321	-1007.707874	154.2717545	-4.710147	158.9819	3.03
53	-1023.74193	-1023.679979	-1023.746657	162.6523505	-12.4107385	175.0631	3.132
58	-3579.062549	-3579.004253	-3579.066745	153.056148	-11.016598	164.0727	3.039

Appendix 2: UV-Vis Absorption Data

Table 1: Changes in isatin **41** absorption at 426 nm: 2mM isatin titrated with aliquots of PMBSH of known concentrations

	Isatin 41 Absorption			
[Thiol] / (mM)	n = 1	n=2	A (average)	ΔA
0	1.2	1.2087	1.206	0
1.99	0.86	0.87667	0.87	0.336
3.97	0.66	0.67126	0.666	0.54
5.94	0.54	0.54875	0.542	0.664
7.89	0.45	0.45838	0.453	0.753
9.84	0.38	0.38956	0.385	0.821
11.76	0.33	0.33992	0.336	0.87
13.68	0.3	0.30033	0.299	0.907
15.58	0.27	0.26859	0.269	0.937
17.48	0.24	0.24589	0.245	0.961
19.35	0.23	0.22517	0.226	0.98

Table 2: Changes in imidazoleindolone **52** absorption at 392nm: 2mM imidazoleindolone titrated with aliquots of PMBSH of known concentrations

	Imidazoleindolone 52 Absorption			
[Thiol] / (mM)	n = 1	n = 2	A (average)	ΔA
0	1.301	1.3007	1.30085	0
3.97	1.2955	1.2896	1.29255	0.0083
5.94	1.2951	1.288	1.288	0.01285
7.89	1.2914	1.2853	1.285	0.01585
9.84	1.2851	1.2807	1.2807	0.02015
11.76	1.2804	1.2763	1.2763	0.02455
13.68	1.2743	1.2719	1.2731	0.02775
15.58	1.2693	1.2668	1.26805	0.0328
17.48	1.2646	1.2635	1.26405	0.0368
19.35	1.2586	1.2583	1.2584	0.04245

Table 3: Changes in pyrimidoindolone **57** absorption at 461 nm: 1mM ketone titrated with aliquots of PMBSH solutions of known concentrations

	Pyrimidoindolone 57 Absorption	
[Thiol] / (mM)	n = 1	ΔA
0	2.1384	0
0.995	2.1235	0.0149
1.985	2.1137	0.0247
2.97	2.1008	0.0376
3.945	2.0888	0.0496
4.92	2.0779	0.0605
5.88	2.0641	0.0743
6.84	2.0512	0.0872
7.79	2.0362	0.1022
8.74	2.0144	0.124
9.675	1.9988	0.1396

Table 4: Changes in Br-imidazoleindolone **58** absorption at 394.7 nm: 2mM ketone titrated with aliquots of PMBSH and of known concentrations

	Imidazoleindolone 58 Absorption			
[Thiol] / (mM)	n = 1	n = 2	A (average)	ΔA
0	1.1762	1.1832	1.1797	0
1.99	1.1706	1.1672	1.1689	0.0108
3.97	1.1611	1.1589	1.16	0.0197
5.94	1.1505	1.1477	1.1491	0.0306
7.89	1.1403	1.1383	1.1393	0.0404
9.84	1.1289	1.128	1.12845	0.05125
11.76	1.1205	1.1185	1.1195	0.0602
13.68	1.1099	1.1091	1.1095	0.0702
15.58	-	1.1009	1.1009	0.0788
17.48	1.0924	1.0913	1.09185	0.08785
19.35	1.0799	1.0817	1.0808	0.0989

Table 5: Changes in Br-imidazoleindolone **59** absorption at 400.8 nm: 2mM ketone titrated with aliquots of PMBSH solutions of known concentrations

[Thiol] / (mM)	**Imidazoleindolone 59 Absorption**	
	n = 1	ΔA
0	1.54	0
1.99	1.53	0.01
3.97	1.5237	0.0163
5.94	1.5168	0.0232
7.89	1.506	0.034
9.84	1.494	0.046
11.76	1.4829	0.0571
13.68	1.4701	0.0699
15.58	1.4577	0.0823
17.48	1.4455	0.0945
19.35	1.4323	0.1077

Table 6: Changes in sulfonamide-imidazoleindolone **60** absorption at 392.5 nm: 1mM ketone titrated with aliquots of PMBSH solutions of known concentrations

	Imidazoleindolone 60 Absorption	
[Thiol] / (mM)	n = 1	ΔA
0	0.7405	0
0.995	0.73792	0.00258
1.985	0.73557	0.00493
2.97	0.73396	0.00654
3.945	0.73157	0.00893
4.92	0.72937	0.01113
5.88	0.72745	0.01305
6.84	0.7245	0.016
7.79	0.72301	0.01749
8.74	0.72097	0.01953
9.675	0.71814	0.02236

Appendix 3: Crystal Data and Structure Refinement for the Ketal Protected Triazoleindolone 212[j]

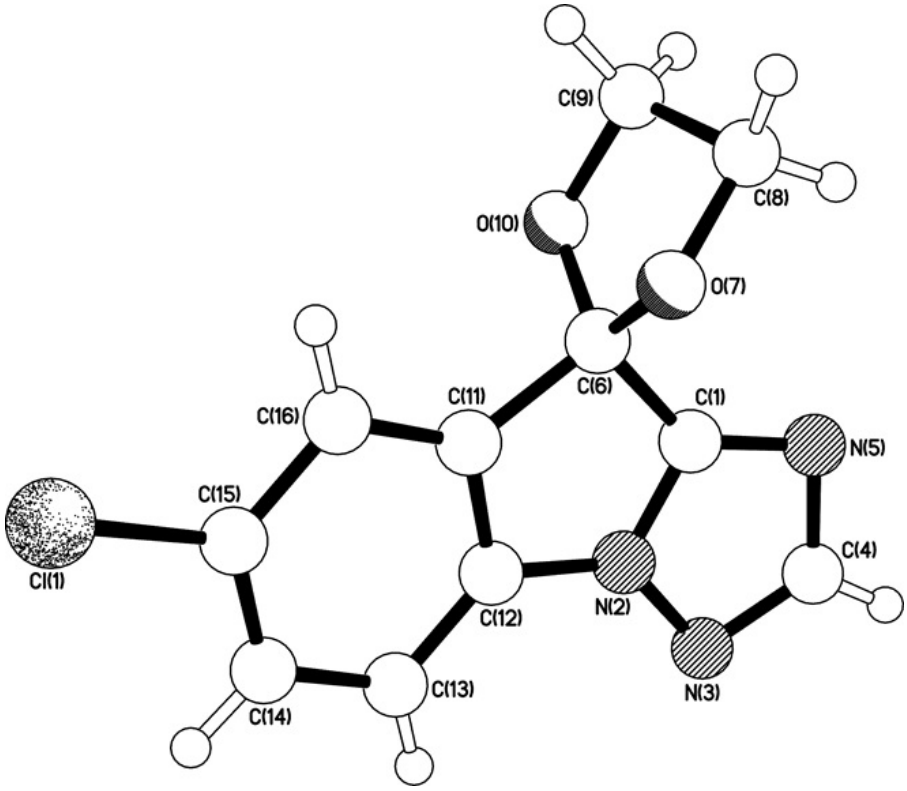


Figure 1: The determined regiochemistry of the ketal-protected triazoleindolone **212**

Initial tests were used to identify the atoms in the C(1)-based five membered-ring. The table below lists atoms 2 to 5 and each line specifies whether each atom was modelled as either carbon or nitrogen, with the resulting R-factor obtained from model refinement. The lower the R-factor, the more optimal the arrangement.

Table 1: Modelling the favourable spatial distribution of the carbon and nitrogen atoms

2	3	4	5	R-factor
C	C	C	C	7.56
N	C	C	C	6.96
C	N	C	C	7.05
C	C	N	C	8.23
C	C	C	N	7.19
N	N	C	N	5.62*
N	N	N	N	6.22

[j] The crystallography experiment was conducted by Dr Andrew J.P. White, Chemical Crystallography Laboratory, Department of Chemistry, Imperial College London.

The top line with all four atoms modelled as carbon serves as the baseline. The next four lines make it clear that the atoms at positions 2, 3 and 5 work better as nitrogen than carbon, and that the atom at position 4 works better as carbon than nitrogen. The penultimate line shows the clear improvement in the structure when all of the four atoms are modelled correctly, and the last line was a check that the four nitrogen model was not optimal. Hence, it was concluded that 2, 3 and 5 are nitrogen atoms and 4 is a carbon. Subsequently hydrogen atoms on C(4) and N(3) were located from difference electron density maps.

Crystal Analysis Data

Temperature	173 K	
Diffractometer, wavelength	OD Xcalibur 3, 0.71073 Å	
Crystal system, space group	Monoclinic, C2/c	
Unit cell dimensions	a = 13.9404(6) Å	α = 90°
	b = 7.3853(3) Å	β = 93.511(4)°
	c = 20.7391(10) Å	γ = 90°
Volume, Z	2131.17(16) $Å^3$, 8	
Density (calculated)	1.556 Mg/m^3	
Absorption coefficient	0.350 mm^{-1}	
F(000)	1024	
Crystal colour / morphology	Colourless tabular needles	
Crystal size	0.49 x 0.28 x 0.09 mm^3	
θ range for data collection	3.43 to 32.65°	
Index ranges	-20<=h<=19, -5<=k<=11, -31<=l<=29	
Reflns collected / unique	11813 / 3618 [R(int) = 0.0276]	
Reflns observed [F>4σ(F)]	2831	
Absorption correction	Analytical	
Max. and min. transmission	0.972 and 0.863	
Refinement method	Full-matrix least-squares on F^2	
Data / restraints / parameters	3618 / 0 / 154	
Goodness-of-fit on F^2	1.092	
Final R indices [F>4σ(F)]	R1 = 0.0532, wR2 = 0.1122	
R indices (all data)	R1 = 0.0723, wR2 = 0.1203	
Largest diff. peak, hole	0.354, -0.306 $eÅ^{-3}$	
Mean and maximum shift/error	0.000 and 0.001	

Table 2: of Bond lengths [Å] and angles (°) for the ketal-protected triazoleindolone **212**

C(1)-N(5)	1.322(2)
C(1)-N(2)	1.339(2)
C(1)-C(6)	1.524(2)
N(2)-N(3)	1.351(2)
N(2)-C(12)	1.415(2)
N(3)-C(4)	1.327(3)
C(4)-N(5)	1.375(3)
C(6)-O(7)	1.404(2)
C(6)-O(10)	1.420(2)
C(6)-C(11)	1.532(2)
O(7)-C(8)	1.446(2)
C(8)-C(9)	1.502(3)
C(9)-O(10)	1.438(2)
C(11)-C(16)	1.382(2)
C(11)-C(12)	1.397(2)
C(12)-C(13)	1.372(2)
C(13)-C(14)	1.398(3)
C(14)-C(15)	1.380(3)
C(15)-C(16)	1.399(2)
C(15)-Cl(1)	1.7411(18)
N(5)-C(1)-N(2)	110.17(15)
N(5)-C(1)-C(6)	139.86(16)
N(2)-C(1)-C(6)	109.85(14)
C(1)-N(2)-N(3)	111.69(14)
C(1)-N(2)-C(12)	112.57(14)
N(3)-N(2)-C(12)	135.22(15)
C(4)-N(3)-N(2)	100.43(15)
N(3)-C(4)-N(5)	116.30(17)
C(1)-N(5)-C(4)	101.41(15)
O(7)-C(6)-O(10)	107.08(13)
O(7)-C(6)-C(1)	112.44(14)
O(10)-C(6)-C(1)	111.99(14)
O(7)-C(6)-C(11)	112.87(14)
O(10)-C(6)-C(11)	112.49(13)
C(1)-C(6)-C(11)	100.03(13)
C(6)-O(7)-C(8)	103.55(14)
O(7)-C(8)-C(9)	102.12(15)
O(10)-C(9)-C(8)	103.75(15)
C(6)-O(10)-C(9)	107.55(14)
C(16)-C(11)-C(12)	119.91(15)
C(16)-C(11)-C(6)	129.80(15)
C(12)-C(11)-C(6)	110.28(14)
C(13)-C(12)-C(11)	123.48(16)
C(13)-C(12)-N(2)	129.42(16)
C(11)-C(12)-N(2)	107.07(14)
C(12)-C(13)-C(14)	116.68(16)

C(15)-C(14)-C(13)	120.29(16)
C(14)-C(15)-C(16)	122.88(16)
C(14)-C(15)-Cl(1)	118.46(13)
C(16)-C(15)-Cl(1)	118.65(14)
C(11)-C(16)-C(15)	116.76(16)